Reevaluating the membrane organization, phase behaviour, aggregation, and fusion of the model membranes under different external influences

Ph.D. Thesis

By

SOUMYA KANTI DE

DISCIPLINE OF CHEMISTRY

INDIAN INSTITUTE OF TECHNOLOGY INDORE

AUGUST 2021

Reevaluating the membrane organization, phase behaviour, aggregation, and fusion of the model membranes under different external influences

A THESIS

Submitted in partial fulfillment of the
requirements for the award of the degree
of
DOCTOR OF PHILOSOPHY

by

SOUMYA KANTI DE

DISCIPLINE OF CHEMISTRY
INDIAN INSTITUTE OF TECHNOLOGY INDORE
AUGUST 2021

INDIAN INSTITUTE OF TECHNOLOGY INDORE

I hereby certify that the work which is being presented in the thesis entitled **Reevaluating the membrane organization, phase behaviour, aggregation, and fusion of the model membranes under different external influences** in the partial fulfillment of the requirements for the award of the degree of **DOCTOR OF PHILOSOPHY** and submitted in the **DEPARTMENT OF CHEMISTRY, Indian Institute of Technology Indore**, is an authentic record of my own work carried out during the time period from SEPTEMBER 2015 to AUGUST 2021 under the supervision of **DR. ANJAN CHAKRABORTY**, Associate Professor, Discipline of Chemistry, Indian Institute of Technology Indore.

The matter presented in this thesis has not been submitted by me for the award of any other degree of this or any other institute.

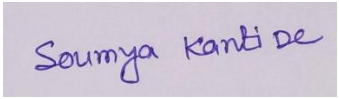

29.08.2021
Signature of the student with date
SOUMYA KANTI DE

This is to certify that the above statement made by the candidate is correct to the best of my knowledge.

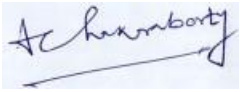

29.08.2021
Signature of Thesis Supervisor with date
DR. ANJAN CHAKRABORTY

SOUMYA KANTI DE has successfully given his Ph.D. Oral Examination held on **20.01.2022**.

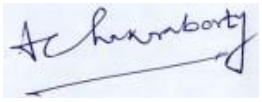

24.01.2022
Signature of Thesis Supervisor with date
DR. ANJAN CHAKRABORTY

ACKNOWLEDGEMENTS

First and foremost, I would like to pay my sincere gratitude towards my supervisor Dr. Anjan Chakraborty, for his invaluable guidance, encouragement, and help throughout the whole course of the thesis work. His thorough knowledge, superior command over the subject, precious advice and constant enthusiasm have made me sail through the Ph.D. journey much more efficiently. Not only he helped me to overcome every single academic difficulty, but also stood firmly by my side whenever I ran into any problematic situation. I am greatly indebted to him for his support, motivation, and guidance.

I express my sincere obligation to my PG Student Progress Committee (PSPC) members, Dr. Tridib Kumar Sarma and Dr. Debasis Nayak for their valuable suggestions and guidance. I would also like to thank all the faculty members of Discipline of Chemistry, IIT Indore for their guidance and help during the course of the thesis work. I would like to thank the sophisticated instrument centre (SIC), Indian Institute of Technology Indore for providing in-house research equipment. I would like to thank Dr. Tridib Kumar Sarma and his group members for their selfless cooperation and help during my Ph. D. programme.

I want to express my heartfelt thanks to Mr. Kinny Pandey, Mr. Ghanshyam Bhavsar, Mr. Manish Kushwaha and Mrs. Vinita Kothari for their technical support without which it would not be possible to continue my work. I would like to thank Dr. Ravinder Kumar for his selfless cooperation and help during confocal microscopy experiments. I would like to acknowledge all the technical and non-technical staff of IIT Indore for their assistance and service.

I want to express my heartfelt thanks to all members of our laboratory. I extend my heartiest gratitude to Dr. Anupam Das and Dr. Nishu Kanwa for their constant guidance, help, and support at all the ups and downs of the Ph.D. programme. I convey my deep thanks to my other group members, Dr. Chandan Adhikari, Mr. Mirajuddin Ahamed, Mr. Avijit Maity, Mr. Debanjan

Bagchi, Mr. Aditya Kumar Bharti, Ms. Kavana M, and Ms. Ananya Patnaik for their selfless co-operation and help to make my work successful.

I have been lucky enough to have some excellent friends and seniors in my life, whom I want to acknowledge deeply. I would like to record my thanks to Ankan, Sayan, Rohit, Pramodh, Soumitra, Tapas, Rishi, Arghya, Sayantan, Amitabha, Surya, Shyama, Chiranjit, Neha, Daisy, Siddharth, Abhiram, Vidhi, Amrita, Jamuna, Yogajivan, Anupama, Madhurima, Amit Sir, Premansh Sir, Devraj, Richa, Vishesh and many more in my friend circle. I express my heartiest gratitude to my fantastic roommates cum friends; Dr. Debashis Majee, Dr. Biju Majumdar, Dr. Soumen Biswas, and Dr. Sayan Maity who have been with me in every ups and downs of my professional and personal life. Also, I want to extend a special thanks to my some dearest friends Subhro, Rakesh, Suvendu, Ruhul, Sunipa and Arpita for always being there with me. Thank you for believing in me, encouraging me, making me laugh, and turning my every tiring and busy day into a joyful evening.

I am profoundly indebted to my family and relatives (Didu, Masi, meso, mamu, moni, tubun, tutun, sona, bunu, aditya and puchku) for their support, immense care, and prayerful assistance in many ways during the span of this research work. Last but definitely not least, I want to express my acknowledgment and love to the four most important people of my life. Maa, Baba, Kaku, and Boni, you should know that your care, support, belief, and unconditional love are worth more than I can express on paper. I am forever indebted to them for giving me the opportunities, encouragement, and experiences that have made me who I am.

There are many more who have directly or indirectly contributed to making this journey successful. I am grateful to each and every one of you who have been responsible for facilitating me to complete my research work.

Soumya Kanti De

IIT Indore

Dedicated to

My Family

ABSTRACT

It is well known that Alec Bangham discovered and proposed the idea of using liposomes as the drug delivery systems. Since then, liposomes have become an indispensable part of research and clinical applications in the field of nanomedicine, due to the several advantages e. g. loading ability of both hydrophobic and hydrophilic drugs, tunable size and surface charge, biodegradability, and biocompatibility, etc. One of the main advantages is that lipid vesicles can mimic the cellular membranes which can be conveniently designed in vitro using lipids and simplify the in *vivo* complex membrane environment for easier analysis. Lipid vesicles are prone to fuse which limits their application as a delivery system and several modifications have been introduced to enhance the targeted delivery. Therefore, in order to modify and stabilize their structures, they are often treated with external interactive species e. g. nanoparticles, biomolecules, polymers, etc. On the other hand, membrane fusion is a fundamental process in many important biological processes such as viral infection, endocytosis, and exocytosis, etc. This process both in *vivo* and in *vitro* is usually controlled by external agents called fusogens. The most common fusogens are large molecules like proteins and peptides and they play a vital role in different processes of cells such as self-reproduction, fusion, and fission which are also crucial steps for mimicking the origin of cellular life. Phospholipid vesicle formation in cells e. g. vesicular transport and organelle biogenesis are critically dependent on membrane fission, which is induced by highly evolved proteins. Therefore, both the stabilization and destabilization of the lipid vesicles have been considered of great interest due to their own perspective. Thus the interactions of lipid vesicles with external species are extremely important to understand the potential changes in the membrane properties. These interactions can influence the hydration-dehydration, rigidity, and fluidity of the lipid bilayer. Even minor changes in the membrane structure and properties can have larger impacts on several important biological functions.

Several complex biological processes are associated with the changes in the membrane phase state. For example, the fluid mosaic model suggested by

Singer and Nicolson proposed that the fluid state of membrane lipids is critical for membrane function. On the other hand, the initial membrane phase state of the delivery system can be changed to either an ordered or disordered phase state by different external entities which consequently affects the releasing ability of the payload from the delivery system. The determination of the membrane phase state required complex instrumentations. Therefore, it is always important and recommended for quick determination of the membrane phase state using simple techniques. The dynamical properties of the membrane were previously investigated by using organic membrane probes (e. g. PRODAN, LAURDAN, ANS, etc.). However, to study the morphological changes in the lipid vesicles via imaging technique (i. e. for confocal microscopy) we had to use external dyes (e. g. Rhodamine B) or lipid-tagged dyes (modified dyes) due to the multiple disadvantages of these organic membrane probes. In this context, luminescence carbon dots (CDs) have several advantages over the conventional organic membrane probes owing to their tunable photoluminescence, high quantum yield, excellent photostability, and broad excitation-emission spectral range. Therefore, a CD-based membrane probe should be advantageous compare to the organic membrane probe, which possibly discovers a new horizon for the bioimaging models.

The membrane interaction studies account for the underlying mechanisms and the resultant influence at the nano-bio interface which eventually affects the cellular processes. Thus, a better understanding of the interactions at the membrane interface is required, which can help us to bridge the gap between the lipid systems in *vivo* and in *vitro*.

Objective: The principal aim of this thesis is to investigate the factors potentially responsible for the alteration of the membrane phase state i.e. hydration-dehydration of the lipid bilayer and its effect on the fusion of the lipid vesicles. The investigation of the underlying mechanism behind the interaction between external entities and membranes and the subsequent impact on the membrane are the key objectives of the current thesis. Thus the current thesis demonstrates the interactions of different metal ions, aromatic amino acids, and carbon dots with model lipid membranes. The lipid bilayers of varying chain lengths, surface charges, and phase transition temperatures

(T_m) were chosen for different spectroscopic as well as imaging studies. The knowledge gained from the spectroscopic and imaging studies regarding membrane phase state may help to understand the different cellular processes like aggregation, and fusion processes induced by external small molecules and ions. The thesis aims for addressing and exploring the following crucial area:

a) We investigated the effect of metal ions on the lipid bilayer by using simple spectroscopic techniques. We put effort to correlate the hydration or dehydration of the lipid bilayer with the aggregation or the colloidal stability of the lipid vesicles.
b) Using a series of trivalent metal ions and a comparative study with the divalent metal ions helped us to understand how the difference in the ionic radius and effective charge of the metal ions affect the lipid-metal ions interaction. We studied the impact of metal ion-induced dehydration of the lipid bilayer on the aggregation and fusion of the lipid vesicles. We also investigate how the aggregation of the lipid vesicles can fit in the framework of the existing theoretical model.
c) Amyloid structures of amino acids are responsible for several major human neurodegenerative diseases. Therefore, the thesis accounts for determining the nature of the interaction between lipid vesicles and aromatic amino acids. We investigated the role of the side chain of the aromatic amino acids in the lipid-amino acid interaction. With the help of live confocal microscopy imaging, the fate of the lipid vesicle during the formation of the amyloid structure was investigated, which helped us to understand the underlying cytotoxic behaviour of the amyloid structure.
d) In the thesis, to the best of our knowledge, for the first time, we explore the opportunity of a CD-based membrane sensor. We reported that the CD-based sensor can be used as an alternative membrane probe like the previously reported organic membrane probe (e. g. PRODAN, LAURDAN, ANS, etc.). We also studied how the organization of the lipid membrane i. e. liquid-crystalline phase and

sol-gel phase influences the photo-stability of a CD, which will potentially help to develop the CD-based bio-imaging systems.

e) The thesis demonstrates how we can probe the interaction of various interactive entities with lipid vesicles by exploiting the properties of a fluorescent membrane probe by means of different spectroscopic methods. Our study demonstrates that the simple steady-state fluorescence and imaging techniques efficiently detect the changes in the membrane dynamics.

Summary of the research work:

The contents of each chapter included in the thesis are discussed as follows.

Chapter 1. Basic introduction

The interaction of different metal ions, proteins, peptides, amino acids, and carbon dots with lipid vesicles is discussed in the introduction. The introduction part also summarizes the changes in the membrane organization by these external entities on different lipid vesicles.

Chapter 2. Spectroscopic evidence for hydration and dehydration of lipid bilayers upon interaction with metal ions: a new physical insight

The binding of metal cations to lipid membranes has been a vital area of research over the past few decades. In this section, we investigated the interaction of the lipid bilayer of different hydrophobic chain lengths and phase transition temperatures with a series of different divalent metal ions (Zn^{+2}, Ca^{+2}, and Mg^{+2}). We chose three different zwitterionic phospholipids, namely DPPC, DMPC, and POPC, which possess the same zwitterionic head groups, but widely different phase transition temperatures (41 °C, 24 °C, and -20 °C for DPPC, DMPC, and POPC respectively). Our study revealed that the divalent metal ions interact strongly with the lipid with saturated tails i.e. DPPC and DMPC bilayers while the interaction is much less prominent with the POPC lipid bilayers. We also found that among the metal ions Zn^{+2} and Ca^{+2} drastically dehydrate the lipid bilayer whereas Mg^{+2} hydrates the lipid

bilayer. We observed that at lower pH, H^{+}possibly preoccupies the phosphate group and thus preventing the metal ions from binding to the lipid head groups. Importantly the dynamic light scattering measurement (DLS) confirmed that with increasing gelation or dehydration of the lipid vesicles the aggregation increased whereas the hydrated lipid bilayer was colloidal stable and did not undergo aggregation.

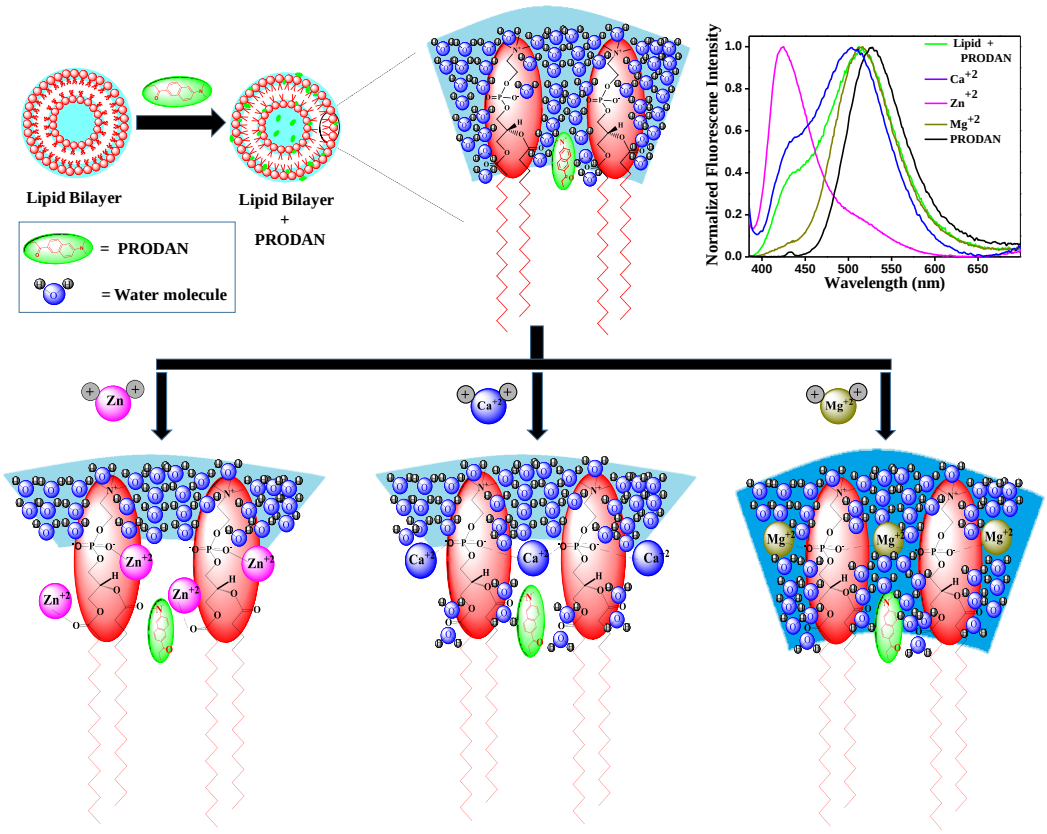

Scheme 1: Pictorial representation of the effect of various metal ions in lipid bilayers. The scheme shows that Zn^{+2} and Ca^{+2} drastically dehydrate the lipid bilayer by removing the water molecule from the lipid head group whereas Mg^{+2} hydrates the lipid bilayer by caring water molecule to the lipid bilayer.

Chapter 3. Influence of Trivalent Metal Ions on Lipid Vesicles: Gelation and Fusion Phenomena.

In this section, we investigated the interaction of 1,2-dimyristoyl-sn- glycero-3-phosphocholine (DMPC) lipid vesicles with a series of trivalent metal ions of the same group, namely, Al^{+3}, Ga^{+3}, and In^{+3} to get a distinct view of the effect of ionic radius of the metal ions on lipid vesicles. We found that trivalent metal ions interact strongly with the lipid vesicles and result in

dehydration of the surface of the lipid vesicles. This interaction is strongest in the case of In^{+3} owing to the higher ionic radius as compared to Al^{+3} and Ga^{+3}. The DLS measurements, CLSM, and AFM imaging revealed that the addition of In^{+3} to the lipid vesicles induced aggregation and fusion, possibly due to the cross-linking ability and higher dehydration of lipid bilayer by In^{+3}. The fusion phenomena were further correlated to the well-celebrated DLVO theory. The confocal imaging indicated the dye leakage possibility of the DMPC vesicles during the aggregation and fusion in the case of In^{+3} whereas we did not observe such behaviour in the case of Al^{+3} and Ga^{+3}. On the contrary, we observed the formation of a more compact vesicle upon the addition of Al^{+3} or Ga^{+3}. One important observation is that, unlike divalent metal ions, trivalent metal ions induced gelation of the lipid vesicles even at a very low pH. The observation indicated the importance of the charge of the metal ions and also exhibited that the trivalent metal ions can stabilize the lipid vesicles even at a lower pH.

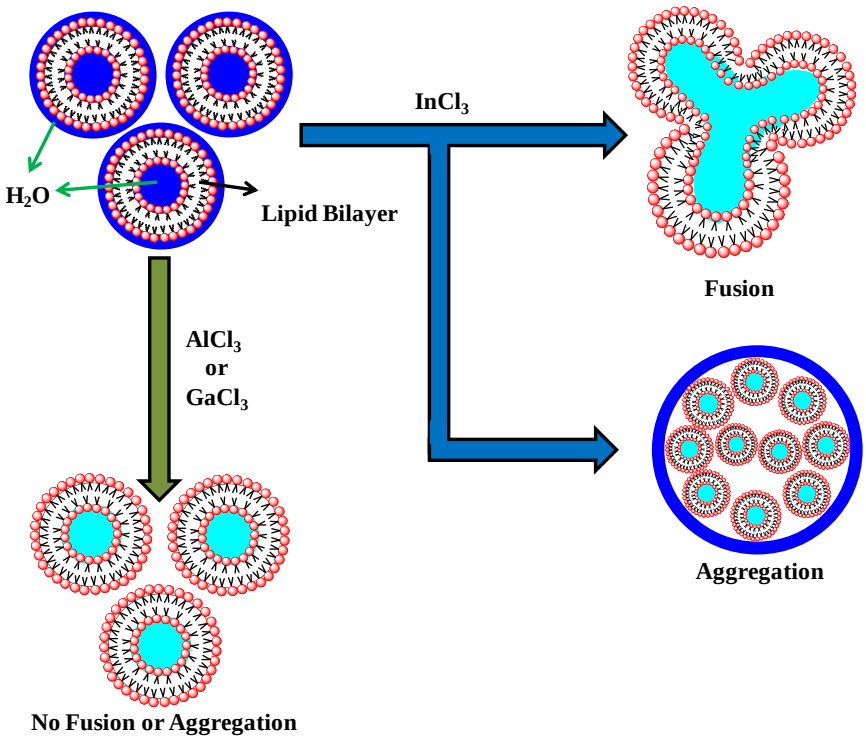

Scheme 2: Pictorial representation of the effect of various trivalent metal ions in lipid bilayers. All the metal ions extensively dehydrate the lipid bilayer by removing the water molecules from the interfacial region. The addition of In^{+3} brings aggregation and fusion whereas the same concentration of Al^{+3} and Ga^{+3} stabilizes the lipid vesicles.

Chapter 4. Interaction of monomeric and self-assembled aromatic amino acids with model membranes: self-reproduction phenomena.

Membrane-protein interaction is a complex process and critically important for mimicking the origin of cellular life. Therefore, in this section, we have investigated the possible mode of interaction of the monomeric and self-assembled amino acids with the model lipid membranes. To unravel the factors behind the interaction between monomeric amino acids with the lipid membrane, we have selected three different surface charged, zwitterionic, negative, and positively charged model membranes (DMPC, DMPG, and DOTAP respectively). We also used a series of amino acids consisting of L-phenylalanine (L-Phe), L-tryptophan (L-Trp), and L-histidine (L-His) to investigate the role of the side chain of the amino acids in lipid–amino acid interaction. As the spontaneous formation of amyloid structures of proteins or peptides or amino acids is responsible for several major human neurodegenerative diseases, we therefore also studied the effect of amino acid amyloid on the structure of the model membrane. Our study revealed that the zwitterionic amino acids rapidly dehydrate the negatively charge lipid bilayer compare to the zwitterionic and positively charged lipid bilayer. This observation leads to the conclusion that the initial interaction is electrostatic in nature that takes place between the NH_3^+ group of the amino acid and the phosphate group (PO_4^-) of the lipid bilayer. The time-dependent study also revealed that the extent of dehydration by these amino acids follows the order L-Trp > L-Phe > L-His and suggests that apart from hydrophobicity, the bulkiness of the side chains plays a crucial role to determine the extent of dehydration of the lipid bilayer. From confocal microscopy and AFM imaging study, we observed the formation of amyloid structure from the aggregated lipid vesicles in the case of zwitterionic DMPC lipid vesicles. However, in the case of negatively charge DMPC/DMPG lipid vesicles, the amyloid structure captured the lipid molecules inside their amyloid structures and form the supported lipid bilayer. The live confocal microscopy imaging revealed that the formation of amyloid aggregates of the amino acids resulting in the formation of supported phospholipid membrane and aggregated vesicles via

fusion and self-reproduction of the lipid vesicles. Our results also suggested that the formation of the aggregated structure of lipid vesicles via fusion is an intermediate of the fibril-lipid membrane complex or supported bilayer.

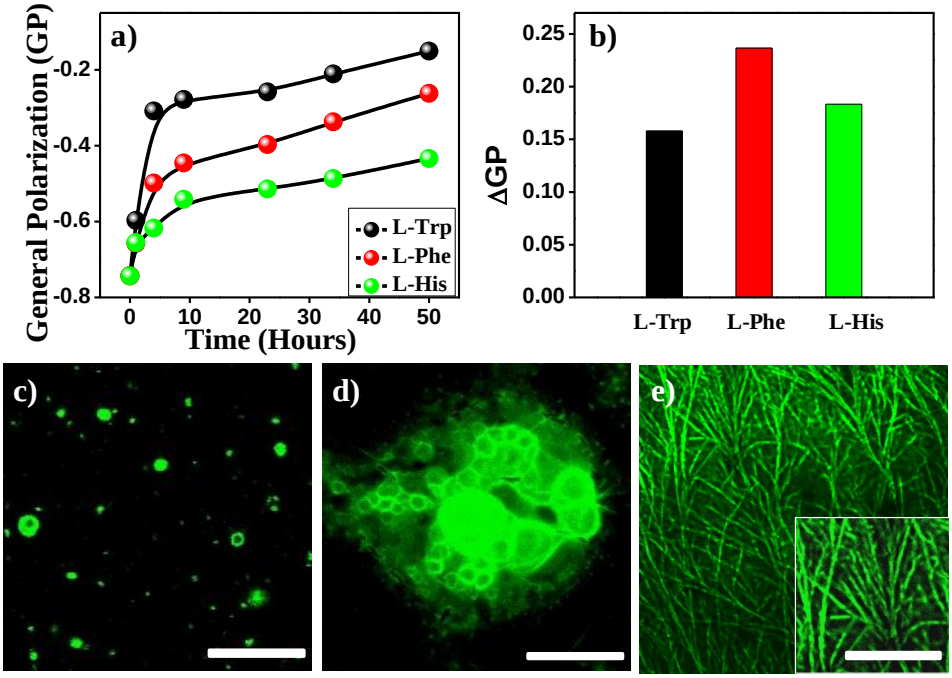

Scheme 3: (a) Time-dependent general polarization plot of the area of DMPC/DMPG-PRODAN fluorescence emission at a fixed concentration of amino acids and (b) change in general polarization (ΔGP) after 4 hours. Confocal images of (c) blank lipid vesicles, (d) DMPC-Phe, and (e) DMPC/DMPG-Phe in the presence of 1 mol% NBD-PE (scale bar 5 μm).

Chapter 5. Lipid phase (ordered/disordered) dependent distinct emission behaviour of hydrophobic carbon dots: the emergence of C-dots based membrane probe.

Simple and quick determination of the membrane phase state is highly advantageous. In this section, we reported a phase-dependent distinct emission profile of lipid encapsulated hydrophobic carbon dots (H-CDs), which can be observed through naked eyes under a UV lamp, thus promoting a unique fluorescence sensor for the membrane phase state. The phase-dependent distinct emission behaviour of the H-CDs have investigated using three representative zwitterionic phospholipid membranes with a wide difference in their phase transition temperatures (T_m), namely, 1,2-dioleoyl-sn-glycero-3-phosphocholine (DOPC, T_m = -20 °C), 1,2-dimyristoyl-sn-glycero-3-

phosphocholine (DMPC, T_m = 23 °C), and 1,2-dipalmitoyl-sn-glycero-3-phosphocholine (DPPC, T_m = 42 °C). We found that, at room temperature, DOPC being in the liquid-disordered state displayed intense blue fluorescence, DPPC vesicle remaining sol-gel-ordered state exhibited high intense red fluorescence, whereas the DMPC vesicles having a T_m near 23 °C remains in an in-between state of order and disorder state at RT, displayed a merge pink fluorescence. Most importantly, the H-CDs embedded lipid bilayer can monitor the changes in membrane dynamics by the membrane active ions or even small molecules, similar to the previously used organic membrane probes (e. g. Prodan, ANS, Laurdan, DPH, etc.).

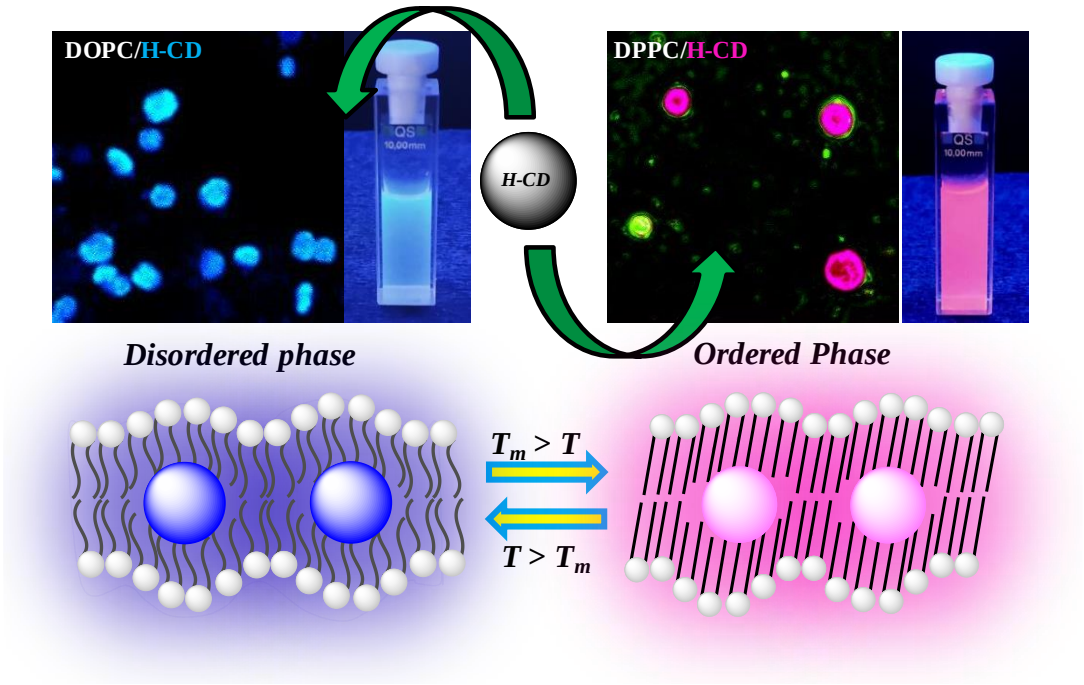

***Scheme 4**:* Confocal microscopy imaging, photograph under UV chamber, and pictorial representation of the distinct emission behaviour of the monomeric hydrophobic carbon dots (H-CDs) in the different phases of the lipid bilayer. DOPC is in liquid-crystalline or disordered phase exhibit blue emission while DPPC is in a sol-gel phase or ordered phase exhibit red luminescence in presence of the same H-CDs.

Chapter 6. Conclusion and future outlook

Research efforts reported in this thesis describe the binding of various metal ions, aromatic amino acids, and carbon dots and their impact on membrane organization, phase behaviour, aggregation, and fusion of the lipid vesicles. Our study demonstrates that minor changes in the interactive entities

(hydration free energy, ionic radius, and effective charge of the metal ions, also the side chain of the aromatic amino acids) can hugely influence the membrane organization and phase behaviour. In addition to that, variation in the charge and phase transition temperature (T_m) of lipid vesicles also plays a significant role in the alteration of the interaction pattern. Therefore, one major effort was to identify membrane phase states by carbon dots (CDs) and to build up the possibility of a CD-based membrane probe. As a future prospect, these studies may add new dimensions to understand the lipid membrane-based assemblies and potential usage in bioimaging and several bio-inspired applications.

LIST OF PUBLICATIONS

1. **S. K. De,** N. Kanwa, M. Ahamed and A. Chakraborty. Spectroscopic evidence for hydration and dehydration of lipid bilayers upon interaction with metal ions: a new physical insight. *Phys. Chem. Chem. Phys*., **2018**, *20*, 14796-14807. DOI: 10.1039/C8CP01774C.
2. **S. K. De**, N. Kanwa and A. Chakraborty. Influence of Trivalent Metal Ions on Lipid Vesicles: Gelation and Fusion Phenomena. *Langmuir* **2019**, *35*, 6429-6440. DOI: 10.1021/acs.langmuir.9b00682.
3. **S. K. De** and A. Chakraborty. Interaction of monomeric and self-assembled aromatic amino acids with model membranes: self-reproduction phenomena. *Chem. Commun.,* **2019**, *55*, 15109-15112. DOI: 10.1039/C9CC08495A.
4. **S. K. De**, A. Maity, D. Bagchi and A. Chakraborty. Lipid phase dependent distinct emission behaviour of hydrophobic carbon dots: C-dots based membrane probe. *Chem. Commun.,* **2021**, DOI: 10.1039/D1CC01941D.

5. **S. K. De**, A. Maity and A. Chakraborty. Underlying Mechanisms for the Modulation of Self-Assembly and the Intrinsic Fluorescent Properties of Amino Acid-Functionalized Gold Nanoparticles. *Langmuir* **2021**, *37*, 5022–5033. DOI:10.1021/acs.langmuir.1c00431.
6. A. Maity, **S. K. De** and A. Chakraborty. Interaction of Aromatic Amino Acid-Functionalized Gold Nanoparticles with Lipid Bilayers: Insight into the Emergence of Novel Lipid Corona Formation. *J. Phys. Chem. B* **2021**, **125**, 2113–2123. DOI: 10.1021/acs.jpcb.0c10079.
7. N. Kanwa, **S. K. De**, A. Maity and A. Chakraborty. Interaction of aliphatic amino acids with zwitterionic and charged lipid membranes: hydration and dehydration phenomena. *Phys. Chem. Chem. Phys.*, **2020**, *22*, 3234-3244. DOI: 10.1039/C9CP06188F.
8. N. Kanwa, A. Patnaik, **S. K. De**, M. Ahamed and A. Chakraborty. Effect of Surface Ligand and Temperature on Lipid Vesicle–Gold Nanoparticle Interaction: A Spectroscopic Investigation. *Langmuir* **2019**, *35*, 1008-1020. DOI: 10.1021/acs.langmuir.8b03673.

9. N. Kanwa, **S. K. De**, C. Adhikari and A. Chakraborty. Spectroscopic Study of the Interaction of Carboxyl-Modified Gold Nanoparticles with Liposomes of Different Chain Lengths and Controlled Drug Release by Layer-by-Layer Technology. *J. Phys. Chem. B* **2017**, *121*, 11333-11343. DOI: 10.1021/acs.jpcb.7b08455.
10. S. Bishnoi, S. Rehman, S. B. Dutta, **S. K. De**, A. Chakraborty, D. Nayak and S. Gupta. Optical-Property-Enhancing Novel Near-Infrared Active Niosome Nanoformulation for Deep-Tissue Bioimaging. *ACS Omega*, **2021**. DOI: 10.1021/acsomega.1c02632.

(Publication 5-10 are not included in the thesis)

TABLE OF CONTENTS

NOMENCLATURE

α	Alpha
β	Beta
γ	Gamma
τ	Fluorescence Lifetime
a_i	Relative Amplitude
ϕ	Quantum Yield
Å	Angstrom
χ	Chi
λ	Wavelength
μ	Micro
π	Pi
Σ	Summation
ns	Nanosecond
ps	Picosecond
nm	Nano Molar
mM	Milli Molar

μM	Micro Molar
η	Viscosity
Kp	Partition Coefficient
ε	Molar Extinction coefficient
cm	Centimeter
μm	Micrometer
nm	Nanometer
°	Degree
N_A	Avogadro Number
K	Kelvin
mL	Milliliter
mV	Mili Volt
μL	Microliter
a. u.	Arbitrary Unit
λ_{ex}	Excitation Wavelength
λ_{em}	Emission Wavelength
pH	The negative logarithm of hydronium-ion concentration
pK_a	Dissociation constant of an acid in ground state
ζ	Zeta Potential

ACRONYMS

AFM	Atomic force microscopy
ANS	8-Anilinonaphthalene-1-sulfonic acid
CA	Citric acid
CDs	Carbon dots
CLSM	Confocal laser scanning microscopy
CMC	Critical Micelle Concentration
DMPC	1,2-dimyristoyl-sn-glycero-3-phosphocholine
DMPG	1,2-dimyristoyl-sn-glycero-3-phospho-(1'-rac-glycerol) sodium salt
DOPC	1,2-dioleoyl-sn-glycero-3-phosphocholine
DOTAP	1,2-dioleoyl-3-trimethylammonium- propane chloride salt
DPPC	1,2-dipalmitoyl-sn-glycero-3-phosphocholine
DSC	Differential Scanning Calorimetry
DTSA	Dithiosalicylic acid
DLS	Dynamic Light Scattering
DNA	Deoxyribonucleic acid
FT-IR	Fourier transformed infrared
FWHM	Full Width Half Maxima

H-CD	Hydrophobic carbon dot
His	Histidine
HR-TEM	High resolution transmission Electron Microscope
IRF	Instrument Response Function
M-CD	Multicolour carbon dot
NMR	Nuclear Magnetic Resonance
O.D.	Optical Density
oPD	o-Phenylenediamine
PAN	1-(2-Pyridylazo)-2-naphthol
Phe	Phenylalanine
POPC	2-Oleoyl-1-palmitoyl-sn- glycero-3-phosphocholine
SDS	Sodium Dodecyl Sulfate
TCSPC	Time Correlated Single Photon Counting
ThT	Thioflavin T
Trp	Trptophan
Tyr	Tyrosine
UV	Ultraviolet–visible
XPS	X-ray photoelectron spectroscopy

LIST OF FIGURES

LIST OF SCHEMES

LIST OF TABLES

Chapter 1

Interaction of different external entities with model membranes

1.1 Introduction

Plasma membrane or cell membrane is the outer covering of the cell and is composed of proteins, lipids, and carbohydrates. The proportions of the components in the membrane vary within the non-identical living cells. Therefore, the cell membranes have a complex structure. The impact of the bio-molecules on the cell membrane is very difficult to study due to this intricacy and the highly dynamic nature of the cell membrane. Therefore, simplified artificial model membranes (e. g. liposome, supported lipid bilayer) have been used to investigate the impact of individual biomolecules in the different types of membrane. The interactions of the biomolecules with the membrane are responsible for various fundamental biological processes. Thus these studies will help to understand the interactions at the membrane interface. Lipid membranes are very prone to fuse and they are often treated with external interactive species (e. g. nanoparticles, biomolecules, polymers, etc.) to stabilize their structures. Contrarily, membrane fusion is an essential process for mimicking the origin of cellular life. For example, proteins and peptides play an indispensable part in various cycles of cells such as self-reproduction, fusion, and fission. Therefore, the interactions of lipid membranes with external species are an indispensable part of the biological research. These interactions can influence the hydration-dehydration, rigidity, and fluidity of the lipid bilayer. More importantly, this information helps understand the collective role of different biomolecules in biological processes and bridge the gap between the lipid systems in vivo and in vitro.

1.2 Model membranes

The major constituents of the cell membrane are lipids (phospholipids and cholesterol), carbohydrates, and proteins. Singer and Nicholson proposed the

fluid mosaic model in 1972 to elucidate biological membrane organization and this model predicted that lipids and proteins diffuse freely within the plane of the cell membrane *[1, 2]*. Therefore, membrane constituents are generally randomly arranged throughout the cellular membrane. Further studies reveal several large membrane domains and lateral microdomain structures also contribute to the complexity of the structure of cellular membrane *[3, 4]*. Therefore, several simplified artificial membrane systems (model membranes) have been discovered which can mimic the essential lipid bilayer structure *[5-10]*. The most commonly known artificial model lipid membranes are supported lipid bilayers (SLBs) *[5, 6]* (Figure 1a), lipid monolayers *[7, 8]* (Figure 1b), and liposomes *[9, 10]* (Figure 1c). The simplified model membranes are frequently utilized by researchers to predict the distinctive role of individual components and their organization and dynamics in the complex cellular membrane.

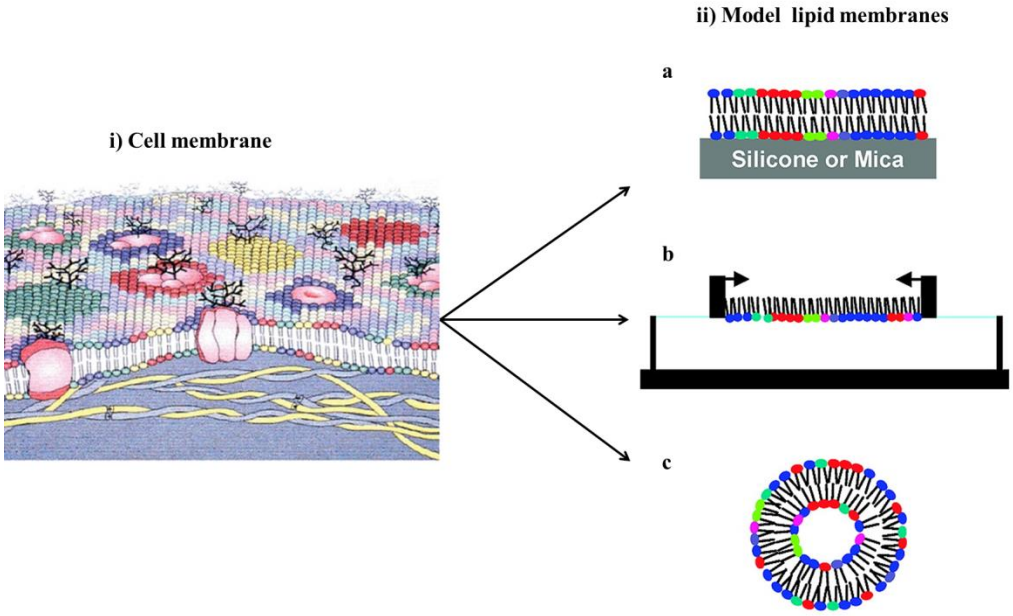

Figure 1.1: Pictorial representation of cellular membrane and various model systems. (i) Cell membrane depicting membrane lipid asymmetry and (ii) different model membrane systems: a) supported lipid bilayer, b) lipid monolayer and c) liposomes [11].

Lipid Monolayer: Lipid monolayer generally forms at the air/water interface. The lipid monolayer represents the simplest model to study the effect of external entities. Different parameters for instance temperature, subphase, and composition of lipids can be picked to imitate physiological conditions.

However, because of their monolayer structures, these model membranes are mostly utilized to investigate the associations with the lipid head groups.

Supported Lipid Bilayer: Supported lipid bilayers (SLBs) are 2-D thin-film coating composed of a single phospholipid bilayer which is developed by fusion of lipid vesicles onto a solid template *[12]*. Generally, they can be formed by the Langmuir-Blodgett method. A combination of the Langmuir-Blodgett and Langmuir-Schaeffer methods was also applied to form the SLBs *[13, 14]*. Formation of SLB requires initial dispersion in mixed organic solvents, and in some cases limits the potential incorporation of the many biological molecules into the bilayer because of conceivable denaturation in mixed solvents in the course of the solvent-exchange process *[15, 16]*.

Liposome: Liposomes are artificial spherical vesicles, composed of at least one lipid bilayer with an enclosing internal aqueous environment. On account of their structural similarity with cell membranes, they are frequently utilized as the simplest cell models. *[17]*. As compared to other model membranes, liposomes have a unique capability to incorporate both hydrophilic and hydrophobic entities inside their hydrophilic aqueous core and hydrophobic lipid bilayer, respectively *[18]*. Several *in vitro* studies on cellular membranes including drug delivery and cytotoxicity assays utilize liposomes as a model membrane.

Each of these models has its own advantages and disadvantages but importantly all the models mimic the lipid bilayer structure of the cellular membrane. Each of these models contributes towards finding the answer to a specific question on lipid bilayer behaviour and contributes to enlarge our knowledge. There is space for fundamental research and still important improvements to make, like studying the membrane organization-phase behaviour, aggregation, fusion, and stabilizing the lipid vesicles.

1.3 Liposome: general introduction, applications and disadvantages

1.3.1 Lipid Vesicle: general introduction

In 1961, lipid vesicles or liposomes were discovered by Dr. Alec D. Bangham, a British haematologist at the Babraham Institute, in Cambridge *[19]*. Lipid vesicles or liposomes were discovered accidentally when the negative stain was added to dried phospholipids to check the institute's new electron microscope. Bangham proposed “liposomes” and interpreted them as swollen phospholipid vesicles composed of single or multiple lipid bilayers. Since then liposomes are an indispensable part of biophysics, biochemistry, and biology *[20-22]*.

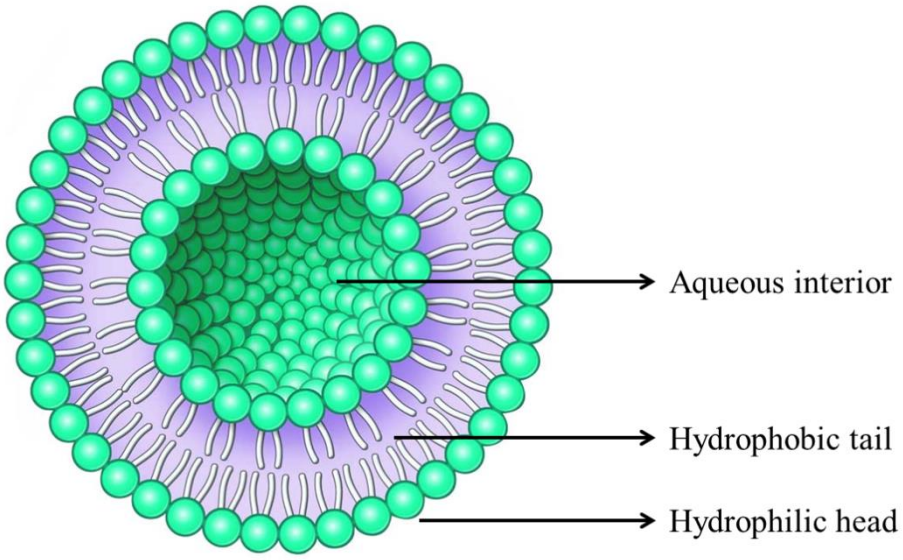

Figure 1.2: Structure of a unilamellar liposome. A liposome consists of a phospholipid bilayer with an aqueous core. [https://www.essentique.com]

Lipid membranes are composed of lipids that are generally non-toxic and biocompatible in nature. A lipid molecule consists of a hydrophilic polar head and two non-polar hydrophobic tail groups. The lipid head group can be zwitterionic, negative, and positively charged whereas the tail group can be saturated, unsaturated, or both. The self-assembly of the lipid molecules into liposomes is a rapid-spontaneous process in an aqueous environment and van der Waals attractive forces between the hydrophobic tails are the major driving force for the arrangement from lipid to lipid vesicles *[23]*. Water molecules are released from the hydrocarbon tails of membrane lipids during the formation of liposomes as the tails become sequestered in the nonpolar interior of the bilayer. Therefore, the formation of liposomes is entropy-driven

[23]. There are several other key factors that can affect the formation of lipid vesicles for example composition, concentration, the phase state of the lipids, and various environmental conditions for example ionic strength, temperature, and solution pH *[24-28]*. Numerous important functions of the cellular membrane significantly depend on the phase state of the lipid bilayer *[29-31]*. Lipid molecules in the membrane can be present in two extreme phases of bilayer i. e. gel-ordered phase and fluid-disordered phase *[32]*. In this sol-gel phase hydrocarbon chains are arrange in a way that they are fully elongated and closely packed. However, in the liquid crystalline phase or liquid-disordered phase the hydrocarbon chains are randomly oriented and loosely packed *[32]*. The phase state of the lipid bilayer often describe with the help of phase transition temperature (T_m). The T_m is defined as the temperature required to induce a change in the lipid physical state from the ordered gel phase to the disordered liquid crystalline phase.

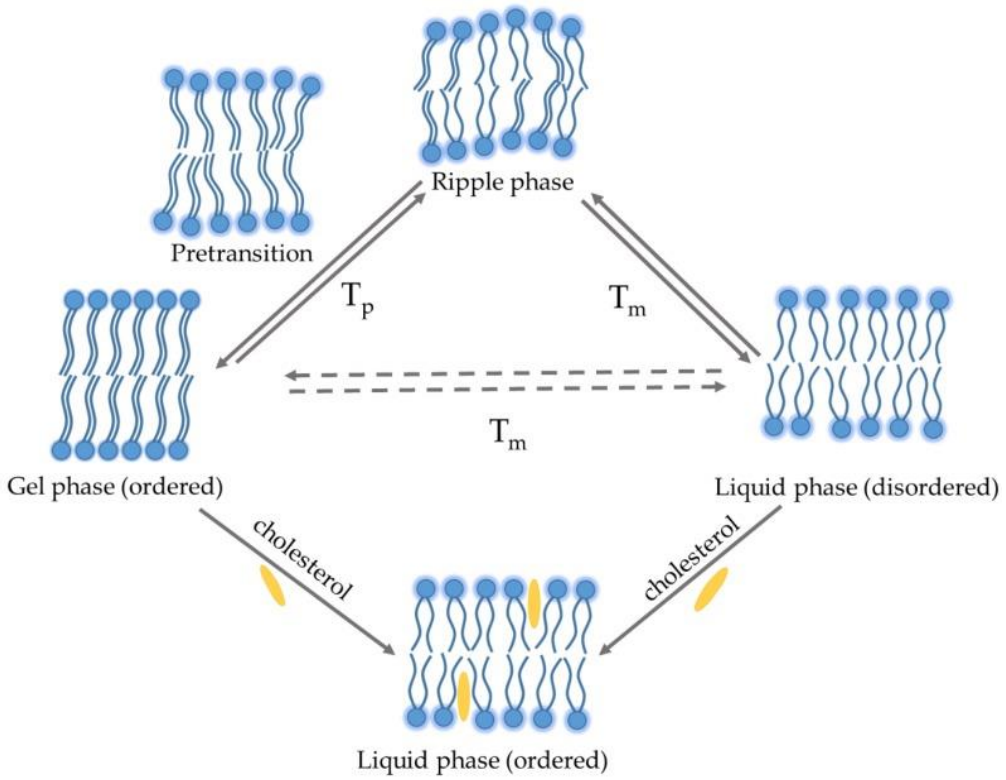

Figure 1.3: Thermotropic behaviour of phospholipid bilayer in an aqueous medium. T_p: pre-transition temperature, T_m: phase transition temperature [32].

There are several factors which directly affect the phase transition temperature, however, the length and degree of unsaturation of the acyl chains

have the most prominent effect *[33, 34]*. As the acyl chain length increased, the van der Waals interaction between neighbouring lipid molecules is stronger. Therefore, the system required more energy to disturb the arranged packing and increases the phase transition temperature. Introducing an unsaturation into the acyl chain puts a crimp in the chain which reduces the van der Waals interaction between them and decreases the phase transition temperature. For example, DLPC with 12 carbon atoms exhibits a T_m near -1 °C whereas the DPPC with 16 carbon atoms exhibits a T_m near 42 °C. On the other hand, DOPC, which has same carbon atoms as DPPC but exhibits a T_m near -18 °C due to presence of a double bond in both acyl chains. Therefore, the choice of the lipid bilayer is highly important because lipid bilayer having higher T_m forms stable lipid vesicle compared to lipid bilayer with lower T_m.

It has been well known that the composition of the lipid head group significantly affects the membrane physicochemical behaviour. It has been shown that the presence of inverted-cone shape lipids (which induce positive curvature) such as lysophosphatidylcholine (LPC) in the outer leaflet of membranes diminish the possibility of fusion, whereas fusion was promoted by the presence of cone-shaped lipids (which induce negative curvature) *[35]*. It has been also reported that small vesicles are less stable against fusion. Therefore, apart from phase state and lipid composition, the properties of lipid vesicles depend on the size and lamellarity *[36]*. The facile synthesis of liposomes offers tuneable size variation, ranging from 20 nm to several micrometers (~ 50 µm). The amphipathic nature and self-assembling characteristics of lipid bilayers influence the hydrophobic layers (or lamellarity) of the bilayers. Therefore, depending on the size and number of phospholipid layers, lipid vesicles or liposomes are broadly classified into three groups which are as follows: *[21, 37]*

Single unilamellar vesicle (SUV): SUVs are homogeneous single lipid bilayer with a size around 100-200 nm. They are susceptible to aggregation and fusion owing to their higher tension on the surface. SUVs are generally prepared by reducing the size of LUV or MLV using a bath sonicator or probe sonicator or by using the ethanol injection method *[21]*.

Large unilamellar vesicle (LUV): LUVs are also composed of a single lipid bilayer with a size between 200 nm to 1 µm. LUVs are synthesized by reverse-phase evaporation, ether injection, and active loading methods. They are mainly useful for capturing hydrophilic therapeutics with a high capacity of encapsulation due to the high aqueous volume to lipid ratio (71/mole lipid). Extended LUV with a very large size (size > 1 µm- 20 µm) is called Giant Unilamellar Vesicle (GUV).

Multi-lamellar vesicle (MLV): MLVs are formed with more than one lipid bilayer. MLVs have a size ranging from 500 nm to 2.5 µm and are mainly prepared by the thin-film hydration method. Classically, a few unilamellar vesicles will frame within the other with a more modest size, making a multilamellar construction of concentric phospholipid circles isolated by layers of water.

1.3.2 Application of the liposomes

Liposomes offer several advantages with a wide range of physicochemical and biophysical properties, including biocompatibility, capacity for self-assembly, easy control over vesicle diameter, ability to carry both hydrophilic and hydrophobic payloads, etc. *[21]*. Additionally, due to their capability to compartmentalize their inside aqueous environment from the outside environment, they are often used as a drug delivery system *[38]*. The first application of liposomes as a model system was to test a theory regarding the action of general anaesthetics, which proposed that anaesthetics interact with the lipid bilayer and somehow inhibited the nervous function *[39]*. Since then, liposome is an indispensable part of research as a model membrane to understand the effect of different biomolecules (proteins, peptides, carbohydrates, etc.), nanomaterials (nanoparticles, quantum dots, carbon dots, etc.), and drugs *[40-42]*. These studies help us to gain insight into the collective role of different external entities on lipid bilayer property which consequently affect several cellular functions.

Biological membranes exist in small ionic species-rich aqueous environment (Na^+, K^+, Ca^{2+}, Fe^{2+}, Mg^{2+}, Zn^{2+} etc) *[43]*. Therefore, lipid vesicles are often used to investigate the effect of these ions in biological processes, such as

transport of ions across the membranes, controlling the gating ion channels, and regulating membrane potential *[44]*. Precise regulation of the flow of energy, metabolites, nutrients, and information in cell membrane were largely regulated by membrane-bound proteins. Therefore, lipid vesicles are often used to study the underlying mechanism of the several proteins and peptides-based interactions and how the lipid-protein interactions regulate the essential membrane-bound processes *[45, 46]*.

The interactions of drug molecules with the membranes are crucial for the preparation of an effective drug delivery system. However, due to the intricacy of biological membranes these studies are very challenging to investigate. Therefore, lipid vesicles are generally utilized to understand the collective role of different lipids or different drugs in drug–membrane interactions. Till now, several liposome-based delivery systems have been approved by FDA (e.g. DOXIL, Daunosomes, Amphotech, etc.). Nucleic acids with different sizes and degrees of base pairing have been investigated with lipid vesicles and researchers have been tried to find out how this interaction influences the lipid bilayer *[47]*. Further the effects of sugar and individual nucleobases also have been studied to understand how the different bases and the sugar in RNA were localized within the membrane and how they affect the vesicles stability *[48]*.

Therefore, the lipid vesicles or liposomes are vigorously used as delivery systems for several entities (e. g. drugs, proteins, peptides, DNA, RNA etc.). However, due to the drug delivery centric view of the scientific community, it has been often neglected that the lipid vesicles greatly help us to understand the effect of the individual biomolecules on the phase state of the lipid bilayer, which consequently affects several biological processes.

1.3.3 Fusion of the liposomes: advantages and disadvantages

Lipid vesicles are widely used as a delivery system. However, applications of the lipid vesicles are generally restricted by their instability, particularly, liposomes with sizes less than 200 nm are susceptible to fuse with each other, leading to premature release of the payload *[49-52]*. Further, several small drug molecules (e. g. halothane, meloxicam, piroxicam, tenoxicam, and chlorpromazine, etc.) have the ability to fuse the lipid vesicles *[53-55]*. In this

regard, the interaction between foreign materials (nanoparticles, polymers, biomolecules, etc.) has been used to stabilize the lipid vesicles to improve targeted and controlled delivery *[56, 57]*. On the other hand, drug molecules that can induce fusion at physiological conditions have potential application for targeted delivery *[58]*. Understanding the underlying mechanism of this fusion influenced by drug molecules will help us to use the drugs to fuse membranes in a controlled way as it is a fundamental process in many biochemical/ biotechnological processes *[58]*.

It is also well known that the fusion of lipid bilayer is a fundamental process in many important biological processes such as endocytosis, exocytosis, and viral infection, etc. *[59]*. Fusion of the membrane was first observed when metal ions are added to the lipid bilayer. Almost after two decades of work, it has been found that Ca^{2+} and Mg^{2+} induce membrane fusion effectively *[60-62]*. Depending upon membrane composition, several other ions such as Zn^{2+}, Mn^{2+}, Ba^{2+}, $La^{3+,}$ and Sr^{3+} also induce membrane fusion *[63-66]*. Proteins and peptides participate in a crucial role in different cycles of cells like self-reproduction, fusion, and fission which are also crucial steps for mimicking the origin of cellular life *[46, 47]*. Formation of phospholipid vesicle in cells e. g. vesicular transport and organelle biogenesis are predominantly dependent on membrane fission, which is influenced by protein molecules *[67]*.

Therefore, both facilitating and prevention of the fusion to the lipid vesicles have been attracted significant interest. Fusion of the lipid vesicles is a time-dependent process or it requires active or passive participation of various fusogenic agents. A wide range of biomolecules (like proteins, peptides, ions, etc.) or drug molecules can act as a fusogenic agent. Therefore it is important to study the fusion process of vesicles in order to find out a way to control it. Natural starting points for studying membrane fusion are aggregation of liposomes. The aggregation of colloidal particles, such as lipid vesicles, has been studied by using the DLVO theory *[68]*. DLVO theory predicts the interaction potential between two distinct lipid vesicles as a combined effect of attractive van der Waals and repulsive electrostatic interaction as a function of distance *[69]*. The van der Waals interaction between the lipid vesicles depends on the membrane phase state, which further depends on the

organization of the lipid molecules in the lipid bilayer. Therefore, membrane organization, phase state, aggregation, and fusion of the lipid vesicles are mutually dependent.

1.3.4 Membrane probes: a unique method to study lipid organization

Several studies such as infrared (IR) spectroscopy, atomic force microscopy (AFM), mass spectrometry, nuclear magnetic resonance (NMR), small angle X-ray diffraction, and differential scanning calorimetry (DSC) measurements have been used to get the various information about the change in phase state of the bilayer *[70-74]*. As seeing is the believing, an optical technique remains unique for in situ studies of different phase states in live cells. Over the previous decade, the sensitivity and resolution of optical microscopy went through sensational enhancements. As a result, fluorescent microscopy imaging techniques by membrane probes are one of the most popular-commonly used techniques to investigate the lipid bilayer phase state. These membrane probes are designed in such a way that they exhibit different emission behaviour in the order and disorder phase of the lipid. Different membrane probes (e. g. cholesterol derivatives, PE head group labeled, SM acyl chain labeled and SM head group labeled) have been successfully applied to determine the different micro-domain (known as lipid rafts) in the bilayer *[75]*. However, there are some other probes such as LAURDAN, PRODAN, ANS, etc. which indicate the degree of water penetration into the lipid bilayer because of their unique fluorescence property *[76, 77]*. As water penetration in the bilayer has been linked with lipid packing and fluidity, these probes have been broadly used in investigating membrane properties by using simple steady-state fluorescence, lifetime, and anisotropy measurements *[78, 79]*. These molecules have a dipole moment arising from their excitation and relaxation of the surrounding water molecules. Thus, they exhibit fluorescence characteristics depending on the degree of solvent relaxation. However, most of the probes have some limitations. The choice of the probes extensively depends on the lipid bilayer and on the fluorescence strategies to be utilized. The fluorescent membrane probes are still an overgrowing field and they have been used extensively over the last decade. Still there are enough spaces for

new membrane sensitive probes specially the nanomaterial based membrane sensitive probes.

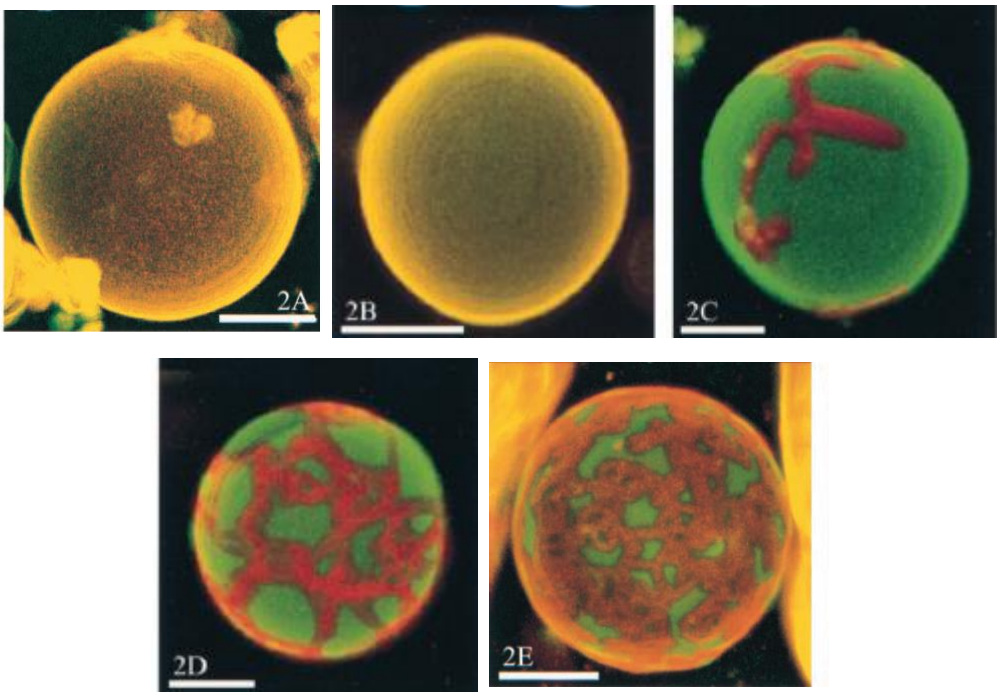

Figure 1.4: Visualization of phase separation by using membrane probes in the binary lipid mixture of DLPC/DPPC. The images show a progression of increasing DPPC concentration relative to DLPC at DLPC/DPPC values: 1/0 (2A), 0.80/0.20 (2B), 0.60/0.40 (2C), 0.40/0.60 (2D), and 0.20/0.80 (2E). An ordered phase region shows red emission from DiI-C20 and the fluid phase region exhibits green emission from Bodipy-PC [80].

1.4 Interaction of lipid vesicles with different external entities

1.4.1 Interaction with the metal ions

Metal ions are fundamental elements in biological systems and their absence can cause different disorders. They help to regulate the function of numerous cells (e. g. the brain, nerve cells, muscle cells, and the heart), cellular communications, maintain electrical charges, osmotic pressure, transport oxygen, and assist several different biological processes *[81]*. Therefore, over the past few decades, the binding of metal ions to the lipid membrane has been an important area of research to understand the role of metal ions in various biological processes.

Monovalent cations, like Na^+, K^+, Rb^+, and Cs^+, interacts strongly with the negatively charged PC/PS lipid bilayer, whereas the interaction is much weaker in case of zwitterionic PC lipid *[82-84]*. Monovalent salts dehydrate the carbonyl region of the negatively charged PC/PS bilayer and an increase in the bilayer rigidity is observed from both simulations and experimental measurements *[82]*. On the other hand, the divalent ions adsorb rapidly even in case of zwitterionic lipid vesicles *[85, 86]*. The effect of several divalent metal ions (e. g. Ca^{2+}, Mg^{2+}, Mn^{2+}, Zn^{2+}, $Ba^{2+,}$ etc.) with the lipid vesicles have been studied *[87-90]*. Recently, it has been observed that the adsorption of Ca^{2+} ions decreases this negative charge of the lipid vesicles, and this phenomenon affects the modulation of T-cell activation *[91]*. Among these metal ions, Ca^{2+} and Mg^{2+} significantly induce the membrane fusion compared to other divalent metal ions *[60, 62]*. Binder and coworkers studied the effect of Na^+, K^+, Li^+, Mg^{2+}, Ca^{2+}, Be^{2+}, Sr^{2+}, Ba^{2+}, Cu^{2+} and Zn^{2+} on the POPC bilayer with the help of Infrared (IR) spectroscopy and they found that all these divalent cations and Li^+ stabilize the gel phase of the lipid bilayer *[90]*. Interestingly, they also observed that the water molecules can penetrate into the carbonyl region of the lipid bilayer in the presence of Mg^{2+}, Ba^{2+}, Sr^{2+} and Ca^{2+}. On the other hand, Be^{2+}, $Zn^{2+,}$ and Cu^{2+} remove the water molecules from the carbonyl groups. Alsop and coworkers established that the interaction of divalent metal ions with the lipid bilayer extensively depends on the location or interaction position of the ions in the bilayers *[72]*. They observed that Ca^{2+} and Zn^{2+} strongly interact with the carbonyl group of the lipid bilayer and exhibit insignificant swelling of the lipid bilayers. On the other hand, Fe^{2+} and Mg^{2+} were observed to be situated close to the phosphate groups and cause an expansion in the hydration water molecules in the lipid bilayer. Although trivalent metal ions do not present in the biological system, however, the effect of these metal ions has been studied in the literature *[92-94]*. The impact of lanthanide ions (La^{3+} and Gd^{3+}) on the stability of the lipid vesicles has been also investigated extensively *[95, 96]*. Interestingly, Verstraeten and coworkers reported the binding of trivalent La^{3+}, Y^{3+}, and Sc^{3+} to the negatively charged PC: PS lipid bilayer and these ions follows the order of $La^{3+} > Y^{3+} > Sc^{3+}$ *[97]*.

Metal ions interact with the lipid bilayer via coulombic interaction, thus negatively charged lipid bilayer interacts strongly than zwitterionic lipid bilayer. Garcia-Celma and coworkers reported that Ca^{2+} binds more strongly with zwitterionic DPPC lipid vesicles than Mg^{2+} *[83]*, whereas Binder and coworkers reported that Zn^{2+} binds more strongly with the zwitterionic POPC vesicles than Ca^{2+} *[90]*. Therefore, the extent of interaction by these metal ions not exclusively depends on ion charge. Several other factors, such as ionic radius, hydration free energy of the ions, the binding position of the ions possibly also have combined effects on the lipid bilayer. These metal ions either dehydrate or hydrate the lipid bilayer. Therefore, these metal ions significantly alter the membrane bilayer organizations which consequently affect the phase transition temperature (T_m) of the lipid. The alteration of the membrane phase further leads to the aggregation and fusion of the bilayer. In this context, even after decades of studies on lipid-metal ion interaction, this field still amazes us. Therefore, the systematic investigation will help us to find out some missing points of an 'ion-lipid jigsaw puzzle'.

1.4.2 Interaction with proteins and amino acids

Both lipids and proteins are indispensable components of the cellular membrane. While lipids are the foundational structural components of cellular membranes, different proteins are answerable for accomplishing particular membrane functions and constitute ~30-50% of the cellular composition *[98]*. The position of these proteins and peptides in the cellular membranes is governed by the composition, orientation, and hydrophobicity *[23, 99-101]*. Lipid composition and lipid-protein interactions modulate the physical properties of membranes and affect membrane protein functions, such as ion channels *[102]*. The interaction between these lipid bilayers and proteins or peptides also plays significant roles in numerous membrane-associated biological processes for example recognizing membrane potential, membrane phase alteration, membrane anchoring, signalling and endocytosis, etc. *[103-106]*. Depending upon the biological functions, membrane-active peptides are broadly divided into two major categorised, antimicrobial and cell-penetrating or fusion peptides *[100]*. Studying the interaction between lipid and proteins or peptides enlighten the underlying mechanism and help us to understand

how the proteins bring several changes in the lipid membrane micro-environment *[23]*. However, the mechanisms by which lipids affect protein conformation and activity (or vice versa) are still not fully understood.

The lipid-protein interaction is a complex process due to the presence of a variety of functional groups in the protein structure. A recent study demonstrates that different proteins in the same complex membrane environment show different interactions with the lipids and provide a complex insight into the mechanistic pathway *[107]*. However, the basic understanding has been seen in a less complex system *[107]*. The most common problem of lipid-protein interaction is lack of simplicity which sometimes leads to poorly justified conclusions and interpretation *[107]*. Therefore, the interaction of amino acids with the lipid membrane gains significant interest due to its inherent transparency and simplicity. Rather than protein and peptide, amino acids with variable charge, hydrophilicity, and hydrophobicity of the side chain admirably enlighten the mode of interactions between protein and lipids. Recently, it has been found that the side chain of the amino acids significantly affects the alteration of membrane surface tension, phase morphology, membrane folding, and transport of metabolites *[108-110]*. Several studies have been performed regarding the association of peptides with the lipid bilayer; however, the basic mechanism of the lipid bilayer interaction with the help of amino acids is still a subject of examination.

On the other hand, the aggregation of protein and peptide into the amyloid-fibrils and their growth in the cellular membrane is the trademark of several neurodegenerative diseases are known as amyloidosis *[111-114]*. The formation mechanism of the amyloid fibril structure has been well studied; however, much importance has been paid to the formation of amyloid structure in presence of biological membrane due to understanding the disease-related fibrillations *[115-118]*. Studies have indicated that the various physicochemical properties of the membrane regulate the protein fibrillations via coulombic and van der Waals interaction between lipids and proteins. It has been observed that biological interfaces enhance fibril nucleation and growth *[119, 120]*. However, specific phospholipid bilayers sometimes have a partial or complete inhibitory effect on fibrillation *[121, 122]*. Recently it

has been proposed that besides proteins and peptides, several amino acids also self-assemble into amyloid-like fibrils, showing similar structural, biochemical and biophysical properties with the conventional amyloid structure *[123-125]*. It has been observed that the amyloid assemblies of proteins, peptides or amino acids induce apoptotic cell death. Few potential mechanisms have been proposed to explain the activation of apoptosis. In the case of amyloid diseases, it is reported that the interaction of the amyloid fibrils with the membrane initiates the usual toxicity. Thus, in this regard, the interaction between the amyloid assemblies with the model lipid bilayer is significantly important to understand the mechanistic insight into the underlying cytotoxic behaviour of the protein-peptides or amino acids.

1.4.3 Interaction with carbon dots

Xu et. al. in 2004, first discovered the fluorescent carbon dots during single-walled carbon nanotubes purification *[126]*. Carbon dots (CDs) are described as quasi-spherical zero-dimensional semiconductor nanomaterials with sizes less than 10 nm *[126]*. CDs generally have a luminescence carbonaceous core with sp2 characters which is responsible for non-toxic behaviour. While the surface of the CDs possesses a variety of functional groups (such as amino, carbonyl, hydroxyl, and carboxylic acid, etc.) and allows a diverse range of physicochemical properties and applications *[127]*. Specific functionalization on the surface of CDs is responsible for its tuneable dispersibility, photoluminescence and special recognition or sensing applications. When the C-dots are excited from UV to visible region, many C-dots exhibit unique excitation dependent (λ_{ex}) emission spectra. The fluorescence properties of the c-dots are dependent on the size, shape, surface ligands, and defects *[128-130]*.

Continuous evaluation of the structure-function relationship between organic fluorescence probe (OFP) with the membrane, *[131, 132]* evaluation of the green fluorescence protein (GFP) *[133, 134]*, and evaluation of quantum dots (QDs) *[135-137]* over last decades have provided diverse field option in biomedical research for monitoring several biological processes. However, after the discovery of highly fluorescent CDs, researchers found CDs as

successful alternatives to conventional imaging probes which have several limitations. Inefficient insertion into the plasma membrane (in case of OFP), weak fluorescent signal, and rapid photobleaching of the conventional dyes make long-term imaging complicated and restrict their versatile applications in biomedical fields *[138]*.

In this context, CDs have multiple advantages over conventional imaging probes e. g. tunable photoluminescence, high quantum yield, resistance to photobleaching, and most importantly easy-cheep-large scale synthesis, etc. Also, carbon dots are largely non-toxic and environmental friendly compared to semiconductor quantum dots (QDs). Due to their excellent chemical and photochemical properties, CDs have attracted great interest as a bioimaging tool to the scientific community. There are several studies where CDs are used as bioimaging tools for live cells. CD-based labelling strategies for cancer cell imaging, *[139-141]* stem cell imaging, *[142-144]* and neuron imaging *[145-147]* have been developed to understand the biological processes.

One of the modern bioimaging tools is organic membrane probes which actually help to determine the bilayer organization. In the past two and a half decades or so, nanomaterials overwhelm numerous areas. Newly developed fluorescent nanomaterials i. e. quantum dots and carbon dots have several advantages over conventional organic dyes. However, till now, nanomaterial-based membrane sensitive probe is still unattainable. Therefore, the germination of nanomaterial-based membrane sensitive probe is a demand of the current decade. So; in this thesis, we focus on the interaction of CDs with different phase states of the lipid vesicles.

Compared to other bio-imaging models the interaction of CDs with lipid vesicles is generally less explored. Depending on the surface functionalization, c-dots can interact differently with the bilayer membrane. While hydrophobic c-dots insert inside the hydrophobic core of the bilayer, hydrophilic c-dots are located either on the interface or within the aqueous core. Nandi and coworkers reported the C-dot conjugated lipid molecules to visualize the lipid vesicles and to study the membrane dynamics by membrane-active ions and molecules *[148, 149]*. Pritzl and coworkers studied the trans-membrane

Förster resonance energy transfer (FRET) by using donor and acceptor in the different leaflet of the lipid bilayer to understand the membrane dynamics *[150]*. Kanwa and coworkers reported that C-dots derived from different isomers of the same carbon precursor (phenylenediamine) interact differently with the lipid vesicles and alter the membrane organization *[151]*. They found that the ortho-CD interacts strongly and stabilizes the lipid vesicles, while the meta-CD and para-CD bring aggregation to the vesicles. However, it is still unclear the extent of lipid membrane organization onto the physical and chemical properties of the C-dots.

1.5 Motivation and organization of the thesis

The principal aim of the research works included in this thesis is to explore the interaction of biomimetic lipid vesicles with different external entities including metal ions, amino acids, and carbon dots. The lipid bilayers varying chain lengths, surface charges, and phase transition temperatures (T_m) have been used to investigate the external-entities induced changes in the lipid organization, aggregation, and fusion. The metal ion-induced changes in the membrane organization have been studied by varying the binding position, ionic radius, effective charge, and hydration free energy of the metal ions. The interactions of amino acids with the model membranes simplify the mechanism of membrane protein interaction and the underlying cytotoxicity of the amyloid aggregation. The change in the membrane phase state organization is the general phenomenon of this type of interaction. Therefore, the thesis also takes an initiative for the carbon dot (CD) based membrane sensitive probes and studying the effectiveness of CDs to detect the changes in the membrane dynamics. The studies reported here help in understanding the mechanisms involved in cellular processes and serve to bridge the gap between in vivo and in vitro systems. The following sections represent a short description of the contents and organization of the thesis:

Chapter 2 is dedicated to investigate the interactions of different metal ions (Zn^{+2}, Ca^{+2}, and Mg^{+2}) with zwitterionic phospholipid bilayers of different chain lengths namely DPPC, DMPC, and DOPC. The effect of the membrane phase state during the interaction with the divalent metal ion has been

explored. It is observed that the divalent metal ions interact strongly, with the increasing ordered phase of the lipid bilayer and follows the order of DPPC> DMPC> DOPC. Among these three metal ions, Zn^{2+} and Ca^{2+} dehydrate the lipid bilayer surface by removing the water molecules from the zwitterionic head group region. On the other hand, Mg^{2+} significantly hydrates the lipid bilayer owing to its higher hydration free energy, and Mg^{2+} is unwilling to bind with the lipid bilayer by losing water from its hydrated shell. The DLS measurement reveals that the lipid vesicles undergo instantaneous aggregation at physiological pH however this phenomenon is less prominent at lower pH (~5.0). Moreover, membrane sensitive probe PRODAN is used to investigate the effects of different metal ions with the different lipid bilayers and reinserts the fact that simple fluorescence technique is useful to gain important information regarding membrane phase state.

In **Chapter 3,** we investigate the effect of size, effective charge, and hydration free energy of these metal ions by using a series of trivalent metal ions of the same group, namely, Al^{3+}, Ga^{3+}, and In^{3+} on the zwitterionic DMPC lipid vesicles. All these metal ions dehydrate the lipid bilayer and the interaction is stronger in the case of In^{3+} owing to the higher ionic radius as compared to that of Al^{3+} and Ga^{3+}. A comparative study with the divalent metal ions indicates that the trivalent metal ions interact strongly than divalent metal ions at both physiological and acidic pH. The DLVO theory with the help of zeta potential measurements suggests that a lower concentration of In^{3+} stabilizes the lipid vesicles more than Al^{3+} and Ga^{3+}. However, at higher concentrations of metal salts, the lipid vesicles have a tendency to form aggregated structures in the presence of metal ions in the following order, $In^{3+} > Ga^{3+} > Al^{3+}$. The DLS measurement, confocal microscopy, and AFM imaging studies reveal that the In^{3+} brings fusion and subsequent aggregation to the lipid vesicles whereas Al^{3+} and Ga^{3+} stabilize the lipid vesicles.

Chapter 4 explores the effect of monomeric and self-assembled aromatic amino acids on model membranes. Phenylalanine, tryptophan, and histidine have been used to investigate the effect of side chains on the model membrane. These amino acids extensively dehydrate the negatively charged lipid vesicles compared to zwitterionic and positively charged vesicles. Amino

acids with larger side chain interact strongly than amino acids with smaller side chain and the order was found Trp> Phe> His. This observation leads to conclude that the initial interaction is electrostatic and instantly takes place between the NH_3^+ group of the amino acid and the phosphate group (PO_4^-) of the lipid bilayer. However, amino acids which have higher hydrophobicity interact slowly with the bilayer and the time-dependent changes are more prominent for the Phe compare to Trp and His. Phe and Trp self-assembled into amyloid-like aggregates and results in supported phospholipid membranes as well as deformed aggregated vesicles via fusion of the liposome. Live-confocal microscopy imaging reveals that during the formation of the fibril structure of Phe, both the self-reproduction and fusion of lipid vesicles take place. Self-reproduction of the vesicles is an important step for mimicking the origin of cellular life and our study reveal that besides the proteins and peptides, the fusion and self-reproduction of lipid vesicles are also driven by the amino acids.

Chapter 5 makes an effort to discover a successful carbon dots base membrane sensitive probe. As luminescence carbon dots (CDs) have several advantages over the conventional organic membrane probes and visual detection of the membrane phase state will be highly advantageous. We observe unique distinct emission behaviour of hydrophobic carbon dots (H-CDs) embedded within the ordered and disordered phase of the lipid membrane. The H-CDs exhibit a blue fluorescence in the disordered phase or fluid phase (L_d) and shows a red emission in the sol-gel phase or ordered phase (L_o) of the lipid. This distinct emission behaviour of lipid encapsulated hydrophobic CDs (H-CDs), observed through naked eyes under a UV lamp, promoting a unique fluorescence sensor for the membrane phase state. Interestingly, these H-CDs embedded in lipid bilayer can monitor the changes in membrane dynamics by the membrane active ions or even small molecules. The further study demonstrates that compared to the fluid phase the gel phase of the membrane stabilizes the photoluminescence property of the CDs. This will help to develop better bioimaging models.

1.6 References

[1] Singer, S.J., Nicolson, G.L. (1972), The fluid mosaic model of the structure of cell membranes, Science, 175, 720-731. (DOI: 10.1126/science.175.4023.720)

[2] Nicolson, G.L. (2013), Update of the 1972 Singer-Nicolson Fluid-Mosaic Model of Membrane Structure, Discoveries (Craiova), 1, e3. (DOI: 10.15190/d.2013.3)

[3] Vereb, G., Szollosi, J., Matko, J., Nagy, P., Farkas, T., Vigh, L., Matyus, L., Waldmann, T.A., Damjanovich, S. (2003), Dynamic, yet structured: The cell membrane three decades after the Singer-Nicolson model, Proc. Natl. Acad. Sci. U S A, 100, 8053-8058. (DOI: 10.1073/pnas.1332550100)

[4] Sezgin, E., Levental, I., Mayor, S., Eggeling, C. (2017), The mystery of membrane organization: composition, regulation and roles of lipid rafts,Nat. Rev. Mol. Cell Biol., 18, 361-374. (DOI: 10.1038/nrm.2017.16)

[5] Tamm, L.K., McConnell, H.M. (1985), Supported phospholipid bilayers, Biophys. J.,47,105-113 (DOI: 10.1016/s0006-3495(85)83882-0)

[6] Castellana, E.T., Cremer, P.S. (2006), Solid supported lipid bilayers: From biophysical studies to sensor design, Surf. Sci. Rep., 61, 429-444. (DOI: 10.1016/j.surfrep.2006.06.001)

[7] Baoukina, S., Monticelli, L., Risselada, H. J., Marrink, S. J., Tieleman, D.P. (2008), The molecular mechanism of lipid monolayer collapse, Proc. Natl. Acad. Sci. U S A, 105, 10803-10808. (DOI: 10.1073/pnas.0711563105)

[8] Maget-Dana, R. (1999), The monolayer technique: a potent tool for studying the interfacial properties of antimicrobial and membrane-lytic peptides and their interactions with lipid membranes, Biochim. Biophys. Acta, 1462, 109-140. (DOI: 10.1016/s0005-2736(99)00203-5)

[9] Eytan, G.D. (1982), Use of liposomes for reconstitution of biological functions, Biochim. Biophys. Acta, 694, 185-202. (DOI: 10.1016/0304-4157(82)90024-7)

[10] Rigaud, J.-L., Pitard, B., Levy, D. (1995), Reconstitution of membrane proteins into liposomes: application to energy-transducing membrane proteins, Biochim. Biophys. Acta, 1231, 223-246. (DOI: 10.1016/0005-2728(95)00091-v)

[11] Peetla, C., Stine, A., Labhasetwar, V. (2009), Biophysical interactions with model lipid membranes: applications in drug discovery and drug delivery, Mol. Pharm.,6,1264-1276. (DOI: 10.1021/mp9000662)

[12] Ferhan, A. R., Yoon, B. K., Park, S., Sut, T. N., Chin, H., Park, J. H., Jackman, J. A., Cho, N. J. (2019), Solvent-assisted preparation of supported lipid bilayers, Nat. Protoc.,14, 2091-2118. (DOI: 10.1038/s41596-019-0174-2)

[13] Clausell, A., Busquets, M.A., Pujol, M., Alsina, A., Cajal, Y. (2004), Polymyxin B-lipid interactions in Langmuir-Blodgett monolayers of Escherichia coli lipids: a thermodynamic and atomic force microscopy study, Biopolymers, 75, 480-490. (DOI: 10.1002/bip.20165)

[14] Liu, J., Conboy, J.C. (2005), Structure of a gel phase lipid bilayer prepared by the Langmuir-Blodgett/Langmuir-Schaefer method characterized by sum-frequency vibrational spectroscopy, Langmuir, 21, 9091-9097. (DOI: 10.1021/la051500e)

[15] Kell, D. (1979), Physiochemical Aspects of Protein Denaturation, FEBS Lett., 105, 390-390. (DOI: 10.1016/0014-5793(79)80660-2)

[16] Griebenow, K., Klibanov, A.M. (1996), On Protein Denaturation in Aqueous−Organic Mixtures but Not in Pure Organic Solvents, J. Am. Chem. Soc., 118, 11695-11700. (DOI: 10.1021/ja961869d)

[17] WEISSMANN, G.S.a.G. (1968), Phospholipid spherules (liposomes) as a model for biological membranes, J. Lipid Res., 9, 310-318.

[18] Alavi, M., Karimi, N., Safaei, M. (2017), Application of Various Types of Liposomes in Drug Delivery Systems, Adv. Pharm. Bull.,7, 3-9. (DOI: 10.15171/apb.2017.002)

[19] Bangham, A. D., Horne, R.W. (1964), Negative staining of phospholipids and their structural modification by surface-active agents as observed in the electron microscope, J. Mol. Biol., 8, 660-IN610. (DOI: 10.1016/s0022-2836(64)80115-7)

[20] Barenholz, Y. (2012), Doxil(R)--the first FDA-approved nano-drug: lessons learned, J. Control. Release, 160, 117-134. (DOI: 10.1016/j.jconrel.2012.03.020)

[21] Akbarzadeh, A., Rezaei-Sadabady, R., Davaran, S., Joo, S.W., Zarghami, N., Hanifehpour, Y., Samiei, M., Kouhi, M., Nejati-Koshki, K. (2013), Liposome: classification, preparation, and applications, Nanoscale Res. Lett., 8, 102. (DOI: 10.1186/1556-276X-8-102)

[22] Khanniri, E., Bagheripoor-Fallah, N., Sohrabvandi, S., Mortazavian, A.M., Khosravi-Darani, K., Mohammad, R. (2016), Application of Liposomes in Some Dairy Products,Crit. Rev. Food Sci. Nutr., 56, 484-493. (DOI: 10.1080/10408398.2013.779571)

[23] Escriba, P.V., Gonzalez-Ros, J.M., Goni, F.M., Kinnunen, P.K., Vigh, L., Sanchez-Magraner, L., Fernandez, A.M., Busquets, X., Horvath, I., Barcelo-Coblijn, G. (2008), Membranes: a meeting point for lipids, proteins and therapies, J. Cell. Mol. Med., 12, 829-875. (DOI: 10.1111/j.1582-4934.2008.00281.x)

[24] Castile, J. D., Taylor, K.M.G. (1999), Factors affecting the size distribution of liposomes produced by freeze–thaw extrusion, Int. J. Pharm., 188, 87-95. (DOI: 10.1016/s0378-5173(99)00207-0)

[25] Caracciolo, G., Pozzi, D., Capriotti, A. L., Cavaliere, C., Piovesana, S., Amenitsch, H., Laganà, A. (2015), Lipid composition: a “key factor” for the rational manipulation of the liposome–protein corona by liposome design,RSC Advances, 5, 5967-5975. (DOI: 10.1039/c4ra13335h)

[26] Barenholz, Y., Bombelli, C., Bonicelli, M. G., di Profio, P., Giansanti, L., Mancini, G., Pascale, F. (2011), Influence of lipid composition on the thermotropic behavior and size distribution of mixed cationic liposomes, J. Colloid Interface Sci., 356, 46-53. (DOI: 10.1016/j.jcis.2010.11.062)

[27] Putri, D.C.A., Dwiastuti, R., Marchaban, M., Nugroho, A.K. (2017), Optimization of Mixing Temperature and Sonication Duration in Liposome Preparation, Journal of Pharmaceutical Sciences and Community, 14, 79-85. (DOI: 10.24071/jpsc.142728)

[28] Shaker, S., Gardouh, A.R., Ghorab, M.M. (2017), Factors affecting liposomes particle size prepared by ethanol injection method, Res. Pharm. Sci., 12, 346-352. (DOI: 10.4103/1735-5362.213979)

[29] Lee, A.G. (2003), Lipid–protein interactions in biological membranes: a structural perspective, Biochim. Biophys. Acta, 1612, 1-40. (DOI: 10.1016/s0005-2736(03)00056-7)

[30] Elson, E. L., Fried, E., Dolbow, J. E., Genin, G. M. (2010),Phase separation in biological membranes: integration of theory and experiment, Annu. Rev. Biophys, 39, 207-226. (DOI: 10.1146/annurev.biophys.093008.131238)

[31] Jouhet, J. (2013), Importance of the hexagonal lipid phase in biological membrane organization, Front Plant Sci, 4, 494. (DOI: 10.3389/fpls.2013.00494)

[32] Franze, S., Selmin, F., Samaritani, E., Minghetti, P., Cilurzo, F. (2018),Lyophilization of Liposomal Formulations: Still Necessary, Still Challenging, Pharmaceutics, 10, (DOI: 10.3390/pharmaceutics10030139)

[33] Schick, M.J. (1987), Handbook of lipid research 4–the physical chemistry of lipids, by Donald M. Small, Plenum, New York, 1986, 672, Journal of Polymer Science Part C: Polymer Letters, 25, 86-87. (DOI: 10.1002/pol.1987.140250211)

[34] Barenholz, Y. (2018), Handbook of Nonmedical Applications of Liposomes Volume III: From Design to Microreactors,

[35] Stiasny, K., Heinz, F.X. (2004), Effect of membrane curvature-modifying lipids on membrane fusion by tick-borne encephalitis virus, J. Virol., 78, 8536-8542. (DOI: 10.1128/JVI.78.16.8536-8542.2004)

[36] Lin, C. M., Li, C. S., Sheng, Y. J., Wu, D. T., Tsao, H. K. (2012), Size-dependent properties of small unilamellar vesicles formed by model lipids, Langmuir, 28, 689-700. (DOI: 10.1021/la203755v)

[37] Pattni, B.S., Chupin, V.V., Torchilin, V.P. (2015), New Developments in Liposomal Drug Delivery, Chem. Rev., 115, 10938-10966. (DOI: 10.1021/acs.chemrev.5b00046)

[38] Agmo Hernandez, V., Karlsson, G., Edwards, K. (2011), Intrinsic heterogeneity in liposome suspensions caused by the dynamic spontaneous formation of hydrophobic active sites in lipid membranes, Langmuir, 27, 4873-4883. (DOI: 10.1021/la1049919)

[39] Johnson, S.M., Miller, K.W., Bangham, A.D. (1973), The opposing effects of pressure and general anaesthetics on the cation permeability of liposomes of varying lipid composition, Biochim. Biophys. Acta, 307,42-57. (DOI: 10.1016/0005-2736(73)90023-0)

[40] Hadjidemetriou, M., McAdam, S., Garner, G., Thackeray, C., Knight, D., Smith, D., Al-Ahmady, Z., Mazza, M., Rogan, J., Clamp, A., Kostarelos, K. (2019), The Human In Vivo Biomolecule Corona onto PEGylated Liposomes: A Proof-of-Concept Clinical Study, Adv. Mater., 31, e1803335. (DOI: 10.1002/adma.201803335)

[41] Semple, S.C., Chonn, A., Cullis, P.R. (1996),Influence of cholesterol on the association of plasma proteins with liposomes, Biochemistry, 35, 2521-2525. (DOI: 10.1021/bi950414i)

[42] Bonté, F., Juliano, R.L. (1986), Interactions of liposomes with serum proteins, Chem. Phys. Lipids, 40, 359-372. (DOI: 10.1016/0009-3084(86)90079-4)

[43] Lo Nostro, P., Ninham, B.W. (2012), Hofmeister phenomena: an update on ion specificity in biology, Chem. Rev., 112, 2286-2322. (DOI: 10.1021/cr200271j)

[44] Vella, F. (1998),The cell. A molecular approach,Biochemical Education, 26, 98-99. (DOI: 10.1016/s0307-4412(98)00065-x)

[45] Pereto, J., Lopez-Garcia, P., Moreira, D. (2004), Ancestral lipid biosynthesis and early membrane evolution, Trends Biochem. Sci., 29, 469-477. (DOI: 10.1016/j.tibs.2004.07.002)

[46] Lombard, J., Lopez-Garcia, P., Moreira, D. (2012), The early evolution of lipid membranes and the three domains of life, Nat. Rev. Microbiol., 10, 507-515. (DOI: 10.1038/nrmicro2815)

[47] Michanek, A., Kristen, N., Hook, F., Nylander, T., Sparr, E. (2010), RNA and DNA interactions with zwitterionic and charged lipid membranes - a DSC and QCM-D study, Biochim. Biophys. Acta, 1798, 829-838. (DOI: 10.1016/j.bbamem.2009.12.009)

[48] Black, R. A., Blosser, M. C., Stottrup, B. L., Tavakley, R., Deamer, D. W., Keller, S. L. (2013), Nucleobases bind to and stabilize aggregates of a prebiotic amphiphile, providing a viable mechanism for the emergence of protocells, Proc. Natl. Acad. Sci. U S A, 110, 13272-13276. (DOI: 10.1073/pnas.1300963110)

[49] Haluska, C.K., Riske, K.A., Marchi-Artzner, V., Lehn, J.M., Lipowsky, R., Dimova, R. (2006),Time scales of membrane fusion revealed by direct imaging of vesicle fusion with high temporal resolution,Proc. Natl. Acad. Sci. U S A, 103, 15841-15846. (DOI: 10.1073/pnas.0602766103)

[50] Lei, G., MacDonald, R.C. (2003), Lipid Bilayer Vesicle Fusion: Intermediates Captured by High-Speed Microfluorescence Spectroscopy, Biophys. J., 85, 1585-1599. (DOI: 10.1016/s0006-3495(03)74590-1)

[51] Marrink, S.J., Mark, A.E. (2003), The mechanism of vesicle fusion as revealed by molecular dynamics simulations, J. Am. Chem. Soc.,125,11144-11145. (DOI: 10.1021/ja036138+)

[52] Zhang, L., Granick, S. (2006), How to stabilize phospholipid liposomes (using nanoparticles), Nano Lett., 6, 694-698. (DOI: 10.1021/nl052455y)

[53] Swift, J.L., Carnini, A., Dahms, T.E.S., Cramb, D.T. (2004), Anesthetic-Enhanced Membrane Fusion Examined Using Two-Photon Fluorescence Correlation Spectroscopy, J. Phys. Chem. B, 108, 11133-11138. (DOI: 10.1021/jp037613t)

[54] Chakraborty, H., Mondal, S., Sarkar, M. (2008), Membrane fusion: a new function of non steroidal anti-inflammatory drugs, Biophys. Chem.,137,28-34 (DOI: 10.1016/j.bpc.2008.06.007)

[55] Mondal, S., Sarkar, M. (2009), Non-steroidal anti-inflammatory drug induced membrane fusion: concentration and temperature effects, J. Phys. Chem. B, 113,16323-16331. (DOI: 10.1021/jp9069527)

[56] Vargas, K.M., Shon, Y.S. (2019), Hybrid lipid-nanoparticle complexes for biomedical applications, J. Mater. Chem. B, 7, 695-708. (DOI: 10.1039/C8TB03084G)

[57] Schulz, M., Olubummo, A., Binder, W.H. (2012), Beyond the lipid-bilayer: interaction of polymers and nanoparticles with membranes, Soft Matter, 8, 4849-4864. (DOI: 10.1039/c2sm06999g)

[58] Mondal Roy, S., Sarkar, M. (2011), Membrane fusion induced by small molecules and ions, J. Lipids, 2011, 528784. (DOI: 10.1155/2011/528784)

[59] Chernomordik, L.V., Kozlov, M.M. (2003), Protein-lipid interplay in fusion and fission of biological membranes, Annu. Rev. Biochem.,72, 175-207. (DOI: 10.1146/annurev.biochem.72.121801.161504)

[60] Poste, G., Allison, A.C. (1973), Membrane fusion, Biochim. Biophys. Acta., 300, 421-465. (DOI: 10.1016/0304-4157(73)90015-4)

[61] Papahadjopoulos, D., Poste, G., Schaeffer, B.E., Vail, W.J. (1974), Membrane fusion and molecular segregation in phospholipid vesicles, Biochim. Biophys. Acta, 352, 10-28. (DOI: 10.1016/0005-2736(74)90175-8)

[62] Papahadjopoulos, D., Vail, W.J., Newton, C., Nir, S., Jacobson, K., Poste, G., Lazo, R. (1977), Studies on membrane fusion. III. The role of calcium-

induced phase changes, Biochim. Biophys. Acta, 465, 579-598. (DOI: 10.1016/0005-2736(77)90275-9)

[63] Ohki, S. (1982), A mechanism of divalent ion-induced phosphatidylserine membrane fusion, Biochim. Biophys. Acta, 689, 1-11. (DOI: 10.1016/0005-2736(82)90182-1)

[64] Breisblatt, W., Ohki, S. (1976), Fusion in phospholipid spherical membranes. II. Effect of cholesterol, divalent ions and pH, J. Membr. Biol., 29, 127-146. (DOI: 10.1007/BF01868956)

[65] Aballay, A., Sarrouf, M.N., Colombo, M.I., Stahl, P.D., Mayorga, L.S. (1995),Zn2+ depletion blocks endosome fusion, Biochem. J., 312, 919-923. (DOI: 10.1042/bj3120919)

[66] Tanaka, T., Yamazaki, M. (2004), Membrane fusion of giant unilamellar vesicles of neutral phospholipid membranes induced by La^{3+}, Langmuir, 20, 5160-5164. (DOI: 10.1021/la049681s)

[67] Do, T.D., de Almeida, N.E., LaPointe, N.E., Chamas, A., Feinstein, S.C., Bowers, M.T. (2016), Amino Acid Metaclusters: Implications of Growth Trends on Peptide Self-Assembly and Structure, Anal. Chem., 88, 868-876. (DOI: 10.1021/acs.analchem.5b03454)

[68] Sabin, J., Prieto, G., Ruso, J.M., Hidalgo-Alvarez, R., Sarmiento, F. (2006), Size and stability of liposomes: a possible role of hydration and osmotic forces, Eur. Phys. J. E, 20, 401-408. (DOI: 10.1140/epje/i2006-10029-9)

[69] Sabin, J., Prieto, G., Messina, P.V., Ruso, J.M., Hidalgo-Alvarez, R., Sarmiento, F. (2005), On the effect of Ca^{2+} and La^{3+} on the colloidal stability of liposomes, Langmuir, 21, 10968-10975. (DOI: 10.1021/la051397t)

[70] Pohle, W., Selle, C., Fritzsche, H., & Binder, H. (1998), Fourier transform infrared spectroscopy as a probe for the study of the hydration of lipid self-assemblies. II. Water binding versus phase transitions, Biospectroscopy, 4, 267-280. (DOI: 10.1002/(SICI)1520-6343)

[71] Kraft, M.L., Weber, P.K., Longo, M.L., Hutcheon, I.D., Boxer, S.G. (2006), Phase separation of lipid membranes analyzed with high-resolution secondary ion mass spectrometry, Science, 313, 1948-1951. (DOI: 10.1126/science.1130279)

[72] Alsop, R.J., Maria Schober, R., Rheinstadter, M.C. (2016), Swelling of phospholipid membranes by divalent metal ions depends on the location of the ions in the bilayers, Soft Matter, 12, 6737-6748. (DOI: 10.1039/c6sm00695g)

[73] Filippov, A., Orädd, G., Lindblom, G. (2003), The Effect of Cholesterol on the Lateral Diffusion of Phospholipids in Oriented Bilayers, Biophys. J., 84, 3079-3086. (DOI: 10.1016/s0006-3495(03)70033-2)

[74] Nicolini, C., Baranski, J., Schlummer, S., Palomo, J., Lumbierres-Burgues, M., Kahms, M., Kuhlmann, J., Sanchez, S., Gratton, E., Waldmann, H., Winter, R. (2006), Visualizing association of N-ras in lipid microdomains: influence of domain structure and interfacial adsorption, J. Am. Chem. Soc., 128, 192-201. (DOI: 10.1021/ja055779x)

[75] Klymchenko, A.S., Kreder, R. (2014), Fluorescent probes for lipid rafts: from model membranes to living cells, Chem. Biol., 21, 97-113. (DOI: 10.1016/j.chembiol.2013.11.009)

[76] Farris, G. W., Farris, F. J. (1979), Synthesis and Spectral Properties of a Hydrophobic Fluorescent Probe: 6-Propionyl-2-(dimethylamino)naphthalenet, Biochemistry, 18, 3075–3078. (DOI: 10.1021/bi00581a025)

[77] Parasassi, T., Gratton, E. (1995), Membrane lipid domains and dynamics as detected by Laurdan fluorescence, J. Fluoresc., 5, 59-69. (DOI: 10.1007/BF00718783)

[78] Wang, H., Zhang, X., Liu, Y., Liu, J. (2018), Stabilization of Liposomes by Perfluorinated Compounds, ACS Omega., 3, 15353-15360. (DOI: 10.1021/acsomega.8b02448)

[79] Shaham-Niv, S., Rehak, P., Zaguri, D., Kolusheva, S., Kral, P., Gazit, E. (2018), Metabolite amyloid-like fibrils interact with model membranes, Chem. Commun.,54, 4561-4564. (DOI: 10.1039/c8cc01423j)

[80] Korlach, J., Schwille, P., Webb, W.W., Feigenson, G.W. (1999), Characterization of lipid bilayer phases by confocal microscopy and fluorescence correlation spectroscopy, Proc. Natl. Acad. Sci. U S A, 96, 8461-8466. (DOI: 10.1073/pnas.96.15.8461)

[81] Moustakas, M. (2021),The Role of Metal Ions in biology biochemistry and medicine, Materials (Basel), 14, (DOI: 10.3390/ma14030549)

[82] Jurkiewicz, P., Cwiklik, L., Vojtiskova, A., Jungwirth, P., Hof, M. (2012), Structure, dynamics, and hydration of POPC/POPS bilayers suspended in NaCl, KCl, and CsCl solutions, Biochim. Biophys. Acta, 1818, 609-616. (DOI: 10.1016/j.bbamem.2011.11.033)

[83] Garcia-Celma, J.J., Hatahet, L., Kunz, W., Fendler, K. (2007), Specific anion and cation binding to lipid membranes investigated on a solid supported membrane, Langmuir, 23, 10074-10080. (DOI: 10.1021/la701188f)

[84] Clarke, R.J., Lüpfert, C. (1999), Influence of Anions and Cations on the Dipole Potential of Phosphatidylcholine Vesicles: A Basis for the Hofmeister Effect, Biophys. J., 76, 2614-2624. (DOI: 10.1016/s0006-3495(99)77414-x)

[85] Melcrova, A., Pokorna, S., Pullanchery, S., Kohagen, M., Jurkiewicz, P., Hof, M., Jungwirth, P., Cremer, P.S., Cwiklik, L. (2016), The complex nature of calcium cation interactions with phospholipid bilayers, Sci. Rep.,6, 38035. (DOI: 10.1038/srep38035)

[86] Javanainen, M., Melcrova, A., Magarkar, A., Jurkiewicz, P., Hof, M., Jungwirth, P., Martinez-Seara, H. (2017), Two cations, two mechanisms: interactions of sodium and calcium with zwitterionic lipid membranes, Chem. Commun., 53, 5380-5383. (DOI: 10.1039/c7cc02208e)

[87] Barfield, K. D., Bevan, D. R. (1985), Fusion of phospholipid vesicles induced by Zn^{2+}, Cd^{2+}, and Hg^{2+},Biochem. Biophys. Res. Commun., 128, 389-395. (DOI: 10.1016/0006-291x(85)91691-2)

[88] Ohki, S., Arnold, K. (1990), Surface dielectric constant, surface hydrophobicity and membrane fusion, J. Membr. Biol., 114, 195-203 (DOI: 10.1007/BF01869214)

[89] Binder, H., Arnold, K., Ulrich, A.S., Zschörnig, O. (2001), Interaction of Zn^{2+} with phospholipid membranes, Biophys. Chem., 90, 57-74 (DOI: 10.1016/s0301-4622(01)00130-2)

[90] Binder, H., Zschörnig, O. (2002), The effect of metal cations on the phase behavior and hydration characteristics of phospholipid membranes, Chem. Phys. Lipids, 115, 39-61. (DOI: 10.1016/s0009-3084(02)00005-1)

[91] Shi, X., Bi, Y., Yang, W., Guo, X., Jiang, Y., Wan, C., Li, L., Bai, Y., Guo, J., Wang, Y., Chen, X., Wu, B., Sun, H., Liu, W., Wang, J., Xu, C. (2013),Ca^{2+} regulates T-cell receptor activation by modulating the charge property of lipids, Nature, 493, 111-115. (DOI: 10.1038/nature11699)

[92] Sabín, J., Prieto, G., Blanco, E., Ruso, J.M., Angelini, R., Bordi, F., Sarmiento, F. (2007), Interaction of gadolinium with phospholipids bilayer membranes, J. Therm. Anal. Calorim., 87, 199-203. (DOI: 10.1007/s10973-006-7841-6)

[93] Akeson, M.A., Munns, D.N., Burau, R.G. (1989), Adsorption of Al^{3+} to phosphatidylcholine vesicles, Biochim. Biophys. Acta, 986, 33-40. (DOI: 10.1016/0005-2736(89)90269-1)

[94] Tanaka, T., Tamba, Y., Masum, S.M., Yamashita, Y., Yamazaki, M. (2002), La^{3+} and Gd^{3+} induce shape change of giant unilamellar vesicles of phosphatidylcholine, Biochim. Biophys. Acta, 1564, 173-182 (DOI: 10.1016/s0005-2736(02)00444-3)

[95] Bentz, J., Alford, D., Cohen, J., Düzgüneş, N. (1988), La^{3+}-induced fusion of phosphatidylserine liposomes. Close approach, intermembrane intermediates, and the electrostatic surface potential, Biophys. J., 53, 593-607 (DOI: 10.1016/s0006-3495(88)83138-2)

[96] Hammoudah, M.M., Nir, S., Isac, T., Kornhauser, R., Stewart, T.P., Hui, S.W., Vaz, W.L.C. (1979),Interactions of La^{3+} with phosphatidylserine vesicles binding, phase transition, leakage and fusion, Biochim. Biophys. Acta., 558, 338-343. (DOI: 10.1016/0005-2736(79)90270-0)

[97] Verstraeten, S.V., Oteiza, P.I. (2000), Effects of Al(3+) and related metals on membrane phase state and hydration: correlation with lipid oxidation, Arch. Biochem. Biophys., 375, 340-346. (DOI: 10.1006/abbi.1999.1671)

[98] Alberts, B., Johnson, A., Lewis, J., Raff, M., Roberts, K., Walter, P. (2002), Membrane proteins, Mol. Biol. Cell, 4th edition,

[99] Zhao, H., Lappalainen, P. (2012), A simple guide to biochemical approaches for analyzing protein-lipid interactions, Mol. Biol. Cell, 23, 2823-2830 (DOI: 10.1091/mbc.E11-07-0645)

[100] Bechinger, B. (2008), A dynamic view of peptides and proteins in membranes, Cell. Mol. Life Sci., 65, 3028-3039. (10.1007/s00018-008-8125-z)

[101] Barcelo, F., Prades, J., Encinar, J.A., Funari, S.S., Vogler, O., Gonzalez-Ros, J.M., Escriba, P.V. (2007), Interaction of the C-terminal region of the Ggamma protein with model membranes, Biophys. J., 93, 2530-2541. (DOI: 10.1529/biophysj.106.101196)

[102] Gu, R.X., de Groot, B.L. (2020), Lipid-protein interactions modulate the conformational equilibrium of a potassium channel, Nat. Commun.,11, 2162 (DOI: 10.1038/s41467-020-15741-8)

[103] Liu, A., Wenzel, N., Qi, X. (2005), Role of lysine residues in membrane anchoring of saposin C, Arch. Biochem. Biophys., 443, 101-112. (DOI: 10.1016/j.abb.2005.09.007)

[104] Jiang, Y., Ruta, V., Chen, J., Lee, A., MacKinnon, R. (2003), The principle of gating charge movement in a voltage-dependent K^+ channel, Nature, 423, 42-48. (DOI: 10.1038/nature01581)

[105] Duchardt, F., Fotin-Mleczek, M., Schwarz, H., Fischer, R., Brock, R. (2007), A comprehensive model for the cellular uptake of cationic cell-penetrating peptides, Traffic, 8, 848-866. (DOI: 10.1111/j.1600-0854.2007.00572.x)

[106] Zhang, J., Yang, W., Tan, J., Ye, S. (2018), In situ examination of a charged amino acid-induced structural change in lipid bilayers by sum frequency generation vibrational spectroscopy, Phys. Chem. Chem. Phys., 20, 5657-5665. (DOI: 10.1039/c7cp07389e)

[107] Corradi, V., Mendez-Villuendas, E., Ingolfsson, H.I., Gu, R.X., Siuda, I., Melo, M.N., Moussatova, A., DeGagne, L.J., Sejdiu, B.I., Singh, G., Wassenaar, T.A., Delgado Magnero, K., Marrink, S.J., Tieleman, D.P. (2018), Lipid-Protein Interactions Are Unique Fingerprints for Membrane Proteins, ACS Cent. Sci., 4, 709-717. (DOI: 10.1021/acscentsci.8b00143)

[108] Hong, H., Park, S., Jimenez, R.H., Rinehart, D., Tamm, L.K. (2007), Role of aromatic side chains in the folding and thermodynamic stability of integral membrane proteins, J. Am. Chem. Soc., 129, 8320-8327. (DOI: 10.1021/ja068849o)

[109] Domene, C., Vemparala, S., Klein, M.L., Venien-Bryan, C., Doyle, D.A. (2006), Role of aromatic localization in the gating process of a potassium channel, Biophys. J., 90, L01-03 (DOI: 10.1529/biophysj.105.072116)

[110] MacCallum, J.L., Bennett, W.F., Tieleman, D.P. (2007), Partitioning of amino acid side chains into lipid bilayers: results from computer simulations and comparison to experiment, J. Gen. Physiol., 129, 371-377 (DOI: 10.1085/jgp.200709745)

[111] Nguyen, P.H., Derreumaux, P. (2020), Structures of the intrinsically disordered Abeta, tau and alpha-synuclein proteins in aqueous solution from computer simulations, Biophys. Chem., 264, 106421 (DOI: 10.1016/j.bpc.2020.106421)

[112] Chiti, F., Dobson, C.M. (2017), Protein Misfolding, Amyloid Formation, and Human Disease: A Summary of Progress Over the Last Decade, Annu. Rev. Biochem., 86, 27-68. (DOI: 10.1146/annurev-biochem-061516-045115)

[113] Haass, C., Selkoe, D.J. (2007), Soluble protein oligomers in neurodegeneration: lessons from the Alzheimer's amyloid beta-peptide, Nat. Rev. Mol. Cell Biol., 8, 101-112. (DOI: 10.1038/nrm2101)

[114] Hardy, J., Allsop, D. (1991), Amyloid deposition as the central event in the aetiology of Alzheimer's disease, Trends Pharmacol. Sci., 12, 383-388. (DOI: 10.1016/0165-6147(91)90609-v)

[115] Chaparro Sosa, A.F., de Oliveira da Silva, S.M., Morgan, G.P., Schwartz, D.K., Kaar, J.L. (2020), Mixed Phospholipid Vesicles Catalytically Inhibit and Reverse Amyloid Fibril Formation, J. Phys. Chem. Lett, 11, 7417-7422. (DOI: 10.1021/acs.jpclett.0c02074)

[116] Yip, C.M., McLaurin, J. (2001), Amyloid-β Peptide Assembly: A Critical Step in Fibrillogenesis and Membrane Disruption, Biophys. J., 80, 1359-1371. (DOI: 10.1016/s0006-3495(01)76109-7)

[117] Heo, C.E., Park, C.R., Kim, H.I. (2021), Effect of packing density of lipid vesicles on the Abeta42 fibril polymorphism, Chem. Phys. Lipids, 236, 105073. (DOI: 10.1016/j.chemphyslip.2021.105073)

[118] Sabaté, R., Gallardo, M., Estelrich, J. (2005), Spontaneous incorporation of β-amyloid peptide into neutral liposomes, Colloids Surf. Physicochem. Eng. Aspects, 270-271, 13-17. (DOI: 10.1016/j.colsurfa.2005.05.031)

[119] Chi, E.Y., Ege, C., Winans, A., Majewski, J., Wu, G., Kjaer, K., Lee, K.Y. (2008), Lipid membrane templates the ordering and induces the fibrillogenesis of Alzheimer's disease amyloid-beta peptide, Proteins,72, 1-24 (DOI: 10.1002/prot.21887)

[120] Lindberg, D.J., Wesen, E., Bjorkeroth, J., Rocha, S., Esbjorner, E. K. (2017), Lipid membranes catalyse the fibril formation of the amyloid-beta (1-42) peptide through lipid-fibril interactions that reinforce secondary pathways, Biochim. Biophys. Acta Biomembr., 1859, 1921-1929 (DOI: 10.1016/j.bbamem.2017.05.012)

[121] Hellstrand, E., Sparr, E., Linse, S. (2010),Retardation of Abeta fibril formation by phospholipid vesicles depends on membrane phase behavior, Biophys. J., 98, 2206-2214. (DOI: 10.1016/j.bpj.2010.01.063)

[122] Sabate, R., Espargaro, A., Barbosa-Barros, L., Ventura, S., Estelrich, J. (2012), Effect of the surface charge of artificial model membranes on the

aggregation of amyloid beta-peptide, Biochimie, 94, 1730-1738. (DOI: 10.1016/j.biochi.2012.03.027)

[123] Adler-Abramovich, L., Vaks, L., Carny, O., Trudler, D., Magno, A., Caflisch, A., Frenkel, D., Gazit, E. (2012), Phenylalanine assembly into toxic fibrils suggests amyloid etiology in phenylketonuria, Nat. Chem. Biol., 8, 701-706 (DOI: 10.1038/nchembio.1002)

[124] Shaham-Niv, S., Adler-Abramovich, L., Schnaider, L., Gazit, E. (2015), Extension of the generic amyloid hypothesis to nonproteinaceous metabolite assemblies, Sci. Adv., 1, e1500137. (DOI: 10.1126/sciadv.1500137)

[125] Shaham-Niv, S., Arnon, Z.A., Sade, D., Lichtenstein, A., Shirshin, E. A., Kolusheva, S., Gazit, E. (2018), Intrinsic Fluorescence of Metabolite Amyloids Allows Label-Free Monitoring of Their Formation and Dynamics in Live Cells, Angew. Chem. Int. Ed. Engl., 57, 12444-12447. (DOI: 10.1002/anie.201806565)

[126] Xu, X., Ray, R., Gu, Y., Ploehn, H. J., Gearheart, L., Raker, K., Scrivens, W.A. (2004), Electrophoretic analysis and purification of fluorescent single-walled carbon nanotube fragments, J. Am. Chem. Soc., 126, 12736-12737. (DOI: 10.1021/ja040082h)

[127] Bao, L., Zhang, Z.L., Tian, Z.Q., Zhang, L., Liu, C., Lin, Y., Qi, B., Pang, D.W. (2011),Electrochemical tuning of luminescent carbon nanodots: from preparation to luminescence mechanism, Adv. Mater., 23, 5801-5806. (DOI: 10.1002/adma.201102866)

[128] Liu, S., Tian, J., Wang, L., Zhang, Y., Qin, X., Luo, Y., Asiri, A.M., Al-Youbi, A.O., Sun, X. (2012), Hydrothermal treatment of grass: a low-cost, green route to nitrogen-doped, carbon-rich, photoluminescent polymer nanodots as an effective fluorescent sensing platform for label-free detection of Cu(II) ions, Adv. Mater., 24, 2037-2041. (DOI: 10.1002/adma.201200164)

[129] Wang, X., Cao, L., Lu, F., Meziani, M.J., Li, H., Qi, G., Zhou, B., Harruff, B.A., Kermarrec, F., Sun, Y.P. (2009), Photoinduced electron transfers with carbon dots, Chem. Commun., 3774-3776 (DOI: 10.1039/b906252a)

[130] Zhu, S., Zhang, J., Tang, S., Qiao, C., Wang, L., Wang, H., Liu, X., Li, B., Li, Y., Yu, W., Wang, X., Sun, H., Yang, B. (2012), Surface Chemistry Routes to Modulate the Photoluminescence of Graphene Quantum Dots: From Fluorescence Mechanism to Up-Conversion Bioimaging Applications, Adv. Funct. Mater., 22, 4732-4740. (DOI: 10.1002/adfm.201201499)

[131] Kim, E., Lee, Y., Lee, S., Park, S.B. (2015), Discovery, understanding, and bioapplication of organic fluorophore: a case study with an indolizine-based novel fluorophore, Seoul-Fluor, Acc. Chem. Res., 48, 538-547. (DOI: 10.1021/ar500370v)

[132] Klymchenko, A.S. (2017), Solvatochromic and Fluorogenic Dyes as Environment-Sensitive Probes: Design and Biological Applications, Acc. Chem. Res., 50, 366-375. (DOI: 10.1021/acs.accounts.6b00517)

[133] Zhang, S., Ma, C., Chalfie, M. (2004), Combinatorial marking of cells and organelles with reconstituted fluorescent proteins, Cell, 119, 137-144. (DOI: 10.1016/j.cell.2004.09.012)

[134] Remington, S.J. (2011),Green fluorescent protein: a perspective, Protein Sci., 20, 1509-1519. (DOI: 10.1002/pro.684)

[135] Pandey, S., Bodas, D. (2020), High-quality quantum dots for multiplexed bioimaging: A critical review, Adv. Colloid Interface Sci., 278, 102137. (DOI: 10.1016/j.cis.2020.102137)

[136] Yong, K.T., Law, W.C., Hu, R., Ye, L., Liu, L., Swihart, M.T., Prasad, P.N. (2013), Nanotoxicity assessment of quantum dots: from cellular to primate studies, Chem. Soc. Rev., 42, 1236-1250. (DOI: 10.1039/c2cs35392j)

[137] Zrazhevskiy, P., Sena, M., Gao, X. (2010), Designing multifunctional quantum dots for bioimaging, detection, and drug delivery, Chem. Soc. Rev., 39, 4326-4354. (DOI: 10.1039/b915139g)

[138] Fu, Y., Zhang, J., Lakowicz, J.R. (2008), Metal-enhanced fluorescence of single green fluorescent protein (GFP),Biochem. Biophys. Res. Commun., 376,712-717. (DOI: 10.1016/j.bbrc.2008.09.062)

[139] Hamd-Ghadareh, S., Salimi, A., Fathi, F., Bahrami, S. (2017), An amplified comparative fluorescence resonance energy transfer immunosensing of CA125 tumor marker and ovarian cancer cells using green and economic carbon dots for bio-applications in labeling, imaging and sensing, Biosens. Bioelectron., 96, 308-316. (DOI: 10.1016/j.bios.2017.05.003)

[140] Wang, N., Zheng, A.Q., Liu, X., Chen, J.J., Yang, T., Chen, M.L., Wang, J.H. (2018), Deep Eutectic Solvent-Assisted Preparation of Nitrogen/Chloride-Doped Carbon Dots for Intracellular Biological Sensing and Live Cell Imaging, ACS Appl. Mater. Interfaces, 10, 7901-7909 (DOI: 10.1021/acsami.8b00947)

[141] Ruan, S., Qian, J., Shen, S., Chen, J., Zhu, J., Jiang, X., He, Q., Yang, W., Gao, H. (2014), Fluorescent carbonaceous nanodots for noninvasive glioma imaging after angiopep-2 decoration, Bioconjug. Chem.,25, 2252-2259. (DOI: 10.1021/bc500474p)

[142] Shao, D., Lu, M., Xu, D., Zheng, X., Pan, Y., Song, Y., Xu, J., Li, M., Zhang, M., Li, J., Chi, G., Chen, L., Yang, B. (2017), Carbon dots for tracking and promoting the osteogenic differentiation of mesenchymal stem cells, Biomater. Sci., 5, 1820-1827 (DOI: 10.1039/c7bm00358g)

[143] Liu, J. H., Cao, L., LeCroy, G. E., Wang, P., Meziani, M. J., Dong, Y., Liu, Y., Luo, P. G., Sun, Y. P. (2015), Carbon "Quantum" Dots for Fluorescence Labeling of Cells,ACS Appl Mater Interfaces, 7, 19439-19445. (DOI: 10.1021/acsami.5b05665)

[144] Zhang, M., Bai, L., Shang, W., Xie, W., Ma, H., Fu, Y., Fang, D., Sun, H., Fan, L., Han, M., Liu, C., Yang, S. (2012), Facile synthesis of water-soluble, highly fluorescent graphene quantum dots as a robust biological label for stem cells, J. Mater. Chem., 22, 7461-7467. (DOI: 10.1039/c2jm16835a)

[145] Gao, W., Song, H., Wang, X., Liu, X., Pang, X., Zhou, Y., Gao, B., Peng, X. (2018),Carbon Dots with Red Emission for Sensing of Pt(2+), Au(3+), and Pd(2+) and Their Bioapplications in Vitro and in Vivo, ACS Appl. Mater. Interfaces, 10, 1147-1154 (DOI: 10.1021/acsami.7b16991)

[146] Zhou, N., Hao, Z., Zhao, X., Maharjan, S., Zhu, S., Song, Y., Yang, B., Lu, L. (2015), A novel fluorescent retrograde neural tracer: cholera toxin B conjugated carbon dots, Nanoscale, 7, 15635-15642 (DOI: 10.1039/c5nr04361a)

[147] Khan, M.S., Pandey, S., Talib, A., Bhaisare, M.L., Wu, H.F. (2015), Controlled delivery of dopamine hydrochloride using surface modified carbon dots for neuro diseases, Colloids Surf. B. Biointerfaces, 134, 140-146. (DOI: 10.1016/j.colsurfb.2015.06.006)

[148] Nandi, S., Malishev, R., Parambath Kootery, K., Mirsky, Y., Kolusheva, S., Jelinek, R. (2014), Membrane analysis with amphiphilic carbon dots,Chem Commun, 50, 10299-10302. (DOI: 10.1039/c4cc03504f)

[149] Nandi, S., Malishev, R., Bhunia, S.K., Kolusheva, S., Jopp, J., Jelinek, R. (2016),Lipid-Bilayer Dynamics Probed by a Carbon Dot-Phospholipid Conjugate, Biophys. J., 110, 2016-2025. (DOI: 10.1016/j.bpj.2016.04.005)

[150] Pritzl, S. D., Pschunder, F., Ehrat, F., Bhattacharyya, S., Lohmuller, T., Huergo, M. A., Feldmann, J. (2019), Trans-membrane Fluorescence Enhancement by Carbon Dots: Ionic Interactions and Energy Transfer, Nano Lett., 19, 3886-3891. (DOI: 10.1021/acs.nanolett.9b01071)

[151] Kanwa, N., M, K., Chakraborty, A. (2020), Discriminatory Interaction Behavior of Lipid Vesicles toward Diversely Emissive Carbon Dots Synthesized from Ortho, Meta, and Para Isomeric Carbon Precursors, Langmuir, 36, 10628-10637. (DOI: 10.1021/acs.langmuir.0c02207)

Chapter 2

Spectroscopic evidence for hydration and dehydration of lipid bilayers upon interaction with metal ions: a new physical insight

2.1 Introduction

Metal ions have been broadly known for their role in cell structure, cell polarization, and most importantly cell function. Metal ions are fundamental elements for the maintenance of the lifespan of many living systems. Metal ions, such as Ca^{2+}, Na^{+}, and K^{+} are usually present in high concentrations and play major roles in regulating cell polarization and action potentials *[1-2]*. Moreover, divalent metal ions such as Mg^{2+}, Zn^{2+}, and Fe^{2+}, though present in traces, are vital for the regulation and function of a number of membrane associated processes *[3]*. The accumulation of cations on a membrane surface eventually modulates its interaction with the surrounding macromolecules and locally alters the physical properties of the membrane *[3–9]*.

The binding of metal cations to lipid membranes has been a vital area of research over the past few decades *[10–48]*. Numerous studies have been carried out in order to understand the role of ions in membrane stability. The role of metal ions on membrane hydration, the binding mode, and the location of the metal ions have been investigated extensively *[15, 28, 30–34]*. It has been well established that ions interact in a specific manner with membranes. Monovalent alkali cations adsorb on the surface of membranes only in the presence of negatively charged lipids, whereas divalent ions adsorb readily even if the lipid is zwitterionic *[35]*. Consequently, the adsorption of cations on the surface of a membrane causes a net positive charge at the membrane–water interface *[34, 45-46]*. The binding mode of metal ions with lipid and their position in the bilayer depends upon their size, charge, and metal-oxygen bonding characteristics *[5, 39]*. Divalent cations are adsorbed on the lipid bilayer surface and ion-dipole interaction causes conformational modifications

both in the head group and tail group region of the membrane *[47, 48]*. It has been reported that metal ions have different affinities towards lipids depending on their hydrophobic chain lengths along with phase transition temperatures *[18, 20, 31, 50-51]*. The divalent ions predominantly interact with the gel phase over the liquid crystalline phase and increase the phase transition temperature of the lipid bilayer *[36–38]*. The affinity of divalent cations among Ca^{2+}, Mg^{2+}, and Zn^{2+}, follows the order $Zn^{2+} > Ca^{2+} > Mg^{2+}$ *[5,17,39]*. Due to the adsorption of these cations, the area per lipid head group quenches, which results in an increase in the membrane thickness *[22, 38, 49]*. As the position and the mode of binding of metal ions with lipid bilayer are different, therefore, the hydration or dehydration of a lipid bilayer majorly depends on the divalent metal ions. Phosphodiester and the carbonyl group of the glycerol moiety provide a site for the binding of ions with the lipid bilayer. Alsop et al. determined the binding position of the cations of different metal ions by an X-ray diffraction experiment *[39]*. They found that Ca^{2+} and Zn^{2+} bind closer to the glycerol group, while Mg^{2+} and Fe^{2+} bind closer to the phosphate group. Moreover, Binder et al. found that Zn^{2+} strongly interacts with the free electronegative oxygen of the phosphate group *[5, 17]*. In addition, Yang et al. reported that Ca^{2+} coordinates and binds electrostatically with oxygen on four adjacent lipid molecules, and Mg^{2+} binds closer to the phosphate group and coordinates with water-oxygen *[32]*. Various techniques (e.g. NMR, XRD, mass spectrometry, etc.) have been applied to study the interaction between the lipid bilayer and metal ions.

Considering the fact that metal ions display different affinities towards lipids of different hydrophobic chain lengths and phase transition temperatures, we have chosen three different zwitterionic phospholipids, namely DPPC, DMPC, and POPC, and used the chlorides of a series of divalent metal ions (Zn^{2+}, Ca^{2+}, and Mg^{2+}) to investigate the bilayer–metal ion interaction. All the aforementioned phospholipids were selected keeping in mind their same zwitterionic head groups, similar molecular weights (734.039, 677.933 and 760.08 for DPPC, DMPC, and POPC, respectively) but distinctly different phase transition temperatures (42 °C, 24 °C, and -20 °C for DPPC, DMPC, and POPC, respectively) *[52,53]*. The metal ions have different electronic

structures, different binding positions, and different hydration free energies. We used PRODAN, a well-known membrane probe, which emits at 440 nm in the gel phase and at 490 nm in the liquid crystalline phase, to monitor the lipid bilayer–metal ion interaction using steady state and time resolved fluorescence spectroscopy *[54–59]*. We conducted time resolved anisotropy to unravel the confinement of PRODAN molecules upon interaction with the lipid bilayer. Apart from monitoring the emission properties of PRODAN, we conducted DLS and zeta potential measurements to understand the effect of metal ions on the size and charge of the lipid bilayers.

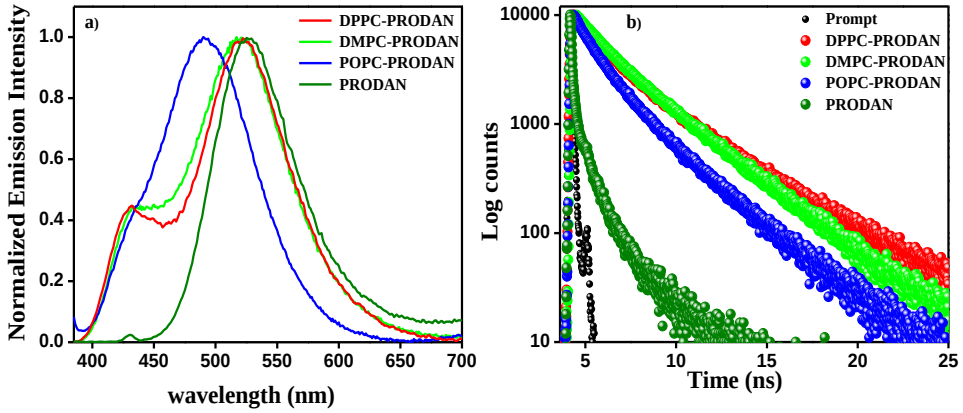

Figure 2.1 a) Normalized Emission spectra of PRODAN impregnated lipid bilayer and b) Time resolved decay curves of PRODAN in the presence of various lipid bilayers at 440 nm.

2.2 Results and Discussion

2.2.1 Results: PRODAN in an aqueous medium exhibits an emission maximum at 540 nm, which is assigned as the twisted intramolecular charge transfer (TICT) band. In the presence of lipid, another band emerges at 440 nm wavelength *[54–59]*. The appearance of a new band at 440 nm is assigned to the local excited (LE) state of PRODAN and it is a characteristic band of the gel phase of the lipid bilayer. The normalized emission spectra, as shown in Figure 2.1, reveal that the band at 440 nm is most prominent for the DPPC and DMPC bilayers. The lifetime decays were fitted with a multi-exponential function by using the equation $D(t) = \sum_{i=1}^{n} a_i \exp(\frac{-t}{\tau_i})$. The lifetime measurements (Table 2.1) indicate that the decays of PRODAN in the different lipid bilayers comprises of three different time constants (τ_1, τ_2, and

τ_3 with amplitudes a_1, a_2, and a_3, respectively). While the first two shorter components, i.e. τ_1 and τ_2, are ascribed to the contribution from the aqueous phase, the longest component, i.e. τ_3, originates from PRODAN in the lipid bilayers.

Table 2.1: Time resolved data for the PRODAN and PRODAN in different lipid bilayers at 440 nm.[#]

	χ^2	**τ_1 (ns)**	**τ_2 (ns)**	**τ_3 (ns)**	**a_1 (%)**	**a_2 (%)**	**a_3 (%)**
PRODAN	1.10	1.80	0.60		0.26	0.74	
DPPC-PRODAN	1.00	1.83	0.58	4.28	0.46	0.22	0.32
DMPC-PRODAN	0.99	1.68	0.37	3.89	0.42	0.13	0.45
POPC-PRODAN	1.19	1.05	0.10	2.89	0.43	0.31	0.27

 # Experimental error in the measurement is around 5%

The emission spectra of PRODAN in different bilayers as a function of the concentration of Zn^{2+} and Ca^{2+} are shown in Figure 2.2a-c and Figure 2.3a-c respectively. Upon the addition of metal ions, namely Zn^{2+} and Ca^{2+} to the PRODAN impregnated bilayers, we observe that the emission intensity of the LE state increases gradually with an increase in the concentration of metal ions for the DPPC and DMPC bilayers. However, in the case of POPC, we did not observe any changes. The overall intensity decreases for both emission sides at the red end (~500 nm) and blue end (~440 nm). We estimated the fractional intensity (P) at the red end (P_R) and blue end (P_B) to understand the change in the fluidity in the presence of metal salts using the following equation:

$$P_B = \frac{I_B}{I_B + I_R} \text{ and } P_R = \frac{I_R}{I_B + I_R}$$

I_B and I_R are the emission intensity at 440 nm and 500 nm respectively *[55]*. The polarization at the blue end increases while that at the red end decreases in DPPC and DMPC bilayers with increasing concentration of Zn^{+2} (Figure 2.2d-e) and Ca^{+2} (Figure 2.3d-e). Interestingly the polarization data (P_B and P_R) remains unchanged in the POPC bilayer even at the highest concentration of Zn^{+2} and Ca^{+2} concentrations (Figure 2.2f & Figure 2.3f).

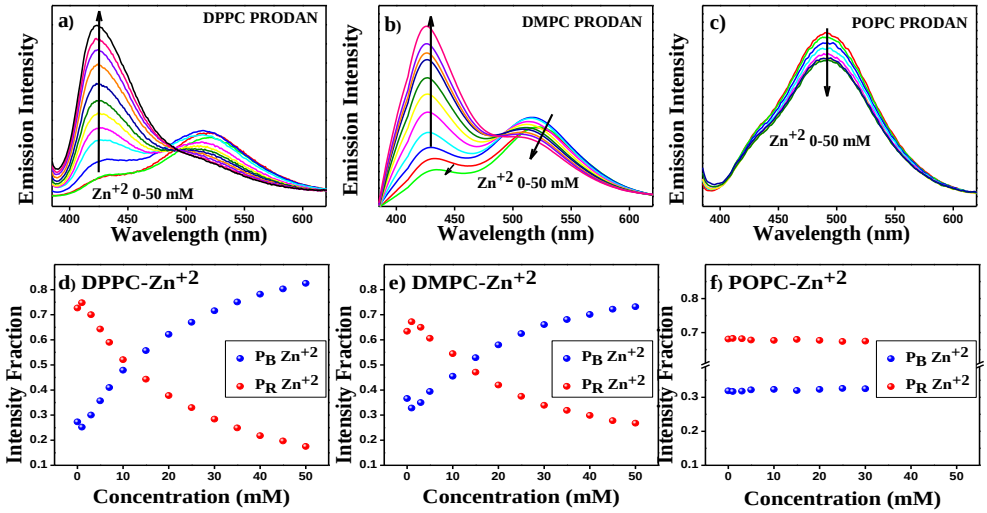

Figure 2.2 Emission spectra of PRODAN at various concentrations of Zn^{2+} in (a) DPPC, (b) DMPC and (c) POPC bilayers. Estimated intensity fraction with increasing concentration of Zn^{2+} in (d) DPPC, (e) DMPC and (f) POPC bilayers.

The lifetime decays of PRODAN for DPPC, DMPC, and POPC bilayers in the presence of Zn^{2+} and Ca^{2+} were measured at 440 nm and they are shown in Figure 2.4. The decay parameters due to the addition of Zn^{2+} and Ca^{2+} as obtained using the non-exponential fitting of the decay curve and given in Table 2.2 and Table 2.3, respectively. It is reveal that up to the concentration of ~3 mM Zn^{2+} (Table 2.2), the component τ_3 decreases from 4.28 ns (32%) to 3.12 ns (28%) in the DPPC bilayer and from 3.89 ns (45%) to 2.95 ns (30%) in the DMPC bilayer, respectively. However, beyond the concentration of 5 mM Zn^{2+}, τ_3 increases from 3.12 ns (28%) to 4.52 ns (67%) in the DPPC bilayer and from 2.95 ns (30%) to 4.33 ns (50%) in the DMPC bilayer. Interestingly, Zn^{2+} does not alter the lifetime components of PRODAN significantly in the POPC bilayer. On the other hand, for Ca^{2+} (Table 2.3), up to ~5 mM, we observe that τ_3 decreases from 4.28 ns (32%) to 2.77 ns (35%) in the DPPC bilayer and from 3.89 ns (45%) to 3.05 ns (46%) in the DMPC bilayer, respectively. However, beyond the concentration of 5 mM Ca^{2+}, we observe a very small increase in τ_3, which increases from 2.77 ns (35%) to 2.97 ns (44%) in the DPPC bilayer while it increases from 3.05 ns (46%) to 3.45 ns (48%) in the DMPC bilayer. Similar to the Zn^{2+}, we did not observe significant changes in the lifetime components in the POPC bilayer in the presence of Ca^{2+}.

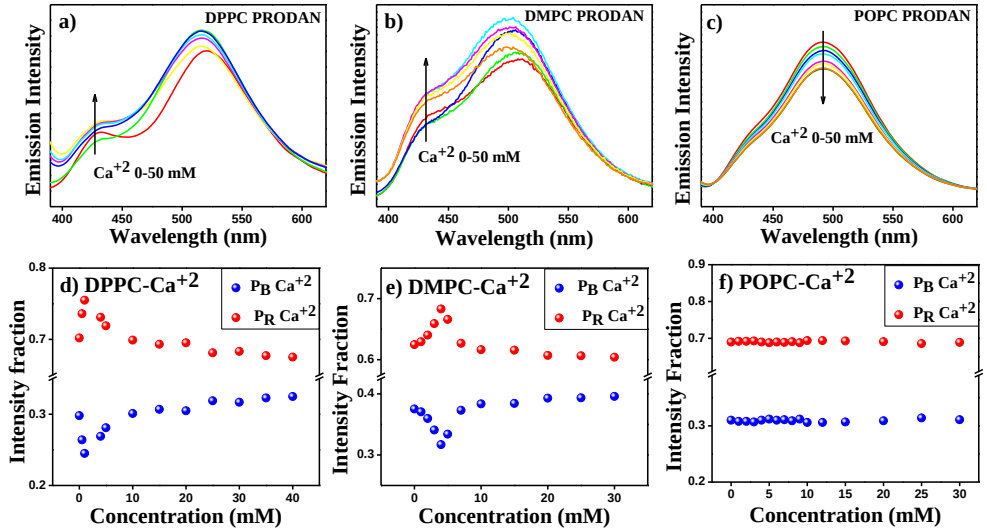

Figure 2.3 Emission spectra of PRODAN for addition of Ca^{2+} (0-40 mM) in a) DPPC b) DMPC and c) POPC. Estimated intensity fraction as a function of concentration of Ca^{2+} in d) DPPC, e) DMPC and f) POPC.

To gain a better insight into the confinement in the vicinity of the lipid bilayer, we performed time resolved anisotropy measurements in the presence of the metal ions. The rotational relaxation in the DPPC and DMPC bilayers in the presence of Zn^{2+} and Ca^{2+} (up to ~5 mM) is shown in Figure 2.5 while the same for the POPC bilayer is shown in figure 2.6. The anisotropy decays indicate that the rotational relaxation becomes faster at low concentrations (~5 mM) of Zn^{2+} and Ca^{2+} in the DPPC and DMPC bilayers compared to the bare lipid bilayer. However, beyond the concentration of 5 mM Zn^{2+}, the rotational relaxation becomes significantly slower for the DPPC and DMPC bilayers. For Ca^{2+}, we observe a very small increase in anisotropy decay for the DPPC and DMPC bilayers. We do not observe any significant changes in anisotropy decay upon the addition of any of the metal ions to the POPC bilayer (Figure 2.6).

After the investigation of the interaction of the lipid bilayers with Zn^{2+} and Ca^{2+}, we studied the interaction of lipid bilayers with Mg^{2+} ions. It is clear from Figure 2.7a–c that in the presence of Mg^{2+}, the PRODAN impregnated bilayers show a decrease in the intensity of the LE band and an increase in the intensity of the TICT band. This result is different from that in the presence of Zn^{2+} and Ca^{2+}. The polarization data reveal that the fractional intensity at the

blue end decreases and that in the red end increases for the DPPC and DMPC bilayers (Figure 2.7d and e). Again, we did not find any change in fractional intensity in the case of the POPC bilayers (Figure 2.7f).

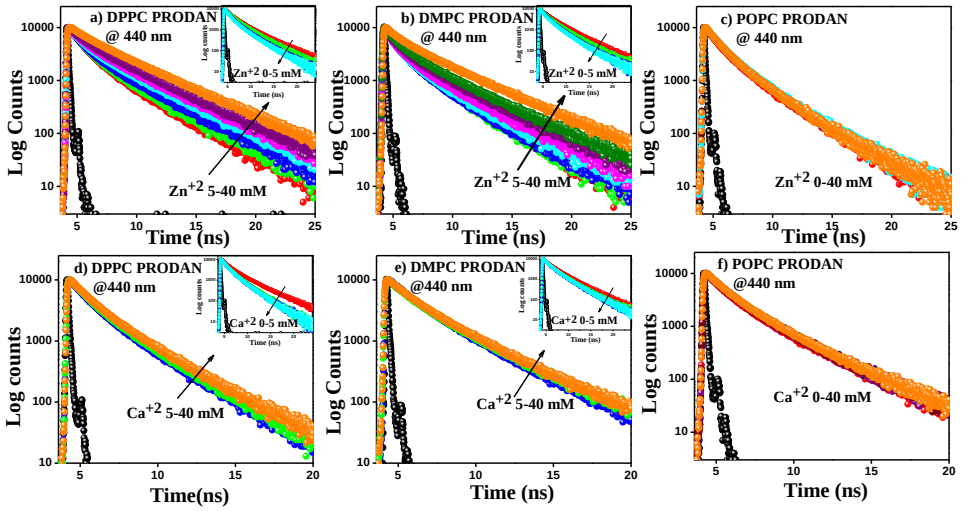

Figure 2.4 Time resolved decay curves of PRODAN in different lipid bilayers at various concentrations of Zn^{2+} for (a) DPPC, (b) DMPC and (c) POPC bilayers at 440 nm (inset shows a decrease in lifetime for the concentration of Zn^{2+} from 0 to 5 mM), and at various concentrations of Ca^{2+} for (d) DPPC, (e) DMPC and (f) POPC bilayers at 440 nm (inset shows a decrease in lifetime for the concentration of Ca^{2+} from 0 to 5 mM).

The lifetime data reveal a significant decrease in the fluorescence lifetime with an increasing concentration of Mg^{2+} (Figure 2.8a-b). The decay parameters for Mg^{2+} as obtained using the fitting of the decay curve are given in Table 2.4. We observe a monotonous decrease in τ_3 and a_3 values in both DPPC and DMPC bilayers. The τ_3 value decreases from 4.28 (32%) to1.99 ns (15%) in the DPPC bilayer and from 3.89 (45%) to 2.40 ns (10%) in the DMPC bilayer. Anisotropy decay at 440 nm (Figure 2.8 d-f) reveal that for the DPPC and DMPC bilayers, the rotational relaxation becomes monotonously faster with increasing concentration of Mg^{2+}. However, for POPC, the decays remain unchanged (Figure 2.8f). Further, we investigated the binding of metal ions at different pH values (pH~7, and pH~5.5) from steady state measurement. The results are summarized in Figure 2.9. We observe significant changes upon the addition of metal ions to the lipid bilayers at pH~7; however, the change is very small as the pH of the system is lowered.

Table 2.2 Lifetime components and normalized amplitudes of time resolved data for lipid bilayer-PRODAN at 440 nm upon increasing the concentration of Zn^{2+} at fixed lipid concentration (0.6 mM)[#]

DPPC	**χ2**	**τ_1 (ns)**	**τ_2 (ns)**	**τ_3 (ns)**	**a_1 (%)**	**a_2 (%)**	**a_3 (%)**
0 mM Zn^{+2}	1.00	1.83	0.58	4.28	0.46	0.22	0.32
1 mM Zn^{+2}	1.07	1.46	0.47	3.56	0.43	0.19	0.39
2 mM Zn^{+2}	1.02	1.26	0.377	3.18	0.45	0.25	0.30
3 mM Zn^{+2}	1.01	1.16	0.341	3.12	0.48	0.24	0.28
5 mM Zn^{+2}	1.13	1.19	0.364	3.52	0.48	0.27	0.25
7 mM Zn^{+2}	1.10	1.24	0.372	3.54	0.45	0.29	0.26
10 mM Zn^{+2}	1.08	1.27	0.357	3.73	0.39	0.33	0.28
15 mM Zn^{+2}	1.04	1.24	0.302	3.90	0.34	0.31	0.35
20 mM Zn^{+2}	1.02	1.38	0.299	4.08	0.31	0.32	0.37
30 mM Zn^{+2}	1.03	1.29	0.301	4.32	0.27	0.25	0.47
40 mM Zn^{+2}	1.02	1.88	0.649	4.52	0.17	0.15	0.67
DMPC	**χ2**	**τ_1 (ns)**	**τ_2 (ns)**	**τ_3 (ns)**	**a_1 (%)**	**a_2 (%)**	**a_3 (%)**
0 mM Zn^{+2}	0.99	1.68	0.37	3.89	0.42	0.13	0.45
1 mM Zn^{+2}	0.985	1.41	0.36	3.48	0.43	0.18	0.39
2 mM Zn^{+2}	1.02	1.35	0.36	3.20	0.45	0.24	0.31
3 mM Zn^{+2}	1.00	1.16	0.29	3.08	0.46	0.20	0.34
5 mM Zn^{+2}	1.04	1.15	0.31	2.95	0.46	0.24	0.30
10 mM Zn^{+2}	1.11	1.04	0.24	3.14	0.44	0.34	0.22
15 mM Zn^{+2}	1.07	1.09	0.25	3.44	0.39	0.41	0.20
20 mM Zn^{+2}	1.06	1.07	0.23	3.56	0.35	0.43	0.22
30 mM Zn^{+2}	1.09	1.08	0.24	3.73	0.33	0.39	0.28
40 mM Zn^{+2}	1.06	1.21	0.27	3.95	0.32	0.35	0.33
50 mM Zn^{+2}	1.14	1.46	0.43	4.33	0.26	0.24	0.50
POPC	**χ2**	**τ_1 (ns)**	**τ_2 (ns)**	**τ_3 (ns)**	**a_1 (%)**	**a_2 (%)**	**a_3 (%)**
0 mM Zn^{+2}	1.19	1.05	0.10	2.89	0.43	0.31	0.27
1 mM Zn^{+2}	1.91	0.97	0.09	2.76	0.37	0.37	0.25
2 mM Zn^{+2}	1.54	1.09	0.07	2.82	0.35	0.42	0.23

3 mM Zn^{+2}	1.24	1.00	0.07	2.81	0.33	0.46	0.21
5 mM Zn^{+2}	1.29	1.01	0.06	2.84	0.29	0.52	0.19
7 mM Zn^{+2}	1.08	1.22	0.31	3.03	0.50	0.19	0.32
10 mM Zn^{+2}	1.05	1.18	0.30	2.96	0.49	0.19	0.32
15 mM Zn^{+2}	1.04	1.21	0.33	2.97	0.49	0.18	0.33
20 mM Zn^{+2}	1.05	1.12	0.25	3.00	0.51	0.16	0.33
30 mM Zn^{+2}	1.02	1.16	0.28	2.92	0.50	0.18	0.33
40 mM Zn^{+2}	1.14	1.23	0.35	2.95	0.48	0.19	0.33

 # Experimental error in the measurement is around 5%.

Table 2.3 Lifetime components and normalized amplitudes of time resolved data for lipid bilayer-PRODAN at 440 nm upon increasing the concentration of Ca^{2+} at fixed lipid concentration (0.6 mM)#

DPPC	**χ2**	**τ_1 (ns)**	**τ_2 (ns)**	**τ_3 (ns)**	**a_1 (%)**	**a_2 (%)**	**a_3 (%)**
0 mM Ca^{+2}	1.008	1.83	0.58	4.28	0.46	0.22	0.32
1 mM Ca^{+2}	1.00	1.23	0.416	2.93	0.43	0.22	0.35
2 mM Ca^{+2}	1.04	1.12	0.33	2.84	0.46	0.21	0.33
3 mM Ca^{+2}	1.08	1.09	0.31	2.78	0.47	0.17	0.36
5 mM Ca^{+2}	1.11	1.05	0.32	2.77	0.48	0.17	0.35
7 mM Ca^{+2}	1.11	1.05	0.336	2.77	0.47	0.13	0.40
10 mM Ca^{+2}	1.00	1.15	0.384	2.79	0.44	0.18	0.38
15 mM Ca^{+2}	1.06	1.11	0.43	2.79	0.44	0.17	0.39
20 mM Ca^{+2}	1.18	1.10	0.35	2.84	0.46	0.13	0.41
30 mM Ca^{+2}	1.12	1.13	0.384	2.90	0.44	0.16	0.40
40 mM Ca^{+2}	1.03	1.16	0.39	2.97	0.44	0.15	0.41
DMPC	**χ2**	**τ_1 (ns)**	**τ_2 (ns)**	**τ_3 (ns)**	**a_1 (%)**	**a_2 (%)**	**a_3 (%)**
0 mM Ca^{+2}	0.99	1.68	0.37	3.89	0.42	0.13	0.45
1 mM Ca^{+2}	1.04	1.50	0.54	3.49	0.40	0.19	0.41
2 mM Ca^{+2}	1.01	1.41	0.48	3.32	0.42	0.18	0.40
3 mM Ca^{+2}	1.095	1.57	0.52	3.26	0.44	0.18	0.38
4 mM Ca^{+2}	1.04	1.34	0.36	3.10	0.43	0.13	0.44
5 mM Ca^{+2}	1.06	1.33	0.40	3.05	0.43	0.11	0.46
7 mM Ca^{+2}	1.08	1.31	0.39	3.07	0.43	0.11	0.46

10 mM Ca^{+2}	1.09	1.36	0.40	3.12	0.42	0.10	0.48
15 mM Ca^{+2}	1.13	1.25	0.41	3.20	0.41	0.09	0.50
20 mM Ca^{+2}	1.12	1.39	0.39	3.37	0.42	0.13	0.45
30 mM Ca^{+2}	1.14	1.27	0.36	3.30	0.41	0.10	0.49
40 mM Ca^{+2}	1.12	1.36	0.35	3.38	0.42	0.15	0.44
50 mM Ca^{+2}	1.21	1.24	0.24	3.45	0.40	0.11	0.48
POPC	**$\chi 2$**	**τ_1 (ns)**	**τ_2 (ns)**	**τ_3 (ns)**	**a_1 (%)**	**a_2 (%)**	**a_3 (%)**
0 mM Ca^{+2}	1.19	1.05	0.10	2.89	0.43	0.31	0.27
1 mM Ca^{+2}	1.06	1.17	0.33	2.82	0.48	0.19	0.33
2 mM Ca^{+2}	1.09	1.13	0.28	2.90	0.49	0.20	0.31
3 mM Ca^{+2}	1.07	1.20	0.35	2.95	0.48	0.17	0.34
5 mM Ca^{+2}	1.01	1.16	0.26	2.91	0.48	0.19	0.33
7 mM Ca^{+2}	1.13	1.13	0.36	2.81	0.48	0.20	0.32
10 mM Ca^{+2}	1.04	1.12	0.30	2.81	0.49	0.19	0.32
15 mM Ca^{+2}	1.08	1.21	0.27	2.80	0.50	0.18	0.32
20 mM Ca^{+2}	1.10	1.15	0.27	2.86	0.47	0.23	0.30
30 mM Ca^{+2}	1.11	1.08	0.29	2.84	0.50	0.20	0.30
40 mM Ca^{+2}	1.11	1.15	0.29	2.80	0.49	0.19	0.32

#Experimental error in the measurement is around 5%.

To investigate metal-induced changes in the size and surface charge of the lipid bilayers, we also performed DLS and zeta potential measurements at different pH values (pH ~ 7, and pH ~ 5.5). The representative DLS results are shown in Figure 2.10 for the DMPC lipid bilayer. For DPPC and POPC, the results are shown in Figure 2.11 and Figure 2.12. We observe that for the DPPC and DMPC bilayers, the size increases significantly upon binding with metal ions at pH ~7, while it remains the same for any of the metal ions upon interaction with the POPC bilayer. Interestingly, at lower pH, we find that none of these metal ions increases the size of the lipid bilayers. The zeta potential results are shown in Figure 2.13. Among the three metal ions, the lipid bilayers have the highest surface charge in the presence of Zn^{2+} followed by Ca^{2+} and Mg^{2+}. Zeta potential data also reveal that surface charge is much higher at pH ~ 7 compared to pH ~ 5.5.

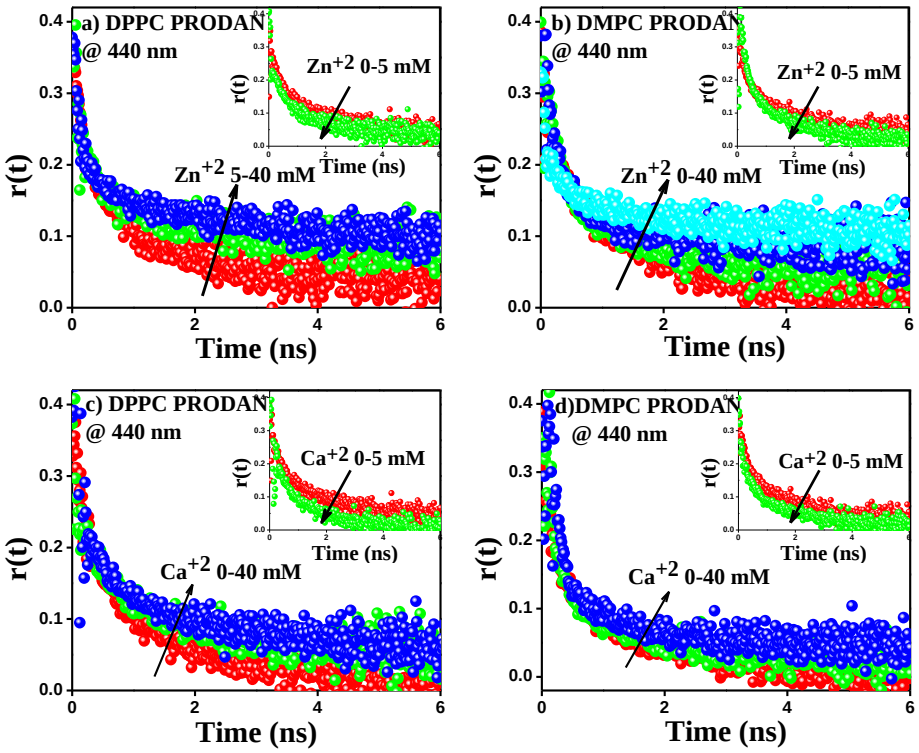

Figure 2.5 Anisotropy decays of PRODAN in lipid bilayers at various concentrations of Zn^{2+} for (a) DPPC and (b) DMPC bilayers at 440 nm (inset shows a decrease in rotational relaxation for Zn^{2+} concentrations from 0 to 5 mM) and at various concentrations of Ca^{2+} for (c) DPPC and (d) DMPC bilayers at 440 nm (inset shows a decrease in rotational relaxation for the concentration of Ca^{2+} from 0 to 5 mM).

2.2.2 Discussion:

2.2.2.1. Interaction of PRODAN with lipid bilayer: Before going into a detailed discussion about the metal ion–lipid bilayer interaction, let us discuss the emission feature of PRODAN in an aqueous medium and different bilayers. It has been reported that PRODAN undergoes intramolecular charge transfer (ICT) in the excited state upon forming a local excited (LE) state. In nonpolar solvents, the LE state predominates while in a polar solvent, the CT state is prevalent *[61]*. Earlier, Maroncelli and co-workers reported the spectral relaxation of PRODAN in terms of a continuous solvation process *[62]*. Thus, PRODAN displays a very high solvatochromic shift ranging from 435 nm to 540 nm in an aqueous medium. The primary factor behind the solvatochromic shift was the high change in dipole moment upon excitation (μ 20 D) *[63]*. Balter et al. reported that hydrogen bonding also contributes to a

very large Stokes shift *[64]*. However, Samanta et al. reported that the change in dipole moment was around 4.5 D *[65]*. PRODAN has been used to study solvation dynamics in organized media such as reverse micelles *[66–68]*. It has been observe that at longer wavelengths, PRODAN precedes with a rise component in reverse micelles, which is attributed to the solvation of PRODAN. It is reported that the LE and CT states display different solvations for PRODAN.

In the lipid bilayer (Figure 2.1), the appearance of a LE band indicates that PRODAN experiences a non-polar environment. The LE band is most prominent in the DPPC and DMPC bilayers while in the POPC bilayer, there is a significant overlap with the TICT band. The $E_{T(30)}$ values for DPPC, DMPC, POPC and DOPC liposomes are 41.7, 47, 52 and 54 kcal/mol, respectively *[54]*. The difference in micropolarity in different liposomes could be attributed to the higher phase transition temperature of DPPC and DMPC due to which these lipid bilayers remain in the sol-gel (SG) phase at experimental temperature. On the other hand, POPC, because of its very low phase transition temperature, remains in the liquid crystalline (LC) phase. Thus, the LE state emission of PRODAN is not distinct in POPC. The lifetime data indicate that t_3, which originates from the lipid bilayers, is in accordance with the phase transition temperature of the lipids used in this study, i.e. DPPC > DMPC > POPC (Table 2.1). The observation indicates that PRODAN molecules experience a more non-polar environment in the gel phase of the DPPC bilayer than in the DMPC or POPC bilayer.

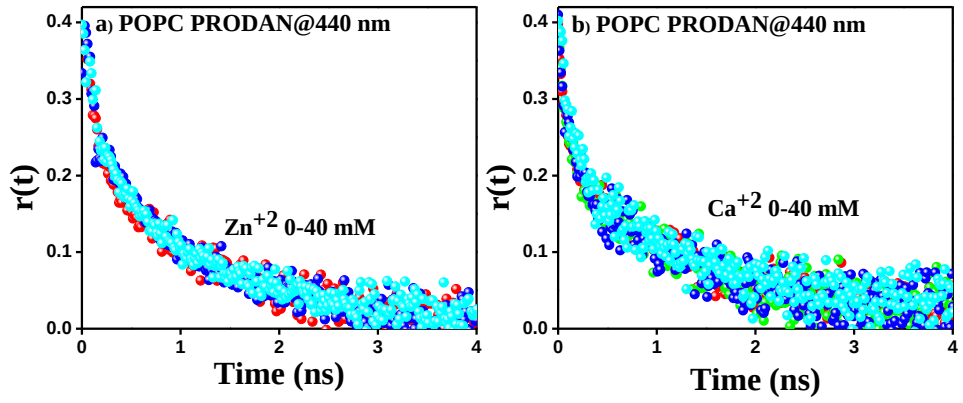

Figure 2.6 Time resolved decay curves of PRODAN in a) POPC-Zn^{+2} (0-40 mM) and b) POPC-Ca^{+2} (0-40 mM) at 440 nm.

2.2.2.2 Interaction of metal ions with the lipid bilayer: In the presence of metal ions, significant changes take place in the emission properties of PRODAN. We summarize the following important observations. (i) The polarization data reveal that with increasing Zn^{2+} concentration, the fractional intensity at the blue end increases and that in the red end decreases for the DPPC and DMPC bilayers. This fact indicates that Zn^{2+} causes gelation in these lipid bilayers possibly by dehydration. However, for the POPC bilayer, the polarization data did not show any significant change, indicating that Zn^{2+} does not interact much with the POPC bilayer. In the case of Ca^{2+}, a similar kind of observation was noted. We observe that a low concentration of metal ion increases the fluidity of both DPPC and DMPC bilayers while at relatively higher concentration, gelation occurs. Similar to Zn^{2+}, we observe that Ca^{2+} does not interact with the POPC bilayer. (ii) When comparing the Zn^{2+} and Ca^{2+} ions in terms of their interaction with the lipid bilayers, we find that Zn^{2+} is more effective in inducing dehydration than Ca^{2+}. Among all the lipid bilayers, DPPC displays the strongest interaction with the metal ions. (iii) In the case of Mg^{2+}, polarization data indicate that the fractional intensity at the blue end decreases with increasing Mg^{2+} concentration. This fact clearly indicates that Mg^{2+} causes hydration in the DPPC and DMPC bilayers. Similar to other metal ions, the POPC lipid bilayer is not very sensitive towards Mg^{2+} concentration. Therefore, in summary, we observe that Zn^{2+} and Ca^{2+} cause dehydration in liposomes while Mg^{2+} hydrates the liposomal surface by carrying water molecules. We have depicted the above phenomena as a pictorial representation in Scheme 2.1 and it is shown that with the addition of Zn^{2+} and Ca^{2+}, the fluidity decreases because of dehydration while in the presence of Mg^{2+}, it increases because of hydration.

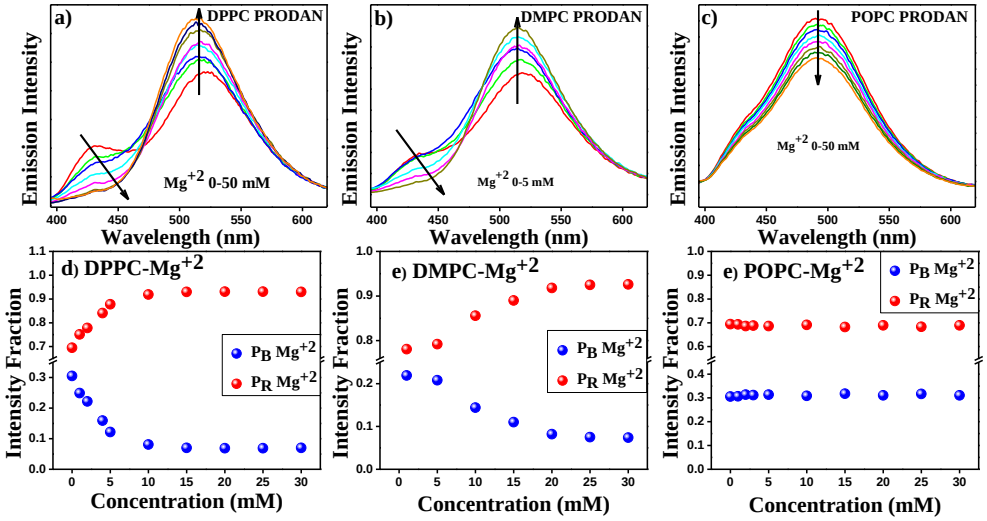

Figure 2.7 Emission spectra of PRODAN at various concentrations of Mg^{2+} for (a) DPPC, (b) DMPC and (c) POPC bilayers. Estimated intensity fraction as a function of concentration of Mg^{2+} in (d) DPPC, (e) DMPC and (f) POPC.

2.2.2.3 Interaction of Zn^{2+} and Ca^{2+} with the DMPC and DPPC lipid bilayer: To account for the above observations, we first discuss the interaction of Zn^{2+} and Ca^{2+} with the DPPC, DMPC, and POPC bilayers because these two metal ions bring about a similar kind of changes in all the lipid bilayers. It is reveal from Figure 2.2d-f and Figure 2.3d-f that the polarization at the blue end increases in the DPPC and DMPC bilayers as a function of Zn^{2+} and Ca^{2+} concentration and this clearly indicates that these metal ions cause gelation in the DPPC and DMPC bilayers (Scheme 2.1). The binding of alkali and alkaline earth metal cations to a phospholipid membrane is endothermic, indicating that the adsorption of the ions to the membrane is mainly entropy-driven. This factor is responsible for the disruption of H bonds between water molecules *[4, 69]*. Thus, we observe the loss of water in the primary hydration shell of lipids upon bonding with metal ions. Our results are consistent with the reports of Binder and co-workers *[5]*.

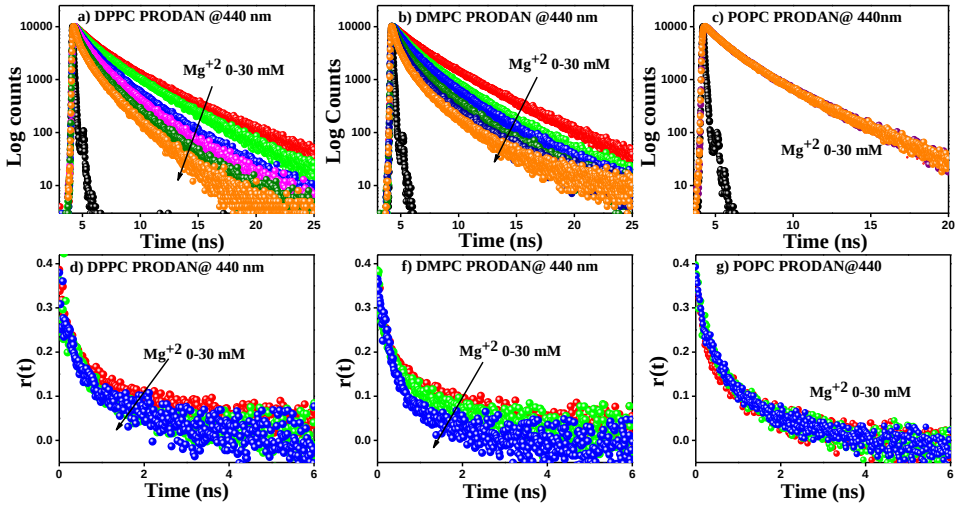

Figure 2.8 Time resolved decay curves of PRODAN in different lipid bilayers at various concentrations of Mg^{2+} for (a) DPPC, (b) DMPC, and (c) POPC bilayers at 440 nm and anisotropy decays of PRODAN in lipid bilayers at various concentrations of Mg^{2+} for (d) DPPC, (e) DMPC, and (f) POPC bilayers at 440 nm.

Table 2.4 Lifetime components and normalized amplitudes of time resolved data for lipid bilayer-PRODAN at 440 nm upon increasing the concentration of Mg^{2+} at fixed lipid concentration (0.6 mM)#

DPPC	**χ2**	**τ_1 (ns)**	**τ_2 (ns)**	**τ_3 (ns)**	**a_1 (%)**	**a_2 (%)**	**a_3 (%)**
0 mM Mg^{+2}	1.008	1.83	0.58	4.28	0.46	0.22	0.32
1 mM Mg^{+2}	1.02	1.44	0.44	3.46	0.41	0.21	0.39
2 mM Mg^{+2}	0.973	1.13	0.33	2.81	0.45	0.25	0.30
3 mM Mg^{+2}	1.17	1.08	0.30	2.74	0.47	0.24	0.29
5 mM Mg^{+2}	1.11	0.96	0.22	2.47	0.45	0.26	0.29
7 mM Mg^{+2}	1.03	0.88	0.195	2.40	0.43	0.35	0.22
10 mM Mg^{+2}	0.98	0.84	0.186	2.34	0.37	0.45	0.18
15 mM Mg^{+2}	1.18	0.77	0.153	2.23	0.33	0.50	0.17
20 mM Mg^{+2}	1.16	0.67	0.14	2.07	0.32	0.51	0.17
30 mM Mg^{+2}	1.07	0.66	0.15	2.04	0.32	0.52	0.16
40 mM Mg^{+2}	1.05	0.68	0.157	1.99	0.30	0.54	0.15
DMPC	**χ2**	**τ_1 (ns)**	**τ_2 (ns)**	**τ_3 (ns)**	**a_1 (%)**	**a_2 (%)**	**a_3 (%)**
0 mM Mg^{+2}	0.99	1.68	0.37	3.89	0.42	0.13	0.45
1 mM Mg^{+2}	1.14	1.42	0.41	3.32	0.45	0.23	0.31

2 mM Mg^{+2}	1.08	1.31	0.35	3.22	0.48	0.21	0.32
3 mM Mg^{+2}	1.07	1.21	0.33	3.06	0.47	0.22	0.31
4 mM Mg^{+2}	1.07	1.20	0.32	2.99	0.42	0.24	0.29
5 mM Mg^{+2}	1.02	1.19	0.33	2.98	0.47	0.25	0.28
7 mM Mg^{+2}	1.11	1.01	0.23	2.74	0.45	0.30	0.24
10 mM Mg^{+2}	1.11	0.96	0.24	2.71	0.42	0.38	0.19
15 mM Mg^{+2}	1.15	0.77	0.15	2.54	0.36	0.51	0.13
20 mM Mg^{+2}	1.06	0.76	0.16	2.54	0.34	0.56	0.10
30 mM Mg^{+2}	1.11	0.72	0.15	2.45	0.33	0.58	0.10
40 mM Mg^{+2}	1.10	0.77	0.16	2.40	0.33	0.58	0.10
POPC	**$\chi 2$**	**τ_1 (ns)**	**τ_2 (ns)**	**τ_3 (ns)**	**a_1 (%)**	**a_2 (%)**	**a_3 (%)**
0 mM Mg^{+2}	1.19	1.05	0.10	2.89	0.43	0.31	0.27
1 mM Mg^{+2}	1.07	1.23	0.349	2.97	0.48	0.18	0.34
2 mM Mg^{+2}	1.11	1.10	0.23	2.90	0.50	0.17	0.33
3 mM Mg^{+2}	1.04	1.25	0.37	3.04	0.49	0.21	0.30
5 mM Mg^{+2}	1.18	1.17	0.25	2.98	0.48	0.17	0.34
7 mM Mg^{+2}	1.04	1.21	0.36	2.96	0.48	0.20	0.32
10 mM Mg^{+2}	1.01	1.19	0.31	2.96	0.49	0.19	0.32
15 mM Mg^{+2}	1.09	1.17	0.23	2.99	0.50	0.18	0.32
20 mM Mg^{+2}	1.10	1.14	0.25	2.94	0.50	0.18	0.32
30 mM Mg^{+2}	1.09	1.04	0.26	2.80	0.47	0.23	0.30
40 mM Mg^{+2}	1.11	1.20	0.29	2.95	0.49	0.19	0.32

 # Experimental error in the measurement is around 5%.

We note that the extent of polarization induced by Zn^{2+} is higher as compared to that caused by Ca^{2+} (Figure 2.2d and 2.3d). The dehydration order of Zn^{2+} and Ca^{2+} is in accordance with the binding order as reported by Binder and coworkers *[5, 17]*. The higher polarization in the case of Zn^{2+} could be due to the fact that Zn^{2+} has a stronger binding with lipid head groups as compared to Ca^{2+}. Binder and co-workers proposed that Zn^{2+} develops a covalent character with the phosphate and carbonyl moieties of the lipid head groups *[5, 17]*. The conformation of the C–O–P–O–C backbone in the phospholipid head group changes upon interaction with Zn^{2+}, which drastically reduces the water

uptake capability of the lipid head group and consequently makes the lipid head group more hydrophobic. Zn^{2+} directly interacts with the carbonyl group and dehydrates the lipid bilayer [17]. The decreased gelation ability of Ca^{2+} as compared to Zn^{2+} most probably stems from the weaker binding of Ca^{2+} with the carbonyl moiety of the lipid head group. Further, the binding position of metal ions, type of binding with the lipid, and hydration free energy of the metal plays crucial roles. It has been reported that Ca^{2+} is positioned a little higher than the Zn^{2+}–carbonyl interaction site of the lipid head group and coordinates with the phosphate group by electrostatic interaction *[5, 34]*. While Zn^{2+} dehydrates both phosphate and carbonyl group regions, apparently Ca^{2+} binds only with the phosphate group, leading to the expulsion of water only from the phosphate group region. The ion obviously concurs with the water of the hydration shell that usually forms H-bonds to the phosphate oxygen. Calcium and phosphate groups possibly form inner-sphere complexes by removing water *[5]*. Interestingly, the polarization data (Figure 2.2 d-e and 2.3 d-e) indicate that initially (at very low concentration of metal ions), the intensity fraction of the blue end decreases upon binding with Ca^{2+} and Zn^{2+}. We propose that very low concentrations of Zn^{2+} and Ca^{2+} (up to ~3–5 mM) increase the fluidity of the interfacial region of the bilayer by hydration or restructuring the lipid bilayer. McManus et al. observed an initial rearrangement of the DPPC bilayer at very low (2–4 mM) concentrations of Ca^{2+} *[41]*. They also found that an increase in the lamellar repeat distance indicates that Ca^{2+} hydrates the lipid bilayer at very low concentrations *[41]*. However, at relatively higher concentrations, the gelation takes place possibly by dehydration of the lipid bilayer as reveal by the increase in intensity fraction at the blue end. Notably, we also found the extent of fluidization is higher in the case of Ca^{2+} than Zn^{2+} (Figure 2.2d-e and 2.3d-e). Ca^{2+} has higher hydration free energy and carries some water molecules in its primary hydration shell, which helps to hydrate the bilayer rather than dehydrate it *[39, 40]*.

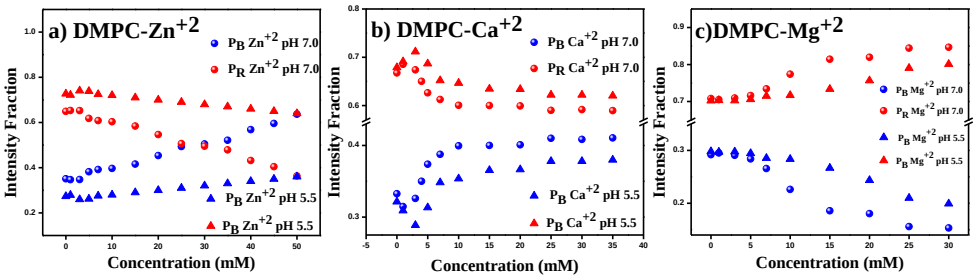

Figure 2.9 Estimated intensity fraction as a function of metal ion concentration a) Zn^{2+}, b) Ca^{2+} and c) Mg^{2+} in DMPC lipid bilayers at pH~7.0 and pH~5.5.

To validate the conjecture of fluidity and subsequent gelation induced by metal ions, we turn to the lifetime measurements that yield some interesting results. Table 2.2 and 2.3, indicate that with the immediate addition of Zn^{2+} and Ca^{2+}, the longest component (τ_3), which originates from the bilayer bound PRODAN molecules, decreases along with its amplitude (a_3) initially up to 3 and 5 mM for Zn^{2+} and Ca^{2+} (Figure 2.4a-b and d-e), respectively. However, at higher concentrations, both the τ_3 and a_3 increase. We explain this observation by taking into account the swelling of the lipid bilayer in the presence of different metal ions. It has been observed that the addition of divalent metal ions increases the lamellar repeat distance by increasing the water layer of the lipid bilayer up to a certain concentration of the metal salt. At relatively higher concentrations, the swelling stops due to screening of the head groups *[18–39]*. In the present case, we observe that τ_3 becomes almost constant in the concentration range of around 5–10 mM of Zn^{2+} and Ca^{2+} in both DPPC and DMPC bilayers. The rapid increase in τ_3 and its amplitude is observe with the further addition of the salts. This observation is consistent with the steady state results. We already mentioned that Zn^{2+} and Ca^{2+} at low concentrations initially restructure the DPPC lipid bilayer, which may increase hydration. Notably, for DMPC, we observe that the hydration effect (at low concentration) is not much more prominent than that of the DPPC bilayer (See Table 2.2 and 2.3). This could be due to the fact that DMPC remains in the liquid crystalline phase (or in between order-disorder phase) and at room temperature, DMPC already carries more water molecules than DPPC. Therefore, both the Zn^{2+} and Ca^{2+} metal ions have a limited scope to hydrate DMPC bilayers than DPPC. The anisotropy measurements also reveal that at

low concentrations of Zn^{2+} and Ca^{2+}, the rotational relaxation becomes significantly faster (inset of Figure 2.5). In general, the rotational relaxation becomes faster if the rigidity of the system is reduced. Thus, the faster rotational relaxation for Zn^{2+} and Ca^{2+} up to 5 mM concentration clearly confirms that the fluidity of the membrane increases, which results in loosening of the packing of the bilayer at low concentrations of these metal ions. Nevertheless, above the concentration of 5 mM metal ions, the rotational relaxation becomes significantly slower in the presence of Zn^{2+}. We note that the rotational relaxation decay in the presence of Zn^{2+} ions possesses a very long tail (Figure 2.5a-b), which indicates that rotation is severely hindered owing to the rigidification of the membrane. The observation is in accordance with the steady state measurements. However, for Ca^{2+}, we observe that rotational relaxation decay did not slow as significantly as in the case of Zn^{2+} (Figure 2.5c-d), which confirms that the dehydration of the membrane and subsequent rigidification induced by Ca^{2+} takes place to a lesser extent than that induced by Zn^{2+}. The observation is in accordance with the steady state and lifetime measurements.

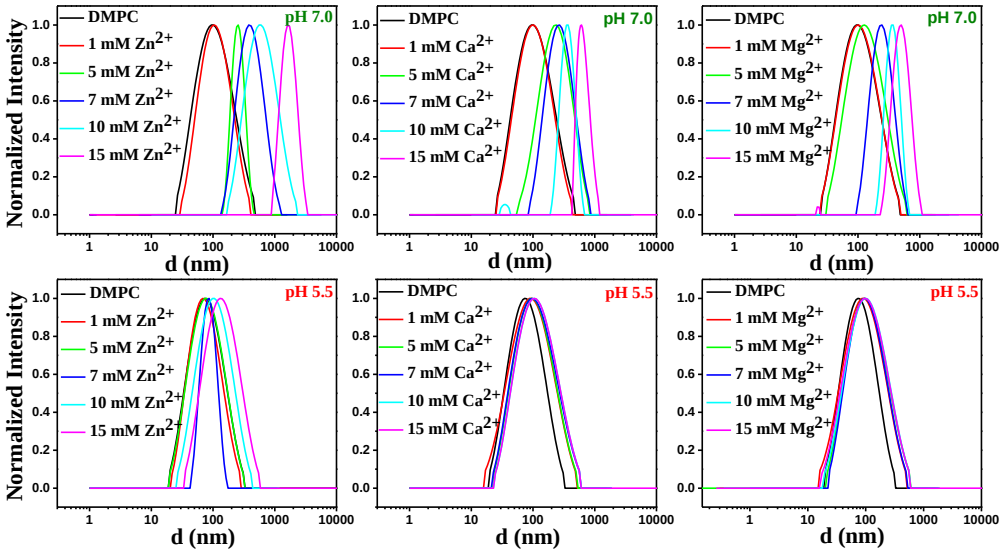

Figure 2.10 Normalized DLS spectra of DMPC lipid bilayers in the presence of different concentrations of metal ions at pH 7.0 and pH 5.5.

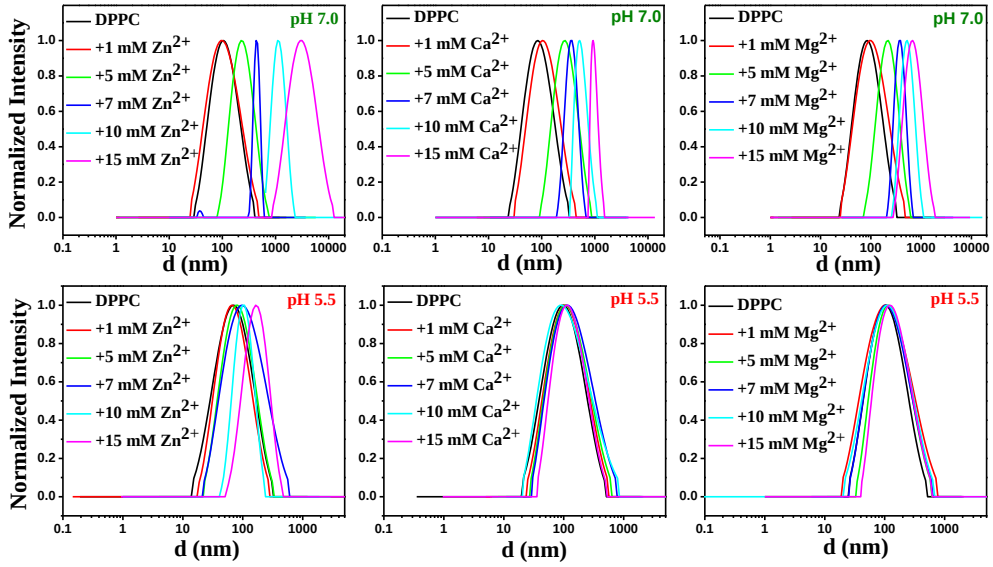

Figure 2.11 Normalized DLS spectra of DPPC lipid bilayers in the presence of different concentrations of metal ions at pH 7.0 and pH 5.5.

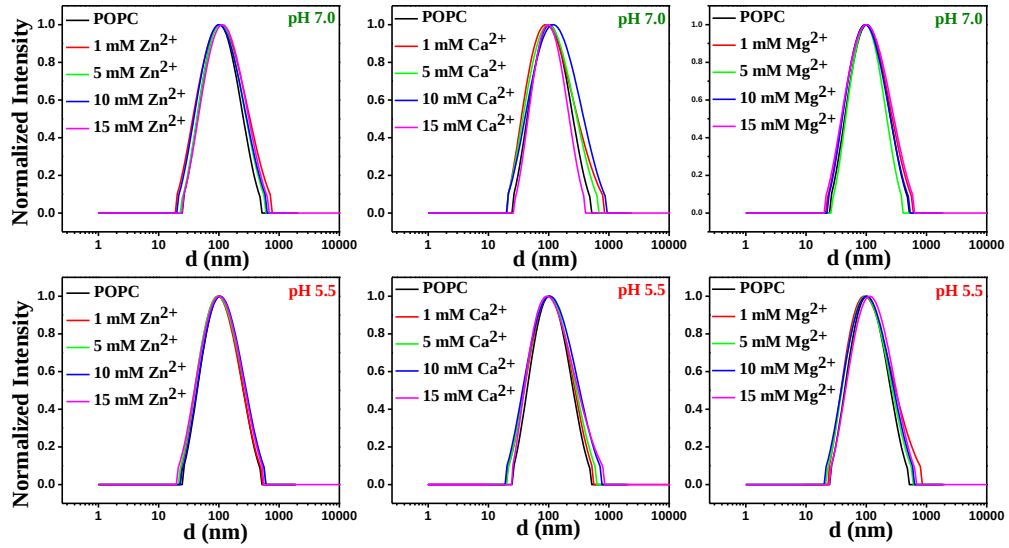

Figure 2.12 Normalized DLS spectra of POPC lipid bilayers in the presence of different concentrations of metal ions at pH 7.0 and pH 5.5.

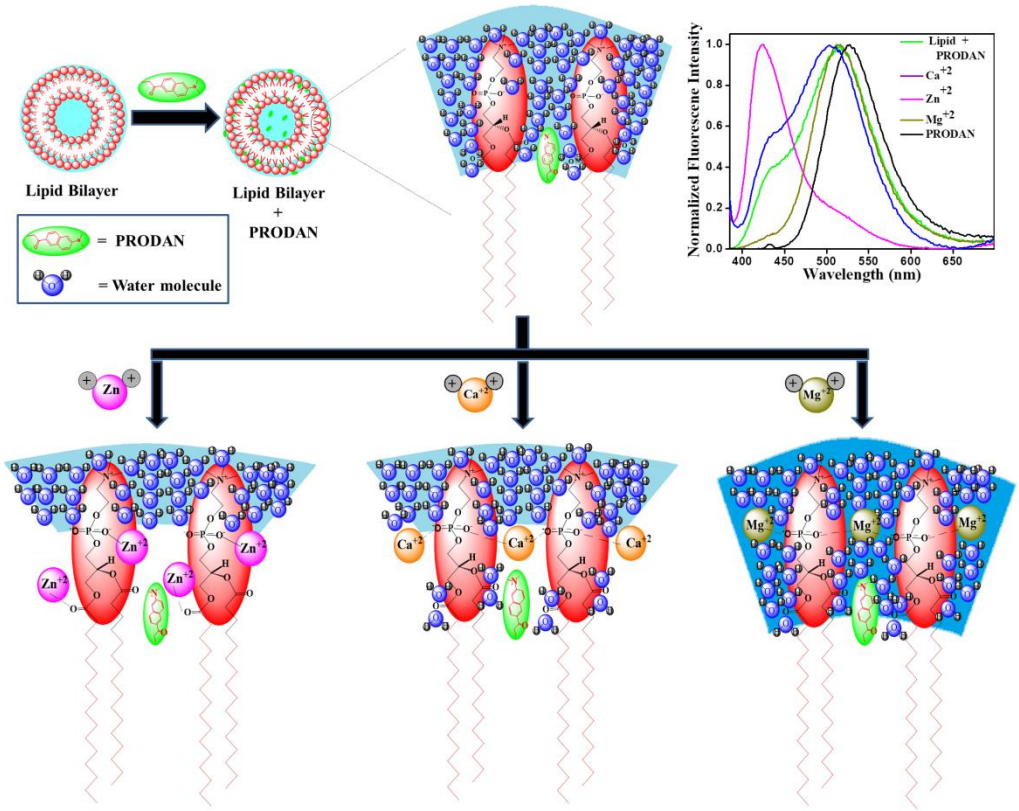

Scheme 2.1 Pictorial representation of the effect of various metal ions in lipid bilayers.

2.2.2.4 Interaction of Zn^{2+} and Ca^{2+} with the POPC lipid bilayer: Although Zn^{2+} and Ca^{2+} have displayed considerable affinity towards the DPPC and DMPC bilayers, much less interaction was observed for these metal ions with the POPC lipid bilayers. The dehydration of the POPC lipid bilayer is not seen either with Zn^{2+} or Ca^{2+} (Figure 2.2c and 2.3c). The weaker interaction of Zn^{2+} and Ca^{2+} is in accordance with earlier reports. Binder and co-workers reported that Zn^{2+} interacts directly with the carbonyl group at low levels of hydration *[17]*. Therefore, it is expected that Zn^{2+} and Ca^{2+} are not likely to interact with the POPC bilayer, which remains in the liquid crystalline phase under the experimental conditions. We can explain the present phenomena in the light of a recent report by Raviv and co-workers *[18]*. It is reported that unsaturated lipids such as POPC or DOPC do not absorb divalent cations Zn^{2+} and Ca^{2+} as strongly as saturated lipids do. The presence of the double bond in the lipid tail significantly reduces the ion adsorption of metal ions for unsaturated lipids. The saturated carbon chains prefer to remain in an all *trans* conformation and create a tightly packed membrane in which the head groups have little configurational and rotational entropy *[18]*. On the other hand,

lipids with unsaturated tails create membranes with relatively loose packing because the hydrophobic tail is kinky due to the *cis* configuration of their double bonds. The relatively loose packing enables free rotation of the head groups. In the case of lipids with saturated tails, head group entropy is significantly lower. Therefore, the binding of divalent cations to membranes with fully saturated tails is stronger because the systems gain ion-dipole enthalpy and lose little head group entropy. The other explanation is that POPC being in the liquid crystalline phase at room temperature will have a higher area per lipid head group as compared to that of DPPC or DMPC lipids, which remain in the gel phase and nearly in the crystalline phase. Therefore, the head group of the POPC lipid bilayer can capture a smaller number of cations than the head groups of DMPC and DPPC, leading to an overall weak interaction.

2.2.2.5 pH-dependent interaction of the metal ions with the lipid vesicles: We checked the effect of pH on the binding of metal ions with the lipid head group. Figure 2.9 illustrates that in an acidic medium (pH ~ 5.50), Zn^{2+} and Ca^{2+} exhibit less binding affinity towards liposomal head groups compared to pH~7.0. The polarization data at lower pH indicate that the extent of dehydration induced by Zn^{2+} and Ca^{2+} is significantly reduced in all the lipid bilayers. Liu et al. reported that at lower pH, H^{+} may bind with the phosphate group, which may prevent the metal ions from binding to the head groups *[70]*.

Table 2.5 Hydrodynamic diameter of DMPC lipid bilayers as obtained from DLS measurement in presence of different concentration of Metal salts (Zn^{+2}, Ca^{+2} and Mg^{+2}).

	Average Size at pH 7.0 (nm)	Average Size at pH 5.5 (nm)
DMPC	90.3	69.8
DMPC+ 1 mM Zn^{+2}	101.4	68.4
DMPC+ 5 mM Zn^{+2}	242.8	69.6
DMPC+ 7 mM Zn^{+2}	365.6	78.1
DMPC+ 10 mM Zn^{+2}	776.6	123.8
DMPC+ 15 mM Zn^{+2}	1605.3	208.4

	Average Size at pH 7.0 (nm)	Average Size at pH 5.5 (nm)
DMPC	90.3	69.8
DMPC+ 1 mM Ca^{+2}	95.6	72.4
DMPC+ 5 mM Ca^{+2}	242.9	85.5
DMPC+ 7 mM Ca^{+2}	349.7	87.6
DMPC+ 10 mM Ca^{+2}	426.7	95.0
DMPC+ 15 mM Ca^{+2}	733.1	95.5
	Average Size at pH 7.0 (nm)	Average Size at pH 5.5 (nm)
DMPC	90.0	69.8
DMPC+ 1 mM Mg^{+2}	93.6	75.6
DMPC+ 5 mM Mg^{+2}	90.3	82.3
DMPC+ 7 mM Mg^{+2}	224.9	85.5
DMPC+ 10 mM Mg^{+2}	332.8	87.6
DMPC+ 15 mM Mg^{+2}	461.8	85.4

Table 2.6 Hydrodynamic diameter of DPPC lipid bilayers as obtained from DLS measurement in presence of different concentration of Metal salts (Zn^{+2}, Ca^{+2}, and Mg^{+2}).

	Average Size at pH 7.0 (nm)	Average Size at pH 5.5 (nm)
DPPC	94.3	84.4
DPPC+ 1 mM Zn^{+2}	98.2	85.1
DPPC+ 5 mM Zn^{+2}	307.6	89.8
DPPC+ 7 mM Zn^{+2}	430.9	97.3
DPPC+ 10 mM Zn^{+2}	982.6	129.5
DPPC+ 15 mM Zn^{+2}	2203.5	189.4
	Average Size at pH 7.0 (nm)	Average Size at pH 5.5 (nm)
DPPC	94.3	84.4
DPPC+ 1 mM Ca^{+2}	97.2	86.1
DPPC+ 5 mM Ca^{+2}	267.6	90.4
DPPC+ 7 mM Ca^{+2}	395.1	97.5
DPPC+ 10 mM Ca^{+2}	978.7	83.7

DPPC+ 15 mM Ca^{+2}	1407.8	101.5
	Average Size at pH 7.0 (nm)	Average Size at pH 5.5 (nm)
DPPC	94.3	84.4
DPPC+ 1 mM Mg^{+2}	97.7	83.8
DPPC+ 5 mM Mg^{+2}	276.1	99.5
DPPC+ 7 mM Mg^{+2}	360.9	86.5
DPPC+ 10 mM Mg^{+2}	513.1	87.1
DPPC+ 15 mM Mg^{+2}	687.5	98.1

Table 2.7 Hydrodynamic diameter of POPC lipid bilayers as obtained from DLS measurement in presence of different concentration of Metal salts (Zn^{+2}, Ca^{+2} and Mg^{+2}).

	Average Size at pH 7.0 (nm)	Average Size at pH 5.5 (nm)
POPC	73.4	82.0
POPC+ 1 mM Zn^{+2}	78.2	86.9
POPC+ 5 mM Zn^{+2}	81.3	84.3
POPC+ 7 mM Zn^{+2}	93.5	87.9
POPC+ 10 mM Zn^{+2}	91.6	86.5
POPC+ 15 mM Zn^{+2}	97.2	81.0
	Average Size at pH 7.0 (nm)	Average Size at pH 5.5 (nm)
POPC	73.4	82.0
POPC+ 1 mM Ca^{+2}	87.3	96.7
POPC+ 5 mM Ca^{+2}	86.6	89.6
POPC+ 7 mM Ca^{+2}	94.4	93.5
POPC+ 10 mM Ca^{+2}	94.3	84.3
POPC+ 15 mM Ca^{+2}	91.5	87.6
	Average Size at pH 7.0 (nm)	Average Size at pH 5.5 (nm)
POPC	73.4	82.0
POPC+ 1 mM Mg^{+2}	89.3	83.6
POPC+ 5 mM Mg^{+2}	85.2	81.5

POPC+ 7 mM Mg^{+2}	85.9	81.4
POPC+ 10 mM Mg^{+2}	96.5	85.1
POPC+ 15 mM Mg^{+2}	95.6	84.9

In order to further study the effect of pH on metal ion binding with the lipid bilayer, we have performed the dynamic light scattering (DLS) measurement of the lipid vesicles in presence of metal ions at different pH values. It is observed that at pH ~ 7, with an increase in the metal salt concentration, the size of DMPC (Figure 2.10 and Table 2.5) and DPPC (Figure 2.11 and Table 2.6) increases significantly, indicating that a strong interaction takes place between these metal ions, causing aggregation of the lipid bilayer. Interestingly, we did not find any kind of strong interaction with the POPC bilayer. The size did not increase for the POPC bilayer (Figure 2.12 and Table 2.7). Recently, Liu et al. reported that Zn^{2+} displays much less affinity towards the DOPC lipid bilayer [70]. Moreover, the isothermal titration calorimetry (ITC) experiments reported by this group reveal that heat change for the DOPC–Zn^{2+} interaction is almost negligible, which indicates that DOPC has a lower binding ability with Zn^{2+} [70]. The result is similar to that obtained from the steady state and DLS measurements. Since both POPC and DOPC possess a double chain in their hydrophobic tail, they display similar behavior towards metal ions. Further at lower pH (~5.50), the size of all lipid bilayers did not increase significantly. This fact indicates that at lower pH, the uptake of metal ions in the lipid bilayer is significantly reduced. We also pointed out that amongst the three metal ions, the addition of Zn^{2+} to the lipid bilayers (Table 2.5, Table 2.6, and Table 2.7) causes a more aggregated structure followed by Ca^{2+} and Mg^{2+}. The zeta potential measurements reveal that the potential goes from a slightly negative value to a highly positive value upon interaction with the metal ions (Figure 2.13 and Table 2.8). On the other hand, zeta potential is reduced significantly at lower pH for all the metal ions. Again, we observe that the POPC bilayer always shows a lower zeta potential value as compared to other lipid bilayers upon interaction with the metal ions (Figure 2.13), indicating the lower absorption of metal ions compared to DMPC and DPPC. This result is consistent with our steady state experiments.

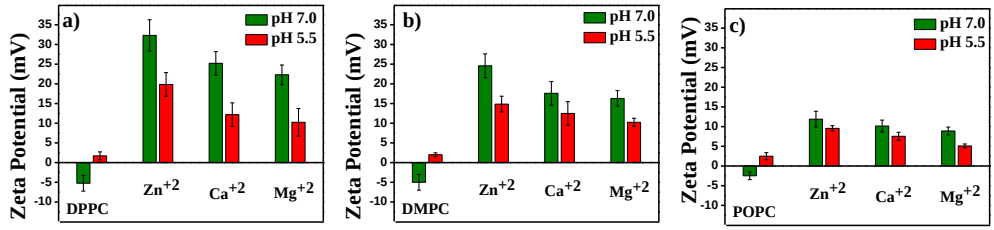

Figure 2.13 Zeta potential of (a) DPPC, (b) DMPC and (c) POPC lipid bilayers in the presence of different metal ions (40 mM) at pH 7.0 (green) and pH 5.5 (red).

Table 2.8 Zeta potential values of lipid bilayers in presence of different metal ions at fixed metal salt concentration (40 mM) at different pH. [#]

	Zeta Potential (mV) at pH 7.0	Zeta Potential (mV) at pH 5.5
DPPC	-5.23	+1.72
DPPC- Zn^{+2}	+32.29	+19.84
DPPC- Ca^{+2}	+25.19	+12.18
DPPC- Mg^{+2}	+22.30	+10.25
DMPC	-5.00	+2.01
DMPC- Zn^{+2}	+24.59	+10.25
DMPC- Ca^{+2}	+17.59	+12.48
DMPC- Mg^{+2}	+16.30	+14.84
POPC	-2.48	+2.49
POPC- Zn^{+2}	+11.89	+9.55
POPC- Ca^{+2}	+10.16	+7.56
POPC- Mg^{+2}	+8.89	+5.09

2.2.2.6 Interaction of Mg^{2+} with the lipid bilayers: While Zn^{2+} and Ca^{2+} induce drastic dehydration in the lipid bilayers, surprisingly; Mg^{2+} did not induce any dehydration in any of the bilayers. We observe that the band at 440

nm decreases continuously while that at 500 nm increases upon the addition of Mg^{2+} (Figure 2.7). The decrease in intensity at 440 nm and concurrent increase at 500 nm clearly indicate that Mg^{2+} induces hydration in the lipid bilayers (Scheme 2.1). The polarization data clearly indicate that the fractional intensity at the blue end steadily decreases with the increasing concentration of Mg^{2+}. Interestingly, in the case of Zn^{2+} and Ca^{2+}, fluidity increases at very low concentrations up to ~3-5 mM and at higher concentrations, significant dehydration takes place. In contrast, we observe that unlike Zn^{2+} and Ca^{2+}, dehydration did not take place for Mg^{2+} up to the concentration of 40 mM (Figure 2.7). The concurrent decays of lifetime measurements and rotational relaxation reveal the continuous increase in the fluidity of the membrane (Figure 2.8). This observation is contradictory to the observation of Binder and co-workers who reported that Mg^{2+} partially removes water from the phosphate group *[5]*. Earlier, it has been reported that metal ions swell the lipid bilayer. Alsop and co-workers reported that among the three metal ions studied in the present work, Mg^{2+} is most effective in swelling the lipid bilayer and the order was found to be $Mg^{2+} > Ca^{2+} > Zn^{2+}$ *[39]*. The hydration phenomena for different metal ions as revealed in the present study are in accordance with the report of Alsop and co-workers *[39]*. The uniqueness of Mg^{2+} over Ca^{2+} in hydrating the lipid bilayer may be explained by taking into account the high barrier of binding energy with lipid molecules. Yang and co-workers reported that Ca^{2+} gains the highest stability when bound to four lipid oxygen of the membrane rather than being hydrated in an aqueous solution. On the other hand, Mg^{2+} being tightly hydrated is reluctant to bind with the membrane by losing any hydrated water *[32]*. The bound state of Mg^{2+} to lipid oxygen is separated from the unbound states in an aqueous solution by a high free energy barrier, which is attributed to the high energy required for the partial dehydration of the first hydration shell of Mg^{2+}. Recently, Allnér and co-workers reported the strong binding of Mg^{2+} with its hydration layer. They also reported that the direct binding of Mg^{2+} with phosphate oxygen is unlikely as it requires a high energy barrier for dehydration *[71]*. From all these studies, it is evident that Mg^{2+} cannot dehydrate the lipid bilayer by forming bonds with the phosphate group. Alsop and co-workers reported that for Mg^{2+}, the number of water molecules in the lipid head group region is

higher than that for Zn^{2+} and Ca^{2+} *[39]*. Our study makes it clear that Mg^{2+} only increases the fluidity of the membrane while Zn^{2+} and Ca^{2+} induce significant dehydration.

2.3 Conclusion

In conclusion, we found that the metal ions interact differently with lipids of different chain lengths. The study reveals that Zn^{2+} and Ca^{2+} interact strongly with the DPPC and DMPC bilayers while the interaction is much less prominent with the POPC lipid bilayers. We found that Zn^{2+} and Ca^{2+} initially increase the fluidity of the membrane by swelling and after a certain concentration; they induce gelation in these lipid bilayers by dehydration. The lifetime measurements and time resolved anisotropy results indicate that Zn^{2+} is more effective in inducing dehydration as compared to Ca^{2+}. In contrast to this finding, we observe that Mg^{2+} does not dehydrate the lipid bilayer. The steady state polarization, lifetime measurements and time resolved data indicate that Mg^{2+} continuously hydrates the lipid bilayer. We explained this observation in light of the hydration free energy of Mg^{2+} and other metal ions.

2.4 References

1. Clarke, R. J., & Lüpfert, C. (1999). Influence of anions and cations on the dipole potential of phosphatidylcholine vesicles: a basis for the Hofmeister effect, Biophys. J., 76, 2614-2624. (DOI: 10.1016/S0006-3495(99)77414-X)

2. Lo Nostro, P., & Ninham, B. W. (2012). Hofmeister phenomena: an update on ion specificity in biology, Chem. Rev., 112, 2286-2322. (DOI: 10.1021/cr200271j)

3. Hofmeister, F. (1888). Zur lehre von der wirkung der salze, Archiv für experimentelle Pathologie und Pharmakologie, 24, 247-260. (DOI: 10.1007/BF01918191)

4. Garidel, P., & Blume, A. (1999). Interaction of alkaline earth cations with the negatively charged phospholipid 1, 2-dimyristoyl-sn-glycero-3-phosphoglycerol: a differential scanning and isothermal titration calorimetric study, Langmuir, 15, 5526-5534. (DOI: 10.1021/la990217a)

5. Binder, H., & Zschörnig, O. (2002). The effect of metal cations on the phase behavior and hydration characteristics of phospholipid membranes, Chem. Phys. Lipids, 115, 39-61. (DOI: 10.1016/S0009-3084(02)00005-1)

6. Garidel, P., & Blume, A. (2005). 1, 2-Dimyristoyl-sn-glycero-3-phosphoglycerol (DMPG) monolayers: influence of temperature, pH, ionic strength and binding of alkaline earth cations, Chem. Phys. Lipids, 138, 50-59. (DOI: 10.1016/j.chemphyslip.2005.08.001)

7. Klasczyk, B., Knecht, V., Lipowsky, R., & Dimova, R. (2010). Interactions of alkali metal chlorides with phosphatidylcholine vesicles, Langmuir, 26, 18951-18958. (DOI: 10.1021/la103631y)

8. Lis, L. J., Lis, W. T., Parsegian, V. A., & Rand, R. P. (1981). Adsorption of divalent cations to a variety of phosphatidylcholine bilayers, Biochemistry, 20, 1771-1777. (DOI: 10.1021/bi00510a010)

9. Tatulian, S. A. (1983). Effect of lipid phase transition on the binding of anions to dimyristoylphosphatidylcholine liposomes, Biochim. Biophys. Acta, Biomembr., 736, 189-195. (DOI: 10.1016/0005-2736(83)90283-3)

10. Tatulian, S. A., Gordeliy, V. I., Sokolova, A. E., & Syrykh, A. G. (1991). A neutron diffraction study of the influence of ions on phospholipid membrane interactions, Biochim. Biophys. Acta, Biomembr., 1070, 143-151. (DOI: 10.1016/0005-2736(91)90156-3)

11. Yeap, P. K., Lim, K. O., Chong, C. S., & Teng, T. T. (2008). Effect of calcium ions on the density of lecithin and its effective molecular volume in lecithin–water dispersions, Chem. Phys. Lipids, 151, 1-9. (DOI: 10.1016/j.chemphyslip.2007.09.001)

12. Lis, L. J., Rand, R. P., & Parsegian, V. A. (1980). Measurement of the Adsorption of Ca^{2+} and Mg^{2+} to Phosphatidyl Choline Bilayers, Bioelectrochem., 2, 41–47. (DOI: 10.1021/ba-1980-0188.ch002)

13. Barfield, K. D., & Bevan, D. R. (1985). Fusion of phospholipid vesicles induced by Zn^{2+}, Cd^{2+}, and Hg^{2+}, Biochem. Biophys. Res. Commun., 128, 389-395. (DOI: 10.1016/0006-291X(85)91691-2)

14. Tsai, H. H. G., Lai, W. X., Lin, H. D., Lee, J. B., Juang, W. F., & Tseng, W. H. (2012). Molecular dynamics simulation of cation–phospholipid clustering in phospholipid bilayers: Possible role in stalk formation during membrane fusion, Biochim. Biophys. Acta, Biomembr., 1818, 2742-2755. (DOI: 10.1016/j.bbamem.2012.05.029)

15. Ohki, S., & Zschörnig, O. (1993). Ion-induced fusion of phosphatidic acid vesicles and correlation between surface hydrophobicity and membrane fusion, Chem. Phys. Lipids, 65, 193-204. (DOI: 10.1016/0009-3084(93)90017-W)

16. Chapman, D., Peel, W. E., Kingston, B., & Lilley, T. H. (1977). Lipid phase transitions in model biomembranes: the effect of ions on phosphatidylcholine bilayers, Biochim. Biophys. Acta, Biomembr., 464, 260-275. (DOI: 10.1016/0005-2736(77)90002-5)

17. Binder, H., Arnold, K., Ulrich, A. S., & Zschörnig, O. (2001). Interaction of Zn^{2+} with phospholipid membranes, Biophys. Chem., 90, 57-74. (DOI: 10.1016/S0301-4622(01)00130-2)

18. Szekely, O., Schilt, Y., Steiner, A., & Raviv, U. (2011). Regulating the size and stabilization of lipid raft-like domains and using calcium ions as their probe, Langmuir, 27, 14767-14775. (DOI: 10.1021/la203074q)

19. Kewalramani, S., Hlaing, H., Ocko, B. M., Kuzmenko, I., & Fukuto, M. (2010). Effects of Divalent Cations on Phase Behavior and Structure of a Zwitterionic Phospholipid (DMPC) Monolayer at the Air−Water Interface, J. Phys. Chem. Lett., 1, 489-495. (DOI: 10.1021/jz9002873)

20. Uhríková, D., Teixeira, J., Lengyel, A., Almásy, L., & Balgavý, P. (2007). Formation of unilamellar dipalmitoylphosphatidylcholine vesicles promoted by Ca^{2+} ions: A small-angle neutron scattering study, Spectrosc., 21, 43-52. (DOI: 10.1155/2007/576282)

21. Lis, L. J., Parsegian, V. A., & Rand, R. P. (1981). Binding of divalent cations to dipalmitoylphosphatidylcholine bilayers and its effect on bilayer interaction, Biochemistry, 20, 1761-1770. (DOI: 10.1021/bi00510a009)

22. Zidovetzki, R., Atiya, A. W., & Boeck, H. D. (1989). Effect of divalent cations on the structure of dipalmitoylphosphatidylcholine and phosphatidylcholine/phosphatidylglycerol bilayers: an 2H-NMR study, Membr. Biochem, 8, 177-186. (DOI: 10.3109/09687688909025830)

23. Roux, M., & Bloom, M. (1990). Calcium, magnesium, lithium, sodium, and potassium distributions in the headgroup region of binary membranes of phosphatidylcholine and phosphatidylserine as seen by deuterium NMR, Biochemistry, 29, 7077-7089. (DOI: 10.1021/bi00482a019)

24. Martín-Molina, A., Rodríguez-Beas, C., & Faraudo, J. (2012). Effect of calcium and magnesium on phosphatidylserine membranes: experiments and all-atomic simulations, Biophys. J, 102, 2095-2103. (DOI: 10.1016/j.bpj.2012.03.009)

25. Gurtovenko, A. A., & Vattulainen, I. (2008). Effect of NaCl and KCl on phosphatidylcholine and phosphatidylethanolamine lipid membranes: insight from atomic-scale simulations for understanding salt-induced effects in the plasma membrane, J. Phys. Chem. B, 112, 1953-1962. (DOI: 10.1021/jp0750708)

26. Petrache, H. I., Gouliaev, N., Tristram-Nagle, S., Zhang, R., Suter, R. M., & Nagle, J. F. (1998). Interbilayer interactions from high-resolution x-ray scattering, Phys. Rev. E, 57, 7014. (DOI: 10.1103/PhysRevE.57.7014)

27. Petrache, H. I., Tristram-Nagle, S., Gawrisch, K., Harries, D., Parsegian, V. A., & Nagle, J. F. (2004). Structure and fluctuations of charged phosphatidylserine bilayers in the absence of salt, Biophys. J, 86, 1574-1586. (DOI: 10.1016/S0006-3495(04)74225-3)

28. Petrache, H. I., Tristram-Nagle, S., Harries, D., Kucerka, N., Nagle, J. F., & Parsegian, V. A. (2006). Swelling of phospholipids by monovalent salt, J. Lipid Res., 47, 302-309. (DOI: 10.1194/jlr.M500401-JLR200)

29. Brotons, G., Dubois, M., Belloni, L., Grillo, I., Narayanan, T., & Zemb, T. (2005). The role of counterions on the elasticity of highly charged lamellar phases: A small-angle x-ray and neutron-scattering determination, J. Chem. Phys., 123, 024704. (DOI: 10.1063/1.1950667)

30. Papahadjopoulos, D., Vail, W. J., Jacobson, K. and Poste, G. (1975). Cochleate lipid cylinders: formation by fusion of unilamellar lipid vesicles, Biochim. Biophys. Acta, Biomembr., 394, 483-491. (DOI: 10.1016/0005-2736(75)90299-0)

31. Uhríková, D., Kučerka, N., Teixeira, J., Gordeliy, V., & Balgavý, P. (2008). Structural changes in dipalmitoylphosphatidylcholine bilayer promoted by Ca^{2+} ions: a small-angle neutron scattering study, Chem. Phys. Lipids, 155, 80-89. (DOI: 10.1016/j.chemphyslip.2008.07.010)

32. Yang, J., Calero, C., Bonomi, M., & Martí, J. (2015). Specific ion binding at phospholipid membrane surfaces, J. Chem. Theory Comput., 11, 4495-4499. (DOI: 10.1021/acs.jctc.5b00540)

33. Petrache, H. I., Zemb, T., Belloni, L., & Parsegian, V. A. (2006). Salt screening and specific ion adsorption determine neutral-lipid membrane interactions, Proc. Natl. Acad. Sci., 103, 7982-7987. (DOI: 10.1073/pnas.0509967103)

34. Melcrová, A., Pokorna, S., Pullanchery, S., Kohagen, M., Jurkiewicz, P., Hof, M., ... & Cwiklik, L. (2016). The complex nature of calcium cation interactions with phospholipid bilayers. Sci. Rep., 6, 1-12. (DOI: 10.1038/srep38035)

35. Jurkiewicz, P., Cwiklik, L., Vojtíšková, A., Jungwirth, P., & Hof, M. (2012). Structure, dynamics, and hydration of POPC/POPS bilayers suspended in NaCl, KCl, and CsCl solutions, Biochim. Biophys. Acta, Biomembr., 1818, 609-616. (DOI: 10.1016/j.bbamem.2011.11.033)

36. Chapman, D., Peel, W. E., Kingston, B., & Lilley, T. H. (1977). Lipid phase transitions in model biomembranes: the effect of ions on phosphatidylcholine bilayers, Biochim. Biophys. Acta, Biomembr., 464, 260-275. (DOI: 10.1016/0005-2736(77)90002-5)

37. Simon, S. A., Lis, L. J., Kauffman, J. W., & MacDonald, R. C. (1975). A calorimetric and monolayer investigation of the influence of ions on the thermodynamic properties of phosphatidylcholine, Biochim. Biophys. Acta, Biomembr., 375, 317-326. (DOI: 10.1016/0005-2736(75)90350-8)

38. Pabst, G., Hodzic, A., Štrancar, J., Danner, S., Rappolt, M., & Laggner, P. (2007). Rigidification of neutral lipid bilayers in the presence of salts, Biophys. J, 93, 2688-2696. (DOI: 10.1529/biophysj.107.112615)

39. Alsop, R. J., Schober, R. M., & Rheinstädter, M. C. (2016). Swelling of phospholipid membranes by divalent metal ions depends on the location of the ions in the bilayers, Soft Matter, 12, 6737-6748. (DOI: 10.1039/C6SM00695G)

40. Huster, D., Arnold, K., & Gawrisch, K. (2000). Strength of Ca^{2+} binding to retinal lipid membranes: consequences for lipid organization, Biophys. j, 78, 3011-3018. (DOI: 10.1016/S0006-3495(00)76839-1)

41. McManus, J. J., Rädler, J. O., & Dawson, K. A. (2003). Does calcium turn a zwitterionic lipid cationic? J. Phys. Chem. B, 107, 9869-9875. (DOI: 10.1021/jp034463d)

42. Marcus, Y. (1994). A simple empirical model describing the thermodynamics of hydration of ions of widely varying charges, sizes, and shapes, Biophys. Chem., 51, 111-127. (DOI: 10.1016/0301-4622(94)00051-4)

43. Adams, E. M., Casper, C. B., & Allen, H. C. (2016). Effect of cation enrichment on dipalmitoylphosphatidylcholine (DPPC) monolayers at the air-water interface, J. Colloid Interface Sci., 478, 353-364. (DOI: 10.1016/j.jcis.2016.06.016)

44. Martín-Molina, A., Rodríguez-Beas, C., & Faraudo, J. (2012). Effect of calcium and magnesium on phosphatidylserine membranes: experiments and all-atomic simulations. Biophys. J., 102, 2095-2103. (DOI: 10.1016/j.bpj.2012.03.009)

45. Melcr, J., Bonhenry, D., Timr, S., & Jungwirth, P. (2016). Transmembrane potential modeling: comparison between methods of constant electric field and ion imbalance, J. Chem. Theory Comput., 12, 2418-2425. (DOI: 10.1021/acs.jctc.5b01202)

46. Jones, M. N. (1995). The surface properties of phospholipid liposome systems and their characterization, Adv. Colloid Interface Sci., 54, 93-128. (DOI: 10.1016/0001-8686(94)00223-Y)

47. Sachs, J. N., Nanda, H., Petrache, H. I., & Woolf, T. B. (2004). Changes in phosphatidylcholine headgroup tilt and water order induced by monovalent salts: molecular dynamics simulations, Biophys. J., 86, 3772-3782. (DOI: 10.1529/biophysj.103.035816)

48. Akutsu, H., & Nagamori, T. (1991). Conformational analysis of the polar head group in phosphatidylcholine bilayers: a structural change induced by cations, Biochemistry, 30, 4510-4516. (DOI: 10.1021/bi00232a020)

49. Huster, D., Paasche, G., Dietrich, U., Zschörnig, O., Gutberlet, T., Gawrisch, K., & Arnold, K. (1999). Investigation of phospholipid area compression induced by calcium-mediated dextran sulfate interaction, Biophys. J., 77, 879-887. (DOI: 10.1016/S0006-3495(99)76939-0)

50. Fink, L., Feitelson, J., Noff, R., Dvir, T., Tamburu, C., & Raviv, U. (2017). Osmotic stress induced desorption of calcium ions from dipolar lipid membranes, Langmuir, 33, 5636-5641. (DOI: 10.1021/acs.langmuir.7b00596)

51. Szekely, O., Steiner, A., Szekely, P., Amit, E., Asor, R., Tamburu, C., & Raviv, U. (2011). The structure of ions and zwitterionic lipids regulates the charge of dipolar membranes, Langmuir, 27, 7419-7438. (DOI: 10.1021/la200264s)

52. Pabst, G., Kučerka, N., Nieh, M. P., & Katsaras, J. (Eds.). (2014). Liposomes, lipid bilayers and model membranes: from basic research to application. CRC press.

53. Das, A., Adhikari, C., & Chakraborty, A. (2016). Lipoplex-mediated deintercalation of doxorubicin from calf thymus DNA–doxorubicin complex, Langmuir, 32, 8889-8899. (DOI: 10.1021/acs.langmuir.6b01860)

54. Thakur, R., Das, A., & Chakraborty, A. (2014). Interaction of human serum albumin with liposomes of saturated and unsaturated lipids with different phase transition temperatures: a spectroscopic investigation by

membrane probe PRODAN, RSC Adv., 4, 14335-14347. (DOI: 10.1039/C4RA01214C)

55. Kanwa, N., De, S. K., Adhikari, C., & Chakraborty, A. (2017). Spectroscopic study of the interaction of carboxyl-modified gold nanoparticles with liposomes of different chain lengths and controlled drug release by layer-by-layer technology, J. Phys. Chem. B, 121, 11333-11343. (DOI: 10.1021/acs.jpcb.7b08455)

56. Jurkiewicz, P., Olżyńska, A., Langner, M., & Hof, M. (2006). Headgroup hydration and mobility of DOTAP/DOPC bilayers: a fluorescence solvent relaxation study, Langmuir, 22, 8741-8749. (DOI: 10.1021/la061597k)

57. Parasassi, T., Krasnowska, E. K., Bagatolli, L., & Gratton, E. (1998). Laurdan and Prodan as polarity-sensitive fluorescent membrane probes, J. Fluoresc., 8, 365-373. (DOI: 10.1023/A:1020528716621)

58. Krasnowska, E. K., Gratton, E., & Parasassi, T. (1998). Prodan as a membrane surface fluorescence probe: partitioning between water and phospholipid phases, Biophys. J., 74, 1984-1993. (DOI: 10.1016/S0006-3495(98)77905-6)

59. Wang, B., Zhang, L., Bae, S. C., & Granick, S. (2008). Nanoparticle-induced surface reconstruction of phospholipid membranes, Proc. Natl. Acad. Sci., 105, 18171-18175. (DOI: 10.1073/pnas.0807296105)

60. Hamilton, D. J., Coffman, M. D., Knight, J. D., & Reed, S. M. (2017). Lipid-coated gold nanoparticles and FRET allow sensitive monitoring of liposome clustering mediated by the synaptotagmin-7 C2A domain, Langmuir, 33, 9222-9230. (DOI: 10.1021/acs.langmuir.7b01397)

61. Rollinson, A. M., & Drickamer, H. G. (1980). High pressure study of luminescence from intramolecular CT compounds, J. Chem. Phys., 73, 5981-5996. (DOI: 10.1063/1.440132)

62. Chapman, C. F., & Maroncelli, M. (1991). Fluorescence studies of solvation and solvation dynamics in ionic solutions, J. Phys. Chem., 95, 9095-9114. (DOI: 10.1021/j100176a016)

63. Weber, G., & Farris, F. J. (1979). Synthesis and spectral properties of a hydrophobic fluorescent probe: 6-propionyl-2-(dimethylamino) naphthalene, Biochemistry, 18, 3075-3078. (DOI: 10.1021/bi00581a025)

64. Balter, A., Nowak, W., Pawełkiewicz, W., & Kowalczyk, A. (1988). Some remarks on the interpretation of the spectral properties of prodan, Chem. Phys. Lett., 143, 565-570. (DOI: 10.1016/0009-2614(88)87067-2)

65. Samanta, A., & Fessenden, R. W. (2000). Excited state dipole moment of PRODAN as determined from transient dielectric loss measurements, J. Phys. Chem. A, 104, 8972-8975. (DOI: 10.1021/jp0009960)

66. Adhikary, R., Barnes, C. A., & Petrich, J. W. (2009). Solvation dynamics of the fluorescent probe PRODAN in heterogeneous environments: Contributions from the locally excited and charge-transferred states, J. Phys. Chem. B, 113, 11999-12004. (DOI: 10.1021/jp905139n)

67. Moyano, F., Biasutti, M. A., Silber, J. J., & Correa, N. M. (2006). New insights on the behavior of PRODAN in homogeneous media and in large unilamellar vesicles, J. Phys. Chem. B, 110, 11838-11846. (DOI: 10.1021/jp057208x)

68. Novaira, M., Moyano, F., Biasutti, M. A., Silber, J. J., & Correa, N. M. (2008). An example of how to use AOT reverse micelle interfaces to control a photoinduced intramolecular charge-transfer process. Langmuir, 24, 4637-4646. (DOI: 10.1021/la704004m)

69. Lehrmann, R., & Seelig, J. (1994). Adsorption of Ca^{2+} and La^{3+} to bilayer membranes: measurement of the adsorption enthalpy and binding constant with titration calorimetry. Biochim. Biophys. Acta, Biomembr., 1189, 89-95. (DOI: 10.1016/0005-2736(94)90284-4)

70. Liu, Y., & Liu, J. (2017). Zn^{2+} induced irreversible aggregation, stacking, and leakage of choline phosphate liposomes, Langmuir, 33, 14472-14479. (DOI: 10.1021/acs.langmuir.7b03209)

71. Allnér, O., Nilsson, L., & Villa, A. (2012). Magnesium ion–water coordination and exchange in biomolecular simulations, J. Chem. Theory Comput., 8, 1493-1502. (DOI: 10.1021/ct3000734)

Chapter 3

Influence of trivalent metal ions on lipid vesicles: gelation and fusion phenomena

3.1 Introduction

The binding of metal cations to lipid membranes has been a vital area of research over the past few decades *[1−14]*. Numerous studies have been carried out to understand the role of ions in membrane stability, their binding mode, the location of metal ions in lipid vesicles, and the effect of metal ions on the membrane phase state *[15, 16]*. It has been well established that metal ions interact with membranes in a specific manner. While monovalent alkali cations adsorb only on the surface of the negatively charged lipid membrane, the divalent ions adsorb readily even if the lipid is zwitterionic *[6, 9, 11, 17]*. The divalent cations are mostly adsorbed on the surface of lipid vesicles, and the ion−dipole interaction causes conformational changes in the head group and also in the tail region of the membrane *[18, 19]*. It is reported that divalent cations favor the gel phase over the liquid-crystalline phase and increase the phase transition temperature of the lipid vesicles *[1, 20, 21]*. Among divalent metal ions, Zn^{2+}, Cu^{2+}, and Ca^{2+} bind strongly, while Sr^{2+}, Ba^{2+}, and some others only interact loosely (including monovalent ions) with the lipid head group *[22−27]*. Electrostatic interaction between the metal ion and the lipid head group is crucial for membrane fusion, aggregation, and leakage of the vesicles. For example, Zn^{2+} can readily absorb on DPPC (1,2-dipalmitoyl-sn-glycero-3-phosphocholine) and DMPC (1,2-dimyristoylsn-glycero-3-phosphocholine) lipid vesicles and at higher concentration of metal salt causes aggregation of lipid vesicles *[28]*. On the other hand, Zn^{2+} and Ca^{2+}-induced vesicle fusion has long been documented, where metal ions bring lipid bilayers closer and rearrange local lipids required for fusion *[28−30]*. Other than the above two metal ions, Cu^{2+}-induced aggregation and fusions of different membranes have been also reported in the literature *[14]*. Although divalent cations interact strongly with the vesicles at physiological pH, some studies

reveal that in the presence of an acidic environment, the interaction with the vesicle significantly decreases *[12, 14, 28*].

While influences of monovalent and divalent metal ions on zwitterionic PC vesicles are well established, the impacts of trivalent metal ions are unexplored. A general perception is that phosphate is chemically inert and only certain high-valent metals can bind *[31−35].* The lanthanide ions (La^{3+}, Gd^{3+}) are known to affect the structure and stability of phospholipid membranes *[33−36]*. Verstraeten et al. reported the binding affinity of Sc^{3+}, Y^{3+}, and La^{3+} to DMPC: DMPS or brain PC: PS and found that the binding ability follows the order of $Sc^{3+} < Y^{3+} < La^{3+}$ *[37]*. Several authors have studied the interactions of La^{3+} with the surface of negatively charged lipid layers composed of phosphoserine (PS) and phosphocholine (DPPC)-phosphatidylinositol (PI), with apparently contradictory results *[38−40]*. Most of the above studies focused on negatively charged vesicles for metal binding. Therefore, systemic studies are required to understand the driving force for the strong interaction of metal ions with zwitterionic lipids. In this context, fluorescence spectroscopic studies including steady state, time-resolved, and different techniques could be very useful to understand the rigidification of the lipid vesicles, leakage, fusion, and aggregation of the vesicles using various membrane-sensitive probes or dyes. Although there are reports in the literature on the interaction of monovalent and divalent ions with the lipid vesicles, the literature lacks studies on the same between lipid vesicles and trivalent metal ions. Moreover, for a particular group of metal ions, with the increase in the radii for the same charge, i.e., with the change in charge density of metal ions, the extent of interaction is not reported elsewhere. Since there are plenty of studies regarding interaction with monovalent and bivalent metal ions, it is imperative to draw a parallel with trivalent ions regarding the interaction with lipid vesicles. Keeping all of these in mind, in this investigation, we use a series of trivalent metal ions, namely, Al^{3+}, Ga^{3+}, and In^{3+}, of the same group and a zwitterionic lipid, namely, 1,2-dimyristoyl-sn-glycero-3-phosphocholine (DMPC) to unravel the effect of size, effective charge, and hydration free energy of these metal ions on lipid vesicles. The steady-state and time resolved techniques have been employed to explore the sensitivity of

membrane probes N,N-dimethyl-6-propionyl-2- naphthylamine (PRODAN) and 8-anilino-1-naphthalenesulfonic acid (ANS) toward changes in the surface properties of the DMPC vesicles *[41−45]*. The findings of the spectroscopic measurements were further validated by time-resolved anisotropy measurements. Conventional PC vesicles are reported to exhibit moderate colloidal stability due to the aggregation/ fusion processes that can prevent drug-loaded vesicles from reaching a targeted site in biomedical applications *[46]*. Therefore, the studies of the aggregation and fusion processes of the PC lipid vesicles are necessary if efficient drug delivery systems are to be designed *[32]*. In the present article, we studied the aggregation and fusion of lipid vesicles induced by metal ions using dynamic light scattering (DLS) measurements and confocal microscopy. The Derjaguin-Landau-Vervey-Overbeek (DLVO) theory has been used to explain our observations from DLS measurements and confocal microscopy. We have also compared the results of trivalent metal ions with those of bivalent metal ions in terms of rigidification of the lipid vesicles.

3.2 Results and Discussion

3.2.1 <u>Behaviour of PRODAN in lipid bilayers, general polarization and area fraction calculations</u>: PRODAN is a membrane-sensitive probe and undergoes partition in lipid vesicles and aqueous medium *[41, 42]*. PRODAN in an aqueous medium exhibits an emission maximum at 540 nm. In presence of lipid, another band emerges at 440 nm wavelength. The appearance of the new band at 440 nm is assigned to be the local excited (LE) state of PRODAN and it is a characteristic band of the gel phase of the lipid bilayer. Using a special spectral feature of PRODAN, area fraction and general polarization plots are very important to investigate the phase transition between the liquid crystalline phase and gel phase of the lipid bilayer. We estimated the area fraction (A) at the red end (A_R) and blue end (A_B) to understand the change in the fluidity in presence of metal salts using the following equation:

$$A_R = \frac{A_{490}}{A_{440}+A_{490}} \text{ and } A_B = \frac{A_{440}}{A_{440}+A_{490}} \quad (3.1)$$

Where, A_{440} and A_{490} are the emitted area under 440 nm and 490 nm, respectively. Whereas the General polarization (GP) value provides a quantitative measurement of what proportion of the PRODAN molecules are surrounded mainly by the liquid-crystalline or mainly by gel-phase phospholipids. We estimated the General polarization (GP) by flowing equation:

$$GP = \frac{A_{440} - A_{490}}{A_{440} + A_{490}} \qquad (3.2)$$

We monitor the emission properties of PRODAN as a function of metal ion concentration to study the interaction of lipid vesicles with trivalent and bivalent metal ions.

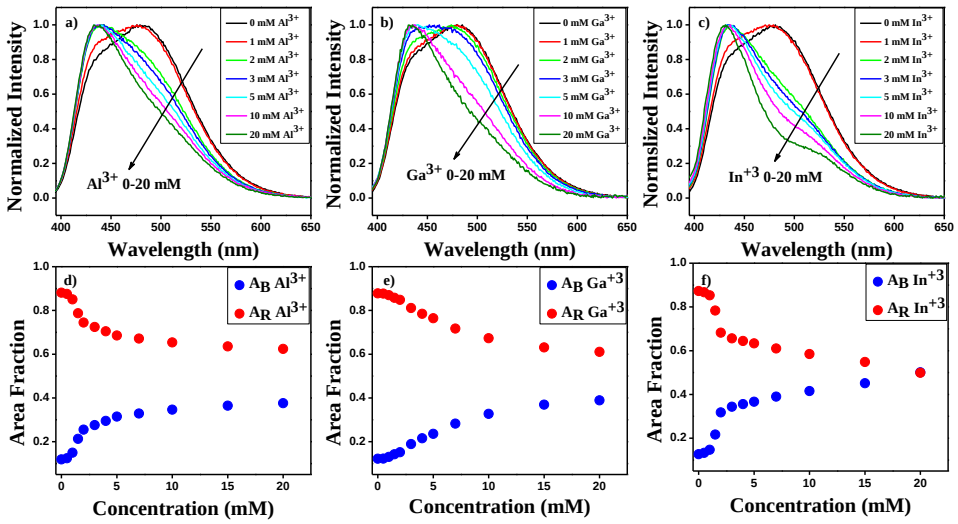

Figure 3.1 Normalized emission spectra of PRODAN in DMPC vesicles at different concentrations of metal salts (0−20 mM): (a) Al^{3+}, (b) Ga^{3+}, and (c) In^{3+} and their corresponding plots (d−f) for the area fraction versus concentration of metal salts at 440 (blue emission, A_B) and 500 nm (red emission A_R) and at 25 °C and pH 7.0.

3.2.2 <u>Metal-induced gelation of lipid vesicles at pH~7.0 using PRODAN as a probe</u>: The addition of metal ions (Al^{3+}, Ga^{3+}, and In^{3+}) to the PRODAN-impregnated vesicles causes a shift in the emission band to a shorter wavelength (Figure 3.1). The band at 440 nm becomes dominating over the band at 540 nm. The observation is primarily ascribed to the gelation of the lipid vesicles induced by metal ions. The gelation is more evident from the area fraction plot of fluorescence emission spectra. Figure 3.1d−f reveals that the area fraction corresponding to the blue end (A_B) increases while that in the

red end (A_R) decreases. This feature confirms that significant gelation takes place in lipid vesicles upon the addition of trivalent metal ions. For better understanding, we have also plotted the generalized polarization data (Figure 3.2 b). We observe that at low concentration the generalized polarization data increases rapidly for all of the three metal ions. The feature suggests that lipid vesicles undergo gelation in the presence of metal ions. Further, it is revealed from Figure 3.2 that up to 3−5 mM concentration of metal ions, the maximum gelation takes place in the case of In^{3+}. However, at a higher concentration of metal salt, the gelation reaches a saturation level for all metal ions. This result is different from that obtained for bivalent metal ions (Chapter 2). We reported earlier that in the case of bivalent metal ions, rehydration of lipid vesicles takes place at a low concentration of metal salts and the gelation initiates at a higher metal salt concentration for Zn^{2+} and Ca^{2+} *[28]*. The extent of gelation induced by trivalent metal ions is compared with that of bivalent metal ions by a general polarization parameter, and we found that the gelation induced by trivalent metal ions is much higher as compared to that induced by bivalent metal ions (*Vide infra*). The impact of gelation on the dynamics of vesicle-bound probe molecules was studied by time-resolved measurements including time-resolved anisotropy. The excited lifetime decays of PRODAN for DMPC vesicles in the presence of different metal ions were measured at 440 nm wavelength to monitor the effect of metal ions on the gel phase (Figure 3.3 a-c). The decay parameters of the PRODAN due to the addition of these metal ions as obtained by the fitting of the decay curves are given in Table 3.1. The lifetime data indicate that the decay of PRODAN in the lipid vesicles comprises two-time constants (τ_1 and τ_2 with amplitudes a_1 and a_2, respectively). The shorter component, i.e., τ_1, is around 1.44 ns (37%) and is ascribed to the contribution from the aqueous phase, and the longer component, i.e., τ_2, which is around 4.28 ns (63%), originates from PRODAN in the lipid vesicles *[28, 47]*. Upon addition of these metal ions to the lipid vesicles, both τ_1 and τ_2 increase significantly up to 3 mM. The rate of change of lifetime or the longer component is highest in the case of In^{3+}. However, at a relatively higher concentration of salt, gelation becomes saturated and the lifetime of PRODAN in the presence of different ions remains almost the same.

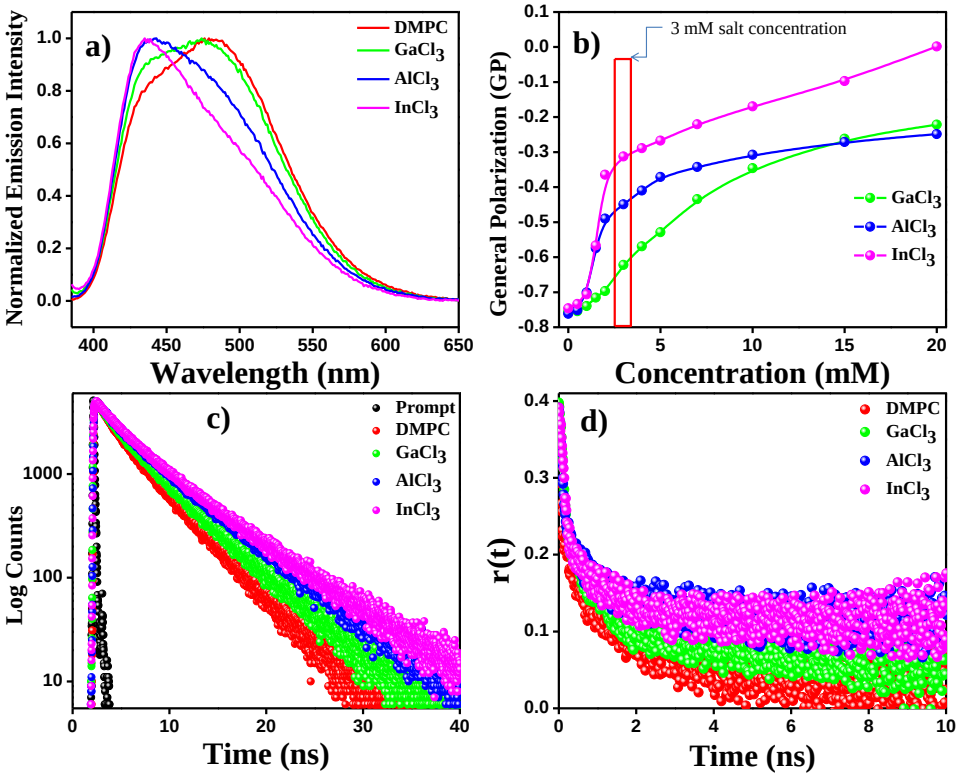

Figure 3.2 (a) Normalized emission spectra of DMPC-PRODAN for the addition of 3 mM Metal salts, (b) Generalized polarization plot of their corresponding area, (c) Time resolved decay curves and (d) anisotropy decays of PRODAN in DMPC lipid bilayers at 3mM concentrations of salts.

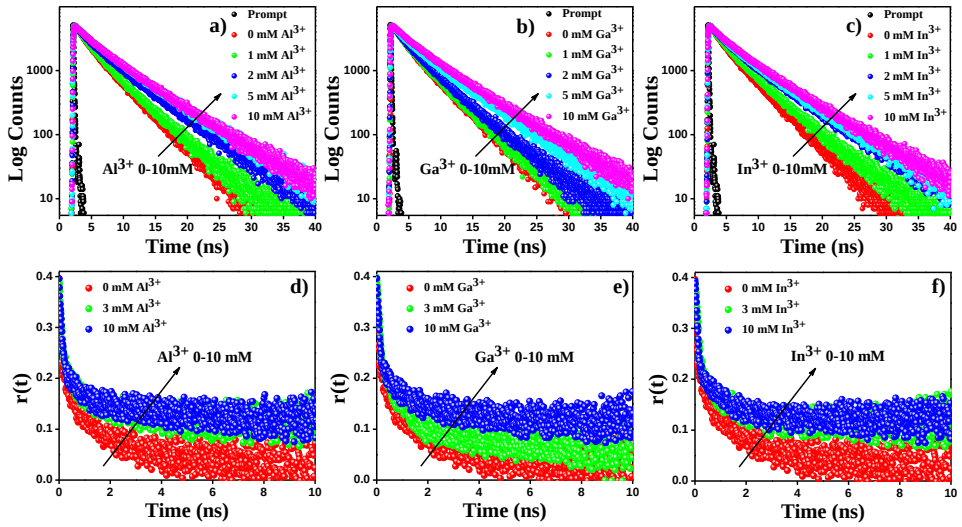

Figure 3.3 Time-resolved decay curves of PRODAN in DMPC lipid vesicles at various concentrations of metal salts of (a) Al^{3+}, (b) Ga^{3+}, and (c) In^{3+} at 440 nm and anisotropy decays of PRODAN in DMPC lipid vesicles at various concentrations of (d) Al^{3+}, (e) Ga^{3+}, and (c) In^{3+} at 440 nm.

To gain a better insight into the confinement of PRODAN in the vicinity of the lipid vesicles, we conducted time-resolved anisotropy measurements in the presence of the metal ions. The time-resolved anisotropy decay curves in the presence of different metal ions are shown in Figure 3.3d−f. The anisotropy decays indicate that the rotational relaxation becomes significantly slower with increasing concentrations of Al^{3+}, Ga^{3+}, and In^{3+} in DMPC vesicles. We note that the rotational relaxation decay in the presence of metal ions possesses a very long tail, which demonstrates that rotation is severely hindered owing to the rigidification of the membrane. The observation is in accordance with the steady-state and lifetime measurements. Interestingly, the observations from trivalent ions are different from those of bivalent ions. In the latter case, the very low concentration of Mg^{2+} salt causes a significant decrease in the lifetime and rotational relaxation time, indicating an initial loosening of the packing of the lipid bilayers *[28]*. In the case of trivalent metal ions, the increase in a lifetime and rotational relaxation confirm that trivalent metal ions are much more effectively dehydrate the vesicles, which renders more confinement for the rotation of the probe molecules. In this context, it is worth mentioning that we experimented with negatively charged lipid vesicles composed of DMPC: DMPG (80:20). We found that the solution turned milky white even at a very low concentration of trivalent salts (0.5 mM). The observation stems from the strong interaction between the negatively charged lipid head group and the positively charged cations. The formation of the insoluble complex upon interaction with the head group indicates that the complex formation takes place between the phosphate group and metal ions.

Table 3.1 Time resolved data for the DMPC-PRODAN at 440 nm upon increasing concentration of Al^{3+}, Ga^{3+} and In^{3+} at fixed lipid concentration of DMPC lipid (0.4 mM).[#]

	χ^2	**τ_1 (ns)**	**τ_2 (ns)**	**a_1**	**a_2**	**$\langle\tau\rangle$ (ns)**
DMPC	1.03	1.44	4.28	0.37	0.63	3.23
1 mM Al^{3+}	1.02	1.50	4.52	0.36	0.64	3.42
2 mM Al^{3+}	1.07	1.96	5.82	0.35	0.65	4.47
3 mM Al^{3+}	1.06	2.15	6.34	0.31	0.69	5.02

5 mM Al^{3+}	1.04	2.15	6.37	0.30	0.70	5.11
10 mM Al^{3+}	1.00	2.40	6.27	0.26	0.74	5.28
1 mM Ga^{3+}	1.04	1.44	4.43	0.34	0.66	3.40
2 mM Ga^{3+}	1.04	1.65	4.90	0.36	0.64	3.73
3 mM Ga^{3+}	1.07	1.87	5.58	0.34	0.66	4.30
5 mM Ga^{3+}	1.03	2.02	6.08	0.32	0.68	4.78
10 mM Ga^{3+}	1.04	2.39	6.45	0.30	0.70	5.23
1 mM In^{3+}	1.02	1.53	4.86	0.37	0.63	3.64
2 mM In^{3+}	1.06	2.10	6.29	0.39	0.61	4.68
3 mM In^{3+}	1.05	2.13	6.40	0.37	0.63	4.83
5 mM In^{3+}	0.98	2.10	6.38	0.35	0.65	4.87
10 mM In^{3+}	1.00	2.06	6.69	0.30	0.70	5.30

 # Experimental error is within 5%.

As the metal ions bind to the lipid vesicles and induce gelation, it might alter the phase transition temperature of the lipid bilayer significantly. We, therefore, conducted temperature-dependent studies to gain an insight into the influences of the metal ions on the phase transition temperature of the lipid. We conducted the temperature-dependent study of the DMPC-PRODAN system in the presence and absence of metal salts (10 mM), from 10 to 40 °C (Figures 3.4 and 3.5). The fluorescence intensity of PRODAN corresponding to the LE state (blue end) decreases, while the intensity of the twisted intramolecular charge transfer state or TICT state (red end) increases with increasing temperature, indicating the changes in the phase state of lipid vesicles from a sol−gel (SG) phase to a liquid-crystalline (LC) phase. We have monitored the alteration of the phase state of the DMPC lipid vesicles using the temperature-dependent steady-state fluorescence area fraction plot of the blue end ($A_B = A_{440}/A_{440} + A_{490}$) of DMPC-PRODAN. Figure 3.5a shows that the decrease in fluorescence area at the blue end is sigmoidal with maximum

changes near the phase transition temperature of vesicles. It is revealed that all of these three metal ions shift the area fraction toward the higher temperature. The changes in the phase state are more clearly notable from the normalized derivative plot of the area fraction (*dA/dT*) with respect to temperature. Figure 3.5b reveals that the phase transition temperature of the DMPC vesicles is estimated at around 23 °C. This result is in good agreement with that reported in the literature. In the presence of 10 mM metal salts, an appreciable shift in the phase transition temperature toward higher temperatures is observed. While Al^{3+} and Ga^{3+} increase the phase transition temperature from 23 to 27 and 28 °C, respectively, In^{3+} shifted the phase transition temperature of DMPC vesicles from 23 to 34 °C. The result confirms that In^{3+} has a much stronger binding effect on lipid vesicles than Al^{3+} and Ga^{3+} and is more effective in increasing the phase transition temperature of DMPC vesicles. Interestingly, the shape of the temperature-dependent curve in the presence of In^{3+} is different from that in the presence of Al^{3+} and Ga^{3+} (Figure 3.5a). The difference may arise due to different modes of binding patterns of In^{3+} with lipid vesicles. We reason that In^{3+} perhaps plays a cross-linking role as observed in the case of Ca^{2+}.

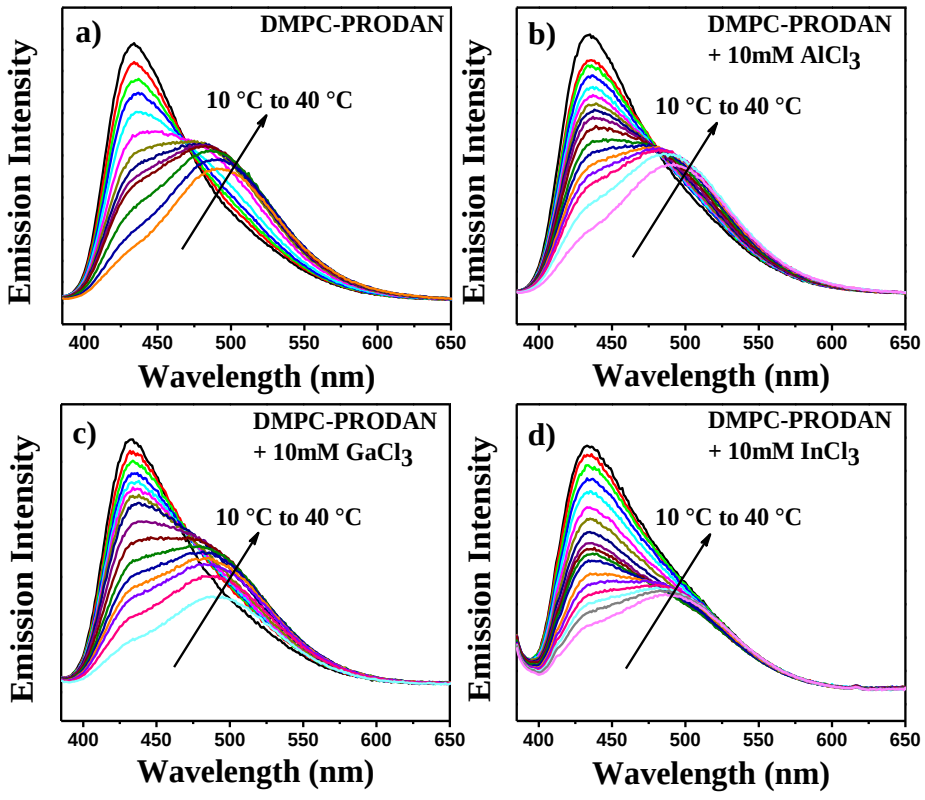

Figure 3.4 Temperature dependent steady state fluorescence spectra of (a) DMPC-PRODAN lipid bilayer and (b), (c) and (d) represents the temperature dependent steady state fluorescence spectra of DMPC-PRODAN in presence of Al^{+3}, Ga^{+3} and In^{+3} respectively.

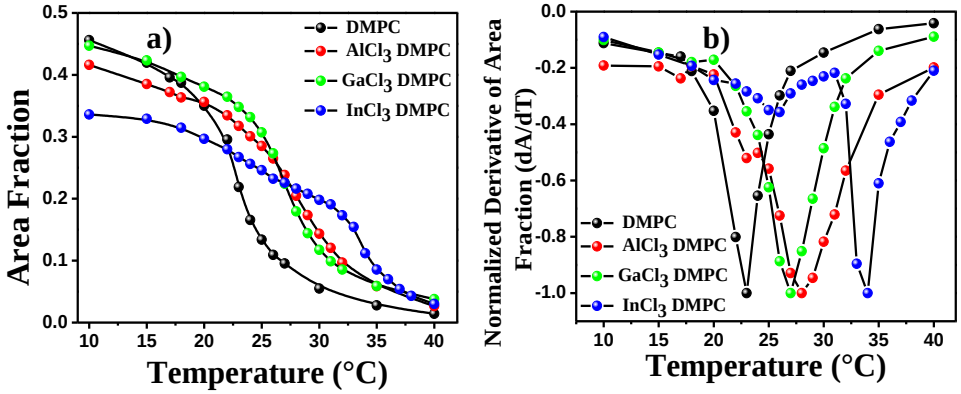

Figure 3.5 (a) Area fraction plot of PRODAN in DMPC vesicles from steady-state fluorescence spectra as a function of temperature (10-40 °C) in presence and absence of metal salts, where DMPC, PRODAN and metal salts concentration are 0.4 mM, 1 µM and 10 mM respectively. (b) Normalized first derivative of area fraction (dA/dT) v/s temperature plot.

While the gel phase of DMPC vesicles displays a significant affinity toward metal ions, the interaction between the lipid membrane and metal ions was significantly reduced in the liquid-crystalline phase. To investigate the effect of metal ions on the LC phase of lipid vesicles, we conducted the experiment at 40 °C where vesicles are present in the LC phase. Interestingly, among these metal ions, the negligible spectral shift was observed for both Al^{3+} and Ga^{3+} (Figure 3.6a,b), while the significant blue shift in emission spectra was observed for In^{3+} at 40 °C (Figure 3.6c). A similar observation was obtained in lifetime and anisotropy measurements (Figure 3.6d−f). The average lifetime of PRODAN in DMPC vesicles at 40 °C temperature is 1.70 ns with lifetime components of 0.93 ns (59%) and 2.81 ns (41%) (Table 3.2). The average lifetime increases to 2.93 ns with lifetime components of 1.46 ns (40%) and 3.92 ns (60%) upon the addition of 20 mM In^{3+}. The rotational relaxation decay also increases significantly with the increasing concentration of In^{3+} (inset of Figure 3.6f). On the other hand, a marginal change was observed in the lifetime and rotational relaxation decay in the presence of Al^{3+} and Ga^{3+} (Figure 3.6d-e). Therefore, from the temperature-dependent study, it is quite clear that In^{3+} has a much more stronger binding to the lipid head group than

that of Al^{3+} and Ga^{3+}, even at a higher temperature. These results also validate the shifted phase transition temperature of the lipid vesicles in the presence of metal ions.

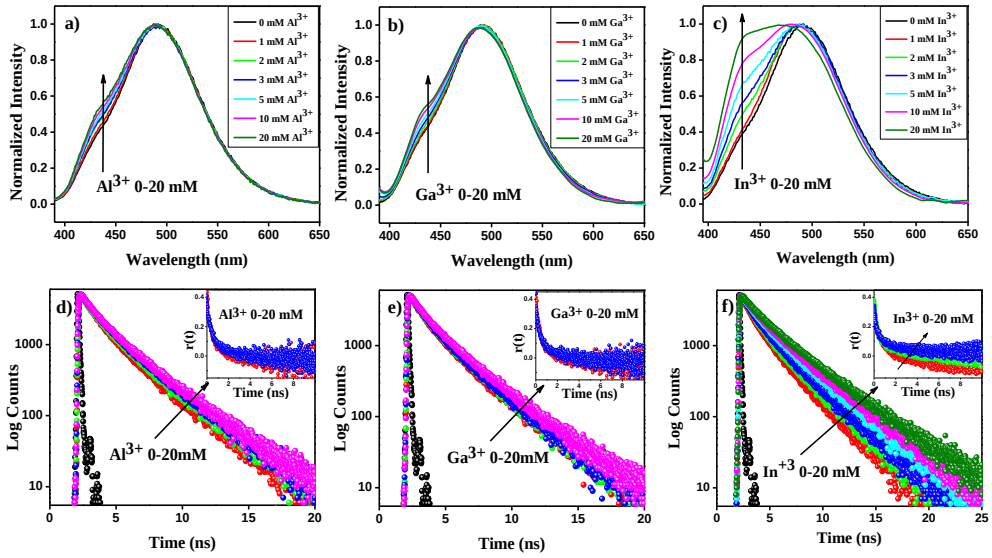

Figure 3.6 (a) Normalized emission spectra of PRODAN in DMPC vesicles at different concentrations (0−20 mM) of metal salts of (a) Al^{3+}, (b) Ga^{3+}, and (c) In^{3+} and time-resolved decay curves at various concentrations of (d) Al^{3+}, (e) Ga^{3+}, and (f) In^{3+} at 440 nm and 40 °C (inset shows anisotropy decays of PRODAN in DMPC lipid vesicles at 440 nm).

Table 3.2 Time resolved data for the DMPC-PRODAN at 440 nm upon increasing concentration of In^{3+} at fixed lipid concentration (0.4 mM) at 40 °C.#

	χ2	**τ_1 (ns)**	**τ_2 (ns)**	**a_1**	**a_2**	**< τ > (ns)**
0 mM In^{3+}	1.17	0.93	2.81	0.59	0.41	1.70
1 mM In^{3+}	1.15	1.00	2.98	0.55	0.45	1.89
2 mM In^{3+}	1.15	1.03	3.07	0.51	0.49	2.03
3 mM In^{3+}	1.04	1.09	3.21	0.46	0.54	2.23
5 mM In^{3+}	1.06	1.14	3.32	0.42	0.58	2.41
10 mM In^{3+}	1.14	1.20	3.50	0.40	0.60	2.59
15 mM In^{3+}	1.23	1.35	3.78	0.43	0.57	2.74
20 mM In^{3+}	1.17	1.46	3.92	0.40	0.60	2.93

 # Experimental error in the measurement is around 5%.

Therefore, our study reveals that among these three metal ions In^{3+} exhibits stronger binding with the lipid head group than Al^{3+} and Ga^{3+} do. Although Al^{3+} interacts with the lipid head group and causes more changes than Ga^{3+} at a low concentration (Figure 3.2b), at the higher concentration, both of these metal ions have an almost comparable effect on the lipid membranes. It has been well reported that the phosphate or carboxylate group on the membrane surface is the probable binding site for the charged metal ions *[23]*. Our experiment does not provide any direct information about any binding energy term. Thus, a theoretical framework may be helpful in explaining the affinities of these trivalent metal ions toward lipid vesicles. The overall free-energy change for complex formation between ions and lipid vesicles is conveniently written as

$$\Delta G^0_{ads} = \Delta G^0_{col} + \Delta G^0_{slov} + \Delta G^0_{chem} \quad (3.3)$$

where ΔG^0_{col} is the change in Coulombic energy due to adsorption, ΔG^0_{solv} is the change due to displacement of the hydration shell associated with the ion and the surface, and ΔG^0_{chem} is any interaction term not included in ΔG^0_{col} such as hydrogen bonding or covalent bonding *[27]*. The metal ions interact with the lipid vesicles through Coulombic interaction. Thus, as the charges of these metal ions are the same, ΔG^0_{col} is mainly dependent on the distance between the charges, i. e. dependent on the ionic radius of the metal ions. Ruso and coworkers studied the interaction of La^{3+} and Al^{3+} toward lipid vesicles, and they found that La^{3+} has a much stronger affinity than Al^{3+} *[27]*. Similarly, Verstraeten and co-workers reported the interaction of Sc^{3+}, Y^{3+}, and La^{3+} toward negatively charged DMPC: DMPS or brain PC: PS *[37]*. Interestingly, they found that La^{3+} and Y^{3+} bind more strongly than Sc^{3+} and the order was found to be $La^{3+} > Y^{3+} > Sc^{3+}$ *[37]*. These studies suggest that metal ions with larger ionic radii exhibit stronger interaction with the lipid head groups. In the present work, we used metal ions from the same group of the periodic table that follows the order of ionic radius as $In^{3+} > Ga^{3+} > Al^{3+}$. Thus, it is expected that In^{3+} probably binds more strongly with the lipid head group than Al^{3+} and Ga^{3+} and this order is in complete agreement with our results. In the case of Al^{3+} and Ga^{3+}, at lower concentrations, Al^{3+} binds strongly than Ga^{3+}, but both these ions produce similar changes at a higher concentration of salts. We

explain this phenomenon in light of hydration free energy. It is known that Ga^{3+} has higher hydration free energy than Al^{3+}. Thus, it is expected that between the bound and unbound states of metal ions with the lipid head group, Ga^{3+} has a higher energy barrier than Al^{3+}. Thus, at a lower concentration, Al^{3+} interacts strongly than Ga^{3+}.

It has also been reported that Coulombic interaction removes the water molecules from the hydration shell. Numerous studies have been reported regarding the dehydration effect of metal ions on the lipid vesicles *[21−23, 28]*. The binding of metal cations to a phospholipid membrane is endothermic, indicating that adsorption of the ions to the membrane is mainly entropy-driven. This factor is responsible for the disruption of hydrogen bonds between water molecules *[23, 48]*. In our study, all of these three metal ions are chaotropic ions. These ions can disrupt the hydrogen bonding network between water molecules. As In^{3+} has the highest ionic radius, it can replace more water molecules from the vicinity of the phosphate group of the lipid vesicles and induce maximum gelation compared with Ga^{3+} and Al^{3+}, which have comparatively smaller ionic radii. Finally, the order was found to be $In^{3+} > Ga^{3+} \geq Al^{3+}$.

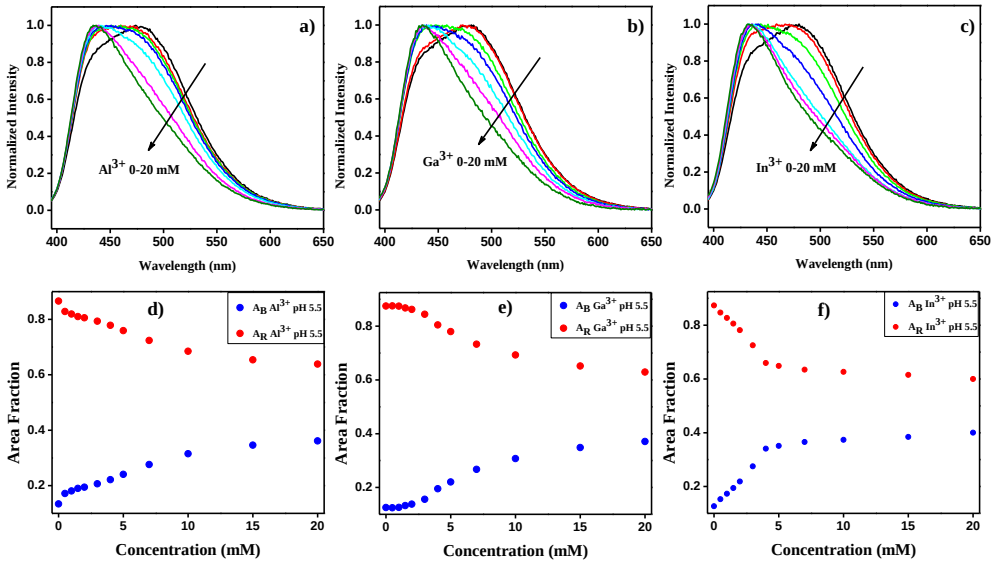

Figure 3.7 Effect of metal ions on DMPC−PRODAN solution at pH 5.5. Normalized emission spectra for the addition of metal salts in different concentrations (0 to 10mM) to DMPC−PRODAN solution for (a) Al^{+3} (b) Ga^{+3} and (c) In^{+3} and their corresponding area

fraction versus concentration of metal salts plots (d-f) for DMPC liposomes at 440 (blue emission) and 500 nm (red emission) at 25 °C.

3.2.3 <u>Metal-induced gelation of lipid vesicles at pH 5.5</u>: We investigated the binding of metal ions at different pH values (pH 7 and pH 5.5) using steady-state measurements (<u>Figure 3.1 and Figure 3.7</u>, respectively). In our previous study (Chapter 2), we found that at lower pH (i.e., 5.5), the extent of gelation by the divalent metal ions (i.e., Zn^{2+} and Ca^{2+}) was significantly reduced *[28]*. Liu et al. reported that at lower pH, H^{+} may bind with the phosphate group and may prevent the metal ions from binding to the phospholipid head groups *[12]*. We plotted the generalized polarization to compare the extent of binding of metal ions (both the divalent and trivalent) toward pH ~7.0 and pH ~5.5. Figure 3.8a reveals that trivalent metal ions interact much more strongly with the lipid head group than divalent metal ions at pH ~7.0. All of these three trivalent metal ions show a higher affinity toward lipid vesicles than Ca^{2+} and Zn^{2+}. We mentioned that divalent metal ions do not effectively interact with the vesicles at lower pH, but interestingly in the present case, even at lower pH, all of these trivalent metal ions induce gelation of lipid vesicles. Although the extent of gelation by trivalent metal ions is significantly reduced at lower pH, it is comparatively higher than that of divalent metal ions (Figure 3.8b). Thus, this study demonstrates that even at lower pH, the trivalent metal ion can interact with the lipid vesicles by inducing more gelation than divalent metal ions.

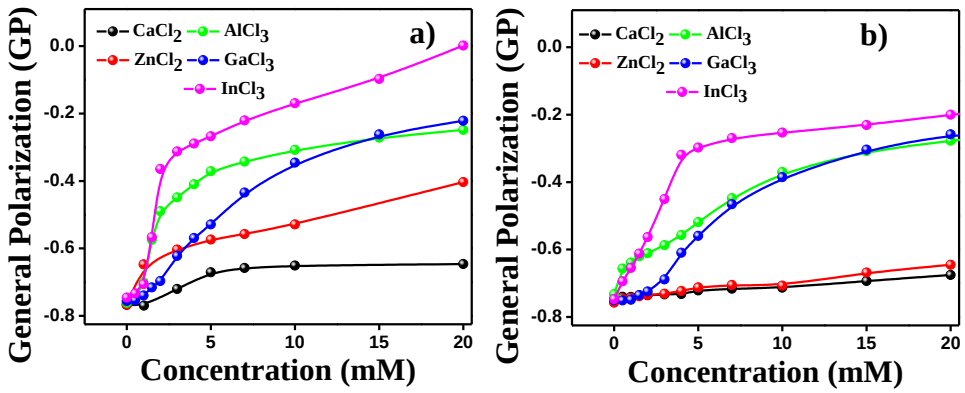

Figure 3.8 Generalized polarization plot of the area of DMPC-PRODAN fluorescence emission versus concentration of different metal ions at (a) pH ~ 7.0 and (b) pH ~ 5.5.

3.2.4 <u>Metal-induced gelation of lipid vesicles at pH 7.0 using ANS as a probe</u>: To probe the gelation of the lipid vesicles induced by trivalent metal ions of different sizes, we took another fluorescence probe, namely, ANS, to study the influences of these metal ions on the lipid vesicles. It is well known that ANS exhibits an emission band at 520 nm in the aqueous phase with a very poor quantum yield. However, in the presence of lipid vesicles, ANS shows a remarkable blue shift and the peak appears at approximately 478 nm due to the presence of a more nonpolar environment. The quantum yield of ANS in lipid vesicles was found to be enhanced by 50 times than in an aqueous medium. As ANS lies near the hydrophilic interfacial region of the lipid vesicles, any changes in the environments affect the spectral properties of ANS. Figure 3.9a-c reveals that the emission spectra of DMPC-ANS are blue-shifted in the presence of metal ions. Among these three metal ions, In^{3+} shows the maximum blue shift, whereas Al^{3+} and Ga^{3+} show a similar spectral shift, which is much lower than that of In^{3+}. The shifting in the emission spectra of ANS upon the addition of metal ions indicates the extrusion of water molecules from the DMPC lipid vesicles. Figure 3.9d shows the fluorescence intensity ratio (I_{474}/I_{518}) of ANS-DMPC vesicles in the presence of metal ions, where I_{474}/I_{518} indicates the hydrophobicity degree at the liposomal membrane surface as reported earlier [49]. In the presence of In^{3+}, the intensity ratio values are much higher than those in the presence of Al^{3+} and Ga^{3+}, whereas these two have a similar effect on the membrane surface. This observation is in complete agreement with our previous observation (using PRODAN as a probe).

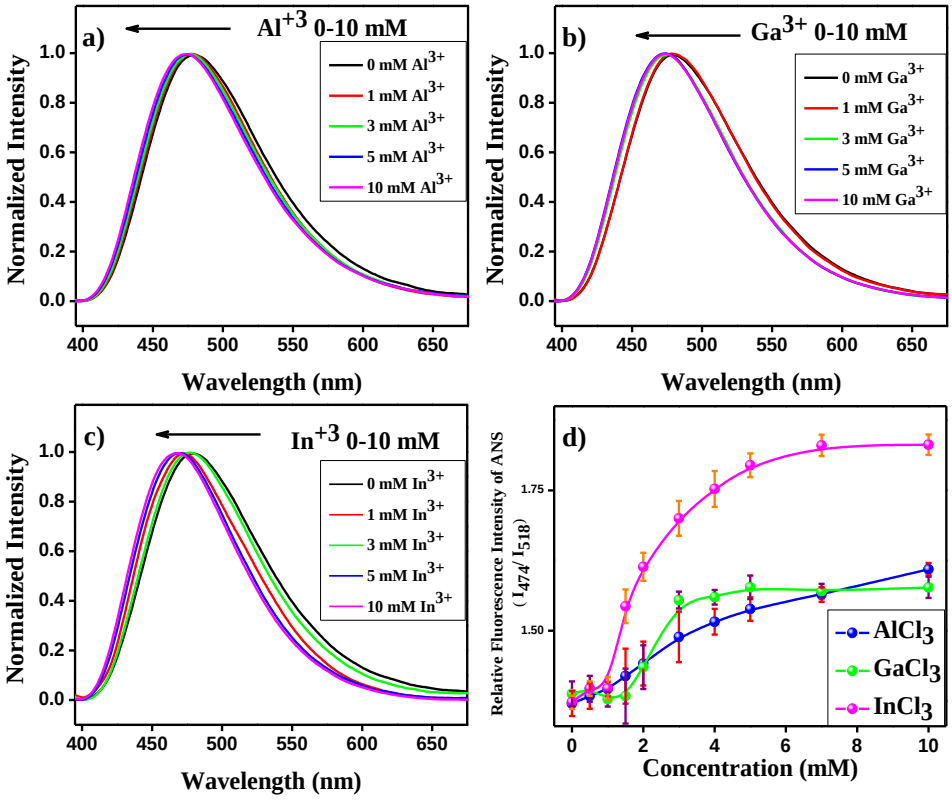

Figure 3.9 Normalized emission spectra of ANS in DMPC vesicles at various concentrations of metal salts (0−10 mM): (a) Al^{3+}, (b) Ga^{3+}, and (c) In^{3+} and (d) relative fluorescence intensity of ANS in DMPC in the presence of metal ions with various concentrations (0−10 mM).

We also conducted the lifetime and time-resolved anisotropy measurements in the presence of metal ions in the DMPC-ANS lipid vesicles. All of the decays are collected at 478 nm and shown in Figure 3.10. The decay parameters due to the addition of metal ions are summarized in Table 3.3. We found that the decay of ANS in lipid vesicles is tri-exponential in nature and the longer component τ_3 is the contribution of ANS, which is impregnated in the lipid vesicle interface. We observed that with increasing the concentration of Al^{3+}, Ga^{3+}, and In^{3+} the average lifetime of ANS in DMPC lipid vesicles increases from 5.54 to 8.25, 8.01, and 9.48 ns respectively. We also noted that the rotational relaxation decay of DMPC-ANS in the presence of metal ions is almost parallel to the X-axis, which confirms the rigidification of membranes in the presence of metal ions. Again, these observations are also in accordance with the results obtained by using PRODAN as a spectral probe.

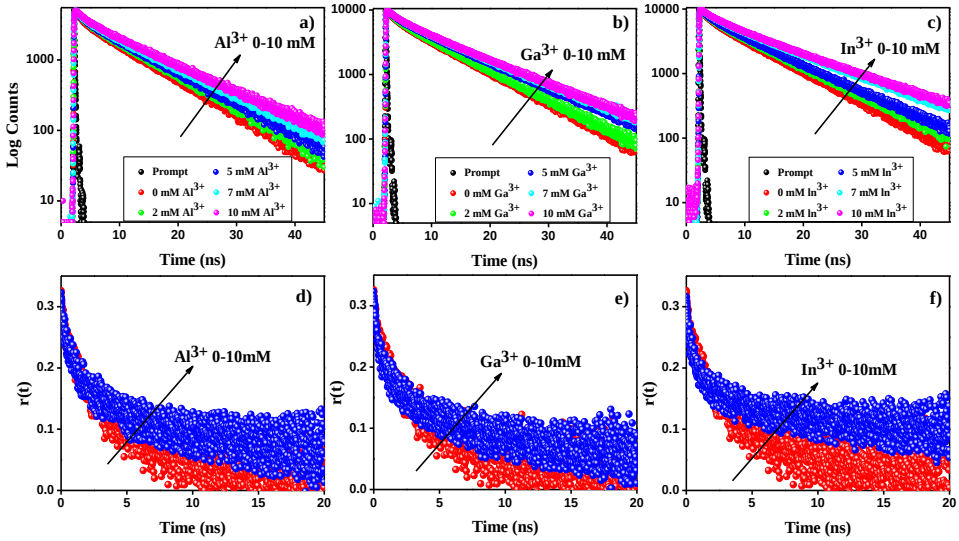

Figure 3.10 Time-resolved decay curves of ANS in DMPC lipid vesicles at various concentrations of (a) Al^{3+}, (b) Ga^{3+}, and (c) In^{3+} at 478 nm and anisotropy decays of ANS in DMPC lipid vesicles at various concentrations of (d) Al^{3+}, (e) Ga^{3+}, and (f) In^{3+} at 478 nm, 25 °C, at pH 7.0.

Table 3.3 Time resolved data for the DMPC-ANS at 478 nm upon increasing concentration of metal salts at fixed lipid concentration (0.4 mM). [#]

DMPC	χ^2	τ_1 (ns)	τ_2 (ns)	τ_3 (ns)	a_1	a_2	a_3	<τ>(ns)
0 mM Al^{+3}	1.03	1.79	0.31	9.09	0.19	0.24	0.56	5.54
1 mM Al^{+3}	1.00	2.38	0.45	9.47	0.17	0.23	0.60	6.17
2 mM Al^{+3}	1.05	2.57	0.46	9.65	0.18	0.22	0.60	6.34
3 mM Al^{+3}	1.03	2.22	0.37	9.74	0.19	0.21	0.61	6.40
4 mM Al^{+3}	1.04	2.90	0.57	10.23	0.17	0.20	0.63	7.01
5 mM Al^{+3}	1.03	3.04	0.53	10.51	0.17	0.21	0.62	7.12
7 mM Al^{+3}	1.01	3.25	0.51	10.86	0.18	0.21	0.61	7.31
10 mM Al^{+3}	1.05	3.29	0.48	11.19	0.19	0.21	0.60	7.44
	χ^2	τ_1 (ns)	τ_2 (ns)	τ_3 (ns)	a_1	a_2	a_3	<τ>
0 mM Ga^{+3}	0.99	1.78	0.29	9.10	0.19	0.24	0.56	5.55
1 mM Ga^{+3}	1.03	1.93	0.32	9.22	0.19	0.24	0.57	5.72

2 mM Ga^{+3}	1.04	2.44	0.45	9.51	0.18	0.24	0.59	6.12
3 mM Ga^{+3}	1.05	3.32	0.52	10.79	0.18	0.22	0.60	7.22
4 mM Ga^{+3}	1.02	3.57	0.52	11.19	0.18	0.22	0.60	7.52
5 mM Ga^{+3}	1.12	3.50	0.53	11.33	0.19	0.21	0.61	7.64
7 mM Ga^{+3}	1.07	3.98	0.62	11.65	0.19	0.21	0.60	7.91
10mM Ga^{+3}	1.01	3.41	0.45	11.66	0.19	0.20	0.61	7.83
	χ^2	**τ_1 (ns)**	**τ_2 (ns)**	**τ_3 (ns)**	**a_1**	**a_2**	**a_3**	**$<\tau>$**
0 mM In^{+3}	0.99	1.78	0.29	9.10	0.19	0.24	0.56	5.55
1 mM In^{+3}	1.08	3.01	0.48	10.03	0.18	0.25	0.57	6.38
2 mM In^{+3}	1.10	3.87	0.60	10.85	0.19	0.25	0.56	6.94
3 mM In^{+3}	1.06	4.15	0.62	13.04	0.20	0.18	0.62	9.07
4 mM In^{+3}	1.01	4.21	0.59	13.47	0.20	0.16	0.63	9.49
5 mM In^{+3}	1.04	4.22	0.52	13.56	0.20	0.17	0.63	9.43
7 mM In^{+3}	1.08	4.12	0.55	13.63	0.21	0.17	0.63	9.46
10 mM In^{+3}	1.00	4.54	0.58	13.76	0.21	0.18	0.61	9.46

 # Experimental error in the measurement is around 5%.

3.2.5 <u>Metal-induced aggregation of lipid vesicles</u>: To investigate the effect of the metal ions on the size of the lipid vesicle, a systematic DLS measurement has been carried out in the presence and in the absence of metal salt. Table 3.4 and Figure 3.11a−c show that the lipid vesicle has a size of around 150 nm. An increase in the concentration of the metal salts up to 30 mM reduces the size of the vesicles to almost half of their original size (Table 3.4). The possible reason for the initial shrinkage in the size of lipid vesicles at a low concentration of metal salt is osmotic pressure *[50]*. One important point needs to be noted that the metal salts also exhibit hydrodynamic size around 200−250 nm, which depicts the possible hydrolysis of metal salts in buffer solution (Table 3.4 and Figure 3.12a). Therefore, as the metal salts undergo hydrolysis, there is a high possibility for the lipid vesicle to interact

with the metal oxide or hydroxide *[61]*. However, in the present case, the significant reductions in the size of lipid vesicle up to 30 mM for all of the metal salts (shown by the arrow in Figure 3.11a–c) indicate that the interaction of lipid vesicle with metal ions is much more dominating and prominent than the interaction with the metal oxide or hydroxide (otherwise addition of metal salts increases the size of the DMPC system due to the higher size of the hydrolyzed metal salt compared to blank DMPC). Moreover, we did not observe any precipitation in the solution in the presence of Al^{3+} and Ga^{3+}. A further increase in the concentration of Al^{3+} and Ga^{3+} has no effect on the size of lipid vesicles (Figure 3.11a-b). This observation is similar to that mentioned in our recent publication, *[47]* where we reported that a gold nanoparticle causes significant shrinkage in the size of lipid vesicles due to gelation. In contrast, In^{3+} was found to increase the size of lipid vesicles rapidly up to 3.7 μM (Figure 3.11c). The observation leads to the conclusion that In^{3+} induces fusion in lipid vesicles. Apparently, there is a specific interaction between lipid molecules and In^{3+} ions. A similar fusion was reported in the case of calcium ions *[51]*. To establish the fusion phenomena, we conducted time-dependent DLS measurements at the highest concentration of metal salts. Figure 3.11d demonstrates that the size of lipid vesicles increases as a function of time in the case of In^{3+}, while the size remains almost unchanged for Al^{3+} and Ga^{3+} with time. Notably, we did not observe any change in the size of the pure metal salt over a period of experimental time (data not shown). Therefore, it is conclusive that at pH ~ 7.0 the fusion is induced by In^{3+} ions.

Table 3.4 Dynamic light scattering (DLS) measurements of hydrated metal salts and DMPC vesicles in presence of different concentration of metal salts.

System	Size (nm)	PDI	System	Size (nm)	PDI
DMPC	154	0.326			
DMPC + 10 mM $AlCl_3$	80.3	0.261	DMPC + 10 mM $GaCl_3$	90.6	0.248
DMPC + 20 mM $AlCl_3$	70.7	0.256	DMPC + 20 mM $GaCl_3$	77.1	0.269
DMPC + 30 mM $AlCl_3$	75.5	0.246	DMPC + 30 mM $GaCl_3$	75.3	0.264
DMPC +40 mM $AlCl_3$	79.1	0.141	DMPC + 40 mM $GaCl_3$	78.7	0.220

DMPC + 50 mM $AlCl_3$	69.4	0.260	DMPC + 50 mM $GaCl_3$	75.4	0.252
DMPC + 70 mM $AlCl_3$	71.0	0.248	DMPC + 70 mM $GaCl_3$	71.7	0.263
DMPC + 10 mM $InCl_3$	87.3	0.295			
DMPC + 20 mM $InCl_3$	63.2	0.301	Salt of $AlCl_3$ in buffer	232.7	0.180
DMPC + 30 mM $InCl_3$	82.9	0.286	Salt of $GaCl_3$ in buffer	215.1	0.256
DMPC + 40 mM $InCl_3$	560.7	0.393	Salt of $InCl_3$ in buffer	220.5	0.218
DMPC + 50 mM $InCl_3$	1276.4	0.425			
DMPC + 70 mM $InCl_3$	3546.1	0.609			

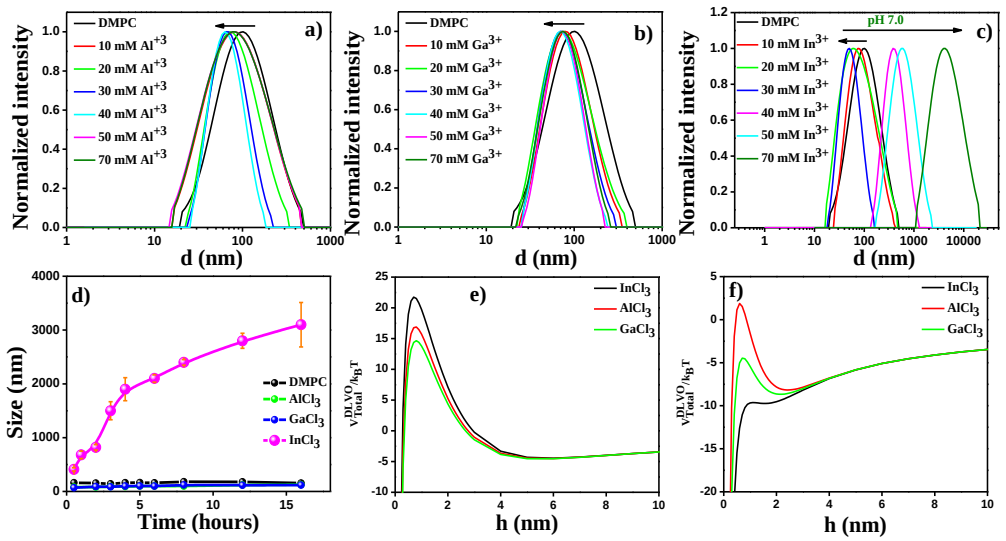

Figure 3.11 Normalized DLS spectra of DMPC lipid vesicles in the presence of different concentrations of (a) Al^{3+}, (b) Ga^{3+}, and (c) In^{3+} at pH 7.0. (d) Plot of the increasing size of lipid vesicles in the presence of metal ions (70 mM) as a function of time. DLVO potential plot of DMPC lipid vesicles as a function of the inter vesicle distance for (e) 10 mM and (f) 50 mM metal salts.

On the other hand, at pH 5.5, we did not find any aggregation of vesicles (Figure 3.12c) in the presence of In^{3+} even at a very high concentration (70 mM). We discussed earlier that at lower pH, H^+ might bind with the phosphate group, which may prevent the metal ions from binding to the phospholipid head groups and preventing the aggregation process.

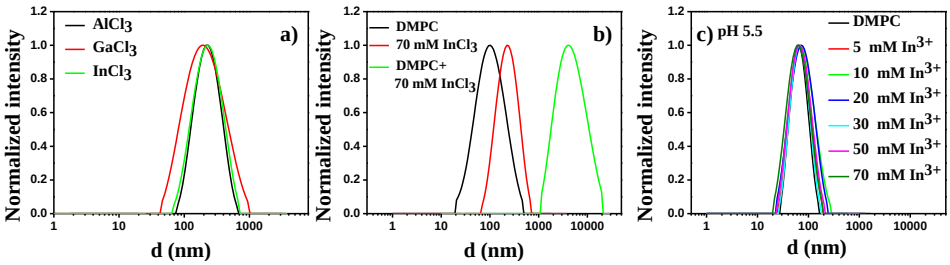

Figure 3.12 Normalized DLS spectra of (a) metal salts (70 mM) in HEPES buffer and (b) DMPC vesicles (black) with 70 mM In^{3+} (green) at pH 7.0. (c) Normalized DLS spectra of DMPC lipid vesicles in the presence of different concentrations of In^{+3} at pH ~5.50.

To validate the experimental results, we employed Derjaguin-Landau-Verwey-Overbeek (DLVO) theory to explain the stability of the DMPC lipid vesicles. The DLVO theory accounts for the interaction potential between lipid vesicles as the sum of electrostatic and van der Waals interactions as a function of distance *[52−55]*. The DLVO theory is a powerful technique in the prediction of the colloidal stability of liposomes. Based on DLVO theory total interaction energy between two surfaces is a sum of electrostatic ($V_{dl}\,(h)$) as well as of the van der Waals forces ($V_{vdw}\,(h)$) and this can be represented as:

$$V_{DLVO}^{Total}(h) = V_{vdw}(h) + V_{dl}(h) \tag{3.4}$$

For the case of sphere-sphere particle of equal radius the electrostatic interactions were calculated with the following expression:

$$V_{vdw}(h) = -\frac{A_{121}}{12}\left\{\frac{1}{X^2+2X} + \frac{1}{X^2+2X+1} + 2\ln\left[\frac{X^2+2X}{X^2+2X+1}\right]\right\} \tag{3.5}$$

and,

$$\mathrm{X} = \frac{h}{a} \tag{3.6}$$

Where A_{121} (J) is the combines Hamaker constant for interaction between two equal radius particles 1 in medium 2. Hamaker constant is a material property and its value is quite uncertain. Distance between the two spherical shells is h and a is the radius of the spherical particles.

Now, the $V_{dl}(h)$ for sphere-sphere interactions of equal radius were calculated with the expression:

$$V_{dl}(h) = 2\pi\varepsilon_o\varepsilon_r\Psi^2 \left[\ln\left(\frac{1+e^{-kh}}{1-e^{kh}}\right)+\ln\ (1-\ e^{-2kh}) \right] \quad (3.7)$$

Where ε_r is the relative dielectric constant of the medium and ε_o ($C^2\ J^{-1}\ m^{-1}$) is the permittivity of the free space. Ψ (V) is the surface potential of the spherical particles. And k (m^{-1}) is the inverse of the diffused layer thickness, known as the Debye-Huckel parameter:

$$k = \left[\frac{2\ N_A I_S\ 1000\ e^2}{\varepsilon_0\varepsilon_r\ k_B T}\right]^{1}/_{2} \quad (3.8)$$

Where N_A (mol^{-1}) is the Avogadro's number, I_s ($mol\ L^{-1}$) is the ionic strength of the medium, k_B ($J\ K^{-1}$) is the Boltzmann constant and T is the temperature.

The zeta potentials of the DMPC lipid vesicles at 10 and 50 mM concentrations of each of the metal ions were measured (Table 3.4). It is revealed that the zeta potentials of DMPC vesicles in the presence of 10 mM Al^{3+}, Ga^{3+}, and In^{3+} are 38.1, 37.2, and 40 mV, respectively. Using the value of the surface charge, we can represent the DLVO potential of the different salts at a particular concentration. Figure 3.11e represents the DLVO potential of DMPC lipid vesicles at 10 mM concentration of the metal salts. We found that at this particular concentration In^{3+} has the maximum potential among all of the metal salts. The fact implies that In^{3+} stabilizes the lipid vesicles much more than the other two metal ions. As the initial size of the lipid vesicles is the same, we conclude that a higher charge of the surface of the vesicle may play an important role in the stabilization of lipid vesicles. This result is in good agreement with our earlier observations from steady-state and TCSPC measurements. Figure 3.11f reveals that at 50 mM concentration of the metal salts, the DLVO potential significantly drops due to the change in the surface charge of metal ions. In this concentration range, the zeta potentials of the surface are 39.3, 35.9, and 30.5 mV for 50 mM concentration of Al^{3+}, Ga^{3+}, and In^{3+} respectively. We observe that the fall in primary maxima is the highest in the case of In^{3+}. The aggregation of the vesicles will occur when the repulsive barrier is lower than k_BT. This suggests that the lipid vesicles have a tendency to form aggregated structures in the presence of metal ions in the following order, $In^{3+} > Ga^{3+} > Al^{3+}$. However, we did not find any kind of aggregation for Al^{3+} and Ga^{3+} up to 100 mM concentrations. This discrepancy

is in good agreement with Ohki et al., *[56]* they reported that according to DLVO theory, neutral PC vesicles might form stable vesicle aggregations due to van der Waals attractive forces. However, they observe that even at very high concentrations of ionic salt no aggregation appears among the PC (SUV) vesicles due to larger distances between the polar head groups.

3.2.6 <u>Confocal laser scanning microscopy (CLSM) and AFM measurements</u>: The DLS data already reveal an increase in the size of DMPC vesicles upon interaction with In^{3+} metal ions at a higher concentration, indicating that an aggregation of lipid vesicles. Moreover, we observe that the In^{3+} induced fusion of the lipid vesicles over a period of time, while fusion did not occur in the case of Al^{3+} and Ga^{3+} ions. This observation is further supported by the DLVO theory, which indicates that aggregation of vesicles is possible at a higher concentration of salt. To visualize the aggregated form of lipid vesicles, we conducted CLSM measurements to capture the aggregated form of the lipid vesicles at a different time interval to monitor the process of aggregation. Figure 3.13a reveals that the DMPC vesicles (in the absence of metal ions) were monodispersed and had a size around ~ 450 nm (Please note that for confocal imaging the multilamellar vesicles were prepared). The addition of Al^{3+} or Ga^{3+} induces gelation or dehydration in lipid vesicles, and this is evident from confocal imaging, which indicates the formation of more compact structures upon the addition of Al^{3+} or Ga^{3+} (Figure 3.13 d-f and g-i). We did not observe any aggregation over a significant time period. This fact confirms that Al^{3+} and Ga^{3+} do not induce aggregation in lipid vesicles despite the fact that they dehydrate the surface of lipid vesicles.

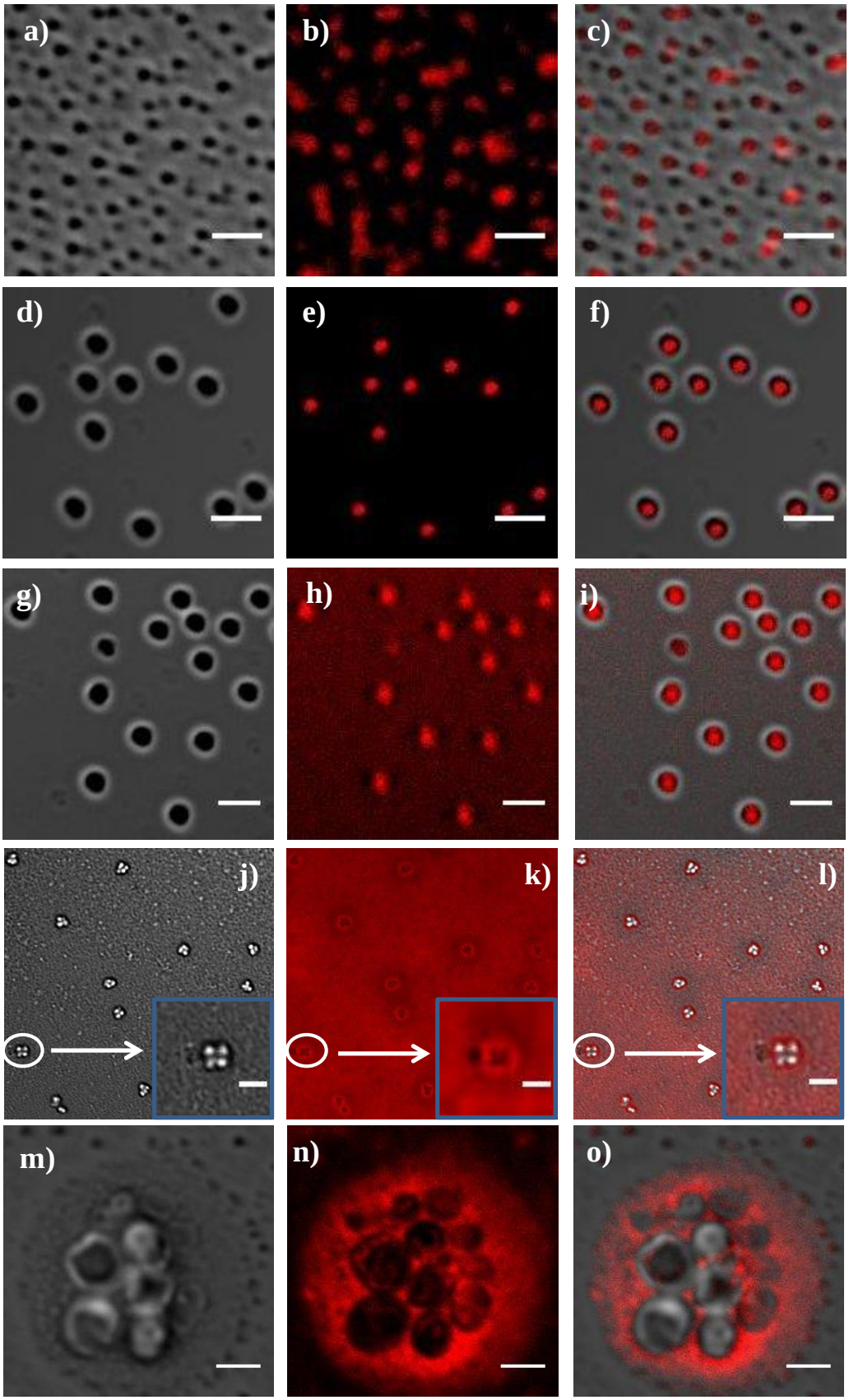

Figure 3.13: Confocal laser scanning microscopy images of DMPC in the presence and absence of metal salts. Bright field, confocal, and merged images of only DMPC vesicles as control with encapsulated Rh-B (a-c), of DMPC vesicles in the presence of 70 mM Al^{3+} (d-f),

Ga^{3+} (g-i) (images taken after 6 h), and of aggregated DMPC vesicles in the presence of 40 mM In^{3+} (j-l) (images taken after 8 h and the encircled section has been zoomed in the figure to illustrate fusion) and 70 mM In^{3+} (m-o) (images taken after 12 h). The scale bar indicates 1 μm.

However, unlike Al^{3+} and Ga^{3+}, we found that In^{3+} induces aggregation to the DMPC vesicles (Figure 3.13j−l). We further observe that after a significant time period the vesicles form giant aggregates consisting of several individuals or aggregated vesicles. We found that in presence of 70 mM In^{3+} and after 12 h, the final size of the vesicles was around 3.5 μm (Figure 3.13m-o). The initial size of the lipid vesicles was 450 nm; therefore the huge increment in the size of the vesicles clearly indicates that the fusion of lipid vesicles takes place in the presence of In^{3+}. This observation is in good agreement with the results obtained from DLS measurements. As we already mentioned that dehydration of DMPC vesicles facilitates their fusion with themselves, we observe that even the low concentration of In^{3+} leads to the aggregation of lipid vesicles if sufficient time is given (data not shown). However, the CLSM study confirms that the DMPC vesicles do not fuse in the presence of Al^{3+} and Ga^{3+} (Figure 8d−f and g−i). The fusion process of different vesicles in the presence of monovalent as well as divalent salts is well reported in the literature *[57−60]*. We conclude that In^{3+} dehydrates DMPC vesicles much more than the rest of the metal ions. The higher dehydration could be the leading reason behind the In^{3+}-induced fusion of DMPC lipid vesicles. As mentioned previously, CLSM imaging revealed some micrometer size aggregated structures of lipid vesicles along with nanometer size vesicles. The results are in good agreement with Liu et al. *[12]* They reported that some vesicles might break in this process and fused onto other ones (or onto the fused larger liposomes), but there were some intact vesicles present that were most likely protected from further interaction with metal ions. We conclude that the intact vesicles may form aggregated structures. It is a well-known fact that fusion causes leakage of the encapsulated dye completely from lipid vesicles. The confocal images indicate that before fusion, the dye was encapsulated inside the vesicles and thus we obtained a few spots of nanometer size (Figure 3.13b-c). The fusion process induced by In^{3+} leads to a huge increase in size, and the encapsulated dye leaks out from the vesicles;

thus, we obtain a very high intensity of the dye in the background during CLSM imaging. The fusion and aggregation also explain the observed leakage of the dye from DMPC vesicles.

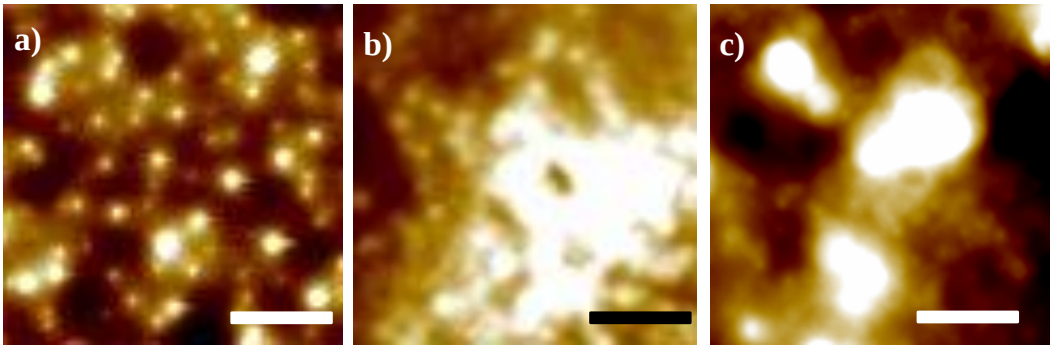

Figure 3.14 Time-dependent atomic force microscopy (AFM) images of DMPC in the presence and absence of In^{3+}. (a) Blank DMPC and in the presence of 70 mM In^{3+} (b) after 2 h and (c) after 6 h. The scale bar indicates 2 μm.

Along with the CLSM images, we also recorded AFM images to visualize the aggregation process of the lipid vesicles in the presence of metal salts (Figure 3.14). The AFM images are in agreement with the CLSM images and reveal that lipid vesicles undergo fusion in the presence of In^{3+}; however, no fusion was induced by either Al^{3+} or Ga^{3+} (data not shown).

3.3 Conclusion

In summary, we have systematically studied the interaction between DMPC lipid vesicles and trivalent metal ions in particular by various spectroscopic measures. We summarized the following important observations:

(1) We find that trivalent metal ions strongly interact with the lipid vesicles and result in dehydration of the surface of the lipid vesicles. This interaction is stronger in the case of In^{3+} owing to the higher ionic radius as compared to that in the case of Al^{3+} and Ga^{3+}. The interaction and the resulting gelation cause a slowing down of the dynamics, which is reflected by the lifetime and time-resolved anisotropy measurements of the lipid vesicle.

(2) One important observation is that trivalent metal ions induce gelation of the lipid vesicles even at a very low pH, whereas divalent metal ions have little effect at low pH. The observation indicates that at a lower concentration trivalent metal ions can stabilize the lipid vesicles even at a lower pH.

(3) The DLS measurements reveal that the average hydrodynamic diameter of DMPC vesicles decreases in the concentration range from 0 to 30 mM upon the addition of all metal salts. Further, an increase in the In^{3+} concentration results in enhancement of the size of lipid vesicles rapidly. In contrast, Al^{3+} and Ga^{3+} did not increase the size of lipid vesicles beyond the concentration of 30 mM. From CLSM imaging, it is confirmed that In^{3+} leads to both aggregation and fusion of DMPC vesicles. The aggregation phenomenon is justified in light of the DLVO theory.

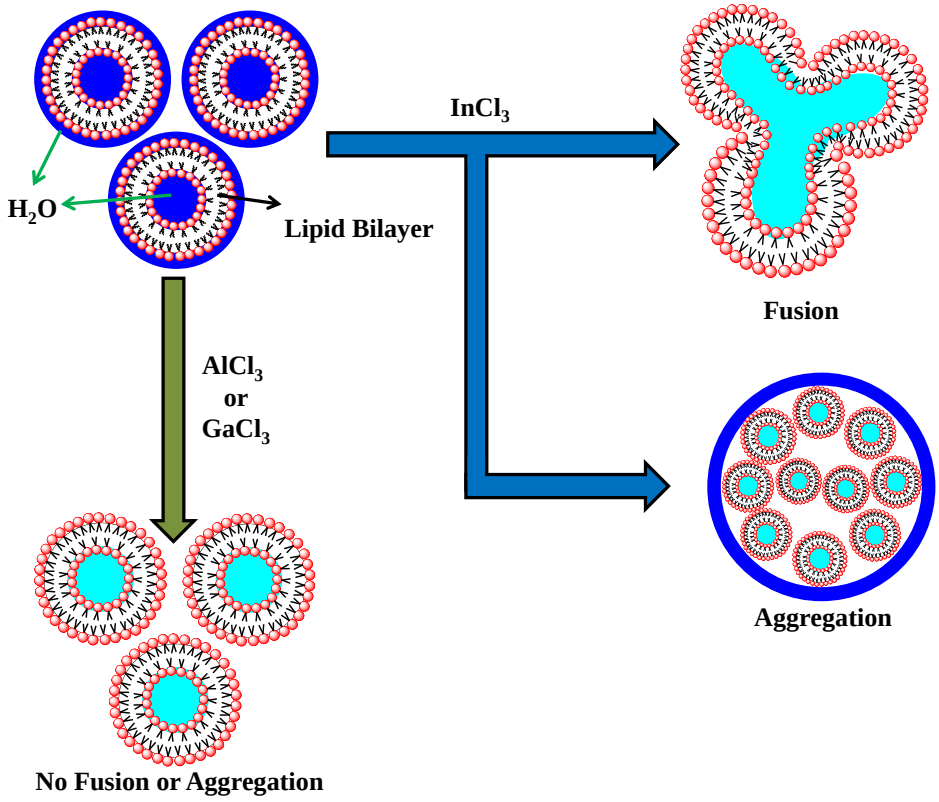

Scheme 3.1 Pictorial representation of the interaction of the trivalent metal ions (Al^{3+}, Ga^{3+} and In^{3+}) with the DMPC lipid vesicles.

3.4 References

1. Chapman D., Peel W. E., Kingston B., Lilley T. H. (1977), Lipid phase transitions in model biomembranes-the effect of ions on phosphatidylcholine bilayers, Biochim. Biophys. Acta, Biomembr., 464, 260-275 (DOI: 10.1016/0005-2736(77)90002-5)

2. Ohki S., Zschörnig O. (1993), Ion-induced fusion of phosphatidic-acid vesicles and correlation between surface hydrophobicity and membrane-fusion, Chem. Phys. Lipids, 65, 193-204 (DOI: 10.1016/0009-3084(93)90017-W)

3. McManus, J. J., Radler J. O., Dawson K. A. (2003), Does calcium turn a zwitterionic lipid cationic?, J. Phys. Chem. B, 107, 9869-9875 (DOI: 10.1021/jp034463d)

4. Petrache H. I., Zemb T., Belloni L., Parsegian V. A. (2006), Salt screening and specific ion adsorption determine neutral-lipid membrane interactions, Proc. Natl. Acad. Sci. U. S .A., 103, 982-7987 (DOI: 10.1073/pnas.0509967103)

5. Szekely O., Steiner A., Szekely P., Amit E., Asor R., Tamburu C., Raviv U. (2011), The structure of ions and zwitterionic lipids regulates the charge of dipolar membranes, Langmuir, 27, 7419-7438 (DOI: 10.1021/la200264s)

6. Jurkiewicz P., Cwiklik L., Vojtíšková A., Jungwirth P., Hof M. (2012), Structure, dynamics, and hydration of POPC/POPS bilayers suspended in NaCl, KCl, and CsCl solutions, Biochim. Biophys. Acta. Biomembr., 1818, 609-616 (DOI: 10.1016/j.bbamem.2011.11.033)

7. Monson C. F., Cong X., Robison A. D., Pace H. P., Liu C., Poyton M. F., Cremer P. S. (2012), Phosphatidylserine reversibly binds Cu^{2+} with extremely high affinity, J. Am. Chem. Soc., 134, 7773-7779 (DOI: 10.1021/ja212138e)

8. Cong X., Poyton M. F., Baxter A. J., Pullanchery S., Cremer P. S. (2015), Unquenchable surface potential dramatically enhances Cu^{2+} binding to phosphatidylserine lipids, J. Am. Chem. Soc., 137, 7785-7792 (DOI: 10.1021/jacs.5b03313)

9. Melcrová A., Pokorna S., Pullanchery S., Kohagen M., Jurkiewicz P., Hof M., Jungwirth P., Cremer P. S., Cwiklik L. (2016), The complex nature of calcium cation interactions with phospholipid bilayers, Sci. Rep., 6, 38035 (DOI: 10.1038/srep38035)

10. Poyton M. F., Sendecki A. M., Cong X., Cremer P. S. (2016), Cu^{2+} binds to phosphatidylethanolamine and increases oxidation in lipid membranes, J. Am. Chem. Soc., 138, 1584-1590 (DOI: 10.1021/jacs.5b11561)

11. Das A., Adhikari C., Chakraborty A. (2017), Interaction of different divalent metal ions with lipid bilayers: impact on the encapsulation of doxorubicin by lipid bilayers and lipoplex mediated deintercalation, J. Phys. Chem. B, 121, 1854-1865 (DOI: 10.1021/acs.jpcb.6b11443)

12. Liu Y., Liu J. (2017), Zn^{2+} induced irreversible aggregation, stacking and leakage of choline phosphate liposomes, Langmuir, 33, 14772-14779 (DOI: 10.1021/acs.langmuir.7b03209)

13. Fink L., Feitelson J., Noff R., Dvir T., Tamburu C., Raviv U. (2017), Osmotic stress induced desorption of calcium ions from dipolar lipid membranes, Langmuir, 33, 5636-5641 (DOI: 10.1021/acs.langmuir.7b00596)

14. Liu Y., Liu J. (2018), Cu^{2+}-directed liposome membrane fusion, positive-stain electron microscopy and oxidation, Langmuir, 34, 7545-7533 (DOI: 10.1021/acs.langmuir.8b00864)

15. Uhrikova D., Kucerka N., Teixeira J., Gordeliy V., Balgavy P. (2008), Structural changes in dipalmitoylphosphatidylcholine bilayer promoted by Ca^{2+} ions: a small-angle neutron scattering study, Chem. Phys. Lipids, 155, 80-89 (DOI: 10.1016/j.chemphyslip.2008.07.010)

16. Yang J., Calero C., Bonomi M., Mart J. (2015), Specific ion binding at phospholipid membrane surfaces, J. Chem. Theory Comput., 11, 4495-4499 (DOI: 10.1021/acs.jctc.5b00540)

17. Eisenberg M., Gresalfi T., Riccio T., McLaughlin S. (1979), Adsorption of monovalent cations to bilayer membranes containing negative phospholipids, Biochemistry, 18, 5213-5223 (DOI: 10.1021/bi00590a028)

18. Sachs J. N., Nanda H., Petrache H. I., Woolf T. B. (2004), Changes in phosphatidylcholineheadgroup tilt and water order induced by monovalent salts: molecular dynamics simulations, Biophys. J., 86, 3772-3782 (DOI: 10.1529/biophysj.103.035816)

19. Akutsu H., Nagamori T. (1991), Conformational analysis of the polar head group in phosphatidylcholine bilayers: a structural change induced by cations, Biochemistry, 30, 4510-4516 (DOI: 10.1021/bi00232a020)

20. Simon S. A., Lis L. J., Kauffman J. W., Macdonald R. C. (1975), A calorimetric and monolayer investigation of the influence of ions on the thermodynamic properties of phosphatidylcholine, Biochim. Biophys. Acta, Biomembr., 375, 317-326 (DOI: 10.1016/0005-2736(75)90350-8)

21. Pabst G., Hodzic A., Strancar J., Danner S., Rappolt M., Laggner P. (2007), Rigidification of neutral lipid bilayers in the presence of salts. Biophys. J., 93, 2688-2696 (DOI: 10.1529/biophysj.107.112615)

22. Binder H., Arnold K., Ulrich A. S., Zschörnig O. (2001), Interaction of Zn^{2+} with phospholipid membranes. Biophys. Chem., 90, 57-74 (DOI: 10.1016/S0301-4622(01)00130-2)

23. Binder H., Zschörnig O. (2002), The effect of metal cations on the phase behavior and hydration characteristics of phospholipid membranes, Chem. Phys. Lipids, 115, 39-61 (DOI: 10.1016/S0009-3084(02)00005-1)

24. Kewalramani S., Hlaing H., Ocko B. M., Kuzmenko I., Fukuto M. (2010), Effects of divalent cations on phase behavior and structure of a zwitterionic phospholipid (DMPC) monolayer at the air-water interface, J. Phys. Chem. Lett., 1, 489-495 (DOI: 10.1021/jz9002873)

25. Tatulian S. A. (1987), Binding of alkaline-earth metal cations and some anions to phosphatidylcholine liposomes, Eur. J. Biochem., 170, 413-420 (DOI: 10.1111/j.1432-1033.1987.tb13715.x)

26. Alsop R. J., Schober R. M., Rheinstadter M. C. (2016), Swelling of phospholipid membranes by divalent metal ions depends on the location of the ions in the bilayers, Soft Matter, 12, 6737 (DOI: 10.1039/C6SM00695G)

27. Ruso J. M., Besada L., Martı´nez-Landeira P., Seoane L., Prieto G., Sarmiento F. (2003), Interactions between liposomes and cations in aqueous solution, J. Liposome Res., 13, 131-145 (DOI: 10.1081/LPR-120020316)

28. De S. K., Kanwa N., Ahamed M., Chakraborty A. (2018), Spectroscopic evidence for hydration and dehydration of lipid bilayers upon interaction with metal ions: a new physical insight, Phys. Chem. Chem. Phys., 20, 14796-17807 (DOI: 10.1039/C8CP01774C)

29. Papahadjopoulos D., Nir S., Düzgünes N. (1990), Molecular mechanisms of calcium-induced membrane fusion, J. Bioenerg. Biomembr., 22, 157-179 (DOI: 10.1007/bf00762944)

30. Martens S., McMahon H. T. (2008), Mechanisms of membrane fusion: disparate players and common principles, Nat. Rev. Mol. Cell Biol., 9, 543-556 (DOI: 10.1038/nrm2417)

31. Caël V., Van der Heyden A., Champmartin D., Barzyk W., Rubini P., Rogalska E. (2003), Interfacial approach to aluminum toxicity: interactions of Al(III) and Pr(III) with model phospholipid bilayer and monolayer membranes, Langmuir, 19, 8697-8708 (DOI: 10.1021/la034907x)

32. Sabín J., Prieto G., Sarmiento F. (2012), Stable clusters in liposomic systems, Soft Matter, 8, 3212-3222 (DOI: 10.1039/C2SM06907E)

33. Sabín J., Prieto G., Blanco E., Ruso J. M., Angelini R., Bordi F., Sarmiento F. (2007), Interaction of gadolinium with phospholipids bilayer membranes, photon correlation spectroscopy and DSC study, J. Therm. Anal. Calorim., 87, 199-203 (DOI: 10.1007/s10973-006-7841-6)

34. Akenson M. A., Munns D. N., Burau R. G. (1989), Adsorption of Al^{3+} to phosphatidylcholine vesicles, Biochim. Biophys. Acta, Biomembr., 96, 33-40 (DOI: 10.1016/0005-2736(89)90269-1)

35. Bürgel S. C., Guillaume-Gentil O., Zheng L., Vörös J., Bally M. (2010), Zirconium ion mediated formation of liposome multilayers, Langmuir, 26, 10995-11002 (DOI: 10.1021/la9047566)

36. Tanaka T., Tamba Y., Masum S. Md., Yamashita Y., Yamazaki M. (2002), La^{3+} and Gd^{3+} induce shape change of giant unilamellar vesicles of phosphatidylcholine, Biochim. Biophys. Acta, Biomembr., 1564, 173-182 (DOI: 10.1016/S0005-2736(02)00444-3)

37. Verstraeten S. V., Oteiza P. I. (2000), Effects of Al^{3+} and related metals on membrane phase state and hydration: correlation with lipid oxidation, Arch. Biochem. Biophys., 375, 340-346 (DOI: 10.1006/abbi.1999.1671)

38. Petersheim M., Sun J. (1989), On the coordination of La^{3+} by phosphatidylserine, Biophys. J., 55, 631-636 (DOI: 10.1016/S0006-3495(89)82860-7)

39. Hammoudah M. M., Nir S., Isac T., Kornhauser R., Stewart T. P., Hui S. W., Vaz W. L. C. (1979), Interactions of La^{3+} with phosphatidylserine vesicles binding, phase transition, leakage and fusion, Biochim. Biophys. Acta, Biomembr., 558, 338-343 (DOI: 10.1016/0005-2736(79)90270-0)

40. Bentz J., Alford D., Cohen J., Duzgunes N. (1988), La^{3+}-induced fusion of phosphatidylserine liposomes. Close approach, intermembrane intermediates, and the electrostatic surface potential, Biophys. J., 53, 593-607 (DOI: 10.1016/S0006-3495(88)83138-2)

41. Parasassi T., Krasnowska E. K., Bagatolli L., Gratton E. (1998), Laurdan and prodan as polarity-sensitive fluorescent membrane probes, J. Fluoresc., 8, 365-373 (DOI: 10.1023/A:1020528716621)

42. Krasnowska E. K., Gratton E., Parasassi T. (1998), Prodan as a membrane surface fluorescence probe: partitioning between water and phospholipid phases, Biophy. J., 74, 1984-1993 (DOI: 10.1016/S0006-3495(98)77905-6)

43. Gutowicz J., Krawczyk A. (1986), Effect of 1-anilinonaphthalene-8-sulphonate on phase transition temperature of dipalmitoylphosphatidylcholine liposomes, Chem. Phys. Lipids, 39, 357-364 (DOI: 10.1016/0009-3084(86)90117-9)

44. Kachel K., Asuncion-Punzalan E., London E. (1998), The location of fluorescence probes with charged groups in model membranes, Biochim.

Biophys. Acta, Biomembr., 1374, 63-76 (DOI: 10.1016/s0005-2736(98)00126-6)

45. Slavík J. (1982), Anilinonaphthalenesulfonate as a probe of membrane composition and function, Biochim. Biophys. Acta, Rev. Biomembr., 694, 1-25 (DOI: 10.1016/0304-4157(82)90012-0)

46. Juliano R. L., Stamp D. Biochem. (1975),The effect of particle size and charge on the clearance rates of liposomes and liposome encapsulated drugs, Biochem. Biophys. Res. Commun., 63, 651-658 (DOI: 10.1016/S0006-291X(75)80433-5)

47. Kanwa N., De S. K., Adhikari C., Chakraborty A. (2017), spectroscopic study of the interaction of carboxyl-modified gold nanoparticles with liposomes of different chain lengths and controlled drug release by layer-by-layer technology, J. Phys. Chem. B,121, 11333-11343 (DOI: 10.1021/acs.jpcb.7b08455)

48. Lehrmann R., Seelig J. (1994), Adsorption of Ca^{2+} and La^{3+} to bilayer membranes: measurement of the adsorption enthalpy and binding constant with titration calorimetry, J. Biochim. Biophys. Acta, Biomembr., 1189, 89-95 (DOI: 10.1016/0005-2736(94)90284-4)

49. Ishigami T., Suga K., and Umakoshi H. (2015),Chiral recognition of L-amino acids on liposomes prepared with L-phospholipid, ACS Appl. Mater. Interfaces, 7, 21065-21072 (DOI: 10.1021/acsami.5b07198)

50. Perkins R., and Vaida V. (2017), Phenylalanine increases membrane permeability, J. Am. Chem. Soc., 139, 14388-14391 (DOI: 10.1021/jacs.7b09219)

51. Zschörnig O., Richter W., Paasche G., Arnold K. (2000), Cation-mediated interaction of dextran sulfate with phospholipid vesicles: binding, vesicle surface polarity, leakage and fusion, Colloid. Polym. Sci., 278, 637-646 (DOI: 10.1007/s003960000295)

52. Sabín J., Prieto G., Messina P. V., Ruso J. M., Hidalgo-Alvarez R., and Sarmiento F. (2005), On the effect of Ca^{2+} and La^{3+} on the colloidal stability of liposomes, Langmuir, 21, 10968-10975 (DOI: 10.1021/la051397t)

53. Sabín J., Prieto G., Sennato S., Ruso J. M., Angelini R., Bordi F., and Sarmiento F. (2006), Effect of Gd^{3+} on the colloidal stability of liposomes, Phys. Rev. E, 74, 031913 (DOI: 10.1103/PhysRevE.74.031913)

54. Chrysikopoulos C. V., Syngouna V. I. (2012), Attachment of bacteriophages MS2 and ΦX174 onto kaolinite and montmorillonite: extended-DLVO interactions, Colloids Surf. B, 92, 74-83 (DOI: 10.1016/j.colsurfb.2011.11.028)

55. Hou W.-C., Moghadam B. Y., Corredor C., Westerhoff P., Posner J. D. (2012), Distribution of functionalized gold nanoparticles between water and lipid bilayers as model cell membranes, Environ Sci Technol., 46, 1869-76 (DOI: 10.1021/es203661k)

56. Ohki S., Ohshima H. (1999), Interaction and aggregation of lipid vesicles (DLVO theory versus modified DLVO theory), Colloids Surf. B, 14, 27-45 (DOI: 10.1016/S0927-7765(99)00022-3)

57. Day E. P., Kwok A. Y., Hark S. K., Ho J. T., Vail W. J., Bentz J., Nir S. (1980), Reversibility of sodium-induced aggregation of sonicated phosphatidylserine vesicles, Proc. Natl. Acad. Sci. U. S. A., 77, 4026-4029 (DOI: 10.1073/pnas.77.7.4026)

58. Henderson I. A., Paxton W. F. (2014), Salt, shake, fuse-giant hybrid polymer/lipid vesicles through mechanically activated fusion, Angew. Chem. Int. Ed., 53, 3372-3376 (DOI: 10.1002/ange.201309433)

59. Kundu N., Banerjee P., Kundu S., Dutta R., Sarkar N. (2017), Sodium chloride triggered the fusion of vesicle composed of fatty acid modified protic ionic liquid: a new insight into the membrane fusion monitored through fluorescence lifetime imaging microscopy, J. Phys. Chem. B, 121, 24-34 (DOI: 10.1021/acs.jpcb.6b09298)

60. Ohki S., Arnold K. (2000), A mechanism for ion-induced lipid vesicle fusion, Colloids Surf., B, 18, 83−97 (DOI: 10.1016/S0927-7765(99)00131-9)

61. We thank anonymous reviewer for pointing out this fact.

Chapter 4

Interaction of monomeric and self-assembled aromatic amino acids with model membranes: self-reproduction phenomena

4.1 Introduction

Membrane fusion is a fundamental process in cell biology like other fundamental processes such as viral infection, endocytosis, and exocytosis *[1-3]*. Phospholipids are a major component of the natural membrane. Phospholipid vesicle formation in cells, such as vesicular transport and organelle biogenesis, is critically dependent on membrane fission, which is induced by highly evolved proteins *[4]*. The proteins and their components, e.g. peptides and amino acids, play a vital role in different processes of cells such as self-reproduction, which is important for the origin of life. Among the essential amino acids, phenylalanine (Phe), tyrosine (Tyr), tryptophan (Trp) and histidine (His) are common aromatic amino acids, which self-assemble into ordered fibrils, showing common structural, biochemical, and biophysical features *[5-6]*. It has been suggested that Phe forms large amyloid-like fibrils in solution, which are responsible for the cytotoxicity observed in PKU *[7-8]*. Recently Vaida et al. found that amino acids even at a high concentration (~120 mM) only tend to form a small cluster in DPPC lipid vesicles; however, they form an amyloid-fibril crystal structure only upon drying the solution even at a lower concentration *[9]*. So, the amino acids in the solution phase, where they are preferably in a monomeric state, and upon drying, where they form an aggregated structure, should offer a different interaction with the lipid bilayer.

Among the natural aromatic amino acids, the interaction of Phe and Trp with the lipid membranes at different pH values is well studied in the literature *[10-11]*. All of these studies mainly focus on the effect of the monomeric unit of amino acids on the lipid bilayer. The spontaneous formation of amyloid-like

structures of these amino acids is recently reported *[12]* and it is believed that these assemblies are responsible for several major human neurodegenerative diseases *[13-14]*. In this regard, the interaction between the amyloid structure of amino acids and the lipid membrane is much more important to understand the underlying cytotoxic behaviour of these amino acids as well as several proteins or peptide based fusion and fission of the lipid membrane.

Recently, Li et al. investigated the interaction of small peptide FF (Phe–Phe) with lipid vesicles. This FF-lipid complex forms a membrane reservoir in phosphate buffered saline and can spontaneously generate phospholipid vesicles *[15-16]*. Sarkar et al. reported that phospholipid vesicles undergo self-reproduction in the presence of a cell-penetrating peptide *[17]*. Self-reproduction of the vesicles is a crucial step for mimicking the origin of life research *[18-19]*. Although numerous studies are available regarding the interaction of peptides and amino acids with lipid membranes, there is hardly any report on the effect of the amino acid amyloid on the lipid vesicles. Therefore; a well-controlled time-dependent investigation of the effect of amino acid amyloid on vesicles is yet to be conducted. This interaction may help us to understand the pathological mechanism of several human neurodegenerative diseases and mimicking critical cell functions. A phospholipid bilayer can be an excellent model for a cell membrane due to its structural similarity with living cells, which has attracted several scientists to study its interaction with amino acids *[20-25]*. We, therefore, intend to study the possible interaction of the model membrane with the monomeric unit of the amino acids and the effect of amino acid amyloid on the structure of the model membrane.

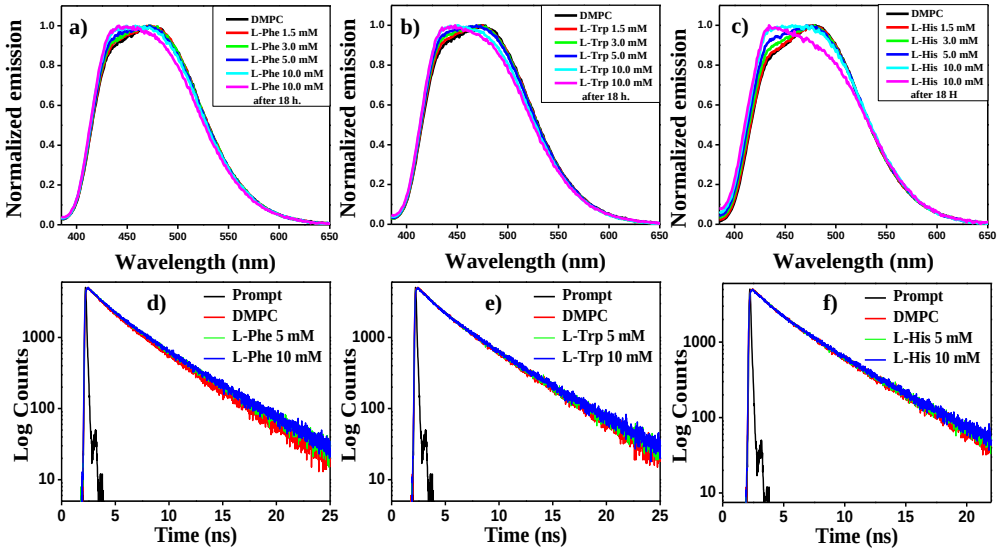

Figure 4.1 Normalized emission spectra (a-c) and time-resolved lifetime decay curves (d-f) of PRODAN in DMPC vesicles at different concentration of amino acids (0-10 mM) for L-Phe (a, d), L-Trp (b, e), and L-His (c, f) respectively.

4.2 Results and Discussion

4.2.1 Interaction of monomeric amino acids with the model membranes:

To unravel the interaction of monomeric amino acids with the lipid membrane, we used three combinations, zwitterionic (DMPC), negative (DMPC/DMPG), and positively charged (DMPC/DOTAP) model membrane. A series of amino acids consisting of L-phenylalanine (L-Phe), L-tryptophan (L-Trp), and L-histidine (L-His) have been used to observe the role of their side chain in lipid–amino acid interaction. We exploited the emission properties of PRODAN by steady-state and time resolved measurement as a function of amino acid concentration and as a function of time to evaluate the interaction of the model membrane with the monomeric unit of the amino acids.

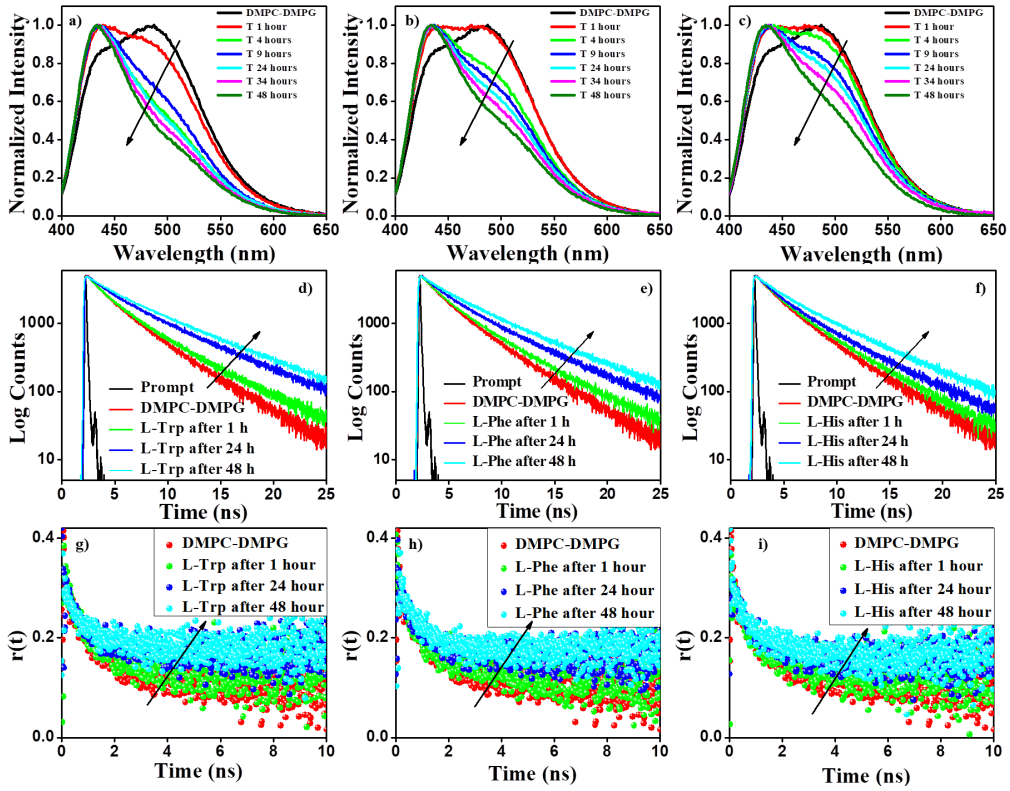

Figure 4.2 Time-dependent normalized emission spectra (a-c), time-resolved lifetime decay (d-f) and anisotropy decay (g-i) of PRODAN in DMPC: DMPG (8:2) vesicles in presence of 10 mM amino acids for L-Trp (a, d, g), L-Phe (b, e, h), and L-His (c, f, i) respectively.

We found that even after prolonged incubation of amino acids in the zwitterionic DMPC membrane, the emission spectra of PRODAN did not change significantly (Figure 4.1). This observation suggests that the interaction between the zwitterionic DMPC membrane and amino acids is very weak and moreover, this interaction is not a time-dependent process (Figure 4.1). To know the exact nature of the interaction, we varied the charge of the lipid membrane by taking negatively charged (DMPC/DMPG) and positively charged (DMPC/DOTAP) membrane. Interestingly, the interaction was found to be very much stronger with the negatively charged (DMPC/DMPG) lipid membrane compared to the zwitterionic one. The substantial blue shift of PRODN (at 1 hour) indicates that amino acids dehydrate the surface of the DMPC/DMPG lipid membrane (Figure 4.2) *[26]*. Furthermore, Figure 4.2 reveals that unlike the zwitterionic DMPC lipid membrane, the dehydration process in the DMPC/DMPG membrane is a time-dependent process that takes place over a period of time. On the other hand, amino acids do not exhibit

significant affinity towards a positively charged DMPC/DOTAP membrane (Figure 4.3). These observations lead us to conclude that the initial interaction is electrostatic in nature and takes place between the NH_3^+ group of the amino acid and the phosphate group (PO_4^-) of the lipid bilayer. Had the CO_2^- group of the amino acid been responsible for the interaction, we would have observed significant interaction with a positively charged DMPC/DOTAP lipid membrane. The time-dependent dehydration of lipid vesicles by the amino acids (Figure 4.2) also reveals that the amino acid is possibly re-configured with time so that the aromatic group can get inserted into the lipid membrane, which results in time-dependent dehydration.

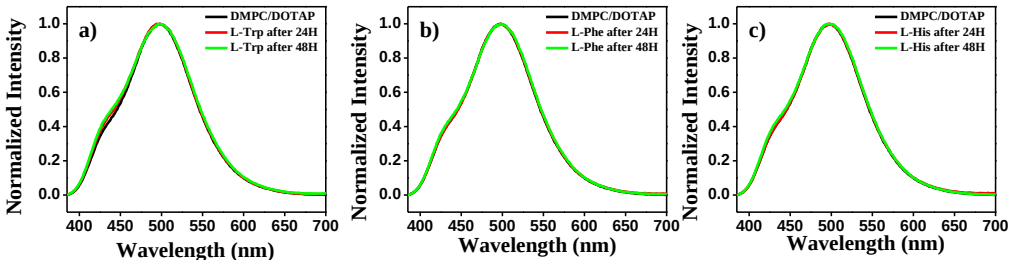

Figure 4.3 Normalized emission spectra of PRODAN in DMPC: DOTAP (8:2) vesicles at different concentration of amino acids (0-10 mM) for L-Trp (a), L-Phe (b), and L-His (c) respectively.

The insertion of the aromatic group into the lipid membrane is facilitated by the hydrophobic interaction. In order to quantify the extent of the gelation, we have plotted the generalized polarization data as a function of time, lifetime and time resolved anisotropy decays (Figure 4.4). The time-dependent general polarization (GP) plot indicates that the Trp has the maximum dehydration effect on the DMPC/DMPG lipid vesicles. The lifetime and anisotropy measurements were performed for the lipid-amino acid assemblies at the maximum incubation and we found a similar observation. The decay parameters of PRODAN in the DMPC/DMPG system due to the addition of these amino acids as obtained by the fitting of the decay curves are given in Table 4.1. We observed that with an increasing incubation time of L-Trp, L-Phe, and L-His, the average lifetime of PRODAN in DMPC/DMPG lipid vesicles increases from 2.92 ns to 5.33, 5.12, and 4.59 ns respectively. Time-dependence increment in the anisotropy decay (Figure 4.2g-i) for all of the

lipid-amino acid systems indicates that the PRODAN molecules sense more rigid environment with time. Figure 4.4c indicates that at a constant amino acid concentration, Trp exhibit the slowest rotational relaxation than Phe and His. Therefore, it is clear that the extent of gelation or dehydration by these amino acids follows the order L-Trp > L-Phe > L-His. Although Phe is slightly more hydrophobic than Trp, it is apparent that because of the bulky group, Trp more efficiently removes water molecules from the interfacial region. Thus we observe that His is even less efficient than Phe to interact with the lipid membrane. The other factors which help tryptophan to interact strongly with the lipid membrane are the hydrogen bonding ability and cationic–π electron interaction *[27-28]*. The phosphate choline bilayer normally has a stronger positive electrostatic potential in the hydrocarbon core which rapidly falls in the interfacial region. The strong electrostatic gradient could trap and hold molecules such as indole, which has a larger dipole *[27]*. Thus between Phe and Trp, Trp has a very strong tendency to direct the polar portion of the molecule toward the lipid–water interface. So, the possibility of interaction with the polar head group region of the bilayer is much more pronounced in the case of Trp than other amino acids. The electrostatic interaction is a rapid phenomenon and mostly causes instantaneous changes in the bilayer. Therefore, we conclude that the initial interaction is electrostatic and time-dependent changes are mostly arising from the hydrophobic interaction between lipid tail group and amino acids side chains. Figure 4.4a indicates that even after 4 hours of incubation the maximum changes were observed from Trp than Phe and His. To observe the effect of hydrophobic interaction of the side chain of the amino acids we have plotted the 'change in the general polarization (ΔGP)' after 4 hours (Figure 4d). Interestingly, we observed that the time-dependent changes (after 4 h) are more prominent in the case of Phe than Trp and His. As we previously mentioned, according to the hydrophobicity scale Phe is more hydrophobic than the other two amino acids. Therefore, higher hydrophobicity of the side chain helps to penetrate deeper into the lipid bilayer in a time-dependent manner.

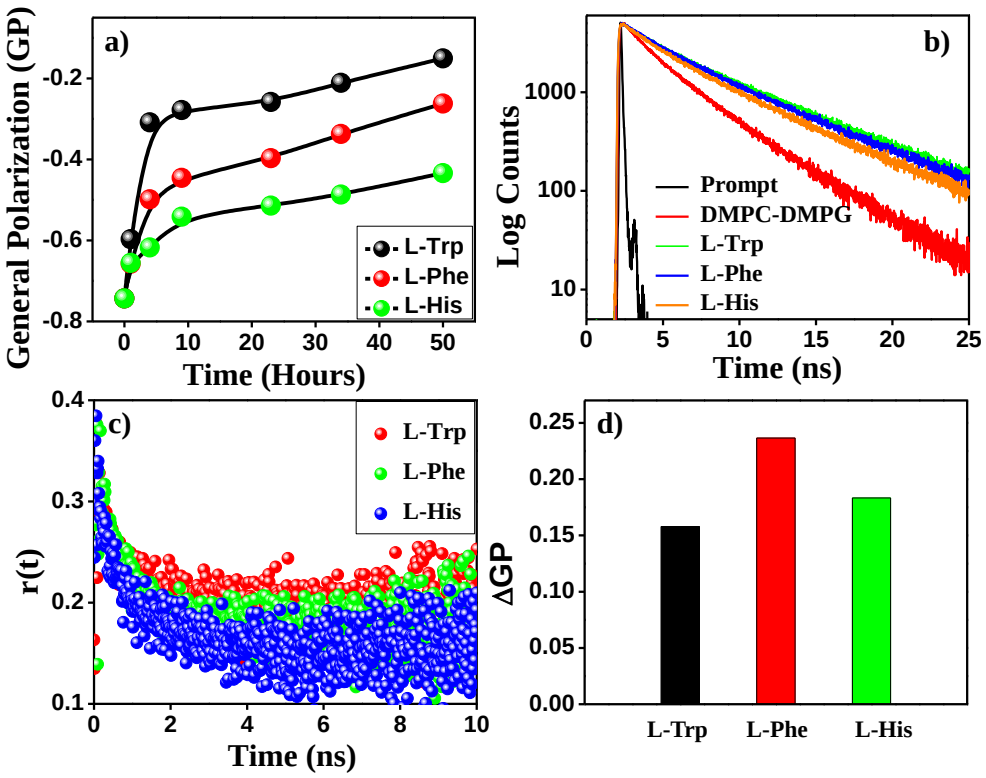

Figure 4.4 Time-dependent (a) general polarization plot of the area of DMPC/DMPG-PRODAN fluorescence emission at a fixed concentration of amino acids; (b) and (c) time-resolved and anisotropy decay curves of PRODAN in DMPC/DMPG, respectively after maximum incubation; (d) change in general polarization after 4 hours.

Table 4.1 Time-resolved lifetime data of PRODAN in DMPC: DMPG (8:2) system in presence of different amino acids collected at 440 nm at different time intervals, where [lipid] = 1 mM and [amino acid] = 10 mM.[#]

	χ^2	τ_1 (ns)	τ_2 (ns)	a_1	a_2	$<\tau>$ (ns)
DMPC/DMPG	1.10	1.50	4.23	0.48	0.52	2.92
Trp T 1 h	1.19	1.69	5.18	0.45	0.55	3.25
Trp T 24 h	1.12	1.86	6.49	0.42	0.58	4.55
Trp T 24 h	1.05	1.89	6.98	0.32	0.68	5.33
Phe T 1 h	1.16	1.76	5.08	0.53	0.47	3.33
Phe T 24 h	1.09	2.00	6.21	0.49	0.51	4.16
Phe T 48 h	1.08	2.28	6.85	0.38	0.62	5.12

His T 1 h	1.09	1.69	4.83	0.51	0.49	3.21
His T 24 h	1.19	1.77	5.49	0.50	0.50	3.61
His T 48 h	1.04	2.11	6.40	0.42	0.58	4.59

 # Experimental error in this measurement is around 5%.

4.2.2 <u>Interaction of self-assembled aromatic amino acids with model membrane:</u> After the spectroscopic investigation of the interaction of the monomeric unit of the aromatic amino acid with the lipid membrane, we studied the interaction of lipid membranes with amino acid assemblies that undergo amyloid formation. As the self-assembly behaviour of His into a well-ordered structure could not be established in water, we limited our investigation to Phe and Trp-assemblies *[5]*. It is important to note that under the current experimental conditions, the amino acid does not undergo aggregate formation in the solution state. We have confirmed this observation by ThT binding assay (Figure 4.5). The ThT emission intensity was collected at 485 nm while excited at 430 nm. The negligible increase in fluorescence intensity of ThT indicates that simply mixing the amino acids in the aqueous medium does not influence the formation of amyloid structure.

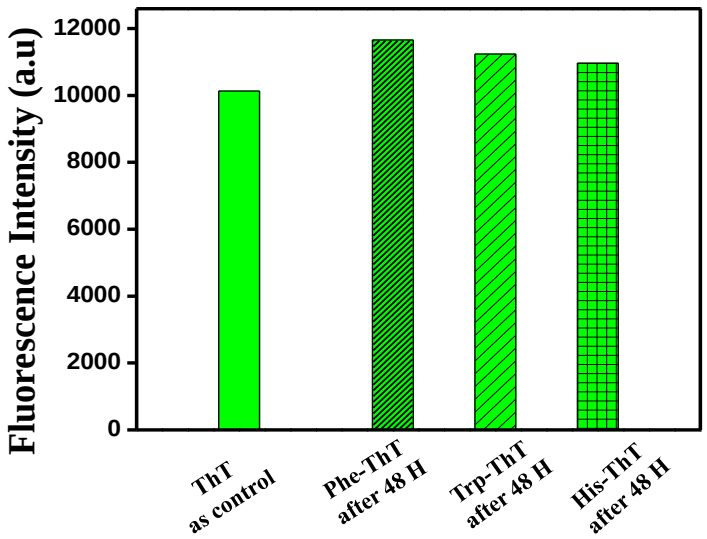

Figure 4.5 Steady-state fluorescence emission spectra of Thioflavin T (ThT) in the presence of different amino acids after 48 hours in a fixed lipid concentration.

Next, we monitored the susceptibility of a membrane incorporated fluorescent lipid probe NBD-PE (λ_{ex} = 460 nm and λ_{em} = 535 nm) using confocal microscopy (using λ_{ex} = 488 nm). To ensure that excess unbound amino acid does not influence the confocal images, we removed excess unbound amino acids by centrifuging the lipid–amino acid mixture. The final concentration of amino acid was around 3.5 and 6.1 mM for DMPC and DMPC/DMPG, respectively. Formations of the amyloid aggregate structure of these amino acids are well-reported in the literature *[12]* and importantly, the blank fibril structures show negligible fluorescence properties upon excitation at 488 nm (Figure 4.6). Therefore, the amyloid does not have the ability to influence the fluorescence of NBD-PE upon excitation at 488 nm.

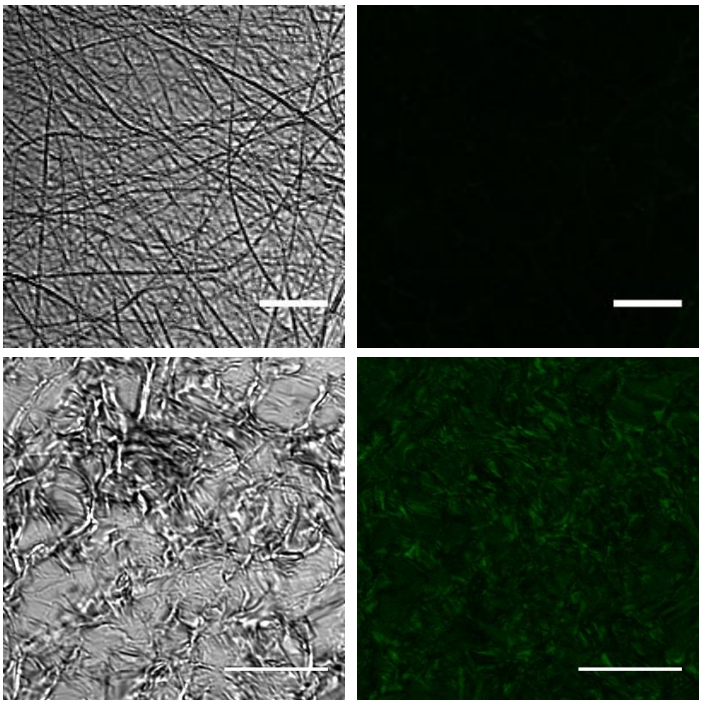

Figure 4.6 Bright field and confocal images of amyloid aggregates of Phe (a, b) and Trp (c, d) upon excitation at 488 nm laser. (Scale bar 10 µm)

Although the monomeric amino acid did not alter the surface properties of DMPC vesicles significantly in the solution state, the amyloids of amino acids bring about severe morphological changes in lipid vesicles. Figure 4.7a depicts the formation of spherical uniform vesicles of zwitterionic lipid of the size around 500–700 nm. The formation of amyloid aggregates of amino acids results in supported phospholipid membranes as well as deformed aggregated vesicles via fusion of the liposome (Figure 4.7b-c). The size of the vesicles

increases up to a few microns. The assembly process for the DMPC-amino system led to the formation of an aggregated structure of the lipid vesicles (Figure 4.7b), in which the size of the lipid vesicle increases several folds compared to blank DMPC vesicles. This indicates that the amyloid structure of amino acids leads to the fusion of lipid vesicles. The negligible presence of the amyloid structure in zwitterionic lipid vesicles (Figure 4.7b-c) is attributed to the less absorption of amino acids on the DMPC surface. A similar observation was found in the case of the DMPC–Trp system (Figure 4.7c). The aggregated lipid vesicles were also observed, but they are morphologically slightly different from the DMPC–Phe system.

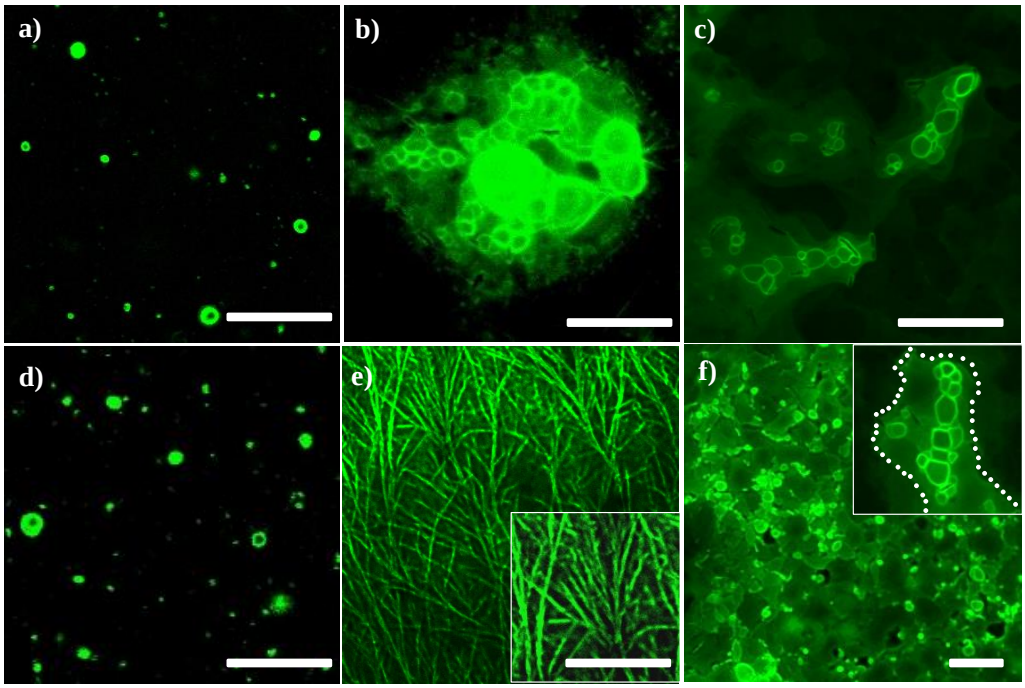

Figure 4.7 Confocal images of DMPC (a) and in the presence of Phe (b) and Trp (c) with 1 mol% NBD-PE. Confocal images of DMPC/DMPG (d) and in the presence of Phe (e) and Trp (f) with 1 mol% NBD-PE (scale bar 5 μm). Images were taken after drying the lipid–amino acid mixture to observe the changes by the amyloid formation.

However, the effects of these amyloid structures on DMPC/ DMPG vesicles were significantly different from that of the pure DMPC system. Figure 4.7e represents the formation of a needle-like fibril structure of Phe in the presence of a DMPC/DMPG membrane. The formation of a dense fibril structure is due to the high absorption of the amino acid (Phe) on DMPC/DMPG vesicles where lipid vesicles are barely seen. This supports our previous observation

that the negatively charged membrane displays a higher affinity towards amino acids. Interestingly, intense fluorescence was observed from all across the fibril–lipid structures upon excitation at 488 nm. The blank fibrils of Phe are non-fluorescent at this wavelength of excitation (Figure 4.6a-b), therefore; the intense fluorescence indicates that lipid vesicles or lipids are located all across the fibril structures. This observation concludes that the presence of a lipid membrane does not affect the formation of a fibril structure of Phe. The intense fluorescence from the fibril structure indicates the formation of a supported bilayer. Interestingly, for Trp, we observe a lipid membrane-amyloid Trp network type structure with the formation of amyloid structures (Figure 4.7f). In the network, lipid vesicles are found distorted and aggregated where Trp assembly is developed beneath the vesicles. As the Trp amyloid shows negligible fluorescence upon excitation at 488 nm (Figure 4.6c-d), the highly intense green fluorescence of the amyloid structure of Trp indicates that like Phe, Trp also induces fusion in lipid vesicles and can capture the lipid membrane inside their amyloid structures. We conducted AFM measurement in support of the above observations. Although it is difficult to take AFM images at a very high concentration of amino acid as the amyloid yields a very rough surface, we took AMF images at a very low concentration of amino acids. Figure 4.8b and d confirms that the zwitterionic DMPC and negatively charged DMPC/DMPG undergo aggregation and fusion upon the formation of amyloid by the amino acids (Phe). Interestingly, similar to the confocal images we observe the fused lipid vesicles on the fibril structure of Phe (Figure 4.8 d). This observation corroborates well with our previous observations.

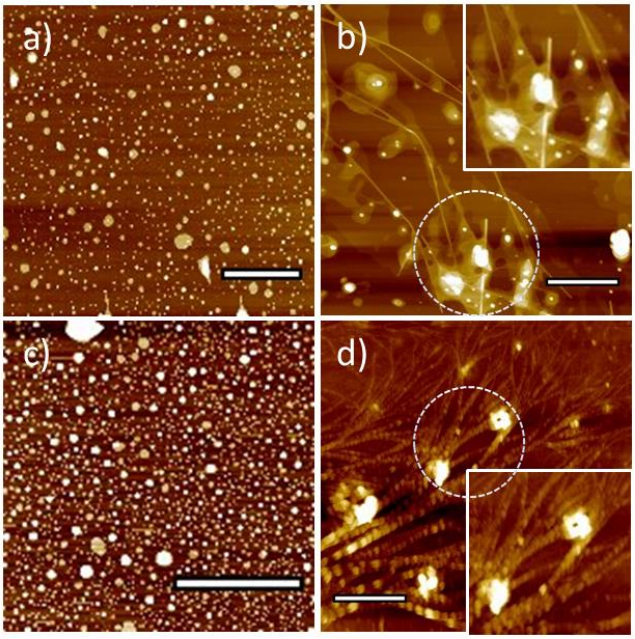

Figure 4.8 Atomic force microscopy (AFM) images of zwitterionic lipid vesicles (DMPC) in absence and presence of Phe (a-b) and negatively charged lipid (DMPC/DMPG) vesicles in absence and presence of Phe (Scale bar 2 µm).

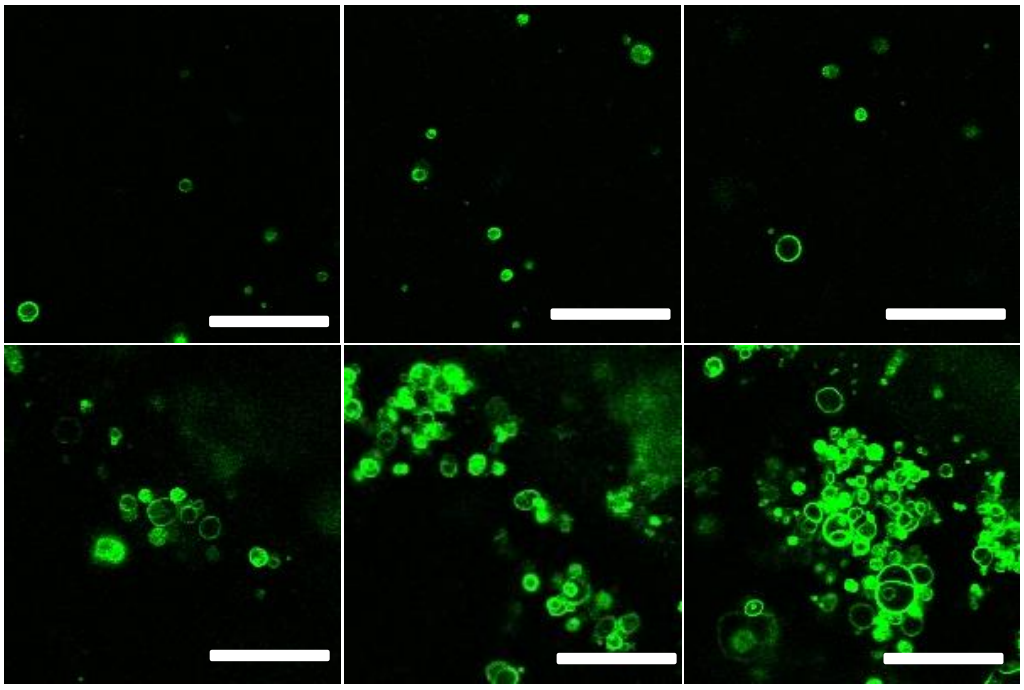

Figure 4.9 Confocal microscopy images of DMPC lipid vesicles in presence of Phe with 1 mol% NBD-PE. Non-aggregated DMPC vesicles in presence of Phe at (a-c) the initial stage of time-lapse imaging and (d-f) aggregated DMPC vesicles during the formation of amyloid aggregates. (Scale bar 5 µm).

To penetrate deeper into the process of morphological changes of lipid vesicles, the vesicle aggregation, vesicle fusion, and amyloid formation were

combined through live imaging during the formation of amyloid aggregates (Figure 4.10-4.11). Initially, well dispersed and non-aggregated DMPC vesicles are found in the system (Figure 4.9a–c). Our live imaging suggests that the pure DMPC lipid vesicles slowly undergo aggregation (Figure 4.9d–f) during the formation of amyloid structures of the Phe. However, the formation of an amyloid structure is not that much prominent as DMPC vesicles do not readily absorb the amino acids. The fusion process and the subsequent increase in the size of DMPC lipid vesicles are observed in Figure 4.10 and also marked by red and blue arrows, which indicates that the final size of some DMPC vesicles is around 3–4 µM while that of the blank DMPC vesicle is around 500–700 nm (Figure 4.7a).

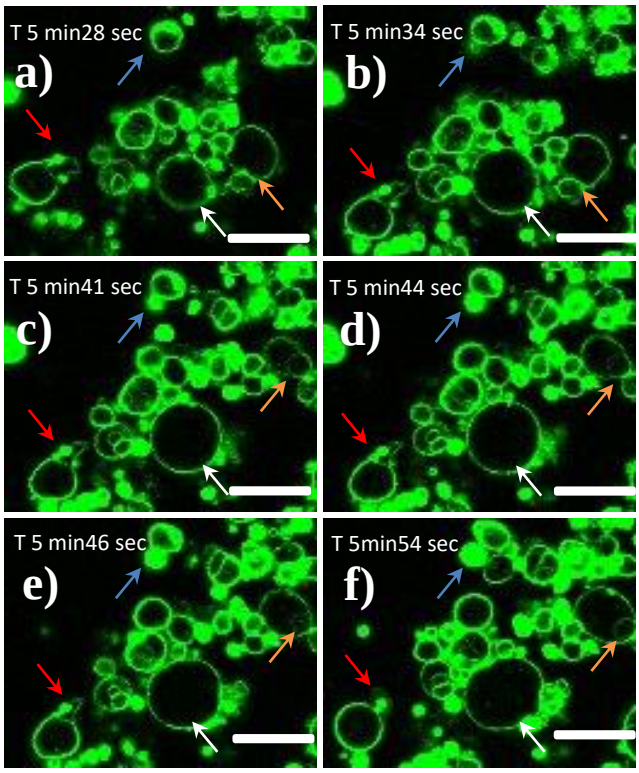

Figure 4.10 Time-lapse imaging of DMPC lipid vesicles showing the fusion of the vesicles during the process of amyloid formation of Phe. Arrows show the changes in vesicle size with time (scale bar 3 µm). Images were taken in a solution phase during the formation of an amyloid structure.

However, the most striking features were obtained when amino acids form the amyloid structure in the presence of (DMPC/DMPG) vesicles. As discussed earlier, negatively charged lipid vesicles (DMPC/DMPG) form a supported bilayer upon formation of amyloid structures of Phe (Figure 4.7e). The live

imaging (Figure 4.11) reveals that during the formation of the fibril structure of Phe, both the self-reproduction and fusion of lipid vesicles take place. It is evident that with time, the DMPC/ DMPG-Phe complex initially exhibits the self-reproduction of the lipid vesicles (Figure 4.11a–h, white arrow). However, these vesicles undergo fusion during the formation of the amyloid fibrils (Figure 4.11i–n, blue arrow). Interestingly, during the fusion processes, we also found the spontaneous formation of lipid vesicles inside the vesicles, which is reported elsewhere as ‘‘vesicle-in-vesicles’’ (Figure 4.11i–l, red arrow) *[16]*. One important observation is that during fusion of the lipid vesicles, they spontaneously generate the ‘‘daughter vesicles’’ (red arrow) until the complete disruption of the lipid vesicles. Our results also suggest that the formation of the aggregated structure of lipid vesicles via fusion is an intermediate of the fibril-lipid membrane complex or supported bilayer. Self-reproduction of vesicles is an important and crucial step for mimicking the origin of cellular life *[18-19]*. The mother vesicles were found to undergo deformation subsequently. Formation of aggregated and self-reproduction of LAPC (L-a-phosphatidylcholine) vesicles in the presence of nona-arginine (R9), a cell penetrating peptide, were recently explored *[17]*. Our results demonstrate that besides the proteins and peptides, the fusion and self-reproduction of lipid vesicles are also driven by their monomeric unites (amino acids).

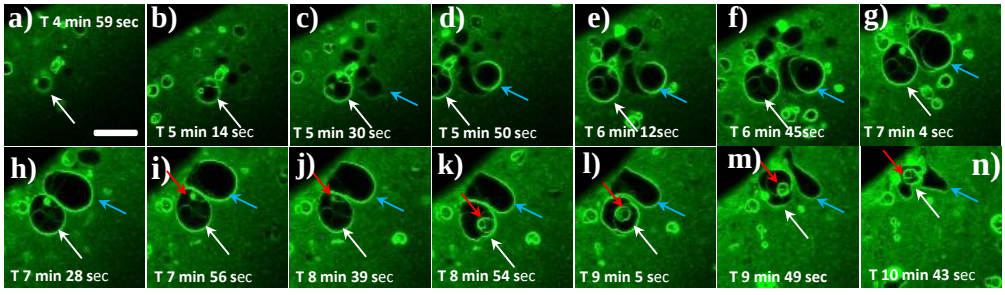

Figure 4.11 Time lapse imaging of DMPC/DMPG lipid vesicles in the presence of Phe during the formation of amyloid fibrils (scale bar 5 µm).

4.3 Conclusion:

In conclusion, the experimental data reveals that in the solution phase, the interaction of amino acids with the lipid bilayer is initially governed by the

electrostatic interaction between $–NH_3^+$ of the amino acid and PO_4^- of the lipid followed by hydrophobic interaction. The time-dependent dehydration of the DMPC/DMPG lipid bilayer takes place by the hydrophobic interaction and reconfiguration of amino acids in the lipid bilayer. The confocal imaging reveals that the zwitterionic lipid vesicles form an aggregated and supported membrane network during the amyloid formation of amino acids. On the other hand, a negatively charged lipid membrane having a higher affinity towards amino acids undergoes self-reproduction and subsequent disruption upon the formation of amyloid structures. This study thus also reveals that the self-reproduction of the vesicles takes place during the process of amyloid-like aggregation.

4.4 References

1. Marrink, S. J., & Mark, A. E. (2003). The mechanism of vesicle fusion as revealed by molecular dynamics simulations, J. Am. Chem. Soc., 125, 11144-11145. (DOI: 10.1021/ja036138+)

2. Marrink, S. J., & Tieleman, D. P. (2013). Perspective on the Martini model, Chem. Soc. Rev., 42, 6801-6822. (DOI: 10.1039/C3CS60093A)

3. Chernomordik, L. V., & Kozlov, M. M. (2003). Protein-lipid interplay in fusion and fission of biological membranes, Annu. Rev. Biochem., 72, 175-207. (DOI: 10.1146/annurev.biochem.72.121801.161504)

4. Do, T. D., De Almeida, N. E., LaPointe, N. E., Chamas, A., Feinstein, S. C., & Bowers, M. T. (2016). Amino acid metaclusters: implications of growth trends on peptide self-assembly and structure, Anal. Chem., 88, 868-876. (DOI: 10.1021/acs.analchem.5b03454)

5. Singh, P., Brar, S. K., Bajaj, M., Narang, N., Mithu, V. S., Katare, O. P., ... & Sharma, R. K. (2017). Self-assembly of aromatic α-amino acids into amyloid inspired nano/micro scaled architects, Mater. Sci. Eng. C, 72, 590-600. (DOI: 10.1016/j.msec.2016.11.117)

6. Ménard-Moyon, C., Venkatesh, V., Krishna, K. V., Bonachera, F., Verma, S., & Bianco, A. (2015). Self-Assembly of Tyrosine into Controlled

Supramolecular Nanostructures. Chem. Eur. J., 21(33), 11681-11686. (DOI: 10.1002/chem.201502076)

7. Adler-Abramovich, L., Vaks, L., Carny, O., Trudler, D., Magno, A., Caflisch, A., Frenkel, D. & Gazit, E. (2012). Phenylalanine assembly into toxic fibrils suggests amyloid etiology in phenylketonuria, Nat. Chem. Biol., 8(8), 701-706. (DOI: 10.1038/nchembio.1002)

8. Shaham-Niv, S., Adler-Abramovich, L., Schnaider, L., & Gazit, E. (2015). Extension of the generic amyloid hypothesis to nonproteinaceous metabolite assemblies. Sci. Adv., 1, e1500137. (DOI: 10.1126/sciadv.1500137)

9. Griffith, E. C., Perkins, R. J., Telesford, D. M., Adams, E. M., Cwiklik, L., Allen, H. C., ... & Vaida, V. (2015). Interaction of L-phenylalanine with a phospholipid monolayer at the water–air interface. J. Phys. Chem. B, 119, 9038-9048. (DOI: 10.1021/jp508473w)

10. Saha, A., SenGupta, S., Kumar, A., & Naik, P. D. (2018). Interaction of l-Phenylalanine with Lipid Monolayers at Air–Water Interface at Different pHs: Sum-Frequency Generation Spectroscopy and Surface Pressure Studies, J. Phys. Chem. C, 122, 3875-3884. (DOI: 10.1021/acs.jpcc.7b11049)

11. Anderson, C. M., Cardenas, A., Elber, R., & Webb, L. J. (2018). Preferential equilibrium partitioning of positively charged tryptophan into phosphatidylcholine bilayer membranes. J. Phys. Chem. B, 123, 170-179. (DOI: 10.1021/acs.jpcb.8b09872)

12. Shaham-Niv, S., Arnon, Z. A., Sade, D., Lichtenstein, A., Shirshin, E. A., Kolusheva, S., & Gazit, E. (2018). Intrinsic Fluorescence of Metabolite Amyloids Allows Label-Free Monitoring of Their Formation and Dynamics in Live Cells. Angew. Chem., Int. Ed., 57, 12444-12447. (DOI: 10.1002/anie.201806565)

13. Williams, R. A., Mamotte, C. D., & Burnett, J. R. (2008). Phenylketonuria: an inborn error of phenylalanine metabolism. Clin. Biochem. Rev., 29, 31.

14. Flydal, M. I., & Martinez, A. (2013). Phenylalanine hydroxylase: function, structure, and regulation, IUBMB life, 65, 341-349. (DOI: 10.1002/iub.1150)

15. Fu, M., Li, Q., Sun, B., Yang, Y., Dai, L., Nylander, T., & Li, J. (2017). Disassembly of dipeptide single crystals can transform the lipid membrane into a network, ACS nano, 11, 7349-7354. (DOI: 10.1021/acsnano.7b03468)

16. Fu, M., & Li, J. (2018). Spontaneous Membrane Generation and Extension in a Dipeptide Single Crystal and Phospholipid Mixed System. Angew. Chem., Int. Ed., 57, 11404-11407. (DOI: 10.1002/anie.201806347)

17. Banerjee, P., Pal, S., Kundu, N., Mondal, D., & Sarkar, N. (2018). A cell-penetrating peptide induces the self-reproduction of phospholipid vesicles: understanding the role of the bilayer rigidity. Chem. Commun., 54, 11451-11454. (DOI: 10.1039/C8CC07176D)

18. Szostak, J. W., Bartel, D. P., & Luisi, P. L. (2001). Synthesizing life, Nature, 409, 387-390. (DOI: 10.1038/35053176)

19. Zhu, T. F., & Szostak, J. W. (2009). Coupled growth and division of model protocell membranes. J. Am. Chem. Soc., 131, 5705-5713. (DOI: 10.1021/ja900919c)

20. Griffith, E. C., & Vaida, V. (2013). Ionization state of L-phenylalanine at the air–water interface. J. Am. Chem. Soc., 135, 710-716. (DOI: 10.1021/ja308089n)

21. Perkins, R., & Vaida, V. (2017). Phenylalanine increases membrane permeability. J. Am. Chem. Soc., 139, 14388-14391. (DOI: 10.1021/jacs.7b09219)

22. MacCallum, J. L., Bennett, W. D., & Tieleman, D. P. (2008). Distribution of amino acids in a lipid bilayer from computer simulations. Biophys. J., 94, 3393-3404. (DOI: 10.1529/biophysj.107.112805)

23. MacCallum, J. L., Bennett, W. F., & Tieleman, D. P. (2007). Partitioning of amino acid side chains into lipid bilayers: results from computer simulations and comparison to experiment. J. Gen. Physiol., 129, 371-377. (DOI: 10.1085/jgp.200709745)

24. Cutro, A. C., & Disalvo, E. A. (2015). Phenylalanine blocks defects induced in gel lipid membranes by osmotic stress, J. Phys. Chem. B, 119, 10060-10065. (DOI: 10.1021/acs.jpcb.5b05590)

25. Rosa, A. S., Cutro, A. C., Frías, M. A., & Disalvo, E. A. (2015). Interaction of phenylalanine with DPPC model membranes: more than a hydrophobic interaction. J. Phys. Chem. B, 119, 15844-15847. (DOI: 10.1021/acs.jpcb.5b08490)

26. De, S. K., Kanwa, N., & Chakraborty, A. (2019). Influence of trivalent metal ions on lipid vesicles: gelation and fusion phenomena, Langmuir, 35, 6429-6440. (DOI: 10.1021/acs.langmuir.9b00682)

27. Norman, K. E., & Nymeyer, H. (2006). Indole localization in lipid membranes revealed by molecular simulation. Biophys. J., 91, 2046-2054. (DOI: 10.1529/biophysj.105.080275)

28. Petersen, F. N., Jensen, M. Ø., & Nielsen, C. H. (2005). Interfacial tryptophan residues: a role for the cation-π effect?. Biophys. J., 89, 3985-3996. (DOI: 10.1529/biophysj.105.061804)

Chapter 5

Lipid phase (order/disorder) dependent distinct emission behaviour of hydrophobic carbon dots: the emergence of C-dots based membrane probe

5.1 Introduction

Lipid vesicles are used to mimic the intercellular and intracellular functions of biological cells and have been employed as potential carriers of drugs, proteins/peptides, enzymes, antigens/antibodies, etc. *[1-2]*. Lipid vesicles protect the encapsulated material from the extracellular environment. It is well documented that the dynamical properties of the membrane e. g. bilayer rigidity-fluidity, lipid mobility have crucial roles in the loading and leakage of the encapsulated species in the delivery system *[3-5]*. The dynamical properties of the membrane were previously investigated by using organic membrane probes both in biomimetic and actual cell systems *[6]*. In this context, luminescence carbon dots (CDs) have several advantages over the conventional organic membrane probes owing to their tunable photoluminescence, high quantum yield, excellent photostability, broad excitation-emission spectral range, and cost-efficient easy large scale synthesis *[7-9]*. However, a CD would act as a membrane probe, if it shows distinct emission properties in sol-gel or ordered (L_o) and liquid-crystalline or disorder (L_d) phase of the membrane and the visual detection of these phenomena will be highly advantageous. In most of the literature, carbon dots are used as biomarkers *[10-11]*, and there is no such report where the bare eyes can detect the distinct emission of the same CD from the different phases of the lipid bilayer. Nandi et al. previously monitored the lipid-membrane dynamics by carbon dot-phospholipid conjugate, and they found a 30 nm blue-shifted emission due to the insertion of the CDs in the lipid bilayer *[12-13]*. However, in most of the studies, the emission profile of the CDs embedded in lipid vesicles does not show any visual colour change from the bare CDs emission.

To the best of our knowledge, till now, the CD-based sensor for different membrane phases has not been reported elsewhere. In this manuscript, for the first time, we report a phase-dependent distinct emission profile of lipid encapsulated hydrophobic CDs (H-CDs), observed through naked eyes under a UV lamp, promoting a unique fluorescence sensor for the membrane phase state. Interestingly, these H-CDs embedded in lipid bilayer can monitor the changes in membrane dynamics by the membrane active ions or even small molecules. This observation is similar to the previously used organic membrane probes (e.g. Prodan, Laurdan, ANS, and DPH, etc.) *[14-15]* and presenting newly emerged CD-based membrane-sensitive probes.

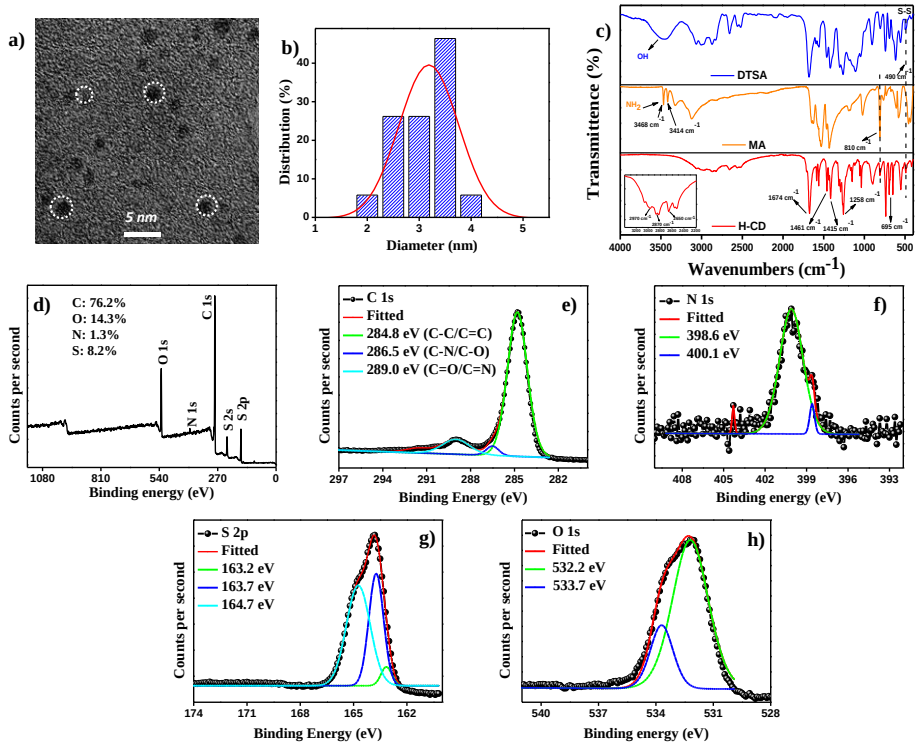

Figure 5.1 a) High-resolution TEM imaging and b) particle size distribution measured by TEM imaging of the H-CDs. C) FT-IR spectrum of dithiosalicylic acid (DTSA), melamine (MA) and the H-CDs. d) XPS spectrum and high-resolution e) C 1s, f) N 1s, g) S 2p, and h) O 1s spectra of the H-CDs.

5.2 Result and discussion:

5.2.1 <u>Synthesis and characterization of the H-CDs</u>: The H-CDs were synthesized from melamine and dithosalicylic acid (DTSA) by a hydrothermal method in an acetic acid medium *[16]*. The HR-TEM image (Figure 5.1a)

reveals that the as-prepared H-CDs are monodispersed with an average size of 3.18 ± 0.07 nm (Figure 5.1 b). The FT-IR (Figure 5.1c) and XPS (Figure 54.1d-h) measurements were also performed to study the chemical structure of the H-CDs. The Fourier transformed infrared (FT-IR) spectra reveals that the surface of the H-CD contains S-S (490 cm^{-1}), C-S (695 cm^{-1}), S-H (2650 cm^{-1}), methylene (2870 cm^{-1} and 2970 cm^{-1}), C=C (1461 cm^{-1}), amide carbonyl (1674 cm^{-1}), C-N (1415 cm^{-1}) and aromatic C-N (1258 cm^{-1}) functional groups, which is good agreement with the Yang and co-workers *[16]*. We also observed that the FT-IR spectra of the MA exhibit a peak at 3468-3414 cm^{-1} which corresponds to the hydrophilic amino group and DTSA exhibits a peak at 3467 cm^{-1} which corresponds to the hydrophilic hydroxyl group. However, after the carbonization and amidation, the hydrophilic amino groups of MA and hydroxyl group of DTSA are disappearing completely in the H-CDs, which possibly contribute to the hydrophobic property of the H-CDs. The full XPS spectra in figure 5.1d displays five typical peaks at 163.8, 227.2, 284.8, 399.8, and 531.8 eV for S 2p, S 2s, C 1s, N 1s, and O 1s, respectively. Suggesting that H-CDs contains C, N, O, and S element and their atomic ratio was found 76.2%, 1.3%, 14.3%, and 8.2% respectively. The high-resolution XPS spectrum of the C 1s band (Figure 5.1e) was deconvoluted into three binding energy peaks, 284.8, 286.5, and 289.0 eV, which are assigned to the C-C/C=C, C-N, and C=O/C=N, respectively. The N 1s band exhibit (Figure 5.1f) two peaks at 398.6 and 400.1 eV, respectively, which is assigned to the pyridinic C3-N and pyrrolic C2-N-H groups. The S 2p band in figure 5.1g shows three peaks at 163.2, 163.7, and 164.7 eV which correspond to the S-C, S-H, and S-S respectively. The O 1s spectra (Figure 5.1h) contain two peaks 532.2 and 533.7 eV for C=O and COH/ C-O-C band, respectively. Therefore, we conclude that H-CD possesses a graphite-like core with defects caused by nitrogen atoms and disulfide bonds, and the surface of the H-CDs is covered with C, N, O, and S containing heterocycles.

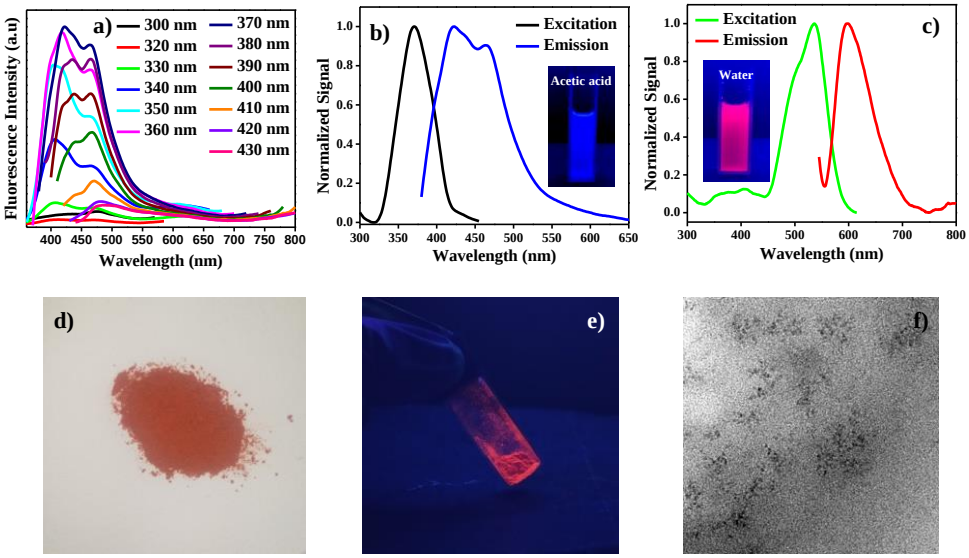

Figure 5.2 a) Excitation-dependent emission spectra of the as-synthesized H-CDs in acetic acid solutions. Excitation and emission spectra of the b) as-synthesized H-CD solution and c) H-CDs in a water medium (inset: photographs of the H-CD solutions under 365 nm ultraviolet radiation). Images of the aggregated H-CDs in d) sunlight, e) under 365 nm UV lamp and f) in HR-TEM.

5.2.2 <u>Optical property and fluorescence mechanism of the H-CDs</u>: The H-CDs in acetic acid solution exhibit excitation-dependent emission spectra (Figure 5.2a) with maximum emission intensity at 423 nm upon excitation at 365 nm (Figure 5.2b). The quantum yield of the H-CDs in acetic acid is estimated to be 5.16%. In the aqueous medium, the H-CD solution forms the aggregated red powder (Figure 5.2d) with intense red emission at ~601 nm at λ_{ex} = 535 nm (Figure 5.2c) with a fluorescence lifetime of around 2.1 ns. The solvent polarity dependent UV-Vis absorption, fluorescence excitation and emission of the H-CDs are studied to understand the emission mechanism. As shown in figure 5.3a, the H-CDs in acetic acid medium exhibit two peaks at 275 nm and 330 nm which correspond to the π-π* transitions of the C=C in the core of the H-CDs. However, with increasing solvent polarity, we observed a decrease in the absorption band at 330 nm with a new peak at 450-500 nm regions, which is attributed to the n-π* transition of the surface states. In an aqueous medium, the H-CDs undergo complete aggregation and we observe a broad absorption band at 450-600 nm region. Therefore, with increasing solvent polarity, we observe a gradual decrease at 330 nm and the appearance of a new peak at 450-600 nm in absorption band regions. The above

observations are supported by excitation spectra (Figure 5.3b) of the H-CDs. We observe the H-CDs in acetic acid exhibit a peak at 280 and 360 nm; however, in an aqueous medium, the H-CDs exhibit a main peak at 535 nm with a low intensity peak at 360 nm. We observed that H-CDs exhibit an intense red emission with increasing polarity of the solvent (Figure 5.3c). Therefore, we conclude that the core of the H-CDs is responsible for blue fluorescence and dominant in the non-polar medium, however, with aggregation, the blue emission quenches and red emission arises from the surface of the H-CDs in the polar medium.

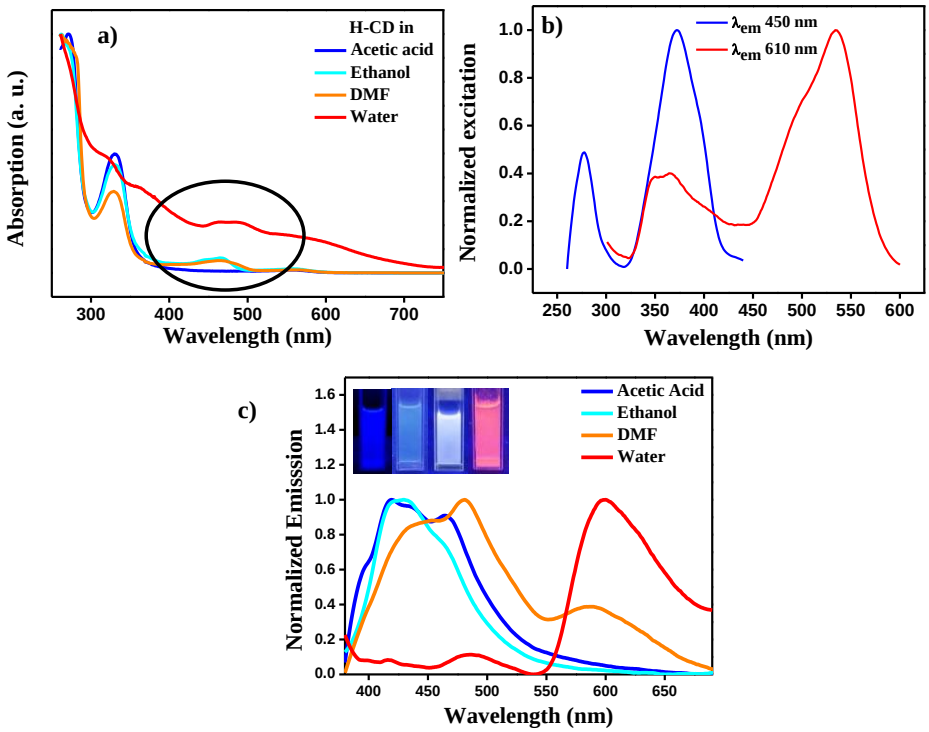

Figure 5.3 a) UV-Vis absorption spectra, b) normalized excitation and c) Fluorescence emission spectra of the purified H-CDs in different solvents (insets: photographs of the H-CDs in different solvents under 365 nm UV lamp).

Concentration dependent emissions of the H-CDs were also studied in both blue and red regions (in acetic acid and water medium, respectively) to get insight into the luminescence mechanism of the H-CDs (Figure 5.4a-b). We found that with increasing concentration of the H-CDs in acetic acid medium, initially, the fluorescence intensity gradually increases in the blue region along with a new peak at 465-470 nm possibly due to the sub-aggregation of the H-

CDs. However, at very high concentration (i.e. 0.5 and 1.0 mg/mL), the emission intensity of the blue end decreases enormously indicating the aggregation-caused quenching (ACQ) of the blue emission (Figure 5.4a). On the other hand, the emission intensity of the H-CDs continuously increases with increasing concentration of the H-CDs at the red region (Figure 5.4b). Polarity dependent aggregation of the H-CDs was investigated visually using bright field and confocal microscopy imaging study. We observe that larger aggregation of the H-CDs in a more polar water medium (Figure 5.4f-h) compared to the ethanol medium (Figure 5.4c-e). The bright field and the confocal microscopy images of the H-CDs in the water medium (Figure 5.4f-h) indicate that red fluorescence originates only from large aggregates whereas dispersed H-CDs exhibit the blue emission from the background. Therefore we conclude that the graphitized cores of the H-CDs are responsible for the blue fluorescence in non-polar medium *[16]*. When the H-CD monomers come in contact with water, their surface hydrophobicity facilitates π-π stacking. Due to the aggregation, the graphitized cores turn off the blue emission via aggregation-caused quenching (ACQ). The aggregation further leads to the restriction of the intramolecular rotation (RIR) of symmetrical heterocycles about their disulfide bonds axes on the surface of the H-CDs, resulting in red emission *[16]*. In a nutshell, the monomeric H-CDs core exhibits blue fluorescence; however, the RIR of the HCDs surface induces the red emission, which is in accordance with the Yang and coworkers.

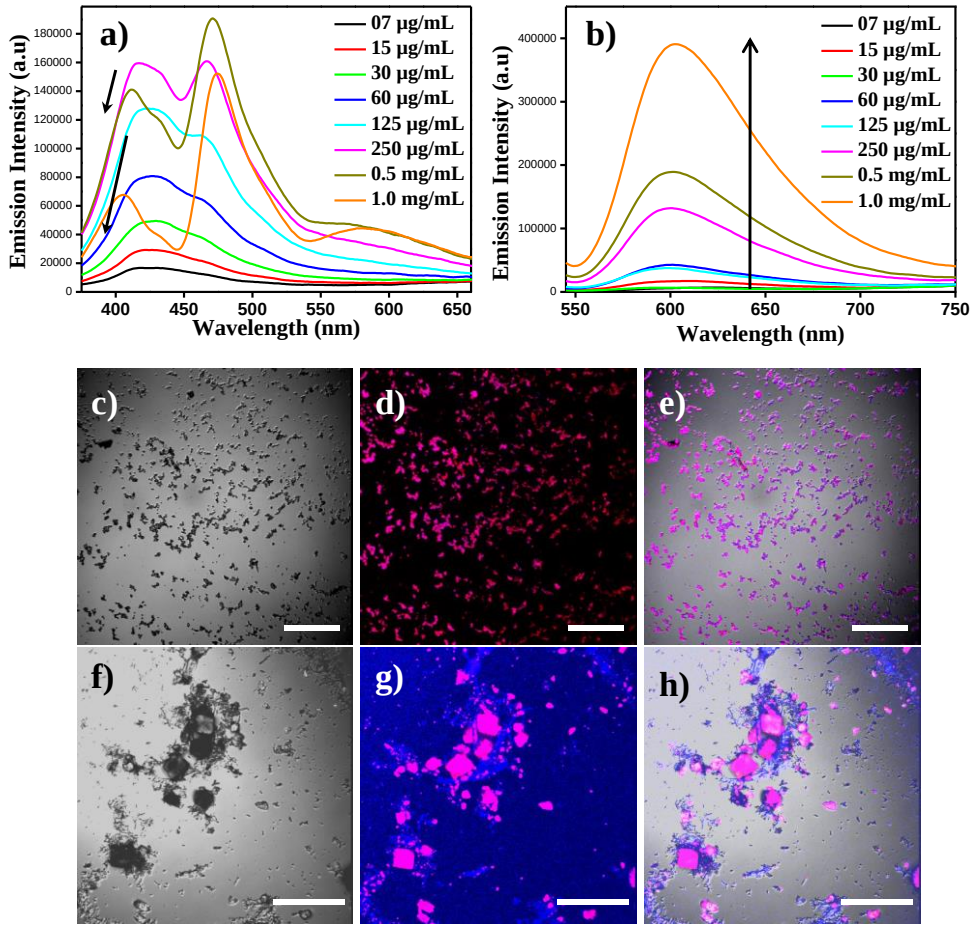

Figure 5.4 Concentration dependent emission of the H-CDs at the blue and red region in a) acetic acid and b) water medium respectively. Bright field, confocal, and merge images of the H-CDs in (c-e) ethanol and (f-h) water medium. The scale bar indicates 10 µm.

5.2.3 <u>Lipid-phase dependent emission behavior of the H-CDs</u>: The phase-dependent distinct emission behaviour of the H-CDs were studied using three representative zwitterionic phospholipid membranes with a wide difference in their phase transition temperatures (T_m), namely, DOPC (T_m= -20 °C), DMPC (T_m= 23 °C) and DPPC (T_m= 42 °C). Therefore, at ambient laboratory conditions, DOPC is in a fluid phase (liquid-crystalline or disordered phase), while DPPC is in a gel phase (sol-gel phase or ordered phase), and DMPC remains near the gel to the fluid transition phase. Figure 5.5a represents the photographs of the H-CDs in three different lipids under 365 nm ultraviolet radiations at room temperature (RT). The lipid-CD assemblies i.e. DOPC-CDs, DMPC-CDs, and DPPC-CDs exhibit blue, pink, and red luminescence respectively at RT, which can be easily observed with bare eyes under UV-

lamp (Figure 5.5a). Since all the lipids contain the same head group, so; the electrostatic interaction between the lipids and CDs should be similar. Therefore, the different emission behaviour of H-CDs is attributed to the different microenvironments and different phases of the lipid bilayers.

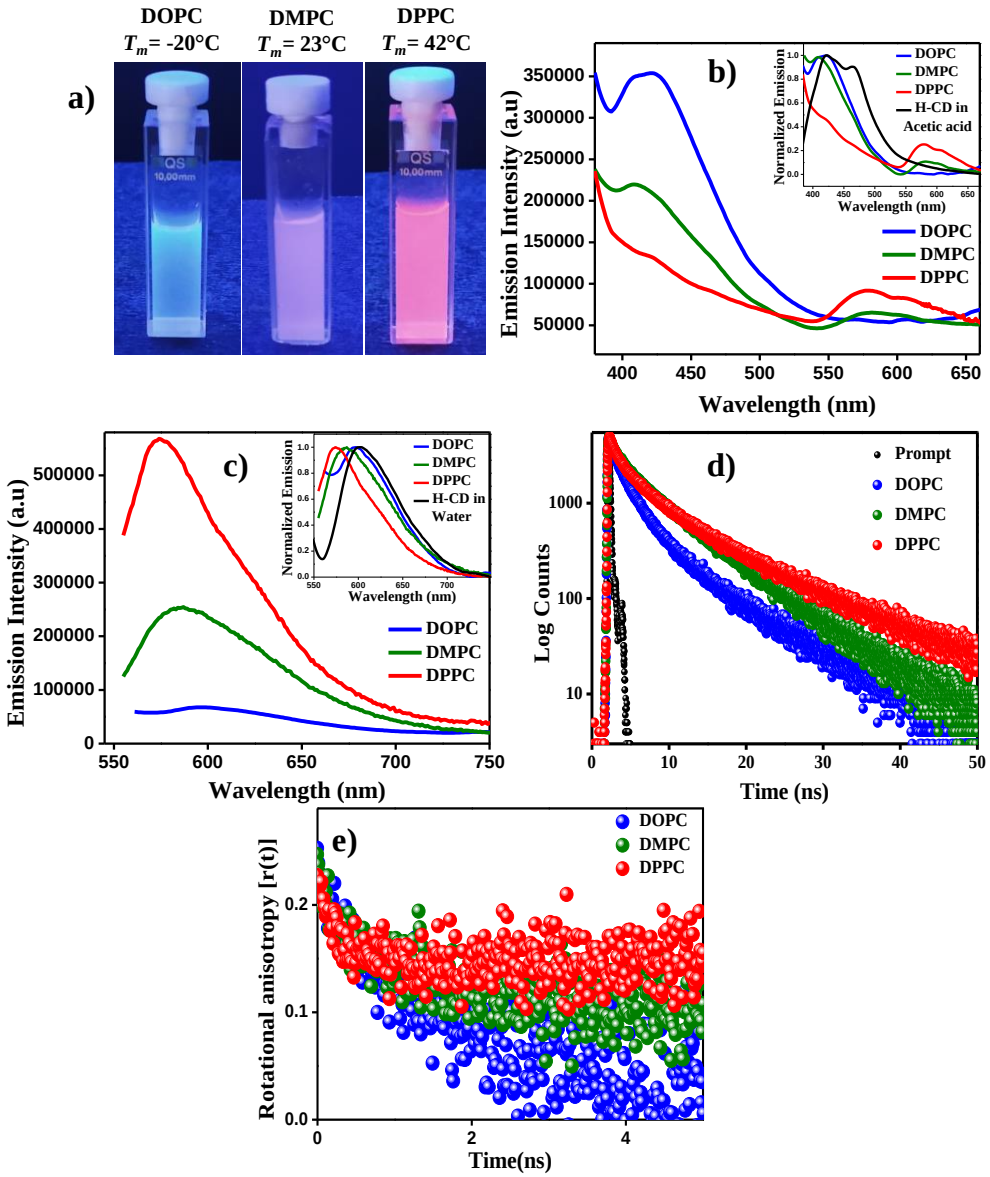

Figure 5.5 a) Photographs of the H-CDs in different lipids under 365 nm ultraviolet radiations. b, c) Steady-state fluorescence emission spectra of the H-CDs in DOPC (blue), DMPC (green), and DPPC (red) lipid vesicles upon excitation at (b) 365 nm and (c) 535 nm (Inset shows the normalized emission spectra of blank H-CDs and lipid-CD assemblies). Lifetime decay (d) and time-resolved anisotropy decay (e) of the H-CDs in different lipid vesicles upon excitation at 485 nm.

Table 5.1 Time-resolved lifetime data of DOPC-CDs, DMPC-CDs and DPPC-CDs collected at 600 nm at λ_{ex} = 485 nm at 25 °C.[#]

	χ^2	a_1	a_2	a_3	τ_1	τ_2	τ_3	$<\tau>$
H-CD in water	1.25	0.48	0.33	0.19	0.338	2.25	6.47	2.13
DOPC-CDs	1.02	0.45	0.45	0.10	0.52	2.45	8.47	2.18
DMPC-CDs	1.04	0.37	0.26	0.37	0.54	2.87	7.37	3.6
DPPC-CDs	1.00	0.35	0.30	0.35	0.53	2.70	9.37	4.3

 # Experimental error in this measurement is around 5%.

Figure 5.5b reveals that DOPC being in the liquid-disordered state, exhibits an intense blue fluorescence around 420 nm at λ_{ex} = 365 nm (Figure 5.5b, blue line) with negligible fluorescence at 597 nm at λ_{ex} = 535 nm at RT (Figure 5.5c, blue line). On the other hand, DPPC vesicle remaining in sol-gel-ordered state at RT exhibit negligible blue fluorescence (Figure 5.5b, red line) and high intense red fluorescence at 580 nm at λ_{ex} = 535 nm (Figure 5.5c, red line) compared to that of DMPC and DOPC. The DMPC having a T_m near 23 °C remains in an in-between state of ordered and disorder state at RT and thus shows an intermediate fluorescence between that of fluid DOPC and gel-phase DPPC vesicles. We observed both blue and red emission upon excitation at 365 nm and 535 nm, respectively (green line in Figure 5.5b and c), resulting in a merged pink luminescence. Therefore, in summary, we found an increasing red emission or decreasing blue emission follows the order of DPPC > DMPC > DOPC. The lifetime and time-resolved anisotropy decay of H-CDs in DPPC, DMPC, and DOPC bilayers were measured at a 600 nm wavelength which corresponds to the ordered phase signal of the lipid. A significant increase in the lifetime (Figure 5.5d) and slow anisotropy decays (Figure 5.5e) were observed which also follows the same order.

From the polarity dependent emission behaviour of the H-CDs (Figure 5.3c), one can infer that the H-CDs are in an aggregated state in case of DPPC rendering the red emission and in monomeric state in case of DOPC showing the blue emission. So, if the aggregation of the H-CDs is responsible for such discrimination, then the blue emission is preferable for DPPC and red emission is preferable for DOPC, as the DOPC bilayer contains more water molecules than DPPC, which is opposite to our observation. Further, the aggregated H-CDs are several micrometer in size (> 3-5 µm, Figure 5.4f-h) therefore, the lipid bilayer which has a bilayer thickness of ~5-50 nm (5 nm in

case of SUV and ~50 nm in case of MLV), capable to uptake the monomeric H-CDs. Thus, we proposed that the sol-gel phase or ordered phase of the lipid bilayer possibly restricts the intramolecular rotation (RIR) of symmetrical heterocycles of the surface molecules in the H-CDs and gives rise to red fluorescence. However, the intramolecular rotation is allowed in the liquid-crystalline phase or disordered phase and in the absence of RIR, the lipid-CDs assembly exhibits blue fluorescence. Therefore, with increasing rigidity or ordered phase of the lipids bilayer (DPPC> DMPC> DOPC), the RIR of symmetrical heterocycles of the H-CDs increases and possibly enhances the red region fluorescence intensity, lifetime, and slower the rotational relaxation of the H-CDs.

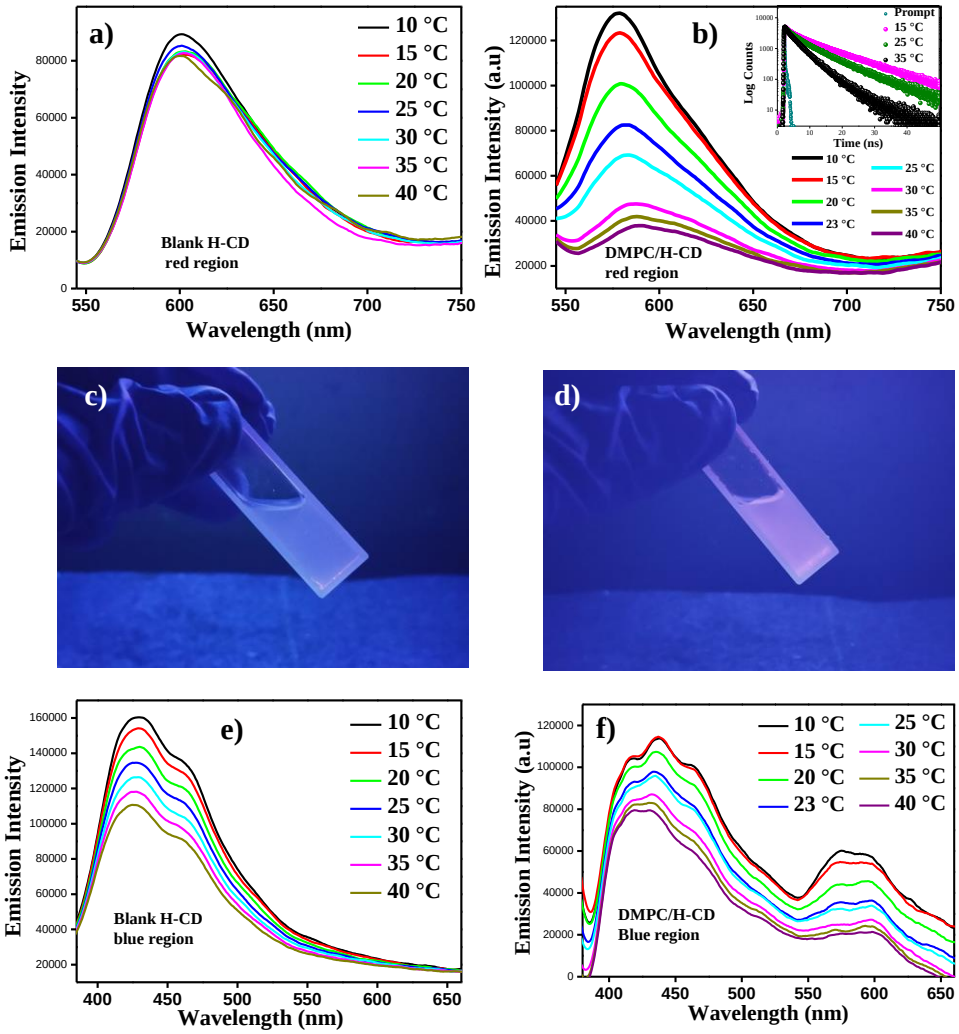

Figure 5.6 Temperature-dependent emissions of the a) blank H-CDs (aqueous medium) b) DMPC-CD assemblies in red region upon excitation at 535 nm. Photographs of the DMPC-

CD assemblies at c) 15 °C and d) 35 °C under a 365 nm UV lamp. Temperature-dependent emission of the e) blank H-CD (in ethanol) and f) DMPC/H-CD in blue region upon excitation at 365 nm.

Further, to bring more insight into the phase-dependent emission properties of the lipid-CD assemblies, we varied the temperatures (Figure 5.6) below and above the T_m of DMPC lipid vesicles. Figure 5.6a indicates that the negligible change in fluorescence intensity (~8%) of the bare H-CDs, which indicates the negligible effect of the temperature on the bare H-CDs red emission. Interestingly, we found that the red region emission of the DMPC-CD assemblies gradually decreases (~72%) with increasing temperature (Figure 5.6b). We also observed a decrease in fluorescence lifetime (λ_{em} = 585 nm) with increasing temperature of the DMPC-CD assemblies (inset of Figure 5.6b). This observation indicates that the red region signal of the lipid-CD assemblies predominantly depends on the lipid phase state. Besides, in bare eyes, the DMPC-CD assemblies exhibit blue colour at 35 °C and pink colour at 15 °C under 365 nm UV lamp, enlighten the phase dependency of the H-CDs in the lipid bilayer (Figure 5.6c-d). Therefore, the observations imply that H-CDs preferably show red emission in the sol-gel phase or ordered phase of the lipid vesicles due to increasing RIR of the symmetrical heterocycles of the H-CDs. We also perform the temperature-dependent study of the DMPC-CD assemblies at the blue region (430 nm). We observe a decrease in the emission of DMPC-CD assemblies (~ 28%) with increasing temperature (Figure 5.6f). One may expect that the blue emission of the H-CDs should be increasing with increasing temperature as the phase of the lipid transforms from order phase to disorder phase (reverse phenomena of the red emission region). However, we did not find such observation in the blue emission region. This discrepancy can be explained by the temperature-induced non-radiative transition from the excited state of the H-CDs. We observe that the blank H-CDs emission (in ethanol), at the blue region decreases by ~35% with increasing temperature (Figure 5.6e). Notably, at 40 °C, we observe that the decrease in fluorescence intensity is higher in the case of bare H-CDs than lipid-CD assemblies (35% and 28% respectively) which indicates that the lipid bilayer, because of its organization, restricts the non-radiative transition of the H-CDs emission compared to blank H-CDs.

5.2.4 Interaction of other carbon dots (o-CDs and M-CDs) with the lipid vesicles: From the above discussion one might speculate that the CDs which exhibit solvent-dependent emission possibly also exhibit the lipid-phase dependent emission. To prove the uniqueness of the H-CDs used in the present work, we have tested some other well-known CDs which exhibit solvent dependent and aggregation-induced emission property or both. Our study reveals that CDs which exhibit the solvent dependent emission or aggregation induced emission do not necessarily show the distinct emission behavior in the different phase states (ordered or disordered state) of the lipid membrane. However, we observe that these CDs generally show little blue shifted emission in lipid membrane from bare CDs emission (in aqueous medium). But till now, there is no report of a CD which exhibits distinct detectable emission under UV lamp or in steady-state fluorescence measurement from both ordered and disordered phase of the lipid. The solvent dependent and aggregation induced emission property of the CDs and their emission in the lipid phase state (ordered and disordered phase) are discussed below:

o-Phenylenediamine (oPD) based carbon dots: Phenylenediamine is a well-known carbon source for the preparation of the versatile carbon dots (CDs) *[9]*. Therefore, we synthesized oPD-based CDs (o-CDs) by one-step hydrothermal treatment by previously reported procedure *[17]*. In this context, the choice of CDs is crucial. We choose o-CDs for three reasons, the as-prepared o-CDs is 1) hydrophobic, 2) shows solvent dependent emission, and 3) the emission peak of the o-CDs was sensitive towards water (i. e. o-CDs used to detect water content in organic solvent) *[17*]. Thus, the o-CDs show significant similarities with the photo physical properties with our reported H-CDs.

As reported previously, *[17]* we found that the as-synthesized o-CD has emission maximum at 570 nm with an excitation spectrum at 410 nm in water medium (Figure 5.7a). The o-CD with decreasing solvent polarity exhibit solvent dependent emission spectra which shift gradually from 570 to 512 nm upon excitation at 410 nm (Figure 5.7b), thus resulting a fluorescence color change from dark yellow to cyan (Figure 5.7c) in UV chamber.

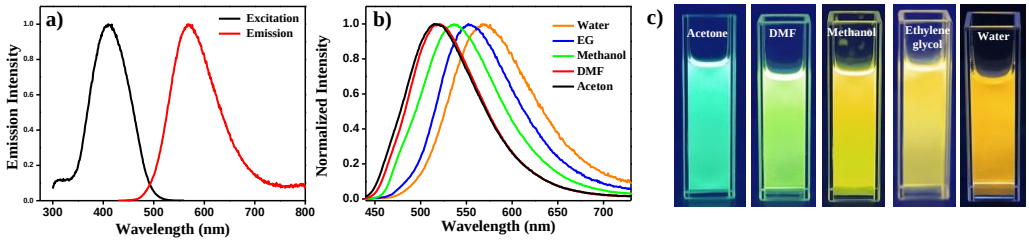

Figure 5.7 a) Excitation and emission spectra of the o-CD in aqueous solution. b) Solvent-dependent mission spectra of the o-CDs excited at 410 nm and c) their photographs in acetone, DMF, methanol, Ethylene glycol and aqueous medium under UV lamp.

After checking the excitation dependent emission spectra, the synthesized o-CDs have been used to detect the different membrane phase state. We used thin-film hydration method to prepare the o-CD based lipid-CD assemblies, same as previously used for the H-CDs. We observe that all the lipid-CD assemblies i. e. DOPC-oCD, DMPC-oCD, and DPPC-oCD exhibit 5-7 nm shifted emission from the bare o-CDs emission in aqueous medium (Figure 5.8a). Figure 5.8b shows the photographs of the o-CDs in three different lipids under 365 nm ultraviolet radiations at room temperature and we did not observe significant difference under the UV lamp. Therefore, despite of hydrophobic nature of o-CDs and H-CDs, solvent dependent emission, and sensitive emission property towards water, the o-CD does not able to sense the membrane phase behavior. On the other hand H-CDs used in the current work successfully detect different phase state of the lipid membranes.

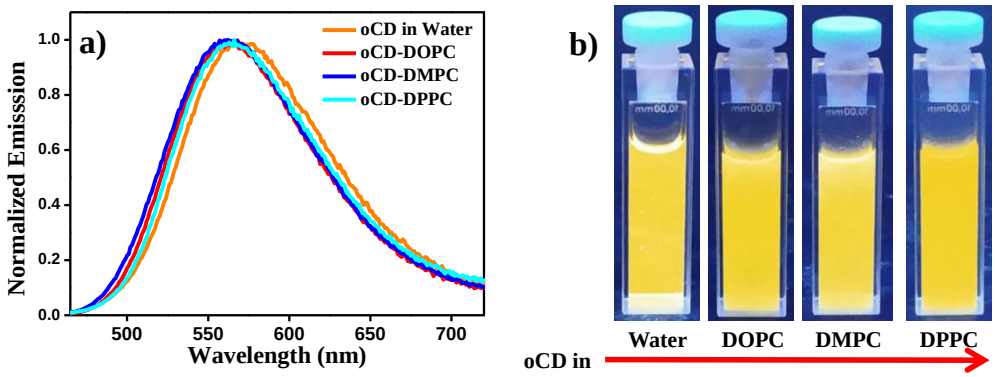

Figure 5.8 a) Steady-state fluorescence emission spectra (λ_{ex} = 410 nm) and b) the photographs of the o-CDs in DOPC, DMPC and DPPC lipid vesicles under Ultra-Violate chamber.

Carbon dots synthesized from citric acid and 1-(2-pyridylazo)-2-naphthol: In this scenario, there is another possibility which cannot be ignored, i. e. the aggregation of the CDs in the bilayer. Aggregation of nanoparticles in the lipid bilayer is well known and it greatly depends on the lipid phase *[18-19]*. So, one can assume that the CDs possibly undergo the phase dependent aggregation in lipid bilayer by increasing the local concentration and exhibit distinct luminescence in different lipid phases.

Therefore, to investigate the above hypothesis, we need to choose CDs which exhibit the concentration dependent emission i.e. with increasing concentration (and consequently aggregation) the CDs should exhibit different color emission. Therefore, we synthesis another carbon dots, namely M-CDs (multicolor carbon dots) by solvothermal treatment of citric acid (CA) and 1-(2-pyridylazo)- 2-naphthol (PAN) by using a previously reported method *[20]*. In this case, the M-CD was chosen for its concentration-tunable fluorescence and solvent-dependent emission property (in water and ethanol).

We observed that the synthesized M-CD in ethanol exhibit excitation dependent emission with three main characteristic peak 370 nm, 440 nm and 590 nm when excitation wavelength changes from 300 to 500 nm (Figure 5.9b). Further, the concentration dependent aggregation of the M-CDs was investigated in ethanolic solution using steady state emission spectra (Figure 5.9a-f). We observed that at lower concentration (0.2 mg/mL) H-CD exhibit a main peak at 370 nm; however with increasing concentration (0.5 mg/mL and 1 mg/mL) the peak at 370 nm gradually decreases. On the other hand, the peak at 440 nm gradually increases. When the concentration of the H-CDs is more than 1.0 mg/mL, we observe the peaks at 370 nm and 440 nm decreases and disappear completely with significant emission at 590 nm. The concentration dependent tunable luminescence property of the M-CDs was also observed in the UV chamber (Figure 5.9g). We observed a white emission at lower concentration, however a red emission was observed at high concentration of M-CDs, as reported earlier *[20]*. The excitation dependent emission of the M-CDs was also measured in water medium (Figure 5.9h). We observe that in addition to the concentration dependent emission, the M-CD exhibit distinct emission in water (cyan colour) and ethanol (white colour) medium (Figure

5.9i). These photophysical properties of the M-CDs are all in accordance with Yan and coworkers *[20]*.

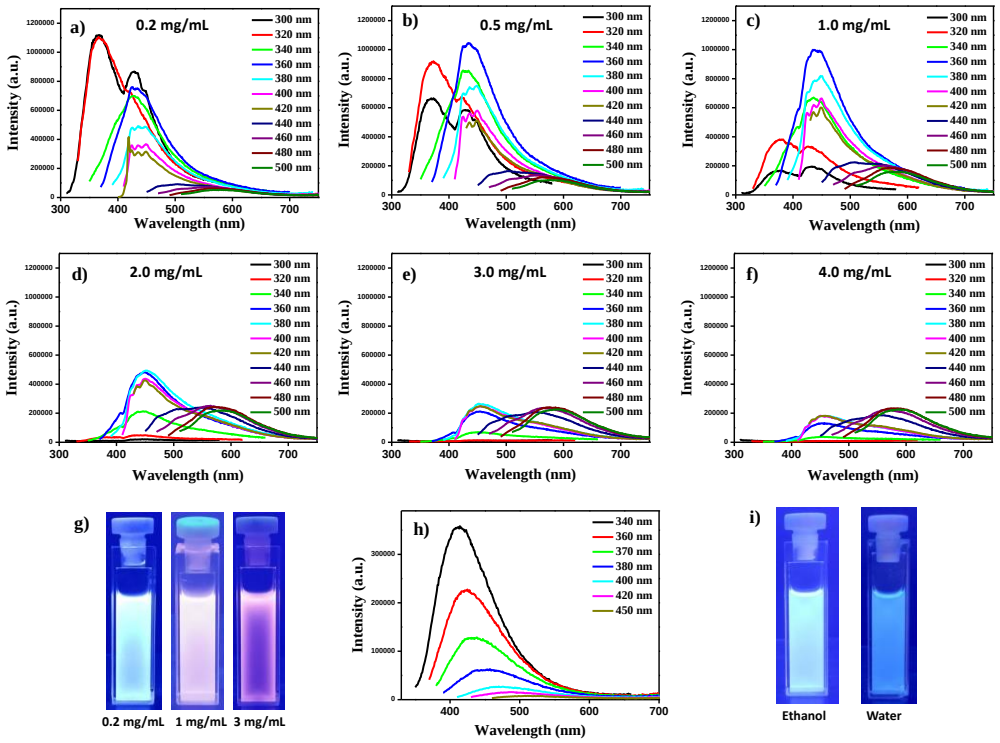

Figure 5.9 Fluorescence spectra of different concentrations a) 0.2 mg/mL, b) 0.5 mg/mL, c) 1.0 mg/mL, d) 2.0 mg/mL, e) 3.0 mg/mL, and f) 4.0 mg/mL of M-CDs in ethanol solution. We kept the scale bar unaltered for each graph for clear view on concentration dependent quenching. g) Photograph of the different concentration of M-CDs under UV lamp. h) Excitation-dependent emission of the M-CDs in aqueous medium. i) Photograph of the M-CDs (0.5 mg/mL) in ethanol and water medium under UV lamp.

Next, we investigated the effect of M-CDs on different phases of the lipid bilayer. We observed that the emission spectra of the M-CDs in an aqueous medium do not alter significantly in presence of either order or disorder phase of the lipid upon excitation at 360 nm (Figure 5.10a). Interestingly, upon excitation at 400 nm, M-CDs in lipid vesicles exhibit a huge blue shifted (~120 nm) emission (Figure 5.10b). However, the spectral shift is almost similar for the ordered (L_o) and disorder (L_d) phase of the lipid and above all, they do not exhibit significant color differences through naked eyes under UV lamp (Figure 5.10c). This observation indicates that despite the aggregation possibility of the M-CDs, the M-CDs are not able to detect the different

membrane phases. The observation further ascertains the unique ability of the H-CDs of our interest to detect different phases of the lipid membrane.

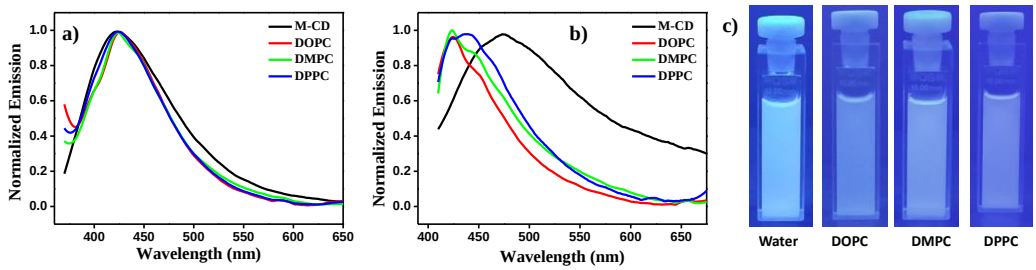

Figure 5.10 Steady-state emission spectra of the M-CDs in DOPC, DMPC, and DPPC lipid vesicles upon excitation at a) λ_{ex} = 360 nm b) λ_{ex} = 400 nm. c) Photograph of the M-CDs (50 µg/mL) in water and in different lipid vesicles under UV lamp.

5.2.5 <u>Confocal microscopy images of lipid/H-CD assemblies</u>: Further, the confocal laser scanning microscopy (CLSM) imaging was performed to gain more insight into the distinct emission behaviour of the lipid-CD assemblies. While we observed significant signal using emission filter 410/480 (blue region) and 490/560 (green region) from the DOPC-CD assemblies, we did not find any signal using emission filter 580/650 (red region) (Figure 5.11a). On the other hand, for DPPC-CD assemblies, a low intense signal in both the blue and green regions was found. However, we observed an intense red signal from the DPPC-CD assemblies (Figure 5.11c). As predicted from the steady-state measurement, the DMPC-CD assembly exhibits blue, green, and red signals altogether because of near the gel to fluid transition temperature at RT (Figure 5.11b). Interestingly, all the lipid-CD assemblies exhibit a significant blue signal, thus confirming the presence of monomeric H-CDs in the lipid bilayer. Therefore, we conclude that all lipid bilayers incorporate the monomeric H-CDs and the RIR of symmetrical heterocycles of H-CDs are restricted in the ordered phase of the lipid membrane rendering the red fluorescence. On the other hand, the intramolecular rotation is allowed in the liquid-crystalline phase or disordered phase of the lipid and in the absence of RIR, the lipid-CD assemblies exhibit a blue fluorescence. Besides, the merged CLSM images for the DPPC, DMPC, and DOPC also show similar observation as shown in the photographs of the H-CDs in different lipids under 365 nm ultraviolet radiations. The merge red and blue signals from

DPPC and DOPC respectively confirm the phase sensitivity of the H-CDs in the different lipid bilayer.

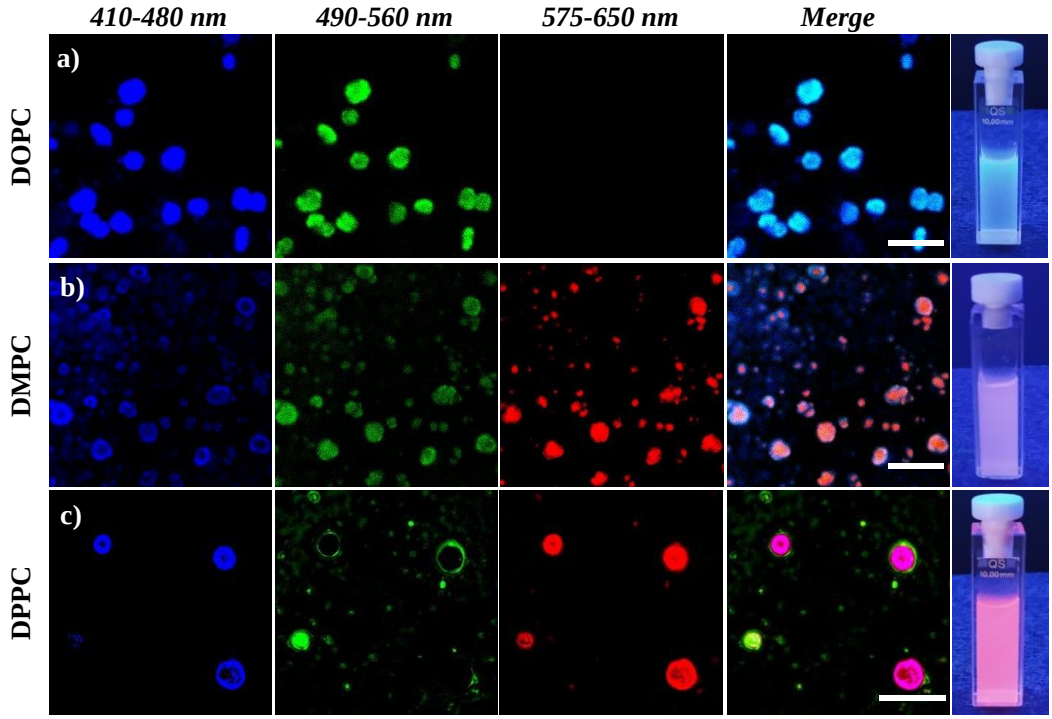

Figure 5.11 Confocal laser scanning microscopy (CLSM) images of the Lipids-CDs assemblies a) DOPC, b) DMPC, and c) DPPC. CLSM images recorded upon excitation using a 405 nm with emission filter EM 410/480 (blue), emission filter EM 490/560 (green), and emission filters EM 575/650 (red). Scale bar corresponds to 10 µm.

5.2.6 <u>Membrane dynamics and photophysical stability of lipid-CD assemblies:</u> Membrane dynamics are generally monitored by organic membrane probes *[6]*. Their emission profiles offer specific information regarding the change in membrane phase state or extent of water penetration into the bilayer. Here, we have investigated the effect of different membrane active ions and biomolecules on the membranes by monitoring the red region signal of lipid-CD assemblies. We found that the addition of In^{3+} to the zwitterionic DMPC-CD assemblies increases the fluorescence intensity, lifetime, and time-resolved anisotropy much more compared to Ca^{2+} (Figure 5.12a-c) indicating that these ions dehydrate the lipid bilayer as reported previously *[14]*. Previously, we have been reported that the small aromatic amino acids (e.g. L-Phe, L-Trp, and L-His) significantly change the membrane dynamics of the DMPC/DMPG vesicles, which follows the order of L-Trp> L-Phe >L-His *[15]*. Interestingly, we also observed a significant increase in the

fluorescence lifetime (Figure 5.11e) and slower rotational relaxation of H-CDs (Figure 5.11f) in negatively charged DMPC/DMPG vesicles upon addition of L-Trp compared to that of L-Phe. Previously, the effects of these membrane-active ions or biomolecules have been investigated with the help of organic membrane probe Prodan and ANS *[8-9]*. The extent of interaction (i.e. In^{3+}> Ca^{2+} and L-Trp> L-Phe) as revealed by the H-CDs collaborates well with our previously reported observation. Therefore, the H-CDs effectively detect the change in the membrane dynamics just like organic probes (Prodan, Laurdan, ANS, etc.).

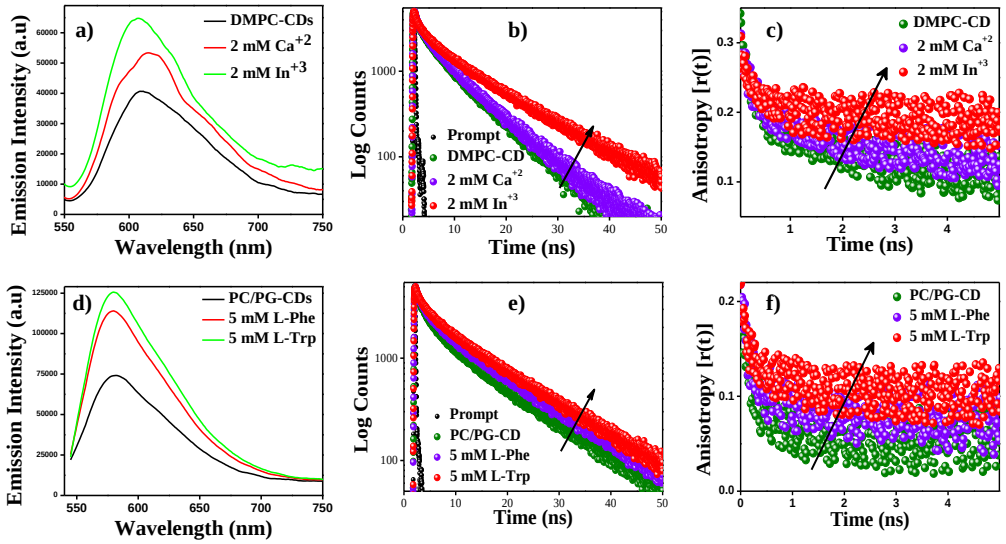

Figure 5.12 Fluorescence emission (a and d), lifetime decay (b and e) and time-resolved anisotropy decay (c and f) of the a-c) DMPC-CD assemblies in presence of 2 mM Ca^{2+} and In^{3+} and d-f) DMPC/DMPG-CD assemblies in presence of 5 mM L-Phe and LTrp upon excitation at 485 nm.

Furthermore, the photostability of the lipid-CDs assemblies was studied to investigate the effect of ordered and disordered phase state of the membrane in emission properties of CDs. We found that the intensity of the H-CDs emission both in water and ethanol medium decreases by ~40 and 55% respectively after 21 days (Figure 5.13a, b). Interestingly, in the disordered phase or in DOPC the PL intensity was stable up to ~7 days; however, PL intensity diminished by 22% after 21 days (Figure 5.13c). On the other hand, the PL intensity of the DPPC-CD assemblies remains unchanged for 21 days (Figure 5.13d), suggesting that the gel phase of the lipid increases the

photostability of the lipid embedded H-CDs. This observation is in accordance with the quantum dot encapsulated lipid bilayer by Salaita and coworkers *[21]*. These studies are important because the insertions of the H-CDs in the lipid bilayer not only detect the change in the membrane dynamics by the small ions or biomolecules but also increase the photostability, providing a CD-based membrane probe like other organic probes.

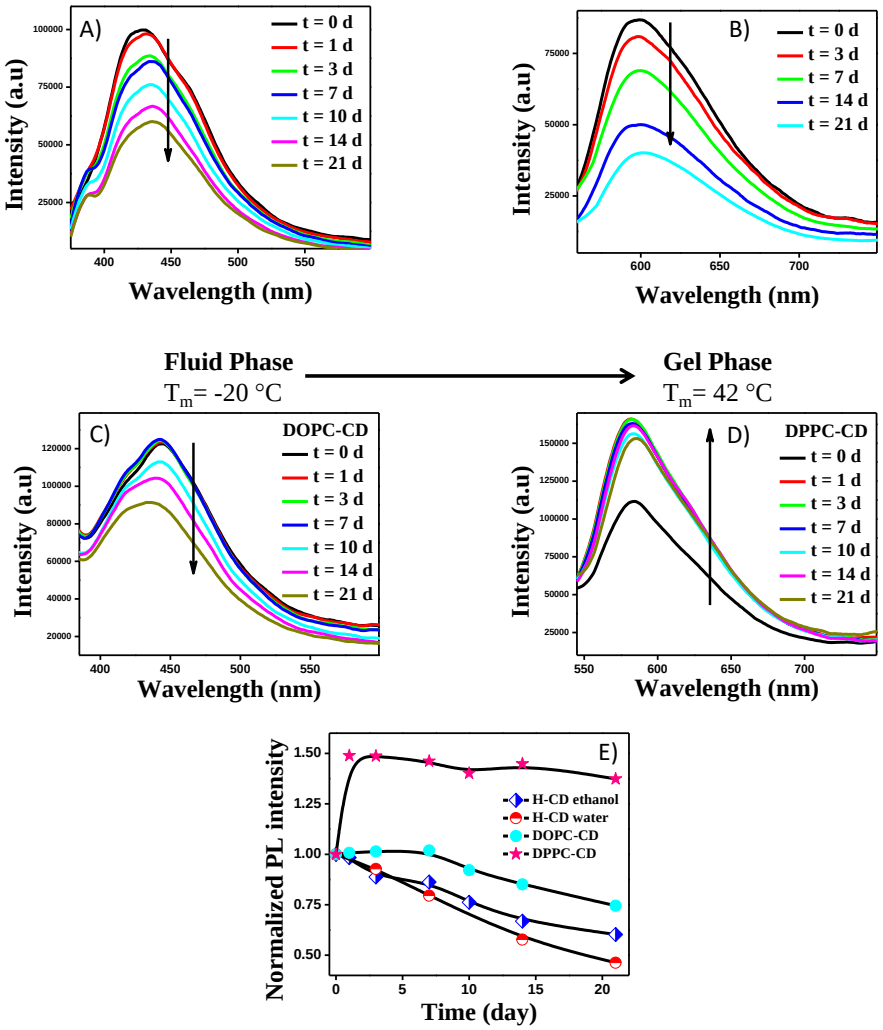

Figure 5.13 Time-dependent fluorescence emission spectra of the blank H-CDs a) in ethanol, b) in an aqueous medium. Membrane-dependent photostability of the lipid-CD assemblies in c) DOPC and d) DPPC. The fluorescence emissions were measure after 0, 1, 3, 7, 10, 14, 21 days upon exposer to ambient light under laboratory condition.

5.3 Conclusion

In conclusion, we exploited the distinct phase-dependent emission properties of a novel hydrophobic CD to identify the membrane phase state through

naked eyes under a UV lamp. The specific binding in the bilayer due to CDs hydrophobic nature and enhance photostability after incorporation in the bilayer of the synthesized H-CDs offer a carbon dot based membrane sensitive probe for regulating the membrane dynamics. We believe that this study will give us an idea to redesign and synthesis of the other CD-based membrane probe for future perspective.

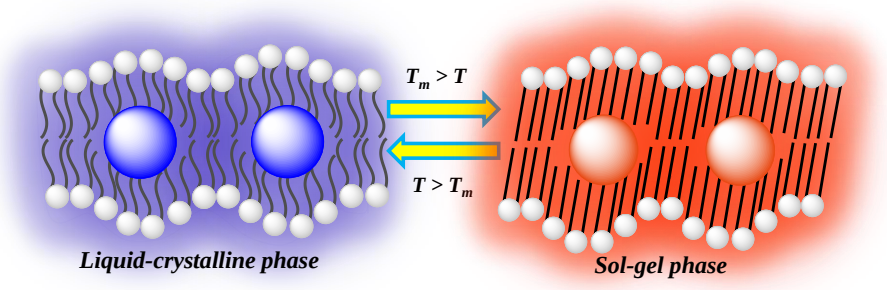

Scheme 5.1 Pictorial representation of the lipid-phase dependent distinct emission behavior of the H-CDs.

5.4 References

1. Bangham, A. D. (1993). Liposomes: the Babraham connection. Chem. Phys. Lipids, 64, 275-285. (DOI: 10.1016/0009-3084(93)90071-A)

2. Banerjee, R. (2001). Liposomes: applications in medicine. J. Biomater. Appl., 16, 3-21. (DOI: 10.1106/RA7U-1V9C-RV7C-8QXL)

3. Stern, T., Kaner, I., Zer, N. L., Shoval, H., Dror, D., Manevitch, Z., ... & Benny, O. (2017). Rigidity of polymer micelles affects interactions with tumor cells. J. Control. Release, 257, 40-50. (DOI: 10.1016/j.jconrel.2016.12.013)

4. Guo, P., Liu, D., Subramanyam, K., Wang, B., Yang, J., Huang, J., ... & Moses, M. A. (2018). Nanoparticle elasticity directs tumor uptake. Nat. Commun., 9(1), 1-9. (DOI: 10.1038/s41467-017-02588-9)

5 Sun, J., Zhang, L., Wang, J., Feng, Q., Liu, D., Yin, Q., ... & Jiang, X. (2015). Tunable rigidity of (polymeric core)–(lipid shell) nanoparticles for regulated cellular uptake. Adv. Mater., 27, 1402-1407. (DOI: 10.1002/adma.201404788)

6. Klymchenko, A. S., Kreder, R. (2014), Fluorescent Probes for Lipid Rafts: From Model Membranes to Living Cells. *Chem. Biol.*, 21, 97−113. (DOI: 10.1016/j.chembiol.2013.11.009)

7. Zhi, B., Cui, Y., Wang, S., Frank, B. P., Williams, D. N., Brown, R. P., ... & Haynes, C. L. (2018). Malic acid carbon dots: from super-resolution live-cell imaging to highly efficient separation. ACS nano, 12, 5741-5752. (DOI: 10.1021/acsnano.8b01619)

8. Pritzl, S. D., Pschunder, F., Ehrat, F., Bhattacharyya, S., Lohmüller, T., Huergo, M. A., & Feldmann, J. (2019). Trans-membrane fluorescence enhancement by carbon dots: Ionic interactions and energy transfer. Nano let., 19, 3886-3891. (DOI: 0.1021/acs.nanolett.9b01071)

9. Jiang, K., Sun, S., Zhang, L., Lu, Y., Wu, A., Cai, C., & Lin, H. (2015). Red, green, and blue luminescence by carbon dots: full-color emission tuning and multicolor cellular imaging, Angew. Chem., Int. Ed., 127, 5450-5453. (DOI: 10.1002/ange.201501193)

10. Du, J., Xu, N., Fan, J., Sun, W., & Peng, X. (2019). Carbon dots for in vivo bioimaging and theranostics, Small, 15, 1805087. (DOI: 10.1002/smll.201805087)

11. Unnikrishnan, B., Wu, R. S., Wei, S. C., Huang, C. C., & Chang, H. T. (2020). Fluorescent carbon dots for selective labeling of subcellular organelles. Acs Omega, 5, 11248-11261. (DOI: 10.1021/acsomega.9b04301)

12. Nandi, S., Malishev, R., Kootery, K. P., Mirsky, Y., Kolusheva, S., & Jelinek, R. (2014). Membrane analysis with amphiphilic carbon dots. Chem. Commun, 50, 10299-10302. (DOI: 10.1039/C4CC03504F)

13. Nandi, S., Malishev, R., Bhunia, S. K., Kolusheva, S., Jopp, J., & Jelinek, R. (2016). Lipid-bilayer dynamics probed by a carbon dot-phospholipid conjugate. Biophys j., 110. 2016-2025. (DOI: 10.1016/j.bpj.2016.04.005)

14. De, S. K., Kanwa, N., & Chakraborty, A. (2019). Influence of trivalent metal ions on lipid vesicles: gelation and fusion phenomena, Langmuir, 35, 6429-6440. (DOI: 10.1021/acs.langmuir.9b00682)

15. De, S. K., & Chakraborty, A. (2019). Interaction of monomeric and self-assembled aromatic amino acids with model membranes: self-reproduction phenomena. Chem. Commun, 55, 15109-15112. (DOI: 10.1039/C9CC08495A)

16. Yang, H., Liu, Y., Guo, Z., Lei, B., Zhuang, J., Zhang, X., ... & Hu, C. (2019). Hydrophobic carbon dots with blue dispersed emission and red aggregation-induced emission. Nat. commun., 10, 1-11. (DOI: 10.1038/s41467-019-09830-6)

17. Chao, D., Lyu, W., Liu, Y., Zhou, L., Zhang, Q., Deng, R., & Zhang, H. (2018). Solvent-dependent carbon dots and their applications in the detection of water in organic solvents. J. Mater. Chem. C, 6, 7527-7532. (DOI: 10.1039/C8TC02184H)

18. Wang, F., & Liu, J. (2015). Self-healable and reversible liposome leakage by citrate-capped gold nanoparticles: probing the initial adsorption/desorption induced lipid phase transition. Nanoscale, 7(38), 15599-15604. (DOI: 10.1039/C5NR04805B)

19. Wang, F., Curry, D. E., & Liu, J. (2015). Driving adsorbed gold nanoparticle assembly by merging lipid gel/fluid interfaces. Langmuir, 31, 13271-13274. (DOI: 10.1021/acs.langmuir.5b03606)

20. Yan, F., Jiang, Y., Sun, X., Wei, J., Chen, L., & Zhang, Y. (2020). Multicolor carbon dots with concentration-tunable fluorescence and solvent-affected aggregation states for white light-emitting diodes. Nano Res., 13, 52-60. (DOI: 10.1007/s12274-019-2569-3)

21. Zheng, W., Liu, Y., West, A., Schuler, E. E., Yehl, K., Dyer, R. B., ... & Salaita, K. (2014). Quantum dots encapsulated within phospholipid membranes: phase-dependent structure, photostability, and site-selective functionalization. J. Am. Chem. Soc., 136, 1992-1999. (DOI: 10.1021/ja411339f)

Chapter 6

Materials and Methods and Instrumentation

6.1 Materials

All the phospholipids, namely, DPPC (1,2-dipalmitoyl-sn-glycero-3-phosphocholine), DMPC (1,2-dimyristoyl-sn-glycero-3-phosphocholine), POPC (1-palmitoyl-2-oleoyl-glycero-3-phosphocholine), DOPC (1,2-dioleoyl-sn-glycero-3-phosphocholine), DOTAP (1,2-dioleoyl-3-trimethylammonium-propane (chloride salt)), DMPG (1,2-dimyristoyl-sn-glycero-3-phospho-(1'-rac-glycerol) (sodium salt)), and NBD-PE (1,2-dioleoyl-sn-glycero-3-phosphoethanolamine-N-(7-nitro-2-1,3-benzoxadiazol-4-yl) (ammonium salt) were purchased from Avanti polar lipids.

All the other chemicals namely PRODAN, ANS, Rhodamine B (Rh-B), Thioflavin T (ThT), 4-(2-hydroxyetyl)- 1-piperazineethanesulfonic acid (HEPES), acetate salts, dithiosalicylic acid (DTSA), o-Phenylenediamine, Citric acid, 1-(2-pyridylazo)-2-naphthol (PAN) were purchased from Sigma-Aldrich. The metal salts zinc chloride ($ZnCl_2$), calcium chloride ($CaCl_2$), magnesium chloride ($MgCl_2$), aluminum chloride ($AlCl_3$), Gallium chloride ($GaCl_3$), indium chloride ($InCl_3$), and the amino acids L-Phenylalanine (Phe), L-Tryptophan (Trp) and L-Histidine (His) were also purchased from Sigma-Aldrich. In chapter 1 the zinc chloride ($ZnCl_2$), and magnesium chloride ($MgCl_2$) were purchased from MERCK. All these chemicals were used without any further purification.

All the solvents i.e. acetic acid, ethanol, DMF, chloroform, acetone, methanol, and ethylene glycol used in the experiments were of the spectroscopic grade obtained from Merck. Milli-Q water was used to prepare all of the lipid vesicles solutions. The resistivity of the Milli-Q water was 18.2 M Ω•cm at 25 °C in our setup. However, in chapter 3 HEPES buffer (for pH~7.0) and acetate buffer (for pH 5.5) have been used to prepare the lipid vesicles.

6.2 Methods

6.2.1 Preparation of PRODAN or ANS solution: Stock solution of PRODAN was prepared in ethanol. The required amount of ethanolic solution of PRODAN was taken in a volumetric flask and dried under vacuum to create a thin film of PRODAN *[1]*. Then, an appropriate amount of buffer or mili-Q was added to it and sonicated for 2 hours. The final concentration of PRODAN was fixed at 1 μM. ANS solution (4 μM) was also prepared by using same above mentioned method.

Chapter 2

6.2.2 Lipid bilayer preparation: Lipid bilayers were prepared using thin film hydration method *[2]*. The lipids were dissolved in a mixture of chloroform and ethanol (2:1), and the solvents were removed completely in rotary evaporator under gentle conditions. The flask containing a dry lipid film was placed under ultra-high vacuum overnight to remove any residual solvent. The film was hydrated with preheated Mili-Q water. The obtained lipid bilayers were extruded through 200 nm track-etched polycarbonate membranes to yield unilamellar bilayer. For the samples that included preparation of PRODAN-loaded lipid bilayer, we use freshly prepared PRODAN solution to hydrate the lipid film. The final lipid and PRODAN concentration was fixed at 0.6 mM and 1 μM respectively. We further confirm that in this concentration range PRODAN molecules does not undergo any kind of aggregation.

To study the effect of pH on binding ability of lipid bilayers with metal ions, the lipid bilayer was prepared at pH~7.00 and pH~ 5.5 using phosphate buffers (I= 10 mM).

Chapter 3

6.2.3 Lipid vesicles preparation: DMPC lipid vesicles were prepared in different buffer solutions as required (10 mM acetate for pH 5.5; and 10 mM HEPES for pH 7.0) *[3]*. The lipids were dissolved in a mixture of chloroform and ethanol, and the solvents were removed completely in rotary evaporator

under gentle conditions (P = 180 mBar, T = 30 °C). The flask containing a dry lipid film was placed under an ultra-high vacuum for overnight to remove any residual solvent. The film was hydrated with a buffer solution, which was already heated above phase transition temperature of the lipids. The obtained lipid vesicles were extruded several times through 200 nm track-etched polycarbonate membranes to yield monodispersed small unilamellar vesicles (SUV). For the samples that included preparation of probe-loaded lipid vesicles, we used freshly prepared PRODAN and ANS solution to hydrate the lipid film. The final concentration of lipid was 0.4 mM while the concentration of PRODAN and ANS were1 μM and 4 μM respectively. We confirmed that in this concentration range any of these probes does not undergo any kind of aggregation. For confocal imaging, the multilamellar vesicles (MLV, 3 mM) were prepared using thin film hydration method and the dye used was rhodamine B (500 nM). After passive loading, the unencapsulated dye was removed by dialysis using a Pur-ALyzer Maxi Dialysis tube (polycarbonate membrane, MWCO 12−14 kDa), purchased from Sigma-Aldrich in HEPES buffer medium (pH ~ 7.0, I= 10 mM).

6.2.4 Preparation of lipid vesicles: Lipid vesicles (DMPC, DMPC/DMPG and DMPC/DOTAP) were prepared by the thin-film hydration method. The ratio of zwitterionic and charged lipid was fixed at 8:2 for preparing the DMPC/DMPG and DMPC/DOTAP lipid vesicles. The required amount of lipids was dissolved in a mixture of chloroform and ethanol, and then the solvents were removed completely in a rotary evaporator under gentle conditions (P = 180 mBar, T = 30 °C). The flask containing a dry lipid film was placed under a high vacuum overnight to remove any residual solvent. The film was hydrated with a preheated HEPES buffer (I= 10 mM) solution, vortexed and stirred for 1 hour above the phase transition of the respective lipid. Lipid dispersion was sonicated for 5 minutes using ultrasonic cell disruptor. Finally, the obtained lipid vesicles were extruded several times through 1 μm track-etched polycarbonate membranes to yield monodispersed small unilamellar vesicles. For confocal microscopy, prior to thin film

preparation, 1 mol% NBD-PE was mixed with the required amount of lipid vesicles, and then the thin film was hydrated with HEPES buffer.

6.2.5 Th-T binding assay: Thioflavin T (ThT) binding assay was performed to unravel any kind of formation of amyloid structures in solution phase. A stock solution of 40 μM ThT was added to the lipid-amino acids mixture to a final concentration of 20 μM ThT, while lipid and amino acid concentration were fixed.

6.2.6 Preparation of Lipid vesicles-amino acid mixture: For all steady-state and time-resolved experiments, the lipid concentration was fixed at 1 mM, and amino acids concentration varied from 0 to 10 mM. For confocal microscopy imaging, 1 mM lipid vesicles were incubated with 10 mM of amino acid. The excess vesicles and unbound amino acids were removed via centrifugation (10000 r/min, 1 min) and exchanged with mili-Q water 3 times. The final concentration of amino acid was around 3.5 and 6.1 mM for DMPC and DMPC/DMPG, respectively. Finally, the lipid-amino acid mixture was re-dispersed in water and vortex for 30 sec, to overcome any vesicle aggregation during the centrifugation process.

Chapter 5

6.2.7 Preparation of Hydrophobic carbon dots (H-CDs):

The hydrophobic carbon dots were prepared by the previously reported method.1Briefly, 100.8 mg melamine and 272 mg dithiosalicylic acids were dissolved into 20 mL acetic acid with ultrasonic treatment and then the solution was transferred into a 40 mL Teflon-lined autoclave and kept at 180 °C for 10 h in an air oven. After the solvothermal treatment, the as-prepared H-CD solution was added to 500 ml of boiled water to form H-CD powder and washed out the residual raw materials and solvent. Finally, purified H-CD powder was achieved through vacuum filtration.

6.2.8 Preparation of carbon dots (o-CDs) from o-Phenylenediamine:

Ortho-phenylenediamine (0.2 g) was dissolved in 20 mL of Mili-Q water, and the solution was transferred into a 40 mL Teflon-lined autoclave and heated at 180 °C for 12 h, as reported previously.2-3 After cooling down naturally, the

as synthesized dark yellow solution was centrifuged to 8000 rpm and filter against 0.22 μm filter to remove the larger aggregates. Finally, the solution was freeze-drying and kept under high-vacuum to get the yellow color powder o-CDs.

6.2.9 Preparation of multicolor carbon dots (M-CDs):

M-CDs were synthesized by a previously reported simple solvothermal method.4 Citric acid (CA, 1.15 g) and PAN (0.07 g) was dissolved in 30 mL ethanol by ultrasonication. Then the mixture was transferred into a 40 mL Teflon-lined autoclave and heated at 200 °C for 7 h. Then, the as synthesized dispersion was filtered by using a microporous membrane (0.22 μm) to remove the larger particles. The excess ethanol was removed by using rotary evaporator and freeze-dried to obtain viscous solids M-CDs for further use.

6.2.10 Preparation of lipid-CD assemblies:

H-CD embedded lipid vesicles or lipid-CD assemblies (DMPC-CD, DPPC-CD, DOPC-CD and DMPC/DMPG-CD) were prepared by hydration of dried Lipid-CD thin-films. The ratio of zwitterionic and charged lipid was fixed at 8:2 for preparing the DMPC/DMPG-CDassemblies. The required amount of lipids and H-CDs were dissolved in a mixture of chloroform and ethanol, and then the solvents were removed completely in a rotary evaporator. The flask containing a dry lipid film was placed under a high vacuum overnight to remove any residual solvent. The film was hydrated with a preheated Milli-Q, vortex for 5 minutes and stirred for 30 minutes above the phase transition of the respective lipid and these cycles were repeated for 3 times.The final concentration of lipid and H-CDs were 1 mM and 50 μg mL-1 respectively. The o-CD and M-CD based lipid-CD assemblies were also prepared by using same above mentioned protocol.

6.3 Instrumentation

6.3.1 Steady-State Fluorescence Measurements: Steady-state fluorescence spectra were recorded using a Fluoromax-4p spectrofluorometer from Horiba JobinYvon (model: FM-100). The excitation and emission slits were 2/2 for all the emission measurements. We maintained temperature (T) at 25°C

throughout all the experiments, otherwise, we mentioned the temperature. The fluorescence quantum yield (QY) was estimated relative to Quinine Sulfate (Φ_{ST}) in water medium by using the following equation:

$$\Phi_S = \Phi_{ST}\left(\frac{I_S}{I_{ST}}\right)\left(\frac{\eta_S^2}{\eta_{ST}^2}\right)\left(\frac{A_{ST}}{A_S}\right) \quad 7.1$$

Here, Φ is the QY, Iis the integrated fluorescence intensity, η is the refractive index of the solvent, and A is the optical density. The subscript "ST" stands for standard and "S" stands for the samples.

6.3.2 Time-Resolved Fluorescence Measurements: For lifetime measurements, we used a picosecond TCSPC (time-correlated single-photon counting) machine from Horiba (Fluorocube-01-NL).We used a filter on the emission side to eliminate the scattered light. The signals were collected at magic angle (54.75°) polarization using a photomultiplier tube (TBX-07C) as a detector with instrument response function ~560 ps. The data analysis was performed using IBH DAS Version 6 decay analysis software.

The decays were fitted with a multi-exponential function.

$$D(t) = \sum_{i=1}^{n} a_i \exp\left(\frac{-t}{\tau_i}\right) \quad 7.2$$

Here D(t) denotes normalized fluorescence decay and a_i is the normalized amplitude of decay components τ_i, respectively. The quality of the fit was judged by reduced chi-square (χ^2) values and corresponding residual distribution. The acceptable fit has a χ^2 near unity.

For the anisotropy decays, the same setup and a motorized polarizer were used in the emission side. The emission intensities at parallel and perpendicular polarizations were collected alternatively until a certain peak difference between parallel and perpendicular decay was achieved. The same software was also used to analyze the anisotropy data. The time-resolved anisotropy decay was described with the following equation:

$$r(t) = \frac{I_{\parallel}(t) - GI_{\perp}(t)}{I_{\parallel}(t) + 2GI_{\perp}(t)} \quad 7.3$$

Where r(t) is the rotational relaxation correlations function, $I_{\parallel}$ (t) and $I_{\perp}$ (t) are the parallel and perpendicular components of the fluorescence and G is the correlation factor.

6.3.3 Dynamic Light Scattering and Zeta potential measurements: DLS and zeta potential of the samples were measured on a NanoPlus particle size analyzer (NanoPlus-3 model). The DLS measurements were conducted at pH values ~5.50 and 7.0 to investigate the effect of pH on metal ion binding interactions with lipid vesicles. The lipid solution was prepared in required buffer solutions (10 mM acetate for pH ~ 5.5 and 10 mM HEPES for pH ~ 7.0). The lipid vesicles were incubated for 12 h in metal salts of different concentrations before DLS measurements. For the time-dependent studies, lipid vesicles were incubated with metal salts and the DLS measurement was conducted at different time intervals.

6.3.4 Confocal laser scanning microscopy (CLSM) imaging: For the confocal imaging of samples, we used a confocal microscope from OLYMPUS, model no. IX-83. A Multiline Ar laser (gas laser) with a desire excitation wavelength was used to study the lipid assemblies. An aliquot of the freshly prepared sample by the previous describe method (see liposome preparation section) was immobilized on a clean cover slide and kept in a vacuum desiccator to remove the solvent. Then the sample containing the cover slide was fixed by a glass slide in a sandwich manner by using transparent nail polish before imaging.

6.3.5 Atomic force microscopy: AFM images were taken by drop-casting the sample on mica substrates via tapping mode at a scan frequency of 0.65−1.0 Hz and were recorded using SmartScan software (model park NX10).

6.3.6 High resolution-Transmission electron microscopy (HR-TEM): High-resolution transmission electron microscopy images were taken by using a field emission gun transmission electron microscope (Model: Tecnai G2, F30) with an acceleration voltage of 300 kV. The diluted solutions of the samples were dried on a carbon-coated copper grid by slow evaporation in the air at room temperature before measurements.

6.3.7 Fourier transformed infrared (FT-IR) and X-ray Photoelectron Spectroscopy (XPS) measurement: The FT-IR spectra of powder samples were obtained by using a Perkin Elmer Spectrum 2 model. The XPS measurements were performed with a Shimadzu, Axis Supra X-ray photoelectron spectrometer. Spectra were acquired using the Al-Kα monochromatic X-ray source (1,486.7 eV) with 0° take of angle (normal to analyzer). The vacuum pressure in the analyzing chamber was maintained at ~2•10-9 Torr during the acquisition process. The survey spectra were collected with pass energy 160 eV, and 1.0 eV step size, dwell time 100 ms. High resolution XPS spectra were collected for C 1s, N 1s, O 1s, and S 2p, with pass energy 20 eV and 0.1 eV step size, dwell time 299 ms. All binding energies were corrected by using the contaminant carbon (C 1s = 284.8 eV) as an internal standard.

6.4 References

1. Thakur, R., Das, A., & Chakraborty, A. (2014) Interaction of human serum albumin with liposomes of saturated and unsaturated lipids with different phase transition temperatures: a spectroscopic investigation by membrane probe PRODAN, RSC Advances, 4, 14335-14347. (DOI: 10.1039/C4RA01214C)

2. Zhang, H. (2017). Thin-film hydration followed by extrusion method for liposome preparation. In Liposomes (pp. 17-22). Humana Press, New York, NY. (DOI: 10.1007/978-1-4939-6591-5_2)

3. Liu, Y., Liu, J. (2017) Zn^{2+} induced irreversible aggregation, stacking and leakage of choline phosphate liposomes, Langmuir, 33, 14472−14779. (DOI: 10.1021/acs.langmuir.7b03209)

4. Yang, H., Liu, Y., Guo, Z., Lei, B., Zhuang, J., Zhang, X., ... & Hu, C. (2019). Hydrophobic carbon dots with blue dispersed emission and red aggregation-induced emission, Nat. commun., 10, 1-11. (DOI: 10.1038/s41467-019-09830-6)

5. Jiang, K., Sun, S., Zhang, L., Lu, Y., Wu, A., Cai, C., & Lin, H. (2015). Red, green, and blue luminescence by carbon dots: full-color emission tuning

and multicolor cellular imaging, Angew. Chem., 127, 5450-5453. (DOI: 10.1002/ange.201501193)

6. Chao, D., Lyu, W., Liu, Y., Zhou, L., Zhang, Q., Deng, R., & Zhang, H. (2018). Solvent-dependent carbon dots and their applications in the detection of water in organic solvents. J. Mater. Chem. C, 6, 7527-7532. (DOI: 10.1039/C8TC02184H)

7. Yan, F., Jiang, Y., Sun, X., Wei, J., Chen, L., & Zhang, Y. (2020). Multicolor carbon dots with concentration-tunable fluorescence and solvent-affected aggregation states for white light-emitting diodes. Nano Research, 13, 52-60. (DOI: 10.1007/s12274-019-2569-3)

Chapter 7

Conclusion and Future aspects

7.1 Conclusion

The binding of different external entities (divalent and trivalent ions, amino acids, carbon dots) and the overall impact on the physiological properties of the model lipid membranes have been discussed in the thesis.

Our study demonstrates that hydration-free energy, ionic radius, cross-linking ability, the effective charge of the metal ions, and the side chain of the aromatic amino acids can hugely influence the membrane organization. For the interaction studies, lipid bilayers of varying chain lengths, surface charges, and phase transition temperatures were explored and we observed that the interactions significantly depend on the membrane organization or the phase state of the membrane.

Therefore, determination of the membrane phase state is crucial for several bio-inspired applications (delivery systems, nano-bio interaction, bioimaging, etc.). Fluorescent microscopy imaging technique by using organic membrane probes are one of the most popular-commonly used technique to investigate the lipid bilayer phase state. Therefore, in this thesis, we also make an effort to find out the nanomaterial-based membrane-sensitive probes. For the first time, we observe phase-dependent distinct emission behaviour of lipid encapsulated hydrophobic carbon dots, which can be observed through naked eyes under a UV lamp.

Several important cellular processes are critically depending on the aggregation and fusion of the membranes. Thus, a better understanding of the process will help us to bridge the gap between the lipid systems in vivo and in vitro.

7.2 Future Aspects

Membrane fusion is a very fundamental process in cell biology. Uncontrolled fusion is problematic in many aspects; therefore, it is important to study the fusion process of vesicles to find out a way to control it. Our study reveals some of the factors that potentially induce membrane fusion. In the future, lessons from these studies possibly help to control the long desire fusion and aggregation of the membrane.

As C-dots have several advantages (particularly the cost-efficient easy large-scale synthesis) over conventional organic membrane probes, we believe that the reported C-dot based membrane probe will attract significant interest to the scientific community. However, several modifications and development have been needed for a better C-dot based membrane-sensitive probe. In the future, the modified new class of c-dots will provide an efficient system for bioimaging modes in biomedical sciences. Thus as a future prospect, these developments are expected to add new dimensions for the development of delivery models, bioimaging, and other bio-inspired applications.